



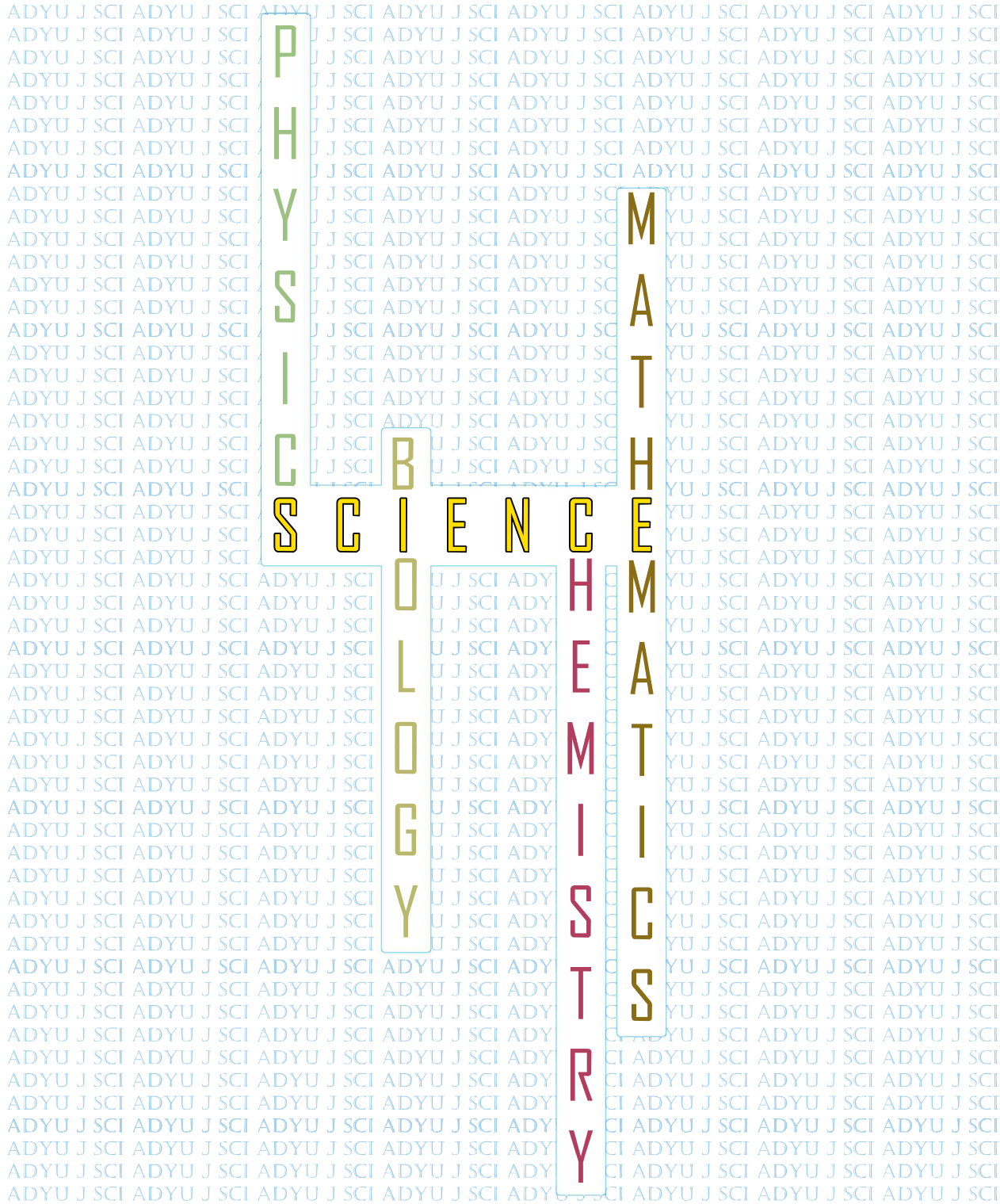
Adiyaman University Journal of Science

June 2022

Volume: 12

Issue: 1

An international peer reviewed journal of science



An open access, peer reviewed, international journal of science. Biannual (June & December). ISSN 2147-1630 | e-ISSN 2146-586X. Publisher: Adiyaman University.

Publication language: English (with Turkish title and abstract)

Issue published date: 30.06.2022

Privilege owner: On Behalf of Rectorate of Adiyaman University, Prof. Dr. Mehmet TURGUT (Rector)

Web site: EN: <https://dergipark.org.tr/en/pub/adyujsci>
TR: <https://dergipark.org.tr/tr/pub/adyujsci>

EDITORIAL BOARD

Editor-in-Chief : Deniz SUNAR ÇERÇİ, Ph.D.

Editors:

Biology : Serdar SÖNMEZ, Ph.D.
: Ertan YOLOĞLU, Ph.D.
Chemistry : Cumhur KIRILMIŞ, Ph.D.
: Gökhan ELMACI, Ph.D.
Mathematics : Selcen YÜKSEL PERKTAŞ, Ph.D.
: Serbay DURAN, Ph.D.
Physics : Salim ÇERÇİ, Ph.D.
: Özge ERKEN, Ph.D.

Statistics Editor: : Tayfun SERVİ, Ph.D.

Section Editors

Biology:

Aydın AKBUDAK, Ph.D.
Bahadır AKMAN, Ph.D.
Birgül ÖZCAN, Ph.D.
Deniz AYAS, Ph.D.
Hasan YILDIZ, Ph.D.
Olga SAK, Ph.D.
Özkan ASLANTAŞ, Ph.D.
Si Hong PARK, Ph.D.
Süphan KARAYTUĞ, Ph.D.

Chemistry:

Sezgin BAKIRDERE, Ph.D.
H. Mehmet KAYILI, Ph.D.
Önder METİN, Ph.D.
Zeynel SEFEROĞLU, Ph.D.
Lokman UZUN, Ph.D.

Mathematics:

Ramazan AKGÜN, Ph.D.
Murat CANDAN, Ph.D.
Feyza Esra ERDOĞAN, Ph.D.

Mehmet Onur FEN, Ph.D.
Öznur GÖLBAŞI, Ph.D.
Mehmet GÜLBAHAR, Ph.D.
Bilge İNAN, Ph.D.
Eylem GÜZEL KARPUZ, Ph.D.
Aynur KESKİN KAYMAKCI, Ph.D.
Mustafa Çağatay KORKMAZ, Ph.D.
James F. PETERS, Ph.D.
Mustafa Çağatay KORKMAZ, Ph.D.
Tahsin ÖNER, Ph.D.

Physics:

Ahmet EKİCİBİL, Ph.D.
Didar DOBUR, Ph.D.
Daniel GREEN, Ph.D.
Faruk KARADAĞ, Ph.D.
Hakan ÖZTÜRK, Ph.D.
Kristina RUSIMOVA, Ph.D.
Latife ŞAHİN YALÇIN, Ph.D.
Mustafa GÜNEŞ, Ph.D.
Paolo GUNNELLINI, Ph.D.

Technical Contact: Serdar SÖNMEZ, Ph.D., ssonmez@adiyaman.edu.tr, sonmezserdar@gmail.com

Language Editors: Münevver AKBAŞ, Hakkı ŞİMŞEK



The articles published in this journal are licensed under a Creative Commons Attribution-NonCommercial-ShareAlike 4.0 International License.

Table of Contents (İçindekiler)

Volume (Cilt): 12 Number (Sayı): 1
June (Haziran) 2022

BIOLOGY

Effects of FOLFIRINOX Components on Pancreatic Adenocarcinoma Cells

FOLFIRINOX Bileşenlerinin Pankreas Adenokarsinom Hücreleri Üzerindeki Etkileri
Sevde ALTUNTAS, Kubra Nur GOKDEMİR 1-8

The Anatomical Surveys on the Two *Salvia* L. Species (Sect. *Hymenosphace*, Sect. *Hemisphace*) Spreading in Mardin (Turkey)

Mardin'de (Türkiye) Yayılış Gösteren İki *Salvia* L. Türü (Seksiyon *Hymenosphace*, Seksiyon *Hemisphace*) Üzerine Anatomik Araştırmalar
Orcun AVSAR 26-39

Microbiological Investigation of the Effects of Olanzapine with Timokinon on the Intestine

Olanzapin ile Timokinon'un Bağırsak Üzerindeki Etkilerinin Mikrobiyolojik Olarak Araştırılması
Ayşe Nilay GÜVENÇ, Sebile AZIRAK, Deniz TAŞTEMİR KORKMAZ, Sedat BİLGİÇ, Nevin KOCAMAN, Mehmet Kaya ÖZER 106-119

Interstitial and Phytal Harpacticoid (Copepoda, Harpacticoida) Fauna of the Mediolittoral Zone of the Biga Peninsula (Çanakkale, Turkey),

Biga Yarımadası (Çanakkale, Türkiye) Mediolittoral Bölgesinin Kumiçi ve Fital Harpacticoid (Copepoda, Harpacticoida) Faunası
Alper KABACA, Serdar SAK, Alp ALPER 120-141

CHEMISTRY

A New Schiff Base Molecule Prepared from Pyrimidine-2-thione: Synthesis, Spectral Characterization, Cytotoxic Activity, DFT, and Molecular Docking Studies

Pirimidin-2-tiyondan Hazırlanan Yeni Bir Schiff Bazı Molekülü: Sentez, Spektral Karakterizasyon, Sitotoksik Aktivite, DFT ve Moleküler Doking Çalışmaları
Zülbiye KÖKBUDAK, Burçin TÜRKMEÑOĞLU, Senem AKKOÇ 9-25

Evaluation of Some Sulfonamide Derivatives as a Potential Inhibitors of the Carbonic Anhydrase IX/XII by ADME and Molecular Docking Method

Karbonik Anhidraz IX/XII'nin Potansiyel İnhibitörleri Olarak Bazı Sülfonamid Türevlerinin ADME ve Moleküler Yerleştirme Metodu ile Değerlendirilmesi
Nuri YORULMAZ, Hilal ÖZTÜRK, Mustafa DURGUN 88-105

MATHEMATICS

New Weyl-Type Inequalities by Multiplicative Injective and Surjective s-Numbers of Operators in Reflexive Banach Spaces

Yansımali Banach Uzaylarda Operatörlerin Çarpımsal İnjektiv ve Surjektiv s-Sayıları ile Yeni Weyl-Tipi Eşitsizlikleri
Lale CONA 40-55

Direct Product of Bitonic Algebras

Bitonic Cebirlerin Direkt Çarpımları
Şule AYAR ÖZBAL 56-69

On Two Efficient Numerical Schemes for Nonlinear Burgers' Type Equations

Lineer Olmayan Burgers Tip Denklemler İçin Etkili İki Nümerik Yöntem Üzerine
Bilge İNAN 70-87

PHYSICS

Effects of Copper Substitution to Mn-site on Magnetic and Magnetocaloric Properties of La_{0.7}Sr_{0.3}Mn_{1-x}Cu_xO₃ Manganites

Mn Bölgesine Bakır Katkılanmasının La_{0.7}Sr_{0.3}Mn_{1-x}Cu_xO₃ Manganitlerinin Manyetik ve Manyetokalorik Özellikleri Üzerindeki Etkileri
Gönül AKÇA, Selda KILIÇ ÇETİN, Mehmet Selim ASLAN, Ahmet EKİCİBİL 142-161



Effects of FOLFIRINOX Components on Pancreatic Adenocarcinoma Cells

Sevde ALTUNTAS^{1,2*}, Kübra Nur GÖKDEMİR³

¹University of Health Sciences, Hamidiye Health Institute, Tissue Engineering Department, 34668, Istanbul, Türkiye

²University of Health Sciences, Experimental Medicine Research and Application Center, Validebag Research Park, 34668, Istanbul, Türkiye
sevde.altuntas@sbu.edu.tr, ORCID: 0000-0002-4803-9479

³Uskudar University, Faculty of Engineering and Natural Sciences, Undergraduate Program of Molecular Biology and Genetics, 34662, Istanbul, Türkiye
kubranur.gokdemir@st.uskudar.edu.tr, ORCID: 0000-0002-4922-8095

Received: 18.09.2021

Accepted: 12.03.2022

Published: 30.06.2022

Abstract

Pancreatic adenocarcinoma is one of the lethal types of cancer worldwide. This study aimed to evaluate the cytotoxic effects of FOLFIRINOX compounds [oxaliplatin (OXA), irinotecan (IRI), fluorouracil (5FU), and leucovorin (LEU)] on a pancreatic adenocarcinoma cell line (PANC-1), both individually and collectively. Cell viability was determined using the colorimetric MTT reagent and apoptosis was assessed using the propidium iodide – Hoechst 33342 staining assay.

Based on cell viability data, 5FU and FOLFIRINOX treatments were more potent against PANC-1 than the other test groups. The apoptotic trend, nevertheless, was not different between them and the control group. Moreover, OXA, LEU, and IRI significantly increase apoptotic cell death. Our findings indicate that 5FU and FOLFIRINOX are comparably effective in reducing the PANC-1 cell viability. In the future, 5FU and FOLFIRINOX may be adapted to local pancreatic adenocarcinoma treatments, but the development of these localized drug release platforms requires further attention as the microenvironment of pancreatic adenocarcinoma inherently contains many unknowns.



Keywords: FOLFIRINOX; PANC-1 cells; Pancreatic Adenocarcinoma; Cytotoxicity; Apoptosis.

FOLFIRINOX Bileşenlerinin Pankreas Adenokarsinom Hücreleri Üzerindeki Etkileri

Öz

Pankreatik adenokarsinoma tüm dünyada en ölümcül kanser türlerinden biridir. Bu çalışma, FOLFIRINOX bileşiklerinin (oksalipatin (OXA), irinotekan (IRI), fluorourasil (5FU) ve leucovorin (LEU)) tekli ve toplu olarak pankreas adenokarsinom hücre hattı (PANC-1) üzerindeki etkilerini hücre canlılığı ve apoptoz için araştırmayı amaçlamıştır. Hücre canlılığı, MTT reaktifi kullanılarak belirlendi ve apoptoz, propidium iyodür – Hoechst 33342 boyama testi kullanılarak değerlendirildi.

Hücre canlılığı sonuçları, FOLFIRINOX uygulamasının diğer test gruplarına kıyasla en yüksek toksisite oranına sahip olduğunu göstermiştir. Ancak apoptotik eğilim kontrol grubundan farklı bulunmadı. Ek olarak, 5FU tekil uygulamada diğer tekil ilaç uygulamalarına nazaran en yüksek toksisiteyi göstermiştir, fakat apoptotik indeksi kontrol grubundan ve FOLFIRINOX tedavisinden farklı bulunmamıştır. Genel olarak, çalışma sonuçları, tedavi rejiminin pankreas adenokarsinom hücre dizileri üzerinde etkili olduğunu gösterdi. Gelecekte, FOLFIRINOX ve 5FU tedavisi lokal pankreas adenokarsinomu tedavilerine uyarlanabilir, ancak pankreas adenokarsinomunun mikroçevresi, doğası gereği pek çok bilinmeyen barındırdığından, bu lokalize ilaç salım platformlarının geliştirilmesi daha fazla dikkat gerektirmektedir.

Anahtar Kelimeler: FOLFIRINOX; PANC-1 hücreleri; Pankreatik Adenokarsinoma; Sitotoksosite; Apoptoz.

1. Introduction

Pancreatic adenocarcinoma (PA) accounts for roughly 2.5% of all malignancies diagnosed globally and is a fatal disease with a rising frequency. The incidence rate and age-standardized rate of pancreatic cancer are 6.4% and 4.9%, respectively. Poor dietary habits are a major cause of disease occurrence [1]. Although the disease has a high prevalence and lethal effect, surgeons and oncologists consider that surgical resection is the only potentially curative treatment for PA in the light of what is known about the disease [2]. Drug screening and drug repurposing studies, therefore, are too critical for PA.

FOLFIRINOX drug combination is one of the PA treatment strategies that has shown promising results when compared to conventional drugs [3]. FOLFIRINOX is known as the abbreviation of the combination chemotherapy regimen consisting of oxaliplatin (OXA), irinotecan (IRI), fluorouracil (5FU), and leucovorin (LEU). In this treatment, OXA targets guanine and cytosine moieties of DNA,

and 5FU blocks DNA synthesis, while IRI is responsible for inhibiting DNA topoisomerase enzymes. One of the vitamin B family members, LEU increases 5FU activity [4].

FOLFIRINOX has been accepted as salvage therapy for PA [5]. The clinical studies demonstrated that FOLFIRINOX treatment for locally advanced or borderline resectable PA seems effective with a manageable toxicity profile [6]. Individually FOLFIRINOX compounds have shown a significantly cellular death profile in independent research studies; however, the cellular level response of the FOLFIRINOX regimen is still unclear and requires more attention. Cytotoxicity profile of FOLFIRINOX may provide an insight for clinicians to low-dose treatment schemes and reduced side effects of the disease [4].

The alterations to the balance between cell proliferation and cell death trigger tumor development with a series of genetic variations during cancer progression. Therefore, monitoring the apoptosis propensity of cell lines is essential to drug applications [7]. The study focused on how the FOLFIRINOX treatment affects the pancreatic adenocarcinoma cell line (PANC-1). The apoptosis trend of the cells was followed after single and multiple drug applications on the cell line in addition to cell viability analyses. We aimed to demonstrate the effects of the FOLFIRINOX compounds individually and collectively on the PANC-1.

2. Material and Methods

2.1. Materials

American Tissue Culture Collection provided a pancreatic ductal adenocarcinoma cell line (PANC1, CRL-1469). Oxaliplatin (O9512), leucovorin (47612), irinotecan (I1406), 5-Fluorouracil (F6627), Dulbecco's Modified Eagle's Medium (DMEM, D3744), fetal bovine serum (FBS, 2327864), trypsin-EDTA (59428C), propidium iodide (PI) (BCC1398), Hoechst bidBenzamide H 33342 trihydrochloride (BCCC5645), and HEPES (H4034) were purchased from Sigma-Aldrich, Germany. L-glutamine (CP21-4047), penicillin-streptomycin (CP21-4079), phosphate-buffered saline (PBS, PBS-1A) were used as received from Capricorn, Germany, and methanol (947.046.2500) was obtained from Isolab, Germany. The 3-(4, 5-dimethylthiazol-2-yl)-2, 5-diphenyltetrazolium bromide (MTT) solution (NC461720) was obtained from Biobasic, Canada.

2.2. Drug Preparation

OXA, LEU, IRI, and 5FU were prepared according to FOLFIRINOX administration protocol [8]. Two milligrams (mg) of drugs were dissolved in one ml of HEPES, HEPES: methanol (3:2 v/v), methanol, dimethylsulfoxide, respectively. Then the final concentrations of the substances were prepared with serial dilutions (Table 1).

Table 1: The analysis concentrations and incubation time for the combinations of OXA, LEU, IRI, and 5FU

Chemicals	Incubation Time (h)	Concentration (mg/m²)
OXA	2	85
LEU	2	400
IRI	0.4	180
5FU	48	400
OXA-LEU	4	85 – 400
OXA-LEU-5FU	52	85 – 400 – 400
OXA-5FU	50	85 – 400
FOLFIRINOX	52.4	85 – 400 – 180 – 400

2.3. Cell viability

The PANC-1 cell line was grown in DMEM medium supplemented with 10% FBS, 1% L-glutamine, and 1% penicillin-streptomycin at 37 °C in a 5% CO₂ atmosphere. The drugs were applied to the cells in a 96-well plate (10⁵ cells/well) at various concentrations (Table 1). After 24 h of treatment, the cell medium was exchanged with MTT solution, and the plates were incubated for 4 hours at 37 °C. The formed formazan crystals were dissolved with dimethylsulfoxide, and optical densities were measured at 590 nm using a plate reader (Biotek, Synergy). The serum-free medium was used as the negative control.

2.4. Propidium iodide – Hoechst 33342 Staining

Hoechst 33342 (2 µg/mL) and PI (1 µg/mL) were dissolved in PBS. The cells were incubated with the solutions for 30 minutes at 37 °C, respectively [9]. After PBS washing, well images were captured using the Operetta CLS High Content Analysis System. In the experiment, apoptotic and total cells were counted from 3 different images and analyzed following the formula:

$$\text{Apoptotic index \%} = \frac{\text{number of apoptotic cells}}{\text{number of total cells}} \times 100$$

2.5. Statistical Analyses

This experiment was performed in triplicate, and negative control was used in the experiment. Results are presented as mean (standard deviation) (n=3). Student t-test and the one-way analysis of variance (ANOVA, Microsoft Excel) was used for statistical analyses.

3. Results and Discussion

3.1. Results

In the FOLFIRINOX treatment, OXA, LEU, IRI, and 5FU are intravenously administered for different dosages and application times as shown Table 1, respectively. However, the drug amount and application time have not affected cell death for individual OXA, LEU, and IRI applications. The application time of individual 5FU on the cell line may have increased cellular toxicity. On the other hand, for the combined applications, synergetic effects of the drugs have been observed on the cell line (Figure 1).

Treatment with 5FU is more toxic towards PANC-1 than OXA, LEU, and IRI ($p < 0.0005$). OXA-LEU combination demonstrated a less toxic effect on the cancer cell compared to different combination scenarios. Additionally, the OXA-LEU-5FU combination shows a statistically similar toxic effect with individual 5FU and OXA-5FU combination ($p > 0.05$). The FOLFIRINOX application caused the highest toxic profile for the cells.

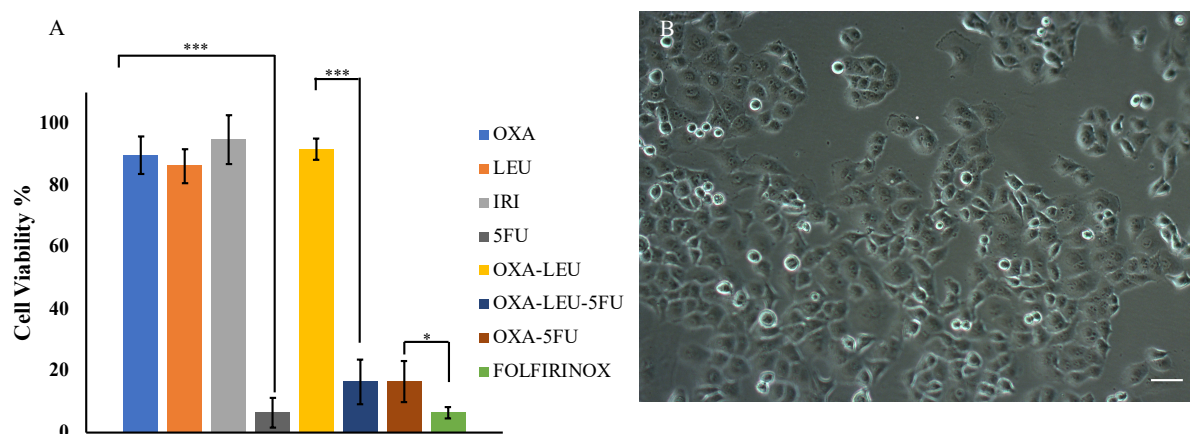


Figure 1: PANC-1 cell line viability analysis for the composition of FOLFIRINOX, (* $p < 0.05$, *** $p < 0.0005$) (A), and optical microscope images of PANC-1 cell line before drug treatments (B)

Since Hoechst 33342 can readily pass cell membranes to dye DNA of living and dead cells, it was used to determine the number of total cells. In contrast, PI was only used to detect dead cells selectively via entering compromised plasma membranes. The analysis demonstrated that cellular

disruption was the main driver for the apoptosis results (Fig. 2). For OXA-treated group, the apoptotic index was consistent with the cell viability percentage ($89.72\% \pm 6.14$) which is one of the highest values among the samples, and the apoptosis trend for the sample ($83.08\% \pm 3.71$) is statistically different from the control group ($67.14\% \pm 1.90$, $p=0.026$). It is indicated that OXA is not toxic for the scenario but leads to early apoptosis of the cells. The same results were observed in the other individual drug applications except for the 5FU samples since application time (48 h) is significantly higher than the other individual drug applications.

The apoptotic trend was found similar to the control group for the drug combinations (OXA-LEU, OXA-LEU-5FU, OXA-5FU). While, the number of cells was decreased (Fig. 2. E-G) when compared to the control group (Fig. 2. I).

The combinations, with the exception of OXA-LEU, had a negative impact on cellular attachment since they were more cytotoxic. Moreover, FOLFIRINOX combination treatment was the most toxic on PANC-1 cells compared to the other drug combinations ($6.53\% \pm 1.79\%$), but the same as the programmed cell death in the control group ($p = 0.31$).

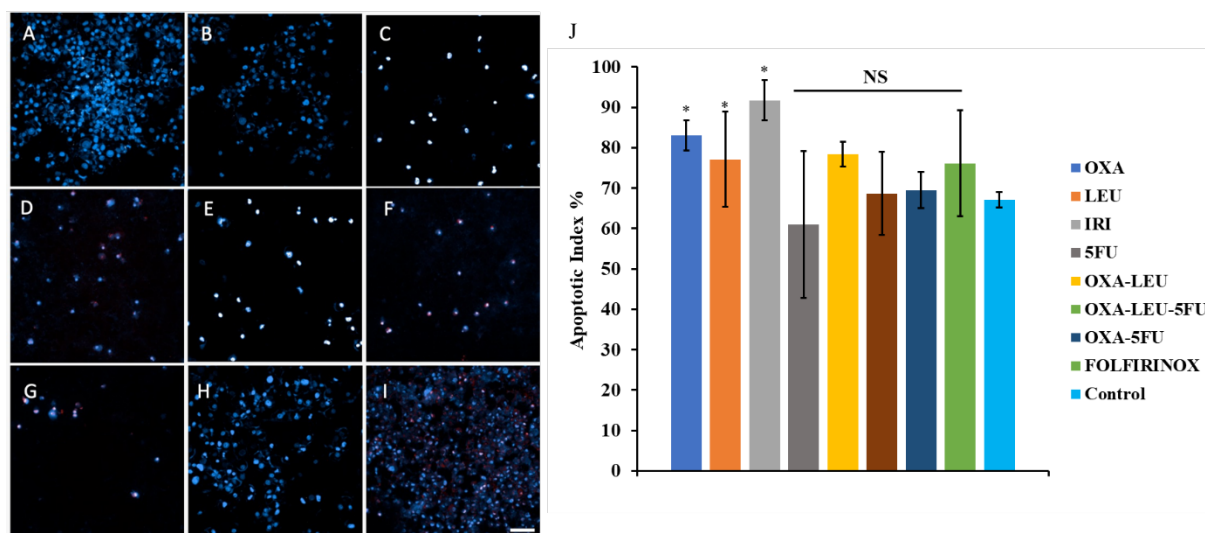


Figure 2: PI - Hoechst 33342 staining images of OXA (A), LEU (B), IRI (C), 5FU (D), OXA-LEU (E), OXA-LEU-5FU (F), OXA-5FU (G), FOLFIRINOX (H), and control (I) groups. Blue indicates Hoechst 33342 staining to determine the number of total cells, while red-pink color, sourced from PI, is selectively detected in apoptotic cells. (J) Apoptotic index values of each drug treatment (* $p < 0.05$, NS: Not Significant)

3.2. Discussion

Although, FOLFIRINOX therapy is currently in the clinical stage for pancreatic cancer, this study found that 5FU alone was comparable to FOLFIRINOX, based on the cell viability analysis. Our cell viability results indicated that 5FU treated samples have substantial cytotoxic effects compared to other 5FU-free treatments. But, the combination of all drugs caused the highest cellular death. It could be due to the synergetic interaction between the drugs, which has previously been described in the treatment of colorectal cancer [4]. However, the controllable cell death profiles of the samples

demonstrated that there is no significant difference between the 5FU-treated samples and FOLFIRINOX-treated samples. The results also support that localized 5FU treatment can be an option for nonresectable tumors.

The PANC-1 cell line was widely used as a PA model in many studies to investigate drug cytotoxicity and disease pathogenesis. In fact, Ma et al. reported that FOLFIRINOX treatment has no significant effect on PANC-1 migration, while gemcitabine exerts anti-proliferative effect on the cell line [10]. It shows that although FOLFIRINOX treatment appears to improve the survival rate of patients with PA, it still requires some tweaking. In our study, the apoptotic index results also supported the findings in the literature since there is no significant difference between the controllable death profile of FOLFIRINOX applied and PBS applied tumor cells.

FOLFIRINOX treatment in a real scenario could be used in localized therapies and with targeted carrier technologies to reduce the intense side effects of the treatment and increase efficiency on PA lesions. For instance, Byrne et al. have used the iontophoretic device model to explain the effectiveness of the local FOLFIRINOX treatment on a mouse model. The study results demonstrated iontophoretic release has promising results for reducing tumor volume compared to standard FOLFIRINOX treatment. However, cell selectivity remains an unanswered question for this study [11]. Alternatively, liposome-based solutions may help to target and encapsulate the drugs since the drugs are mainly water-soluble; however, further experiments are needed to combine the FOLFIRINOX and localized drug carriers.

Although the lipid-based systems have various drawbacks concerning stability and prolonged circulation time in the bloodstream, the systems can be adapted to the localized tumor treatment with a cancer-specific recognition layer. In this way, systemic toxicity can be controlled, and the localized chemotherapy applications may prevent adversely remodeling of the tumor microenvironment, which can cause chemoresistance. Therefore, the local response of the drugs used is important at the cellular level. At the same time, tumor microenvironment designs and personalized drug applications are the main indicators of such designs.

4. Conclusion

Our findings indicate that 5FU and FOLFIRINOX are comparably effective in reducing the PANC-1 cell viability. Moreover, OXA, LEU, and IRI significantly increase apoptotic cell death, whereas 5FU and FOLFIRINOX do not. The findings suggest that the drug combinations can be an option for unresectable nonmetastatic diseases. The local delivery application can be transformed into a locally targeted therapy. The model can also be adaptable for other metastatic tumors.

5. Ethical Declarations

Conflict of Interest Statement: The authors have no conflicts of interest to declare.

Financial Disclosure: The authors declared that this study had received partially financial support from TUBITAK, 121S050.

Author Contributions: All of the authors declare that they have all participated in the paper's design, execution, and analysis and that they have approved the final version.

References

- [1] Schima, W., Ba-Ssalamah, A., Kölblinger, C., Kulinna-Cosentini, C., Andreas Puespoek, A., Götzinger, P., *Pancreatic adenocarcinoma*, *European Radiology*, 17, 638-649, 2007.
- [2] Rhee, H., Park, M.S., *The role of imaging in current treatment strategies for pancreatic adenocarcinoma*, *Korean Journal of Radiology*, 22, 23-40, 2021.2021.
- [3] Vaccaro, V., Sperduti, I., Milella, M., *FOLFIRINOX versus gemcitabine for metastatic pancreatic cancer*, *New England Journal of Medicine*, 365, 768-769, 2011.
- [4] Zoetemelk, M., Ramzy, G.M., Rausch, M., Nowak-Sliwinska, P., *Drug-drug interactions of irinotecan, 5-fluorouracil, folinic acid and oxaliplatin and its activity in colorectal carcinoma treatment*, *Molecules*, 25, 1-20, 2020.
- [5] Kim, J.H., Lee, S., Oh, S.Y., Song, S., Lee, N., Nam, E.M., Lee, S., Hwang, I.G., Lee, H. R., Lee, K.T., Bae, S., Kim, H.J., Jang, J.S., Lim, D.H., Lee, H.W., Kang, S.Y., Kang, J.H., *Attenuated FOLFIRINOX in the salvage treatment of gemcitabine-refractory advanced pancreatic cancer: a phase II study*, *Cancer Communications*, 38, 1-8, 2018.
- [6] Auclin, E., Marthey, L., Abdallah, R., Mas, L., Francois, E., Saint, A., Cunha, A.S., Vienot, A., Lecomte, T., Hautefeuille, V., Fouchardière, C., Sarabi, M., Ksontini, F., Forestier, J., Coriat, R., Fabiano, E., Leroy, F., Williet, N., Bachet, J., Tougeron, D., Taieb, J., *Role of FOLFIRINOX and chemoradiotherapy in locally advanced and borderline resectable pancreatic adenocarcinoma: update of the AGEO cohort*, *British Journal of Cancer*, 124, 1941-1948, 2021.
- [7] Sadeghi, S., Davoodvandi, A., Pourhanifeh, M.H., Sharifi, N., Nezhad, R.A., Sahebnaasagh, R., Moghadam, S.A., Sahebkar, A., Mirzaei, H., *Anti-cancer effects of cinnamon: Insights into its apoptosis effects*. *European Journal of Medicinal Chemistry*, 178, 131-140, 2019.
- [8] Tong, H.X., Zhu, F., Biyuan, L., Tao, L., *The benefits of modified FOLFIRINOX for advanced pancreatic cancer and its induced adverse events: a systematic review and meta-analysis*, *Scientific Reports*, 8, 1-8, 2018.
- [9] Gil-Ad, I., Shtauf, B., Levkovitz, Y., Nordenberg, J., Taler, M., Korov, I, Weizman, A., *Phenothiazines induce apoptosis in a B16 mouse melanoma cell line and attenuate in vivo melanoma tumor growth*. *Oncology Reports*, 15, 107-112, 2006.
- [10] Ma, L., Wei, J., Su, G.H., Lin, J., *Dasatinib can enhance paclitaxel and gemcitabine inhibitory activity in human pancreatic cancer cells*, *Cancer Biology & Therapy*, 20, 855-865, 2019.
- [11] Byrne, J.D., Jajja, M.R.N., Schorzman, A.N., Keeler, A.W., Luft, J.C., Zamboni, W.C., DeSimone, J.M., Yeh, J.J., *Iontophoretic device delivery for the localized treatment of pancreatic ductal adenocarcinoma*, *Proceedings of the National Academy of Sciences of the United States of America*, 113, 2200-2205, 2016.



A New Schiff Base Molecule Prepared from Pyrimidine-2-thione: Synthesis, Spectral Characterization, Cytotoxic Activity, DFT, and Molecular Docking Studies

Zülbiye KÖKBUDAK^{1*}, Burçin TÜRKMENOĞLU², Senem AKKOÇ³

¹Erciyes University, Faculty of Sciences, Department of Chemistry, 38039, Kayseri, Türkiye
zulbiye@erciyes.edu.tr, ORCID: 0000-0003-2413-9595

²Erzincan Binali Yıldırım University, Faculty of Pharmacy, Department of Analytical Chemistry, 24100, Erzincan, Türkiye

burcin.turkmenoglu@erzincan.edu.tr, ORCID: 0000-0002-5770-0847

³Suleyman Demirel University, Faculty of Pharmacy, Department of Basic Pharmaceutical Sciences, 32260, Isparta, Türkiye
senemakkoc@sdu.edu.tr, ORCID: 0000-0002-1260-9425

Received: 07.11.2021

Accepted: 01.04.2022

Published: 30.06.2022

Abstract

Schiff base derivatives are some of the most widely used organic compounds for industrial purposes and they exhibit a broad range of biological activities. In this paper, a new Schiff base derivative (**2**) synthesized from the condensation reaction of 1-amino-5-benzoyl)-4-phenylpyrimidine-2(1*H*)-thione (**1**) with 2-chlorobenzaldehyde. The new compound was characterized by ¹H, ¹³C NMR, and FT-IR. The biological activity property of this compound was tested against two different cancer cell lines and a healthy human cell line. The results demonstrate that molecule **2** has antiproliferative activity. In molecular modeling studies, the interaction site was examined using the epidermal growth factor receptor (EGFR) tyrosine kinase domain. Alignment in molecular docking, surface mapping binding, amino acids, and binding energy calculated. Glide score energy was found to be -9.820 kcal/mol and it predicted that the bonding interaction is strong. Theoretical calculations were made to compare the experimental and theoretical data. These calculations were performed on the 6-31 G* basis set using the Density Functional Theory (DFT) method and Becke-3-Parameter-Lee-Yang-Parr (B3LYP).



Using this method, various parameters, such as frontier molecular orbitals, HOMO-LUMO energy levels, band gap, and chemical reactivity indices were found and interpreted.

Keywords: Cytotoxic activity; Pyrimidine-2-thione; 2-Chlorobenzaldehyde; Schiff base; Molecular docking.

Pirimidin-2-tiyondan Hazırlanan Yeni Bir Schiff Bazı Molekülü: Sentez, Spektral Karakterizasyon, Sitotoksik Aktivite, DFT ve Moleküler Doking Çalışmaları

Öz

Schiff bazı türevleri, endüstriyel amaçlar için en yaygın olarak kullanılan organik bileşiklerden bazılarıdır ve çok çeşitli biyolojik aktiviteler sergilerler. Bu makalede, 1-amino-5-benzoil)-4-fenilpirimidin-2(1*H*)-tion (**1**)'in 2-klorobenzaldehyt ile kondenzasyon reaksiyonundan yeni bir Schiff bazı türevi (**2**) sentezlendi. Yeni bileşik, ¹H, ¹³C NMR ve FT-IR ile karakterize edildi. Bu bileşiğin biyolojik aktivite özelliği, iki farklı kanser hücre hattına ve sağlıklı bir insan hücre hattına karşı test edildi. Sonuçlar, molekül **2**'nin antiproliferatif aktiviteye sahip olduğunu göstermektedir. Moleküler modelleme çalışmalarında etkileşim bölgesi, epidermal büyüme faktörü reseptörü (EGFR) tirozin kinaz alanı kullanılarak incelenmiştir. Moleküler dokingte hizalama, yüzey haritalama bağlanması, amino asitler ve bağlanma enerjisi hesaplandı. Glide skoru enerjisi -9.820 kcal/mol olarak bulunmuş ve bağlanma etkileşiminin kuvvetli olduğu tahmin edilmiştir. Deneysel ve teorik verilerin karşılaştırılması için teorik hesaplamalar yapılmıştır. Bu hesaplamalar, Yoğunluk Fonksiyonel Teorisi (DFT) yöntemi ve Becke-3-Parameter-Lee-Yang-Parr (B3LYP) kullanılarak 6–31 G* temel setinde yapıldı. Bu yöntem kullanılarak sınır moleküler orbitalleri, HOMO-LUMO enerji seviyeleri, bant aralığı ve kimyasal reaktivite indeksleri gibi çeşitli parametreler bulunmuş ve yorumlanmıştır.

Anahtar Kelimeler: Sitotoksik aktivite; Pirimidin-2-tiyon; 2-Klorobenzaldehyt; Schiff baz; Moleküler doking.

1. Introduction

Schiff bases are long-known compounds that are easy to synthesize and purify. For this reason, it attracts the attention of many researchers. Therefore, many compounds have been synthesized and studied extensively. Let us examine the work done from past to present synthesis of such compounds started in 1910. Studies in these years focused on synthesis [1-6]. As the variety and number of synthesized bases increased, researchers began to study the different properties of these substances. In 1970, a series of Schiff bases was synthesized by a group of researchers. The activities of these compounds were screened against lymphoid leukemia in

mouse and Intramuscular Walker sarcoma in rats. None of the compounds showed activity against lymphoid leukemia in mouse. However, activity against Intramuscular Walker Sarcoma was detected in rats [7]. In another study, the researchers synthesized a series of Schiff bases with salicylaldehyde from various aniline derivatives under acetic acid catalysis. *In vitro* antimicrobial activities of these compounds included various Gram-positive (*S. aureus*, *B. subtilis*, *B. cereus*), Gram-negative (*S. typhi*, *S. enterica*, *E. coli*, *P. aeruginosa*) bacteria, and fungi (*C. albicans*, *A. niger*, and *A. fumigatus*). They used antibacterial cefadroxil and antifungal fluconazole as a standard drug. They also tested the cytotoxic activity of these compounds against the human colorectal carcinoma (HCT-116) cell line. They reported that the synthesized bases showed significant activity against Gram-positive, Gram-negative bacteria, and fungi. They reported that 4-((2-bromophenyl) diazenyl)-2-((4-nitrophenylimino) methyl) phenol (SBN-13) showed more cytotoxic activity against the cell line than the standard drug, 5-fluorouracil [8].

Pyrimidines and their derivatives as important fine chemicals have been frequently found in many natural products and drugs and have exhibited a wide range of biological activities, such as anticancer [9], antiviral [10], antimicrobial [11], anti-hepatitis [12] and anti-inflammatory properties [13]. Aminopyrimidine-2-one/thione derivatives appeared to be an important starting compound in synthetic organic chemistry. In recent years, the reactions of aminopyrimidine-2-one/thione derivatives with isothiocyanate [14, 15], 1,3-dicarbonyl compounds [16], aryl chlorides [17] and transition metal complexes [18, 19] have been reported. Nowadays, theoretical, and experimental comparison of N-aminopyrimidine-2-one derivatives have become popular [15, 20, 21]. Therefore, in the present study, the starting material **1** was obtained from the reaction of furan-2,3-dione and acetophenone thiosemicarbazone according to the procedure in the literature [17] (Scheme 1). In the second step, a new Schiff base **2** was synthesized and tested as *in vitro* towards human cell lines for learning its anticancer activity (Scheme 2, Table 1).

It has been determined that the synthesis of new Schiff bases is of great importance for drug development studies [22, 23]. Recently, it has been added to theoretical (the parameters related to ground state calculations of HOMO and LUMO (electronic chemical potential and global hardness, global electrophilicity index and softness) studies in addition to experimental studies of new Schiff-based compounds [23, 24].

In cancer treatment using EGFR inhibitors, cancer cells destroyed, and the side effects of drugs reduced to a minimum. Therefore, they represent a valuable target for the design of an important class of potential anticancer agents.[25-27]. Numerous heterocyclic compounds have been reported as important tyrosine kinase (TK) inhibitors [28-31]. The cellular proliferation properties of EGFR make it heavily responsible in malignant tumors. Most of the abnormal forms

of EGFR in malignant tumors have been reported to occur in many types of cancer, such as lung cancer, colorectal cancer, breast cancer.[32-36].

Molecular docking of the synthesized compound was performed within the binding site of EGFR TK to gain insight into molecular interactions and possible modes of action. Molecular docking was performed using the EGFR protein (PDB ID: 6DUK) as a target [36]. Free energy, chemical hardness, chemical potential, dipole moment, softness, electronegativity, electrophilicity index, nucleophilicity, HOMO (highest occupied molecular orbital), LUMO (lowest unoccupied molecular orbital), and ΔE_{Gap} calculated to understand and interpret the electrostatic and chemical behavior of the synthesized compound.

2. Materials and Methods

2.1. Synthesis and characterization of a new molecule

The reagents and solvents purchased from different chemical companies and used without further purification. 1-amino-5-benzoyl-4-phenylpyrimidine-2(1*H*)-thione (**1**) and 2-chlorobenzaldehyde, used in the synthesis steps. The purities of the compounds routinely monitored using DC Alufolien Kieselgel 60 F254-Merck thin layer chromatography and Camag brand TLC lamp (254/366 nm). This study also used an electrothermal 9100 brand digital melting point device, Shimadzu Model 8400 FT-IR spectrophotometer, Bruker brand 400 MHz (for ¹H NMR) spectrophotometer, and 100 MHz (for ¹³C NMR) spectrophotometer. Starting material **1** was prepared according to literature procedures [9]. The synthesis steps given in Scheme 1.

1-(2-Chlorobenzylideneamino)-5-benzoyl)-4-phenylpyrimidin-2(1*H*)-thione, (2)

Mixtures of compound **1** (1 mmol) 0.429 g and 2-chlorobenzaldehyde, (1 mmol) 0.141 g in 30 mL of ethanol refluxed in the presence of a catalytic amount of *p*-toluene sulfonic acid as catalyst for 6 h. The solvent evaporated after this reaction time. Then, the residue treated with dry diethyl ether and filtered. This Schiff base **2** was purified with crystallization in ethyl alcohol. Yield: 72%; m.p.: 240-242 °C; color: yellow. FT-IR: 3041 (aromatic C-H), 1677 (C=O), 1619.6-1601.9 (C=N and C=C), 1266 (C=S), 765-729 cm⁻¹ (pyrim. ring). ¹H NMR (400 MHz, DMSO): δ (ppm) = 9.28 (s, 1H, N=CH), 9.01 (s, 1H, pyrim. -CH) and 8.21-7.35 (m, 14H, Ar-H). ¹³C NMR (100 MHz, DMSO): δ (ppm) = 192.02 (Ph-C=O), 190.51, 176.03, 167.00, 164.61, 146.78, 145.06, 136.62, 136.45, 136.29, 135.88, 135.58, 135.19, 135.06, 134.33, 131.45, 131.19, 131.10, 130.78, 130.49, 130.29, 130.14, 130.01, 129.70, 129.40, 129.33, 129.19, 128.89, 128.80, 128.59, 128.36, 120.53, 116.50, 112.33 (Ar-C). Elemental analysis for C₂₄H₁₆ClN₃OS (429.92 g/mol) %: Found C: 66.95, H: 3.95, N: 9.60, S: 7.30. Anal. Calc. C: 67.05, H: 3.75, N: 9.77, S: 7.46.

2.2. *In vitro* cytotoxic activity studies

Human colon cancer cell line (DLD-1) (ATCC[®] CCL-221[™]), human liver hepatocellular carcinoma cell line (HepG2) (ATCC[®] HB-8065[™]), and human normal lung cell line (WI-38) (ATCC[®] CCL-75[™]) were purchased from American Type Culture Collection (ATCC, USA).

The cytotoxic activity studies performed completely according to the literature [37, 38]. The DLD-1, HepG2, and WI-38 cells were seeded into sterile 96-well plates at a density of 5×10^3 cells/well. After 24 h, cells were exposed to the Schiff base compound for 48 h. After this period was completed, 5 mg/mL of MTT stock solution was added to each well and the plates were incubated for 3 h.

2.3. Computational details

2.3.1. DFT calculations

Theoretical calculations for the **molecule 2** were calculated using the B3LYP/6-31 G* basis cluster method [39] in the Spartan'08 package program [40]. Minimized structural parameters, HOMO, LUMO, ΔE_{gap} , chemical hardness (η) [41], chemical potential (μ) [42-44], dipole (debye), softness (σ), electronegativity (χ) [41], electrophilicity index (ω), nucleophilicity (ϵ), energy values were determined in the vacuum [45, 46].

2.3.2. Molecular docking study

The Maestro software in the Schrödinger 2021-2 Glide program [47] was used to perform all molecular docking studies [48]. Before the molecular docking study, the crystal structure of the enzyme and the preparation [49] of the ligand are included. The crystal structure (PDB ID: 6DUK) to use as the EGFR obtained from the RCSB Protein Data Bank (<https://www.rcsb.org/structure/6DUK>). Water molecules optimized by removing heteroatoms and co-factors. **Molecule 2**, used as the ligand was prepared and optimized using the LigPrep wizard [50] of the Schrödinger Software Suite and minimized using the OPLS2005 force field [48]. Grid box size was set to 20 Å Radius using the Grid Generation receptor implemented in Glide [48]. Molecular docking calculations performed using the Standard Precision (SP) mode.

2.3.3. *In silico* ADME prediction

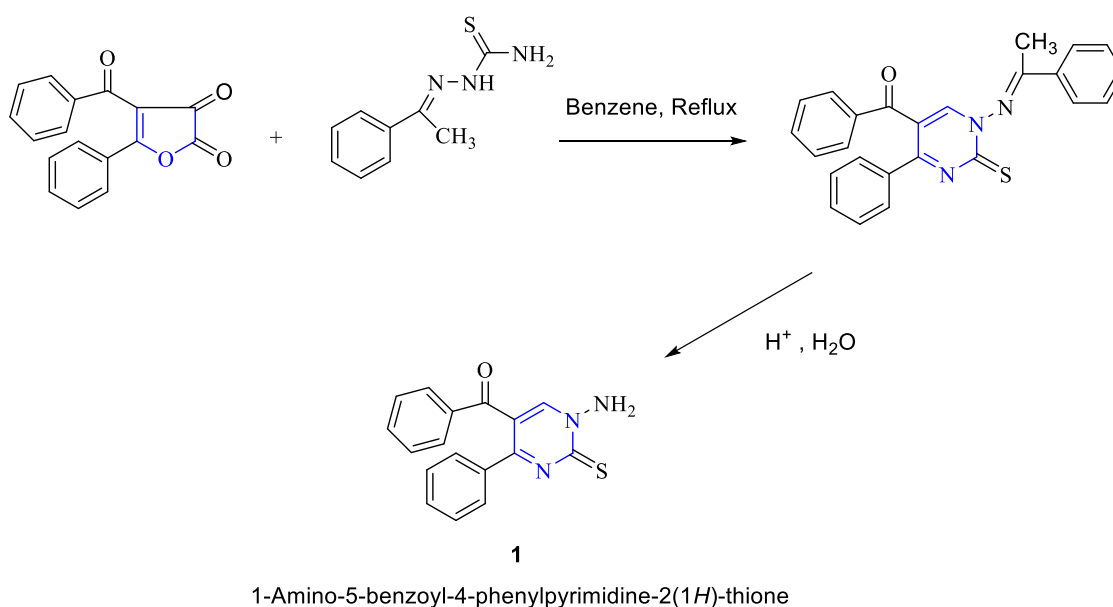
The synthesized compound Schrödinger Maestro 2021-2 QikProp [51] was used to calculate the synthesized compound's Absorption, Distribution, Metabolism, and Excretion (ADME) properties, which were selected together with the standard drug Lapatinib, for its pharmacological properties, such as drug similarity. Various predicted pharmacological parameters calculated.

3. Results and Discussion

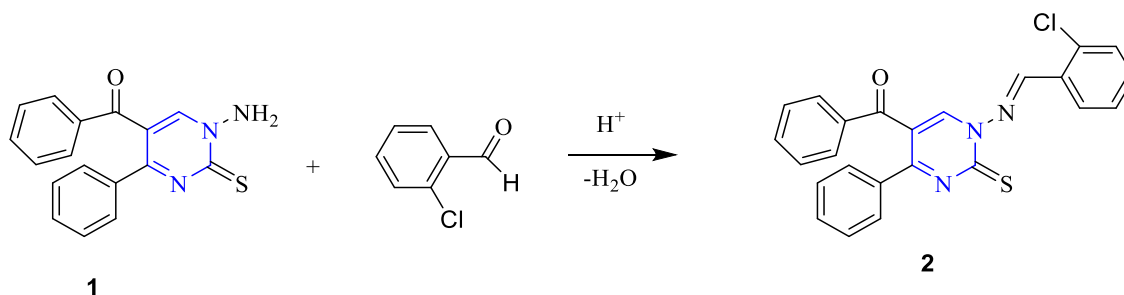
3.1. Experimental

In this study, N-aminopyrimidine-2-thione derivative **1** was used as a key starting material. Compound **1** was prepared according to the literature method by a two-step process (**Scheme 1**) [9]. Reaction of **1** with 2-chlorobenzaldehyde afforded the Schiff base derivative **2** in satisfactory yields (76%) (see experimental section) (**Scheme 2**). The moderate yield of the reaction can be explained by the chemical behavior of aminopyrimidine-2-thione **1** towards the aromatic aldehyde. The carbonyl group represents the electrophilic site in the molecule of the aromatic aldehyde, which can interact with a nucleophile [13-16] (**Scheme 2**).

Molecule **2** was obtained from the reaction of compound **1** and 2-chlorobenzaldehyde in 76% yield. In the FT IR spectrum of molecule **2**, the C=O and C=S absorption bands observed at 1677 and 1266 cm^{-1} , respectively. The signals of N=CH and pyrim. -CH protons were observed at 9.28, 9.01 ppm as singlets in the ^1H NMR spectrum of molecule **2**. The aromatic protons of **2** were observed in the 8.21-7.35 ppm region. A resonated signal recorded by ^{13}C NMR spectrum at 192.02 ppm due to the presence of the (ph-C=O) group. Aromatic carbons of **2** were determined in the 190.51-112.33 ppm region. The results of measurements of **2** are given in the experimental section. The general outline of the reaction studied shown in **Scheme 1**.



Scheme 1: Synthesis of the compound (**1**)



Scheme 2: Synthesis of the compound (2)

3.2. *In vitro* cytotoxic activity studies

The cytotoxic activity of the Schiff base was tested at 5, 10, 20, 50, 100, and 200 μM concentrations against DLD-1, HepG2, and WI-38. The results are given in Table 1.

Table 1: IC_{50} results of molecule in cell lines

Compounds	IC_{50} (μM)		
	HepG2	DLD-1	WI-38
2	91.90	169.90	40.90
Cisplatin	65.23	77.04	28.71

As seen in the results in Table 1, molecule **2** had cytotoxic activity on the HepG2 and DLD-1 cancer cell lines with IC_{50} values of 91.90 and 169.90 μM , respectively. This molecule was found to have a more toxic effect on liver cells than on colon cells. Developed molecule **2** was found to have less activity against both cell lines than cisplatin, which was used as a positive control. Furthermore, molecule **2** did not show selectivity when tested on healthy lung cells, WI-38. It inhibited the proliferation of the WI-38 cells. The dose-dependent effect of molecule **2** on cell viability is given in Fig. 1.

In our recently published work, similar eight compounds were synthesized and tested against colon (DLD-1) and breast (MDA-MB-231) cancer cell lines for 48 h [52]. Except for one, the others showed similar results to the study here. The compound, namely 1-(2,4-dichlorobenzylideneamino)-5-benzoyl-4-phenylpyrimidin-2(1H)-one, demonstrated higher toxic effect on colon cancer cells in comparison to cisplatin, with an IC_{50} value of 34.41 μM . In a conducted study by Devim and coworkers, similar pyrimidine-based compounds were developed and screened against breast and colon cancer cell lines for 48 h [53]. They found that the IC_{50} values of the molecules ranged from 118.90 μM to >200 μM in the DLD-1 cell line. In this study, we found that the efficacy of the molecule **2** was in this range against colon cancer cells with IC_{50} value of 169.90 μM .

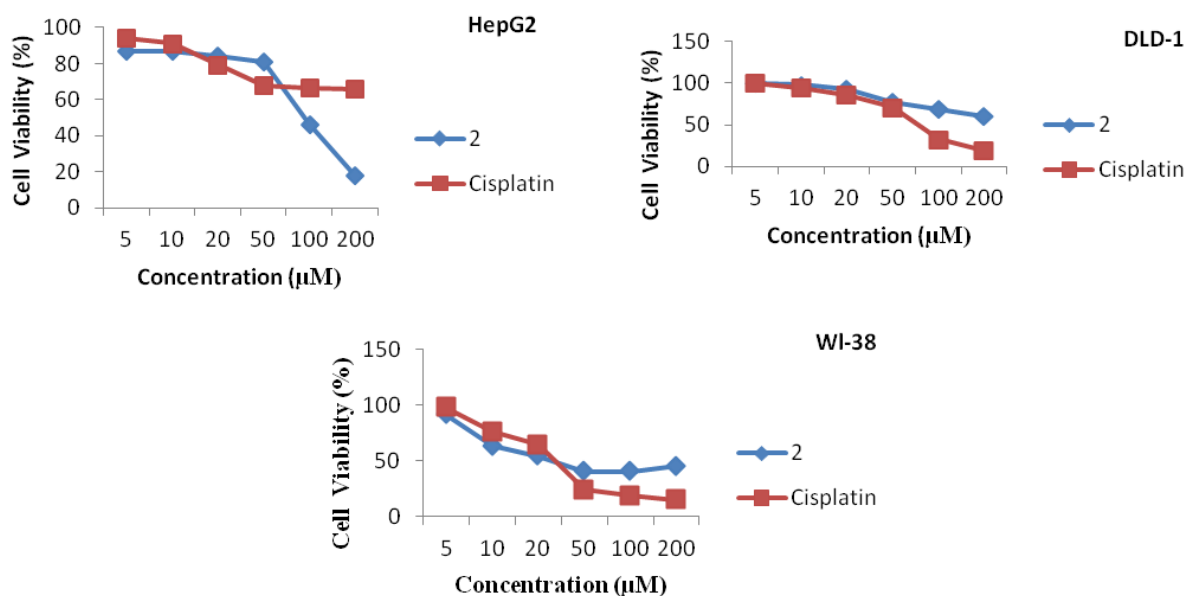


Figure 1: Dose-dependent antiproliferative effect of molecule 2 and cisplatin on HepG2, DLD-1, WI-38 cells for 48 h

As seen in Fig. 1, the viability ratio of cells changed depending on the concentrations tested of molecule 2 and cisplatin for the three cell lines. The highest cell viabilities were seen in 5, 10, and 20 µM concentrations. Viability rates decreased further in concentrations after 20 µM. At 100 µM concentration of molecule 2, cell viability ratios were calculated as 46.48%, 68.56%, and 40.49% for the HepG2, DLD-1, and WI-38 cells, respectively. At 200 µM concentration of molecule 2, the viability rates decreased further and were calculated as 17.86%, 60.13%, and 45.10% for the HepG2, DLD-1, and WI-38 cells, respectively. Some pictures taken for the HepG2 cells are given in Fig. 2.

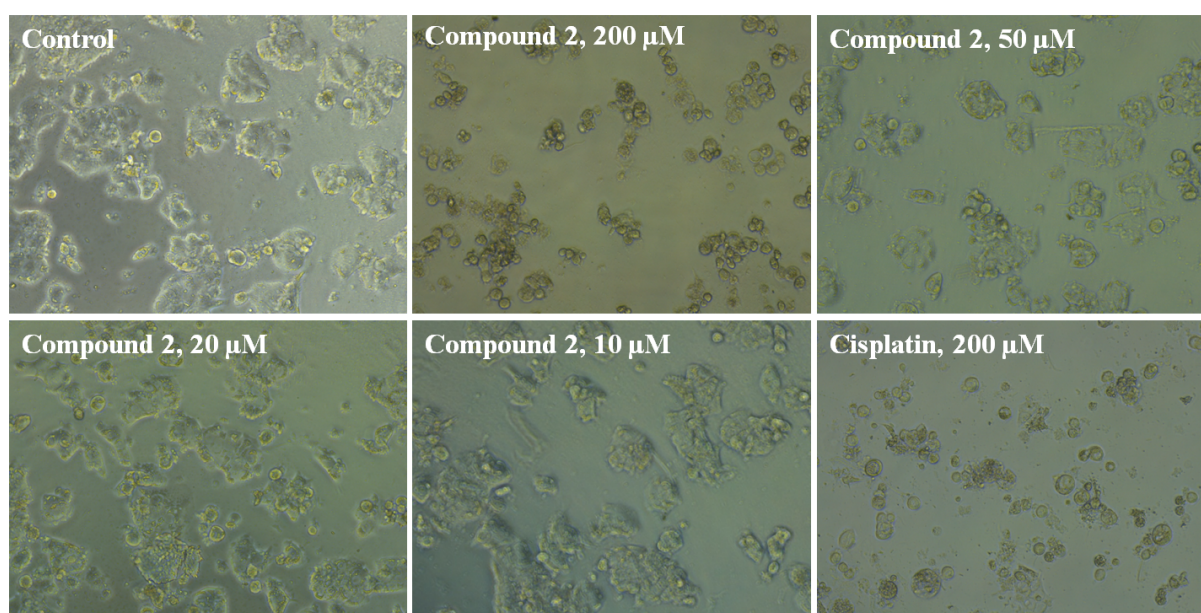


Figure 2: Leica Inverted microscopy images of HepG2 cells

It is seen that the cells in the control grow normally (Fig. 2). However, the cells affected by molecule **2** and cisplatin varied depending on the concentration. It is seen that cell viability rates are high at low concentrations, while viability rates are very low at high concentrations.

3.3. DFT calculations

Quantum chemical calculations used to explain the electronic and chemical properties of compounds. Molecule **2** B3LYP/6-31 G* optimized in the gas phase using the DFT method. The purpose of calculating the frontier molecular orbital energies leads to the identification of the chemically active sites of the molecule. The value of the energy gap plays an important role in the case of organic molecules as it relates to the specific movement of electrons from one energy state to another [54]. In Fig. 3, the energy gap value of molecule **2** is calculated as 3.1896 eV. The energy gap reveals the stability important for the structure [55] and reflects the chemical activity of the molecule [56].

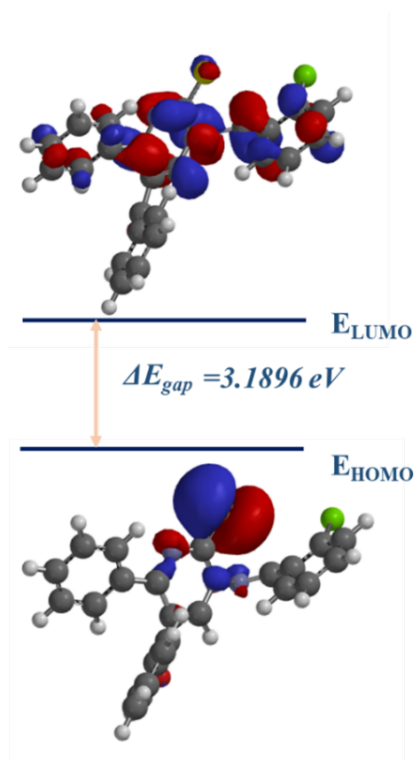


Figure 3: Frontier molecular orbitals of (HOMO-LUMO) with the energy gap of the molecule **2** in vacuum

It is responsible for the kinetic energy and chemical reactivity of the compound, where the energy gap between the HOMO-LUMO orbitals defines the chemical stability and reactivity of the molecule [57]. The energy difference between the investigated compound's HOMO-LUMO is 3.1896 eV. This value indicates that the compound is soft, unstable, and reactive. In Fig. 3, the energy difference between HOMO and LUMO is the data used to interpret the

properties of molecule **2**, such as activity and reactivity. Initially, the structure and optimal energy of studied molecule **2** were calculated using the DFT theory. Table 2 shows the calculated energies of the different frontier molecular orbitals and the molecular reactivity descriptors for ΔE_{Gap} and molecule **2**.

The electrophilicity index, ω value of the molecule, is a value of its electron ability take. A high ω value indicates good electrophilicity, while a low ω value indicates a poor electrophile [58]. The ω value found is 2.7528 eV (strong electrophiles with $\omega > 1.5$ eV [59]), confirming that it is a strong electrophile. The chemical potential, μ gives information about the reaction mechanism. Through the parameters specified in Table 2, the reaction mechanism of molecule **2** can be predicted by defining the interactions and bonds.

Table 2: The parameters of studied molecule **2**

<i>Parameters</i>	<i>Vacuum</i>
<i>Energy</i>	-5308751.29 kcal/mol
<i>E_{HOMO}</i>	-5.4781 eV
<i>E_{LUMO}</i>	-2.2885 eV
<i>ΔE_{Gap}</i>	3.1896 eV
<i>I</i>	5.4781 eV
<i>A</i>	2.2885 eV
<i>Chemical Hardness (η)</i>	2.7391
<i>Dipole (debye)</i>	6.8673
<i>Chemical Potential (μ)</i>	-3.8833
<i>Softness (σ)</i>	0.3651
<i>Electrophilicity index (ω)</i>	2.7528
<i>Electronegativity (χ)</i>	3.8833
<i>Nucleophilicity (ϵ)</i>	0.3633

3.4. Molecular docking study

The purpose of molecular docking analysis was to define parameters such as the interaction region, binding energy, Glide gscore, docking score, and glide emodel in the binding region of molecule **2**, which is the ligand in our study with the suitable protein. Figure 4 shows the binding site of the ligand candidate, which can be an EGFR TK inhibitor, after interacting with 6DUK in silico. Accordingly, amino acid residues in the binding site were determined. In Fig. 5-a, it interacts with amino acids such as Ala743, Ile744, Leu747, Glu749, Thr751, Ile853, Thr854, Asp 855, Gly857, Leu858, and Leu861 in the active binding site. In

addition, there is an H bond interaction with Lys745 amino acid and H₂O and a π - π interaction with Phe856 amino acid.

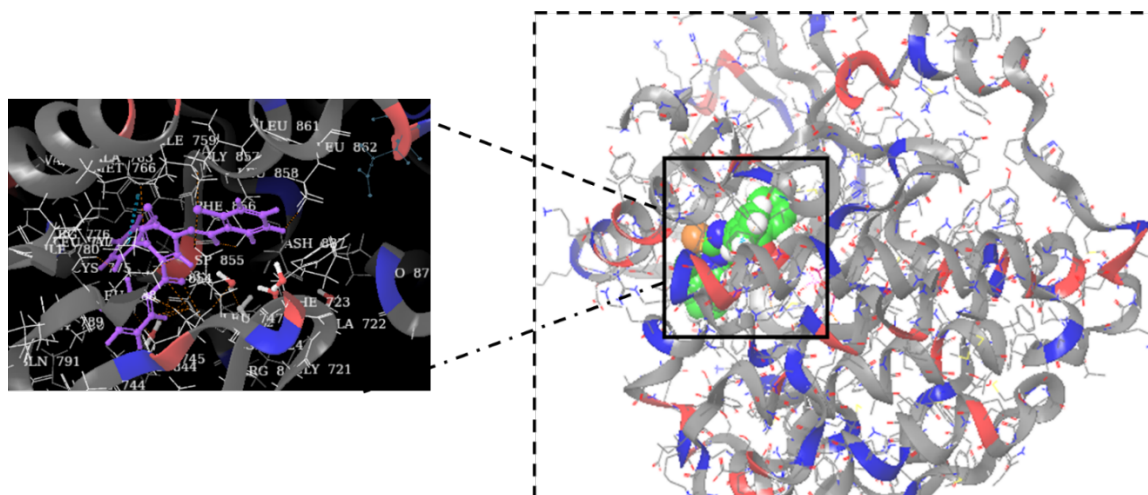


Figure 4: The binding mode of the compound used as molecule **2** with EGFR TK and the binding pattern in its active site

Descriptor parameter values in the binding region such as Glide energy, energy, Glide gscore, docking score, Glide emodel, Glide Lipo, Glide evdw, and Glide erotb given in Table 3. Here, among the conformers of molecule **2**, the conformer with the highest Glide gscore and the best active binding site was selected. With these values, the inhibitory property of ligand molecule **2** on EGFR TK can be interpreted.

Table 3: Parameter values found because of molecular docking of the molecule **2**

<i>Parameters</i>	<i>Values</i>
<i>Glide Energy</i>	-44.683 kcal/mol
<i>Energy</i>	45.229 kcal/mol
<i>Glide Gscore</i>	-9.820 kcal/mol
<i>Docking Score</i>	-9.820 kcal/mol
<i>Glide Emodel</i>	-44.854
<i>Glide Lipo</i>	-5.091
<i>Glide evdw</i>	-42.427
<i>Glide Erotb</i>	0.538

The interaction of the 6DUK protein downloaded from the protein data bank (<https://www.rcsb.org/>) with the **JBJ 1103** ligand is shown in Fig. 5-b. Figure 5-b, it was clearly observed that the ligand **JBJ 1103** entered the same pocket region as molecule **2**.

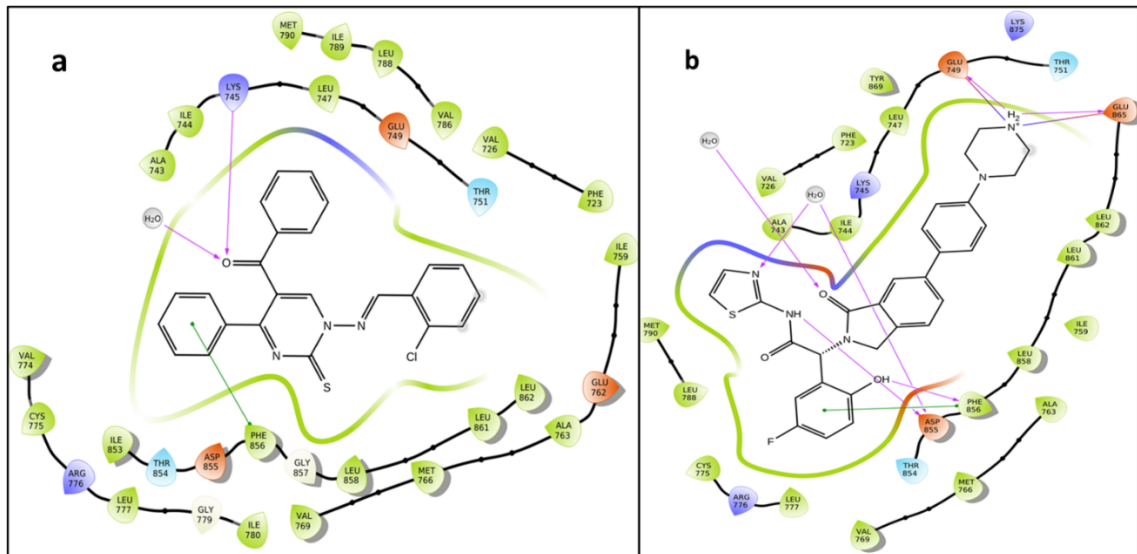


Figure 5: 2D structures of ligands docked into the PDB ID: 6DUK receptor, respectively: a) Molecule **2**, b) Interaction of JBJ 1103 ligand

In Fig. 6, the binding interaction of the ligand in the binding site shown with the binding surface and the electron charge distribution there is determined. It understood from which region the ligand enters the active site of the 6DUK protein and what type of electron density it has.

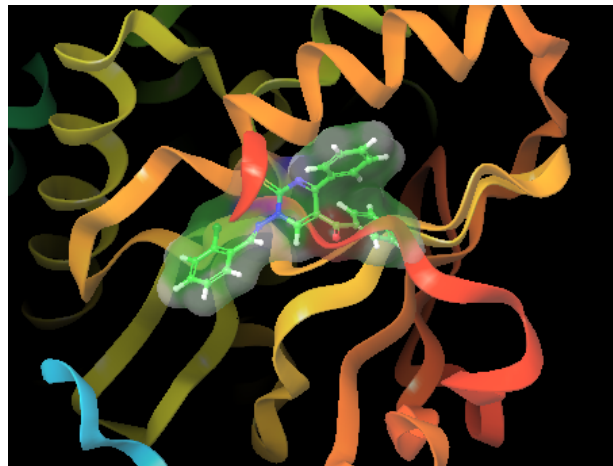


Figure 6: Docked pose of molecule **2** with EGFR (PDB ID: 6DUK)

3.5. In silico ADME prediction

To better understand the general properties of the synthesized compound, lipophilicity (octanol/water distribution coefficient, log P) calculated using the Schrödinger Maestro 2021-2 program. Theoretical estimation of the ADME properties of the compound (molecular weight, log P, number of hydrogen donors and acceptors, etc.) was performed and is shown in Table 4.

Table 4: Physicochemical properties of the synthesized compound for "drug similarity" for the standard drug lapatinib predicted by QikProp

<i>Physicochemical Properties</i>	Compound	Lapatinib
<i>MW</i>	429.923	581.060
<i>SASA</i>	714.633	859.153
<i>HBD</i>	0.000	1.000
<i>HBA</i>	8.250	6.500
<i>QPloGPoct</i>	20.069	27.196
<i>QPlogPw</i>	10.489	12.945
<i>QPlogPo/w</i>	5.249	5.842
<i>QPlogS</i>	-5.951	6.358
<i>#rotor</i>	10	6
<i>QPlogBB</i>	-0.088	-0.069
<i>QPPMDCK</i>	7666.211	3887.880
<i>QPlogKhsa</i>	0.367	0.189
<i>PSA</i>	55.651	42.261
<i>QPlogKp</i>	-0.210	-2.640
<i>Rule of 5</i>	1	2
<i>Rule of 3</i>	1	1

4. Conclusion

In this study, new benzyldeneamino-pyrimidin-2(1H)-thione derivative, including pyrimidine core, was synthesized from the condensation reaction of aminopyrimidin-2(1H)-thione derivative **1** with 2-chlorobenzaldehyde (Scheme 2). The structure of this molecule **2** was determined from the FT-IR, ¹H, ¹³C-NMR spectroscopic data, and elemental analysis. Furthermore, the newly synthesized compound was tested against three different cell lines, and it was found to have a toxic effect on cancer cells. In addition to the synthesis and cytotoxicity studies of molecule **2**, theoretical calculations, such as DFT, molecular docking, and ADME were made. Atomic charges of molecule **2** studied by the DFT method and values, such as HOMO-LUMO energies, ionization potential, electron affinity, electronegativity, electrophilicity index, hardness, and chemical potential calculated.

The molecular docking studies revealed that molecule **2** interacts strongly with the EGFR TK protein, with a Glide gscore and docking score of -9.820 kcal/mol. The docking score of -9.820 kcal/mol shows that it interacts well with Lys745 and H₂O through hydrogen bonding and that the π - π interaction with Phe856 is good. In addition to the molecular docking studies, ADME studies were compared with the data obtained by comparing ligand molecule **2** with the commercially available Lapatinib drug.

Acknowledgements

Burçin Türkmenoğlu would like to thank Erzincan Binali Yıldırım University, Basic Sciences Application and Research Center (EBYU-EUTAM) for the Schrödinger Maestro 2021-2 program. Senem Akkoç would like to thank Suleyman Demirel University Research Fund (TSG-2021-8458) for financial support.

References

- [1] Bogert, M.T., Beal, G.D., *Researches on quinazolines (twenty-ninth paper). A further study of the stilbazoles, hydrazones and schiff bases of the 4-quinazolone group*, Journal of the American Chemical Society, 34, 516-524, 1912.
- [2] Sumerford, W.T., Hartung, W.H., Jenkins, G.L., *Some Schiff Bases with p-Aminothymol*, Journal of the American Chemical Society, 62, 2082-2083, 1940.
- [3] McIntire, F.C., *Some Schiff bases of free amino acids*, Journal of the American Chemical Society, 69, 1377-1380, 1947.
- [4] Stephens, F.F., *Heterocyclic compounds from Schiff's bases*, Nature, 164, 243, 1949.
- [5] Holly, F.W., Cope, A.C., *Condensation products of aldehydes and ketones with o-aminobenzyl alcohol and o-hydroxybenzylamine*, Journal of the American Chemical Society, 66, 1875-1879, 1944.
- [6] Surrey, A.R., *The preparation of 4-thiazolidones by the reaction of thioglycolic acid with Schiff bases*, Journal of the American Chemical Society, 69, 2911-2912, 1947.
- [7] Hodnett, E.M., Dunn, W.J., *Structure-antitumor activity correlation of some Schiff bases*, Journal of Medicinal Chemistry, 13, 768-770, 1970.
- [8] Kaur, H., Lim, S.M., Ramasamy, K., Vasudevan, M., Shah, S.A.A., Narasimhan, B., *Diazenyl schiff bases: Synthesis, spectral analysis, antimicrobial studies and cytotoxic activity on human colorectal carcinoma cell line (HCT-116)*, Arabian Journal of Chemistry, 13, 377-392, 2020.
- [9] Ma, L.Y., Pang, L.P., Wang, B., Zhang, M., Hu, B., Xue, D.Q., *Design and synthesis of novel 1,2,3-triazole-pyrimidine hybrids as potential anticancer agents*, European Journal of Medicinal Chemistry, 86, 368-380, 2014.
- [10] Rai, D., Chen W Fau - Tian, Y., Tian Y Fau - Chen, X., Chen X Fau - Zhan, P., Zhan P Fau - De Clercq, E., De Clercq E Fau - Pannecouque, C., *Design, synthesis and biological evaluation of 3-benzyloxy-linked pyrimidinylphenylamine derivatives as potent HIV-1 NNRTIs*, Bioorganic & Medicinal Chemistry, 21, 7398-7405, 2013.
- [11] Ramiz, M.M.M., El-Sayed, W.A., El-Tantawy, A.I., Abdel-Rahman, A.A.H., *Antimicrobial Activity of New 4,6-Disubstituted Pyrimidine, Pyrazoline, and Pyran Derivatives*, Archives of Pharmacal Research, 33, 647-654, 2010.
- [12] Hwang, J.Y., Windisch, M.P., Jo, S., Kim, K., Kong, S., Kim, H.C., *Discovery and characterization of a novel 7-aminopyrazolo[1,5-a]pyrimidine analog as a potent hepatitis C virus inhibitor*, Bioorganic & Medicinal Chemistry Letters, 22, 7297-7301, 2012.
- [13] Gondkar, A.S., Deshmukh, V.K., Chaudhari, S.R., *Synthesis, characterization and in-vitro anti-inflammatory activity of some substituted 1,2,3,4 tetrahydropyrimidine derivatives*, Drug Invention Today, 5, 175-181, 2013.

- [14] Onal, Z., Daylan, A.C., *Cyclization reactions of 1-pyrimidinyl-3-arylthiourea derivatives with oxalyl dichloride* Asian Journal of Chemistry, 19, 1455-1460, 2007.
- [15] Saracoglu, M., Kokbudak, Z., Yalcin, E., Kandemirli, F., *Synthesis and Dft quantum chemical calculations of 2-oxopyrimidin-1(2h)-yl-urea and thiorea derivatives*, Journal of The Chemical Society of Pakistan, 41, 841-858, 2019.
- [16] Onal, Z., Ceran, H., Sahin, E., *Synthesis of novel dihydropyrazolo[1,5-C]pyrimidin-7(3h)-one/-thione derivatives*, Heterocyclic Communications, 14, 245-250, 2008.
- [17] Cimen, Z., Akkoc, S., Kokbudak, Z. *Reactions of aminopyrimidine derivatives with chloroacetyl and isophthaloyl chlorides*, Heteroatom Chemistry, 29, 2018.
- [18] Aslan, H.G., Akkoc, S., Kokbudak, Z., Aydin, L., *Synthesis, characterization, and antimicrobial and catalytic activity of a new Schiff base and its metal(II) complexes*, Journal of the Iranian Chemical Society, 14, 2263-2273, 2017.
- [19] Aslan, H.G., Akkoc, S., Kokbudak, Z., *Anticancer activities of various new metal complexes prepared from a Schiff base on A549 cell line*, Inorganic Chemistry Communications, 111, 2020
- [20] Kokbudak, Z., Saracoglu, M., Akkoc, S., Cimen, Z., Yilmazer, M.I., Kandemirli, F., *Synthesis, cytotoxic activity and quantum chemical calculations of new 7-thioxopyrazolo[1,5-f]pyrimidin-2-one derivatives*. Journal of Molecular Structure, 1202, 2020.
- [21] Kokbudak, Z., Aslan, H.G., Akkoc, S., *New Schiff Bases Based on 1-Aminopyrimidin-2-(1h)-One: Design, Synthesis, Characterization and Theoretical Calculations*, Heterocycles, 100, 440-449, 2020.
- [22] Elmaci, G., Duyar, H., Aydiner, B., Seferoglu, N., Naziri, M.A., Sahin, E., *The syntheses, molecular structure analyses and DFT studies on new benzil monohydrazone based Schiff bases*, Journal of Molecular Structure, 1162, 37-44, 2018.
- [23] Elmaci, G., Duyar, H., Aydiner, B., Yahaya, I., Seferoglu, N., Sahin, E., *Novel benzildihydrazone based Schiff bases: Syntheses, characterization, thermal properties, theoretical DFT calculations and biological activity studies*, Journal of Molecular Structure, 1184, 271-280, 2019.
- [24] Elmacı, G., Aktan, E., Seferoğlu, N., Hökelek, T., Seferoğlu, Z., *Synthesis, molecular structure and computational study of (Z)-2-((E)-4-nitrobenzylidene) hydrazone)-1, 2-diphenylethan-1-one*, Journal of Molecular Structure, 1099, 83-91, 2015.
- [25] Antonello, A., Tarozzi, A., Morroni, F., Cavalli, A., Rosini, M., Hrelia, P., *Multitarget-directed drug design strategy: A novel molecule designed to block epidermal growth factor receptor (EGFR) and to exert proapoptotic effects*, Journal of Medicinal Chemistry, 49, 6642-6645, 2006.
- [26] Pawar, V.G., Sos, M.L., Rode, H.B., Rabiller, M., Heynck, S., van Otterlo, W.A.L., *Synthesis and Biological Evaluation of 4-Anilinoquinolines as Potent Inhibitors of Epidermal Growth Factor Receptor*, Journal of Medicinal Chemistry, 53, 2892-2901, 2010.
- [27] Yu, H.Q., Li, Y.X., Ge, Y., Song, Z.D., Wang, C.Y., Huang, S.S., *Novel 4-anilinoquinazoline derivatives featuring an 1-adamantyl moiety as potent EGFR inhibitors with enhanced activity against NSCLC cell lines*, European Journal of Medicinal Chemistry, 110, 195-203, 2016.
- [28] Elbastawesy, M.A.I., Aly, A.A., Ramadan, M., Elshaier, Y.A.M.M., Youssif, B.G.M., Brown, A.B., *Novel Pyrazoloquinolin-2-ones: Design, synthesis, docking studies, and biological evaluation as antiproliferative EGFR-TK inhibitors*, Bioorganic Chemistry, 90, 103045, 2019.

- [29] Zhang, Y.L., Chen, L., Li, X.B., Gao, L., Hao, Y.X., Li, B.L., *Novel 4-arylaminoquinazolines bearing N,N-diethyl(aminoethyl)amino moiety with antitumour activity as EGFR(wt)-TK inhibitor*, *Journal of Enzyme Inhibition and Medicinal Chemistry*, 34, 1668-1677, 2019.
- [30] Zhang, Y.L., Chen, L., Xu, H.J., Li, X.B., Zhao, L.J., Wang, W., *6,7-Dimorpholinoalkoxy quinazoline derivatives as potent EGFR inhibitors with enhanced antiproliferative activities against tumor cells*, *European Journal of Medicinal Chemistry*, 147, 77-89, 2018.
- [31] Abbas, H.A.S., Abd El Karim, S.S., *Design, synthesis and anticervical cancer activity of new benzofuran-pyrazol-hydrazono- thiazolidin-4-one hybrids as potential EGFR inhibitors and apoptosis inducing agents*, *Bioorganic Chemistry*, 89, 103035, 2019.
- [32] Guardiola, S., Varese, M., Sanchez-Navarro, M., Giralt, E. *A Third Shot at EGFR: New Opportunities in Cancer Therapy*. *Trends Pharmacol Sci*. 2019, 40, 941-55.
- [33] Leonetti, A., Assaraf, Y.G., Veltsista, P.D., El Hassouni, B., Tiseo, M., Giovannetti, E., *MicroRNAs as a drug resistance mechanism to targeted therapies in EGFR-mutated NSCLC: Current implications and future directions*, *Drug Resistance Update*, 42, 1-11, 2019.
- [34] Rolfo, C., Giovannetti, E., Hong, D.S., Bivona, T., Raez, L.E., Bronte, G., *Novel therapeutic strategies for patients with NSCLC that do not respond to treatment with EGFR inhibitors*, *Cancer Treatment Reviews*, 40, 990-1004, 2014.
- [35] Piotrowska, Z., Sequist, L.V., *Treatment of EGFR-Mutant Lung Cancers After Progression in Patients Receiving First-Line EGFR Tyrosine Kinase Inhibitors A Review*, *Jama Oncology*, 2, 948-954, 2016.
- [36] Recondo, G., Facchinetti, F., Olaussen, K.A., Besse, B., Friboulet, L., *Making the first move in EGFR-driven or ALK-driven NSCLC: first-generation or next-generation TKI*. *Nature Reviews Clinical Oncology*, 15, 694-708, 2018.
- [37] Akkoç, S., *Derivatives of 1-(2-(Piperidin-1-yl)ethyl)-1H-benzof[d]imidazole: Synthesis, Characterization, Determining of Electronic Properties and Cytotoxicity Studies*, *ChemistrySelect*, 4, 4938-43, 2019.
- [38] Akkoç, S., *Antiproliferative activities of 2-hydroxyethyl substituted benzimidazolium salts and their palladium complexes against human cancerous cell lines*, *Synthetic Communications*, 49, 2903-2914, 2019.
- [39] Bozbey, I., Uslu, H., Türkmenoğlu, B., Özdemir, Z., Karakurt, A., Levent, S., *Conventional and microwave prompted synthesis of aryl (alkyl) azole oximes, 1H-NMR spectroscopic determination of E/Z isomer ratio and HOMO-LUMO analysis*, *Journal of Molecular Structure*, 1251, 132077, 2022.
- [40] Wavefunction, I. Spartan'08. Irvine, CA. 1991, 2009.
- [41] Lukovits, I., Bakó, I., Shaban, A., Kálmán, E. *Polynomial model of the inhibition mechanism of thiourea derivatives*, *Electrochimica Acta*, 43, 131-6, 1998.
- [42] Parr, R.G., Pearson, R.G. *Absolute hardness: companion parameter to absolute electronegativity*, *Journal of the American Chemical Society*, 105, 7512-6, 1983.
- [43] Parr, R.G., Donnelly, R.A., Levy, M., Palke, W.E. *Electronegativity: the density functional viewpoint*, *The Journal of Chemical Physics*, 68, 3801-7, 1978.
- [44] Parr, R.G., Chattaraj, P.K. *Principle of maximum hardness*. *Journal of the American Chemical Society*, 113, 1854-5, 1991.

- [45] Parr, R.G., Szentpály, L.v., Liu, S. *Electrophilicity index*, Journal of the American Chemical Society, 121, 1922-1924, 1999.
- [46] Oladipo, S.D., Yusuf, T.L., Zamisa, S.J., Shapi, M., Ajayi, T.J. *Synthesis, crystal structure, Hirshfeld surface analysis and DFT studies of N-(2,6-diisopropylphenyl)-1-(4-methoxyphenyl) methanimine*, Journal of Molecular Structure, 1241, 13620, 2021.
- [47] Schrödinger Release 2021-2: Glide, S., LLC, New York, NY, 2021.
- [48] Anil, D.A., Aydin, B.O., Demir, Y., Turkmenoglu, B., *Design, Synthesis, Biological Evaluation and Molecular Docking Studies of Novel 1H-1, 2, 3-Triazole Derivatives as Potent Inhibitors of Carbonic Anhydrase, Acetylcholinesterase and Aldose Reductase*, Journal of Molecular Structure, 132613, 2022.
- [49] Schrödinger Release 2021-2: Protein Preparation Wizard; Epik, S., LLC, New York, NY, 2021; Impact, Schrödinger, LLC, New York, NY; Prime, Schrödinger, LLC, New York, NY, 2021.
- [50] Schrödinger Release 2021-2: LigPrep, S., LLC, New York, NY, 2021.
- [51] Schrödinger Release 2021-2: Qikprop, L., New York, NY, 2021.
- [52] Kökbudak, Z., Akkoç, S., Karataş, H., Tüzün, B., Aslan, G., *In Silico and In Vitro Antiproliferative Activity Assessment of New Schiff Bases*, Chemistryselect, 7, e202103679, 2022.
- [53] Devim, M., Akkoç, S., Zeyrek, C.T., Aslan, H.G., Kökbudak, Z., *Design, synthesis, in vitro antiproliferative activity properties, quantum chemical and molecular docking studies of novel Schiff bases incorporating pyrimidine nucleus*, Journal of Molecular Structure, 132421, 2022.
- [54] Vagish, C.B., Kumara, K., Vivek, H.K., Bharath, S., Lokanath, N.K., Kumar, K.A. *Coumarin-triazole hybrids: Design, microwave-assisted synthesis, crystal and molecular structure, theoretical and computational studies and screening for their anticancer potentials against PC-3 and DU-145*, Journal of Molecular Structure, 1230, 2021.
- [55] Lewis, D.F.V., Ioannides, C., Parke, D.V., *Interaction of a Series of Nitriles with the Alcohol-Inducible Isoform of P450 - Computer-Analysis of Structure-Activity-Relationships*, Xenobiotica, 24, 401-408, 1994.
- [56] Sheela, N.R., Muthu, S., Sampathkrishnan, S., *Molecular orbital studies (hardness, chemical potential and electrophilicity), vibrational investigation and theoretical NBO analysis of 4-(1H-1,2,4-triazol-1-yl methylene) dibenzonitrile based on abinitio and DFT methods*, Spectrochimica Acta Part A: Molecular and Biomolecular Spectroscopy, 20, 237-251, 2014.
- [57] Sallam, H.H., Mohammed, Y.H.I., Al-Ostoot, F.H., M. A, S., Khanum, S.A., *Synthesis, crystal structure characterization, DFT calculations, Hirshfeld surface analysis and 3D energy frameworks of triazole pyridazine derivatives: Theoretical and experimental studies*, Journal of Molecular Structure, 1246, 131242, 2021.
- [58] Benbouguerra, K., Chafai, N., Chafaa, S., Touahria, Y.I., Tlidjane, H., *New alpha-Hydrazinophosphonic acid: Synthesis, characterization, DFT study and in silico prediction of its potential inhibition of SARS-CoV-2 main protease*, Journal of Molecular Structure, 1239, 130480, 2021.
- [59] Domingo, L.R., Aurell, M.J., Perez, P., Contreras, R., *Quantitative characterization of the global electrophilicity power of common diene/dienophile pairs in Diels-Alder reactions*, Tetrahedron, 58, 4417-4423, 2002.



The Anatomical Surveys on the Two *Salvia* L. Species (Sect. *Hymenosphace*, Sect. *Hemisphace*) Spreading in Mardin (Turkey)

Murat KILIÇ^{1,*}, Fatma MUNGAN KILIÇ¹

¹ Department of Crops and Animal Production, Mardin Artuklu University, 47200 Mardin, Artuklu, Türkiye

muratkilic04@gmail.com, ORCID: 0000-0002-6408-9660

fatmamungankilic@artuklu.edu.tr, ORCID: 0000-0001-6858-3458

Received: 07.11.2021

Accepted: 01.04.2022

Published: 30.06.2022

Abstract

In this study, we investigated two *Salvia* species (sect. *Hymenosphace*, sect. *Hemisphace*) distributed in the province of Mardin in the Southeastern Anatolia Region in terms of anatomy. These species are *S. multicaulis* Vahl. (sect. *Hymenosphace*) and *S. russellii* Benth. (sect. *Hemisphace*). For anatomical investigation, cross-sections taken from roots, stems, leaves, and petioles of the taxa were examined under a light microscope. In anatomical examinations, it was observed that root, stem, leaf, and petiole structures of the taxa were similar but shapes and measurements as well as the the number of tissue layers and pith rows were different. In addition, it was observed that the surface of the *S. multicaulis* species was covered by multicellular and compound hairs. In conclusion, anatomical characters provide information of taxonomic importance, and especially hairiness is important in species differentiation.

Keywords: Anatomy; *Salvia*; *Hymenosphace*; *Hemisphace*; Mardin; Turkey.



Mardin'de (Türkiye) Yayılış Gösteren İki *Salvia* L. Türü (Seksiyon *Hymenosphace*, Seksiyon *Hemisphace*) Üzerine Anatomik Araştırmalar

Öz

Bu çalışma Güneydoğu Anadolu Bölgesi'nde Mardin ilinde yayılış gösteren iki *Salvia* türü (Seksiyon *Hymenosphace*, Seksiyon *Hemisphace*) anatomik açıdan araştırılmıştır. Bu türler *S. multicaulis* Benth. (Seksiyon *Hymenosphace*) ve *S. russellii* Vahl. (Seksiyon *Hemisphace*)'dir. Anatomik inceleme için taksonların kök, gövde, yaprak ve petiollerinden alınan kesitler ışık mikroskopunda incelendi. Anatomik incelemelerde taksonların kök, gövde, yaprak ve petiyol yapılarının benzer olduğu ancak şekil ve ölçülerinin bunlarla beraber doku tabakası ve öz sıra sayılarının da farklı olduğu görüldü. Ayrıca anatomik analizlerde *S. multicaulis* türünün yüzeyinin çok hücreli ve bileşik tüylerle örtülü olduğu gözlemlendi. Sonuç olarak anatomik karakterler taksonomik öneme sahip bilgiler sağlar ve türlerin farklılaşmasında özellikle tüylülük önemlidir.

Anahtar Kelimeler: Anatomi; *Salvia*; *Hymenosphace*; *Hemisphace*; Mardin; Türkiye.

1. Introduction

The Lamiaceae family is one of the largest families in the world. Although there is no fossil record of the family, its origin is thought to date back to 70-90 million years ago [1]. Family members are more common in the Mediterranean phytogeographic region. Due to the high rate of endemism, it is among the first three large families in our country [1]. There are 245 genera and 7,886 species of the Lamiaceae family in the world [2]. In Turkey, Lamiaceae includes 46 genera and more than 870 taxa [3].

The genus *Salvia* L., which is one of the richest members of the Lamiaceae family, is represented by about 1.037 taxa in the world [2]. In Turkey, the genus *Salvia* has about 100 defined taxa in Flora of Turkey which of 50% were recorded as endemic [3-5].

Salvia is a very important genus of the Lamiaceae family as it has many medicinal and aromatic taxa that are widely used, collected from their natural habitats, and utilised locally. The genus *Salvia* is popularly known as sage. Many types of sage are used in the treatment of various diseases [6]. In addition, *Salvia* species have economic importance as they are used as therapeutic, herbal tea, food and decorative purposes and can be utilised in cosmetics, perfumery, and pharmaceutical industries [7,8].

The *Hymenosphace* section, which is mostly grown in Turkey in terms of the number of taxa, has herbaceous and woody semi-shrub forms. On the other hand, the *Hemisphace* section has herbaceous and woody rootstock forms, and is represented by only three species in Turkey [9].

This study aims to investigate the anatomical features of *Salvia multicaulis* and *S. russellii* in detail and also discuss the anatomical importance of the findings with former studies relevant to the section.

2. Materials and Methods

The study area is surrounded by the Tigris basin in Southeastern Anatolia, Batman and Şırnak in the east, Şanlıurfa in the west, north of Diyarbakır and Syria in the south [10] (Fig. 1). Mardin belongs to the Iran-Turanian Phytogeographical Region and includes the Mesopotamian lowland. The region has a Mediterranean, continental, and desert climate and is rich in plant diversity.

In this study, the anatomical features of *S. multicaulis* and *S. russellii* species distributed in Mardin province were investigated. Both species were collected from different populations of Mardin during the flowering and seed formation periods between April 2018 and August 2019. The taxonomic description of the plant was prepared according to Davis [4] and Güner et al. [3]. Some of the plant samples collected from different localities were fixed in alcohol and dried. Samples are stored in Mardin Artuklu University Kızıltepe Animal and Plant Production Department. The places and regions where the plants were collected are given in Table 1.

Root, stem, leaf and petiole samples of species collected from different localities for anatomical examinations were conserved in 70% alcohol. All cross-sections were made manually by using a razor blade. Cross-sections of root, stem, leaf and petiole were stained with safranin and fast-green solutions [11]. Anatomical features of root, stem, leaf and petiole were studied by light microscopy (ISOLAB). The micro-anatomic measurements of tissue and cells of root, stem, leaf and petiole are given in Table 2-5.

3. Results

Transverse sections taken from the root, stem, leaf and petiole of the plants were analysed in detail and the obtained results are outlined below. The taxa are given in alphabetical order.

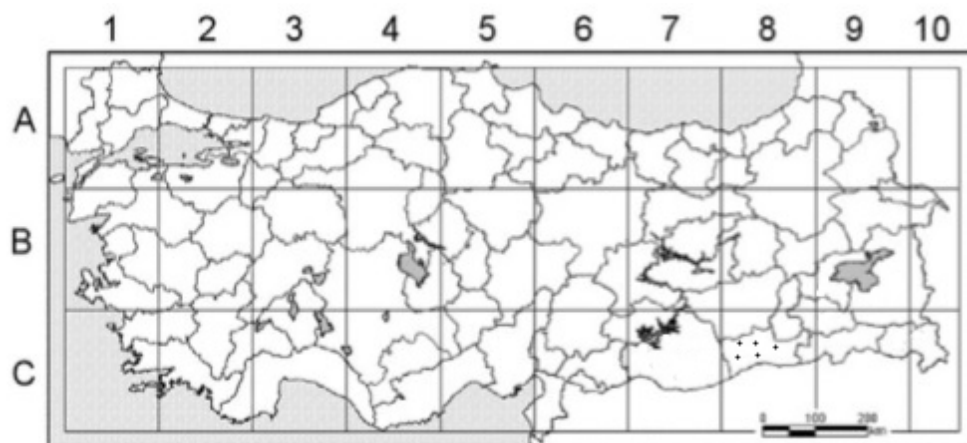


Figure 1: Distribution map of *S. multicaulis* and *S. russellii* taxa (.)

3.1. Root anatomical characteristics

Salvia multicaulis: Peridermis was thick layer, crushed and fragmented at the outermost of the root. Beneath the periderm is multilayered parenchymal cells, which are 6.11-21.97 μ wide. Under the parenchyma, there are several layers of sclerenchyma. There is multi-layer of phloem under sclerenchyma groups. Cambium was unclear. Tracheae conspicuous in the xylem are numerous, and their diameters vary between 19.93-44.35 μ . In the xylem, besides the large tracheas, tracheids and xylem parenchyma have lignified walls. Pith rays consist of 2-4 rowed narrow cells. As the xylem occupies the pith, it is narrow (Fig. 2, Table 2).

Salvia russellii: Peridermis was thick layer, crushed and fragmented at the outermost of the root. Beneath the periderm is multilayered parenchymal cells, which are 9.46-26.31 μ wide. Under the parenchyma, there are several layers of sclerenchyma. There is multi-layer of phloem under sclerenchyma groups. Cambium was unclear. Tracheae conspicuous in the xylem are numerous, and their diameters vary between 16.89-67.12 μ . In the xylem, besides the large tracheas, tracheids and xylem parenchyma have lignified walls. Pith rays consist of 1-2 rowed narrow cells. As the xylem occupies the pith, it is very narrow (Fig. 2, Table 2).

Table 1: *S. multicaulis* and *S. russellii* taxa that were used for anatomical studies and their collected localities.

Species	Locality (Turkey, C8, Mardin)	Date	Coordinates	Altitude	Habitat	Collector's number
<i>S. multicaulis</i>	Artuklu, Yalım Village	27.04.2019	37°19'39"N-40°44'28"E	886 m	rocky, valley edge, <i>Crataegus</i> communities	M. Kılıç, F. Mungankılıç 194, 200, 209, 211
	Artuklu, Eskikale Village, Bakırkırı	27.04.2019	37°19'14"N-40°45'36"E,	1.004 m	roadsides	
	Artuklu, Hamzabey Village, Yalım to Hamzabey road, spring water-cemetery	28.04.2019	37°21'49"N-40°44'10"E	895 m	roadside, slopes	
	Artuklu, Cevizpınar Village, Nehruk Street	04.05.2019	37°21'50"N-40°45'21"E	1087 m	stony slope	
	Artuklu, Hamzabey Village, Yalım to Hamzabey road, Old hippodrome location	18.05.2019	37°22'14"N-40°43'55"E	970 m	roadside, degraded steppe	
	Kızıltepe, Beşdeğirmen village	24.02.2019	37°16'56"N-40°32'56"E	770 m	rocky slopes	
	Kızıltepe, between Uluköy-Ayaz villages	25.05.2019	37°18'09"N-40°37'23"E	737 m	roadside rocky slopes	
	Artuklu, Zınnar	04.05.2020	37°24'41"N-40°41'13"E	1076 m	highland road, roadside slopes, <i>Quercus brantii</i> lower locality	
	Artuklu, Bakırkırı	11.05.2020	37°19'22"N-40°46'04"E	979 m	roadside slopes, <i>Quercus brantii</i> Lower locality	
	Mazıdağı, Derik-Mazıdağı road, Enginköy erosion control area site	16.06.2019	37°28'00"N-40°26'42"E	1.001 m	,barren slopes	
	Mazıdağı, Derik-Mazıdağı road, Enginköy erosion control area upper level, Radio television station lower locality	16.06.2019	37°27'41"N-40°26'55"E	1.089 m	between menengiç and grape gardens	
	Midyat, Eskimidyat, Kooperatif street-833 street, Çetintaş limestone mining road	15.06.2019	37°26'13"N-41°21'06"E	969 m	roadside	
<i>S. russellii</i>	Artuklu, Hamzabey Village, Çağlar-Hamzabey road	09.06.2019	37°22'18"N-40°42'09"E	972 m	fields, gardens	M.Kılıç, F.Mungankılıç 210, 218
	Artuklu, Hamzabey Village, Zınnar locality	22.06.2019	37°22'17"N-40°41'12"E	1.003 m	highland road, <i>Glycyrrhiza</i> community, roadside	
	Midyat, Cumhuriyet Village, location on Adnan Aslan street	15.06.2019	37°25'45"N-41°21'30"E	950 m	vineyards	

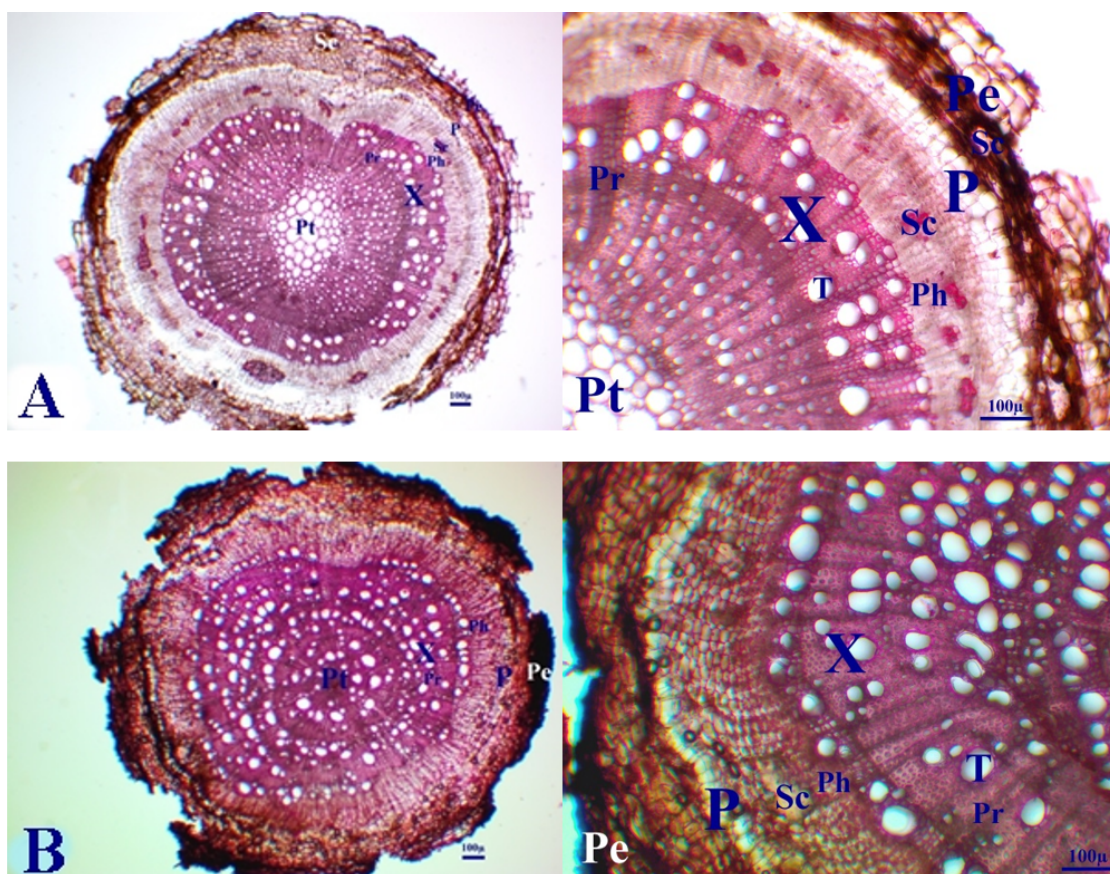


Figure 2: Cross-section of the root of *S. multicaulis* (A) and *S. russellii* (B). Pe: Periderm, P: Parenchyma, Sc: Sclerenchyma, Ph: Phloem, X: Xylem, Pr: Pith ray, T: Trachea, Pt: Pith region

Table 2: Anatomical measurements of root tissues of *S. multicaulis* and *S. russellii*. S.D.: Standard Deviation

Species	Tissue	Width (μ)		Length (μ)	
		Min.–Max.	Mean \pm S.D.	Min.–Max.	Mean \pm S.D.
<i>S. multicaulis</i>	Peridermis cell	12.02–34.25	23.92 \pm 6.99	8.33–21.05	14.40 \pm 3.29
	Parenchyma cell	14.70–44.72	24.76 \pm 9.06	6.11–21.97	12.62 \pm 4.19
	Trachea cell	16.73–66.50	36.98 \pm 13.13	19.93–44.35	32.73 \pm 7.76
	Pith cell	7.88–14.85	11.77 \pm 1.95	7.52–30.37	16.57 \pm 5.50
<i>S. russellii</i>	Peridermis cell	20.59–52.17	32.89 \pm 9.15	11.87–34.34	22.33 \pm 5.80
	Parenchyma cell	9.92–50.67	25.33 \pm 9.56	9.46–26.31	16.66 \pm 5.25
	Trachea cell	13.98–61.54	36.61 \pm 15.15	16.89–67.12	41.90 \pm 15.49
	Pith cell	3.40–8.22	5.90 \pm 1.49	3.40–15.10	11.12 \pm 2.88

3.2. Stem anatomical characteristics

Salvia multicaulis: The stem is quadrangular and has a thin cuticle layer on the outside. Just below, there is a single row of small, square, oval nearly rectangular epidermal cells. There are many glandular and eglandular hairs on the epidermis cells. Most of them are eglandular made up of compound hair. Under the epidermis, there are 6-7 rows of collenchyma cells

concentrated at the corners and 3-4 rows between the corners, and the sizes of these cells are 7.87-25.32 μ . Parenchyma, formed by parenchymatous, cubic, and oval cells was 2-5 rowed at the edges and 4-6 rowed at the corners. 3-5 rows of sclerenchyma were located on the vascular bundles are just above the phloem. Conduction tissue is more developed in the corners. Below the several rows of phloem tissue is an indistinct cambium. In the xylem region, which has wider pith arms, there are large round tracheal cells and many small tracheids between them. The trachea is arranged quite regularly. Wide with 35.03-165.69 μ parenchyma diameter in the center, there is an essence. The cells in the pith region are angular, polygonal, or orbicular parenchymatic cells that grow towards the center and form triangular spaces between them (Fig. 3, Table 3).

Salvia russellii: The stem is quadrangular and has a thin cuticle layer on the outside. Just below, there is a single row of small, square, oval nearly rectangular epidermal cells. There are many single or multicellular eglandular hairs on the epidermis cells. Under the epidermis, there are 6-7 rows of collenchyma cells concentrated at the corners and 3-4 rows between the corners, and the sizes of these cells are 7.75-17.62 μ . Parenchyma, formed by parenchymatous, cubic, and oval cells was 1-2 rowed at the edges and 2-3 rowed at the corners. 3-5 rows of sclerenchyma were located on the vascular bundles are just above the phloem. The parenchyma is tucked towards the corners. Conduction tissue is more developed in the corners. Below the several rows of phloem tissue is an indistinct cambium. In the xylem region, which has wider pith arms, there are large round tracheal cells and many small tracheids between them. The trachea is arranged quite regularly. Wide with 22.07-75.90 μ parenchyma diameter in the center, there is an essence. The cells in the pith region are angular, polygonal, or orbicular parenchymatic cells that grow towards the center and form triangular spaces between them (Fig. 3, Table 3).

3.3. Leaf anatomical characteristics

Salvia multicaulis: The epidermis formed by oval and nearly rectangular cells. The leaf type is bifacial. A thin layer of cuticle with a diameter of 1.86-3.18 μ surrounds the outer part of the leaf. Below the cuticle is the upper epidermis, which contains one and multicellular or compound hairs. Cells are variable in size. Palisade parenchyma cells are in 1-3 rows and their thickness varies between 28.28–55.67 μ , while spongy parenchyma cells are 1-2 rows and between 14.26-24.61 μ . Lower epidermis cells are larger than upper epidermis cells. Xylem and phloem elements are prominent in the bundles. In leaf sections, it was determined that the species had diacytic type stomata. The adaxial surface is slightly convex and has 1-2 rows of collenchyma underneath. The vascular bundles are collateral. The arcuate vascular bundle is

surrounded by parenchyma cells. Just below the parenchyma are the trachea and the xylem consisting of tracheids. The phloem is several layers and is located below the xylem. The abaxial surface is slightly convex and located below it there are 4-5 rows of Collenchyma (Fig. 4, Table 4).

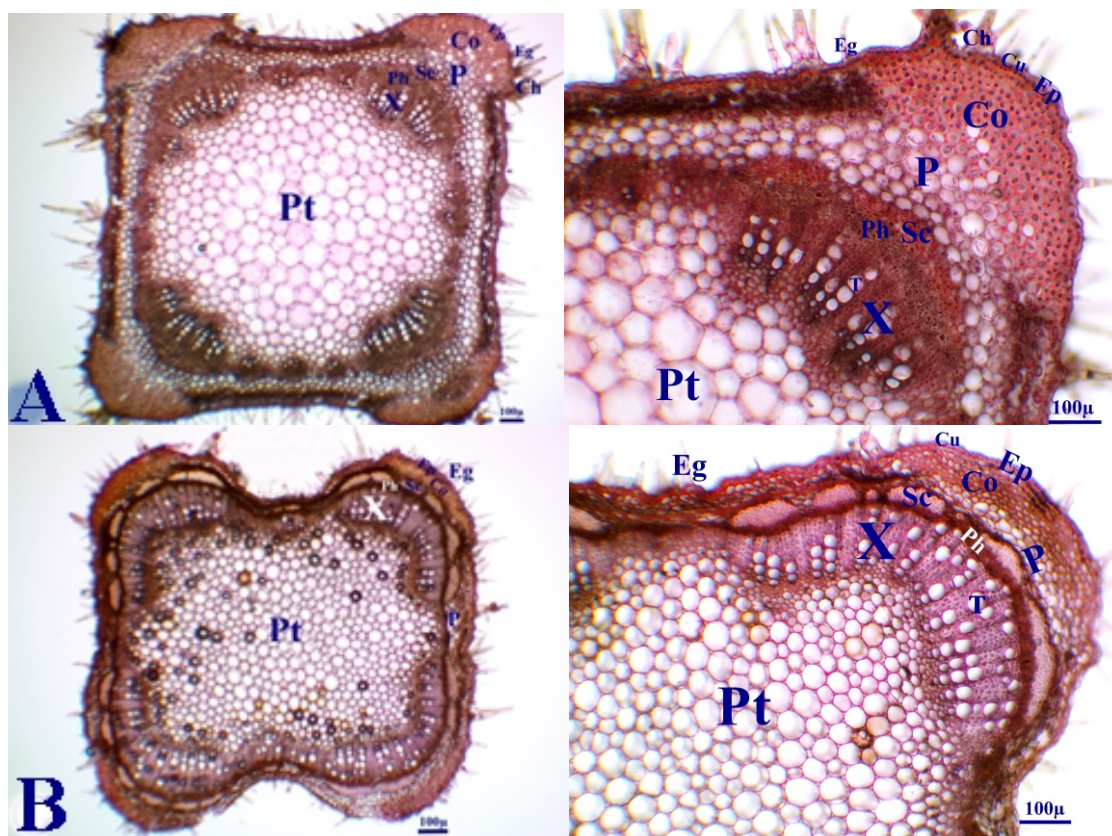


Figure 3: Cross-section of the stem of *S. multicaulis* (A) and *S. russellii* (B). G: Glandular hair, Eg: Eglandular hair, Ch: Compound hair, H: Hair, Cu: Cuticle, Ep: Epidermis, Co: Collenchyma, Crp: Crushed parenchyma

Table 3: Anatomical measurements of stem tissues of *S. multicaulis* and *S. russellii*

Species	Tissue	Width (μ)		Length (μ)	
		Min.–Max.	Mean \pm S.D.	Min.–Max.	Mean \pm S.D.
<i>S. multicaulis</i>	Cuticle	–	–	2.74–8.38	5.86 \pm 1.60
	Epidermis cell	6.56–21.39	12.04 \pm 4.03	5.92–20.92	11.00 \pm 3.49
	Collenchyma cell	9.22–29.34	19.46 \pm 5.23	7.87–25.32	16.47 \pm 4.58
	Parenchyma cell	17.70–61.18	40.64 \pm 12.88	13.22–48.42	31.32 \pm 10.64
	Phloem cell	3.12–13.25	8.10 \pm 2.51	3.05–8.47	5.85 \pm 1.65
	Trachea cell	13.79–34.05	24.02 \pm 6.43	7.98–39.15	20.94 \pm 8.83
	Pith cell	43.44–157.49	95.85 \pm 27.87	35.03–165.69	85.79 \pm 29.89
<i>S. russellii</i>	Cuticle	–	–	2.29–6.27	4.21 \pm 0.94
	Epidermis cell	5.95–18.75	12.23 \pm 3.43	6.52–13.86	9.79 \pm 1.88
	Collenchyma cell	9.33–19.93	14.31 \pm 2.49	7.75–17.62	12.27 \pm 2.90
	Parenchyma cell	9.10–28.93	20.37 \pm 5.40	8.17–23.01	14.34 \pm 4.60
	Phloem cell	2.18–9.00	4.97 \pm 1.81	2.07–5.72	3.87 \pm 1.01
	Trachea cell	9.60–26.38	18.57 \pm 5.13	7.32–31.89	18.93 \pm 7.43
	Pith cell	20.85–73.80	45.19 \pm 14.06	22.07–75.90	48.84 \pm 17.18

Salvia russellii: The epidermis formed by oval and nearly rectangular cells. The leaf type is bifacial. A thick layer of cuticle with a diameter of 5.38-15.62 μ surrounds the outer part of the leaf. Below the cuticle is the upper epidermis, which contains one and multicellular hairs. Cells are variable in size. Palisade parenchyma cells are in 1-3 rows and their thickness varies between 22.38-56.74 μ , while spongy parenchyma cells are 1-2 rows and between 8.49-16.95 μ . Lower epidermis cells are smaller than upper epidermis cells. Xylem and phloem elements are prominent in the bundles. In leaf sections, it was determined that the species had diacytic type stomata. The adaxial surface is slightly concave and has 1-2 rows of collenchyma underneath. The vascular bundles are collateral. The arcuate vascular bundle is surrounded by parenchyma cells. Just below the parenchyma is the trachea and the xylem consisting of tracheids. The phloem is several layers and is located below the xylem. The abaxial surface is slightly convex and located below it there are 1-3 rows of collenchyma (Fig. 4, Table 4).

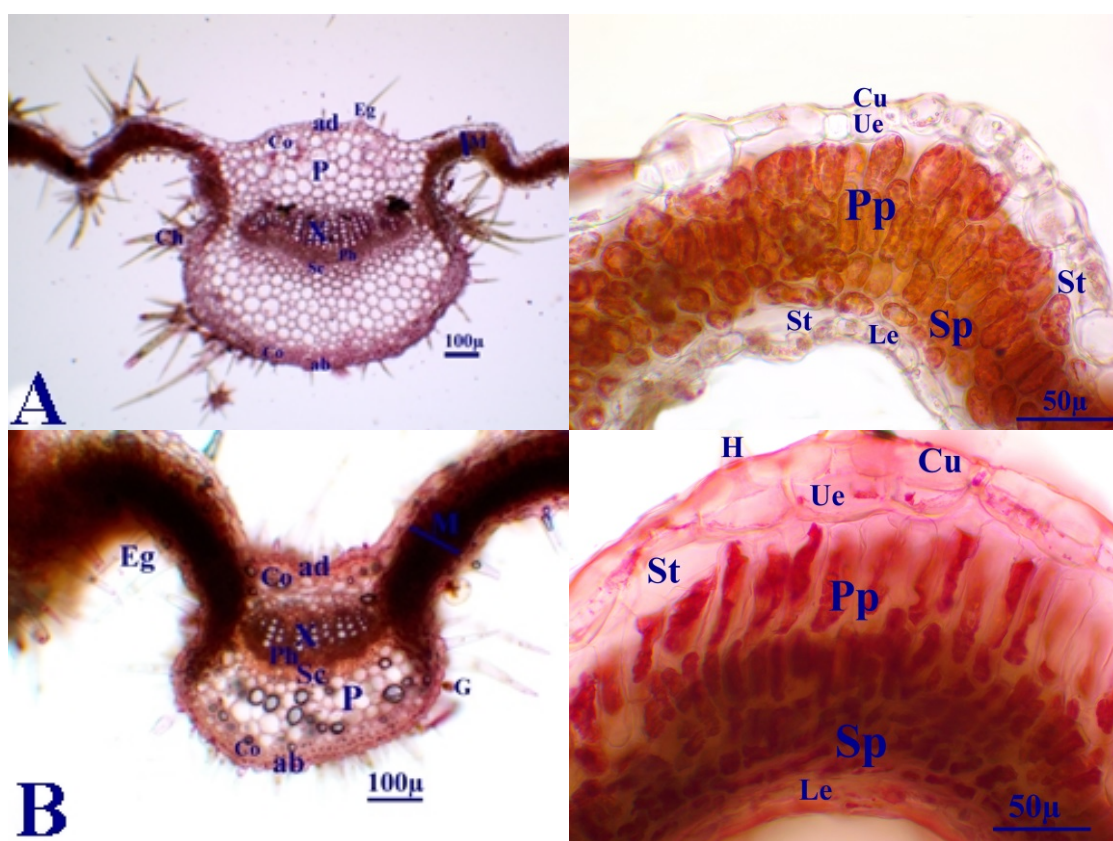


Figure 4: Cross-section of the leaf of *S. multicaulis* (A) and *S. russellii* (B). M: Mesophyll layer, ad: Adaxial surface, ab: Abaxial surface, Ue: Upper epidermis, Le: Lower epidermis, Pp: Palisade parenchyma, Sp: Spongy parenchyma, Hp: Hypodermis, St: Stomata

Table 4: Anatomical measurements of leaf tissues of *S. multicaulis* and *S. russellii*

Species	Tissue	Width (μ)		Length (μ)	
		Min.–Max.	Mean \pm S.D.	Min.–Max.	Mean \pm S.D.
<i>S. multicaulis</i>	Cuticle	–	–	1.86–4.72	3.18 \pm 0.89
	Upper epidermis cell	13.88–39.67	25.53 \pm 9.05	6.44–26.49	17.28 \pm 5.86
	Palisade parenchyma	10.23–23.66	15.33 \pm 3.67	28.28–55.67	43.09 \pm 8.52
	Spongy parenchyma	11.50–19.71	15.45 \pm 2.19	14.26–24.61	17.33 \pm 3.15
	Mesophyll layer	–	–	122.47–193.32	153.23 \pm 19.21
	Lower epidermis cell	5.77–36.66	18.48 \pm 9.21	7.99–35.09	15.69 \pm 7.58
<i>S. russellii</i>	Cuticle	–	–	5.38–15.62	10.38 \pm 2.82
	Upper epidermis cell	10.73–43.30	23.83 \pm 8.41	10.04–33.92	17.06 \pm 5.88
	Palisade parenchyma	5.37–21.95	11.30 \pm 4.14	22.38–56.74	34.58 \pm 10.86
	Spongy parenchyma	7.93–18.94	12.48 \pm 2.94	8.49–16.95	12.00 \pm 2.18
	Mesophyll layer	–	–	75.69–216.74	160.77 \pm 42.95
	Lower epidermis cell	8.99–24.87	16.48 \pm 4.18	5.84–15.55	10.00 \pm 2.79

3.4. Petiol anatomical characteristics

Salvia multicaulis: It is anatomically similar to the midrib of the leaf. There is a thin cuticle layer around the single layer of the epidermis with a diameter of 1.82-5.20 μ , and on it are abundant glandular and eglandular hairs consisting of single, multicellular, or compound hairs. Epidermal cells are different size, square, oval and rectangular. Collenchyma cells are 2-4 rows and thick-walled. Just below is the parenchymatic tissue, which occupies a very large space. Parenchyma cells are 35.02-109.07 μ in diameter. Parenchyma cells are round-cornered, with distinct triangular spaces between them. Conduction tissue is integral in the center of the parenchymatic cells. There are underdeveloped or developed, two small vascular bundles at both corners of the petiole. Fragmented bundles of sclerenchyma are located on the phloem. Phloem is several rows, sieves, and companion cells are not very prominent. The xylem consists of many regularly ordered tracheal elements. Trachea diameters vary between 9.33-20.42 μ (Fig. 5, Table 5).

Salvia russellii: It is anatomically similar to the midrib of the leaf. There is a thick cuticle layer around the single layer of the epidermis with a diameter of 3.66-10.11 μ , and on it are abundant glandular and eglandular hairs consisting of single, multicellular, or compound hairs. Epidermal cells are different is size, square, oval and rectangular. Collenchyma cells are 2-6 rows and thick-walled. Just below is the parenchymatic tissue, which occupies a very large space. Parenchyma cells are 25.57-77.64 μ in diameter. Parenchyma cells are round-cornered, with distinct triangular spaces between them. Conduction tissue is integral in the center of the parenchymatic cells. There are underdeveloped or developed, two small vascular bundles at both corners of the petiole. Fragmented bundles of sclerenchyma are located on the phloem. Phloem is several rows, sieves, and companion cells are not very prominent. The xylem consists

of many regularly ordered tracheal elements. Trachea diameters vary between 15.10-33.93 μ (Fig. 5, Table 5).

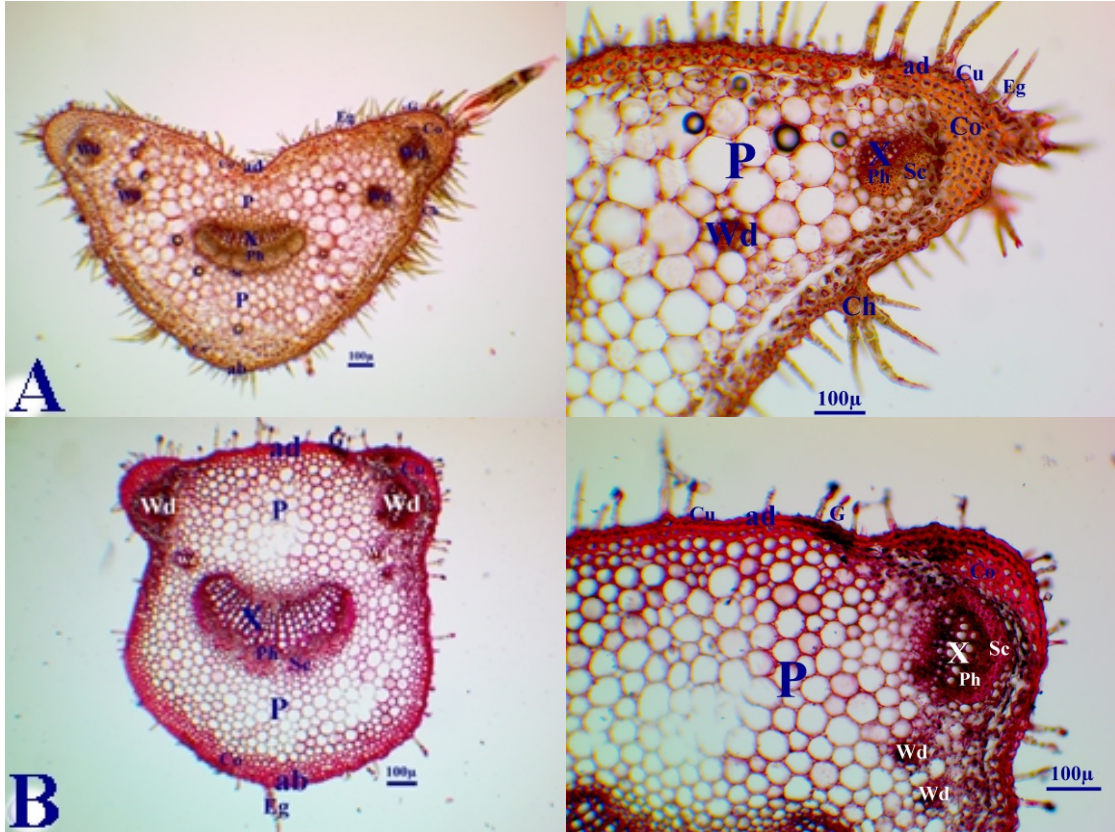


Figure 5: Cross-section of the petiol of *S. multicaulis* (A) and *S. russellii* (B). Mb: Median bundle, Wb: Wing bundle

Table 5: Anatomical measurements of petiole tissues of *S. multicaulis* and *S. russellii*

Species	Tissue	Width (μ)		Length (μ)	
		Min.–Max.	Mean \pm S.D.	Min.–Max.	Mean \pm S.D.
<i>S. multicaulis</i>	Cuticle	–	–	1.82–5.20	3.37 \pm 1.13
	Adaxial epidermis	5.93–16.39	10.85 \pm 3.20	6.43–13.70	10.24 \pm 2.20
	Parenchyma cell	42.38–115.70	73.95 \pm 25.20	35.02–109.07	66.28 \pm 21.43
	Trachea cell	9.19–17.90	13.42 \pm 2.19	9.33–20.42	14.30 \pm 3.17
	Phloem cell	3.37–10.28	6.38 \pm 1.88	2.74–8.58	5.21 \pm 1.57
	Abaxial epidermis	9.89–18.65	13.74 \pm 2.82	6.89–17.43	10.60 \pm 2.83
<i>S. russellii</i>	Cuticle	–	–	3.66–10.11	5.63 \pm 1.66
	Adaxial epidermis	11.12–18.32	15.17 \pm 2.47	7.01–17.06	10.48 \pm 2.38
	Parenchyma cell	24.85–82.66	56.97 \pm 13.71	25.57–77.64	54.52 \pm 14.63
	Trachea cell	13.76–30.01	21.09 \pm 4.69	15.10–33.93	24.96 \pm 5.78
	Phloem cell	6.33–13.61	9.47 \pm 2.11	4.54–10.05	6.53 \pm 1.67
	Abaxial epidermis	10.00–21.36	14.63 \pm 3.24	6.53–16.60	11.01 \pm 2.94

4. Discussion and Conclusion

In this research, *Salvia multicaulis* and *Salvia russellii* which spread to Mardin-Turkey between the years 2018-2020, were examined comparatively in terms of anatomy. The anatomical measurements of the root, stem, leaf and petiole are shown in Tables 2-5, respectively. The *Salvia* taxa used in our study belong to the *Hemisphace* and *Hymenosphace* sections. In this section, we will compare it with the former studies on these sections.

Metcalf and Chalk [12], regarding the root anatomy of the Lamiaceae family, stated that the pith rays of the roots consist of 2-12 or more rows of cells. The pith rays of *S. russellii* (sect. *Hemisphace*) are composed of 1-10 rowed cells [13], and those of *S. blepharochlaena* Hedge & Hub.-Mor. (sect. *Hymenosphace*) are 1-2 rowed [14], [13]; *S. multicaulis* (sect. *Hymenosphace*) are 1-3 rowed [13]. Our studies on the cross-sections of the roots of *S. multicaulis*, and *S. russellii* revealed that the taxa comprise 3-4, 1-2 rowed ray cells respectively. The number of rays seen in the anatomical section of the root is significant in the discrimination of species [15].

The quadrangular stem structure is a distinctive feature of the family, and there is a well-developed collenchyma tissue at the stem corners [12]. We found the same anatomical features in the stem cross-section. Kahraman [13] has examined the stem anatomy of *Salvia* species. It can be seen that some data obtained by Kahraman [13] were similar to the results of our study. However, while Kahraman [13] reported that the collenchyma of the *Hymenosphace* section has 3-7 layers at the corners, 1-5 layers at the edges and parenchyma contain 2-9 layers, and the collenchyma of the *Hemisphace* section has 5-8 layers at the corners, 2-4 layers at the edges, and 1-10 layers on the parenchyma. We have found them to consist of 6-7, 3-4, 2-6, and 6-7, 3-4, 1-3 layers respectively.

In the Lamiaceae family, stomata are usually diacytic. In addition to multicellular, glandular, capitate hairs, various types of hairs are also encountered in family members [16]. In addition, the leaf mesophyll of *Salvia* species is entirely parenchymatic and the midrib is surrounded by collenchymatous cells [12]. According to the mesophyll structure, the leaves of *S. multicaulis* and *S. russellii* are bifacial. The palisade parenchyma has 2-3 rows in *S. multicaulis* and *S. russellii*. But the data obtained by Kahraman [13] regarding the anatomy of the leaf of *S. multicaulis* and *S. russellii* species is different from our study. The structure of palisade parenchyma in the leaf anatomy of *Salvia* species can't be used as a helpful key for distinguishing the species. On the contrary the structure of vascular bundles in the leaf anatomy of *Salvia* species can be used as a helpful key for distinguishing the species [15]. In the midrib of *Salvia* taxa, there are one or two large vascular bundles or absent on sides. It can be seen that

the data obtained by Kahraman [13] regarding the anatomy of the vascular bundles of species is compatible with our study.

The structure of the petiole shows differences between the genera and species. Helpful anatomical characters of the petiole can be determinable in the specified taxonomical structures of some species [17]. According to Metcalfe and Chalk [12], the vascular bundles in the petiole of the Lamiaceae family are very important as a diagnostic feature. In the petiole of *Salvia* taxa, there is a single and lobed large bundle and there are two or three small subsidiary bundles in petiolar wings.

S. verticillata L., as indicated by Kaplan [18], has one broad vascular bundle in the middle of the petiole and one-two small bundle in its wings, *Hemisphace* section [13] has a one-five broad vascular bundle in the centre of the petiole and one-two small bundles in its wings, *Hymenosphace* section [13] has usually one broad vascular bundle in the centre of the petiole and one-two small bundles in its wings, and *S. blepharochlaena* Hedge & Hub.-Mor., [14] has one large bundle in the centre and two small bundles in the wings.

Since the stem part of the plants is less exposed to environmental effects, anatomical studies in vascular plants are mostly conducted on this organ [19]. The stem anatomies of these two species support this information as they show distinctive features.

As a result, it is seen that the anatomical characters in the species provide important taxonomic information. In addition, the presence of anatomical data, as well as morphological characters, shows that species distinction can be made more healthily.

Acknowledgements

We wish to thank Scientific Investigation Project to Coordinate of Mardin Artuklu University (Project No. MAÜ.BAP.18.KMYO.043) for financial support.

References

- [1] Hedge, I.C., *Labiatae of South-West Asia: Diversity, Distribution and Endemism*, Proceedings of The Royal Society of Edinburgh, Section B: Biological Sciences, 89, 23-35, 1986.
- [2] The Plant List. (2021, November 5). Retrieved from <http://www.theplantlist.org/>
- [3] Güner, A., Aslan, S., Ekim, T., Vural, M., Babaç, M.T, eds., *Turkey plant list (Vascular plants)*. İstanbul: Nezahat Gökyiğit Botanik Bahçesi Yayını, 2012.
- [4] Davis, P.H., *Flora of Turkey and the East Aegean Islands*. vol. 7, Edinburgh: Edinburgh University Press, 36-461, 1982.

- [5] Güner, A., Özhatay, N., Ekim, T., Başer, K.H.C., *Flora of Turkey and the East Aegean Islands*. vol. 11, Edinburgh: Edinburgh University Press, 2000.
- [6] Baytop, T., *Türkiye'de Bitkilerle İle Tedavi*. İstanbul: İstanbul Üniversitesi Yayınları, , 158p. 1984.
- [7] Ulubelen, A., *Cardioactive and antibacterial terpenoids from some Salvia species*, *Phytochemistry*, 64, 395-399, 2003.
- [8] Kamatou, G. P. P., Makunga, N. P., Ramogola, W. P. N., Viljoen, A. M., *South African Salvia species: a review of biological activities and phytochemistry*, *Journal of Ethnopharmacology*, 119, 667-672, 2008.
- [9] Hedge, I. C., *Flora of Turkey and the East Aegean Islands*. In P.H. Davis, (Ed.), *Salvia L.*, vol. 7 (pp. 400-461). Edinburgh: Edinburgh University Press, 947 pp, 1982.
- [10] Demir, M. M. (2010) *Mardin City*. Msc Thesis, Istanbul University, İstanbul, Turkey.
- [11] Bozdağ, B., Kocabaş, O., Akyol, Y., Özdemir, C., *A New Staining Method for Hand-Cut in Plant Anatomy Studies*, *Marmara Pharmaceutical Journal*, 20, 184-190, 2016
- [12] Metcalfe, C. R., Chalk, L., *Anatomy of the Dicotyledons*. vol. 2, London: Oxford at The Clarendon Press, 1041-1053pp. 1972.
- [13] Kahraman, A. (2011). *Morphology, Anatomy and Systematics Of The Genus Salvia L. (Lamiaceae) In East And Southeast Anatolia, Turkey*. Phd Thesis, Middle East Technical University, Ankara, Turkey.
- [14] Özkan, M., Özdemir, C., Soy, E., *Morphology, Anatomy, Hair and Karyotype Structure of S. blepharochlaena Hedge and Hub.-Mor. (Lamiaceae), Endemic to Turkey*, *Pakistan Journal of Biological Sciences*, 10, 893-898, 2007.
- [15] Kahraman, A., Celep, F., Doğan, M., *Morphology, anatomy, palynology and nutlet micromorphology of Salvia macrochlamys (Labiatae) in Turkey*, *Biologia*, 65, 219-227, 2010.
- [16] Özörgücü, B., Gemici, Y., Türkan, İ., *Karşılaştırmalı Bitki Anatomisi*, İzmir: Ege Üniversitesi Fen Fakültesi Yayınları, 106-107pp. 1991.
- [17] Akcin, Ö.E., Özyurt, M.S., Şenel, G., *Petiole anatomy of some Lamiaceae taxa*, *Pakistan Journal of Botany*, 43, 1437-1443, 2011.
- [18] Kaplan, F. (2019) *Sakarya ili çevresinde yayılış gösteren bazı Salvia L. (Lamiaceae) taksonları üzerine anatomik, morfolojik ve palinolojik araştırmalar*. Msc Thesis, Düzce Üniversitesi, Türkiye.
- [19] Lopes, L. K. C., Góes-Neto, L. A. A., Feio, A. C., *Stem anatomy and its relevance for the taxonomic survey of Selaginella subg. Gymnogynum (Selaginellaceae)*. *Plant Systematics and Evolution*, 306, 13, 2020.



New Weyl-Type Inequalities by Multiplicative Injective and Surjective s -Numbers of Operators in Reflexive Banach Spaces

Lale CONA^{1,*}

¹Gümüşhane University, Faculty of Engineering and Natural Sciences, Department of Mathematical Engineering, Gümüşhane, Türkiye
lalecona@gumushane.edu.tr, ORCID: 0000-0002-2744-1960

Received: 27.09.2021

Accepted: 05.04.2022

Published: 30.06.2022

Abstract

In this work, two problems are investigated. In general, Weyl-type inequalities of operators in complex reflexive Banach spaces are discussed. First, we obtained the Weyl-type inequalities using arbitrary multiplicative surjective and injective s -numbers that are dual of each other. Second, we introduced the Weyl-type inequalities by multiplicative injective and surjective s -numbers under certain conditions for S and S' operators in complex reflexive Banach space. So, new Weyl-type inequalities are investigated for both dual s -number sequences and dual operators.

Keywords: Dual s - numbers; Dual operators; Multiplicative injective and surjective s -numbers; s -numbers; Weyl-Type inequalities.

Yansımali Banach Uzaylarda Operatörlerin Çarpımsal İnjektiv ve Surjektiv s -Sayıları ile Yeni Weyl-Tipi Eşitsizlikleri

Öz



Bu çalışmada iki problem incelenmiştir. Genel olarak, kompleks yansımali Banach uzaylarında operatörlerin Weyl-tipi eşitsizlikleri üzerinde durulmuştur. İlk olarak, birbirinin duali olan keyfi çarpımsal surjektif ve injektif s -sayılarını kullanarak Weyl-tipi eşitsizlikler elde edilmiştir. İkinci olarak, kompleks yansımali Banach uzayındaki S ve S' operatörleri için belirli koşullar altında çarpımsal injektif ve surjektif s -sayıları ile Weyl-tipi eşitsizlikler ifade edilmiştir. Böylece hem dual s -sayı dizileri hem de dual operatörler için yeni Weyl-tipi eşitsizlikleri araştırılmıştır.

Anahtar Kelimeler: Dual s -sayıları; Dual operatörler; Çarpımsal injektif ve surjektif s -sayıları; s -sayıları; Weyl-Tipi eşitsizlikler.

1. Introduction

The definition of s -number (or singular numbers) was firstly used by E. Schmidt in the theory of non-selfadjoint integral equation. The axiomatic structure of the original s -numbers in Banach spaces was developed by A. Pietsch [1].

Let us first give the theorem which expresses the classical Weyl inequality in Hilbert spaces [2]. Let H be a Hilbert space and $S \in C_\infty(H)$ a compact operator. Then

$$\prod_{k=1}^n |\lambda_k(S)| \leq \prod_{k=1}^n s_k(S)$$

for $n = 1, 2, \dots$

This inequality is an important tool to prove the correlation between eigenvalues and s -numbers. Thus, an important contribution is made to the investigation of the optimum asymptotic behavior of the eigenvalues. A. Pietsch developed the Weyl inequality for operators in Banach spaces [3].

$$\left(\prod_{j=1}^n |\lambda_j(S)| \right)^{\frac{1}{n}} \leq \left(\frac{n}{k} \right)^{\frac{n-k}{2n}} n^{\frac{k}{2n}} \|S\|^{1-\frac{k}{n}} \left(\prod_{j=n-k+1}^n h_j(S) \right)^{\frac{1}{n}}.$$

This inequality applies to any s -number sequence, because the Hilbert numbers are the smallest s -numbers in Banach spaces. We can also look at [4] for better constants.

For these inequalities, the Weyl numbers are considered to be suitable s -numbers. This fact has been confirmed as a result of extensive studies on the eigenvalues about of integral operators moving in function spaces. Researchers obtained similar inequalities by taking different s -

numbers instead of Weyl numbers. These inequalities are generally referred to as Weyl-type inequalities in the literature. We can see several Weyl-type inequalities in [2, 5, 6]. However, various Weyl-type inequalities were obtained for different operators (Riesz operator, Compact operator, etc.) in Banach space [5-7]. We can see some Weyl-type inequalities by injective and surjective s -numbers in [8, 9]. In our study, we will use the multiplicative injective and surjective s -numbers.

In the studies done in the ever-evolving literature, it has been concluded that many problems of the theory of multi-point differential operators can be easily solved on the direct sum of Banach spaces [10, 11]. In this context, some s -number functions of the direct sum of operator defined on the direct sum of Banach spaces, which can contribute to the field, and the s -number functions of the same type of coordinate operators have been investigated [12, 13]. In addition, s -numbers have a very important place for studies related to Lorentz-Schatten sequence classes [17-24].

We denote by B_X the closed unit ball of X . In what follows X, Y, Z , e.t.c . always denote complex Banach spaces. Then $L(X, Y)$ and $C_\infty(X, Y)$ respectively are denote the set of bounded linear operators and compact operators from X into Y . Also, if $X = Y$, it is denoted by $L(X) = L(X, X)$ and $C_\infty(X) = C_\infty(X, X)$. Moreover, S' is a dual operator of S .

2. s -Numbers and basic results

Definition 1. Let $S \in L(X)$. If $S^n \in C_\infty(X, Y)$ for $n \in \mathbb{N}$ then S is called power compact [5-7].

Let's give the definition of an s -number sequence [14].

Definition 2. A rule $s_n(S) : L \rightarrow [0, \infty]$ assigning to every operator $S \in L$ a non-negative scalar sequence $s_n(S)_{n \in \mathbb{N}}$ is called an s -number sequence if the following conditions are satisfied:

(i) Monotonicity:

$$\|S\| = s_1(S) \geq s_2(S) \geq \dots \geq 0 \text{ for } S \in L(X, Y),$$

(ii) Additivity:

$$s_n(S + T) \leq s_n(S) + \|T\| \text{ for } S, T \in L(X, Y) \text{ and } n, m = 1, 2, \dots,$$

(iii) Ideal-Property:

$$s_n(RST) \leq \|R\|s_n(S)\|T\| \text{ for } R \in L(X_0, X), S \in L(X, Y) \text{ and } T \in L(Y, Y_0)$$

(iv) Rank-Property:

$$s_n(S) = 0 \text{ for } S \in L(X, Y) \text{ with } \text{rank}(S) < n$$

(v) Norming Property:

$$s_n(I_n) = 1 \text{ for the identity maps } I_n: l_2^n \rightarrow l_2^n \text{ on } l_2.$$

Let's give important s -number definitions. For $S \in L(X, Y)$ and $n = 1, 2, \dots$, the n -th approximation number is defined by

$$a_n(S) = \inf\{\|S - A\|: A \in L(E, F), \text{rank}(A) < n\},$$

the n -th Gelfand number by

$$c_n(S) := \inf\{\|SJ_M\|: M \subset X, \text{codim}(M) < n\},$$

where $J_M: M \rightarrow X$ is the natural embedding from a subspace M of X into X , and the n -th Kolmogorov number by

$$d_n(S) := \inf\{\|Q_N S\|: N \subset Y, \text{dim}(N) < n\},$$

where $Q_N: Y \rightarrow Y/N$ defines the canonical quotient map from Y into the quotient space Y/N , and the n -th Weyl number by

$$x_n(S) = \sup\{a_n(SA): \|A: l_2 \rightarrow X\| \leq 1\},$$

and the n -th Hilbert number by

$$h_n(S) := \sup\{a_n(BSA): \|A: l_2 \rightarrow X\| \leq 1, \|B: Y \rightarrow l_2\| \leq 1\}.$$

Remark 1. The following inequality exists for s -numbers in Banach spaces

$$h_n(S) \leq s_n(S) \leq a_n(S),$$

where $s_n(S)_{n \in \mathbb{N}}$ is an arbitrary s -number [5, 14].

Now let us express the relation between s -numbers in Hilbert spaces [5, 6].

Let us first give a brief description of the s -number in the classical Hilbert spaces. Suppose H is a Hilbert space and let $S \in C_\infty(H)$. Then $s_n(S) = \lambda_n\left((S^*S)^{\frac{1}{2}}\right)$ are called the singular

numbers of S . We will show the sequence of eigenvalues of the S transformation with $\lambda_n(S)_{n \in \mathbb{N}}$. This sequence is ordered in decreasing absolute value and counted according to their multiplicity,

$$|\lambda_1(S)| \geq \dots \geq |\lambda_n(S)| \geq \dots \geq 0.$$

If S possesses less than n eigenvalues λ with $\lambda \neq 0$ we put $\lambda_n(S) = \lambda_{n+1}(S) = \dots = 0$. It is well known that the sequence of eigenvalues form a null sequence.

Lemma 1. Let X, Y be Hilbert spaces and $S \in C_\infty(X, Y)$. Then we have

$$a_n(S) = c_n(S) = x_n(S) = d_n(S) = h_n(S) = \lambda_n(S^*S)^{\frac{1}{2}},$$

where S^* is the Hilbert adjoint of S .

In addition to these, let's give the following definitions [5, 6].

- a. A s -number sequence $s = (s_n)$ is called injective if, given any metric injection $J \in L(Y, \tilde{Y})$ i.e. $\|Jy\| = \|y\|$ for $y \in Y$, $s_n(S) = s_n(JS)$ for all $S \in L(X, Y)$ and all Banach spaces X .
- b. A s -number sequence $s = (s_n)$ is called surjective if, given any metric surjection $Q \in L(\tilde{X}, X)$ i.e. $Q(B_{\tilde{X}}) = B_X$, $s_n(S) = s_n(SQ)$ for all $S \in L(X, Y)$ and all Banach spaces Y .
- c. If a s -number sequence satisfies (a) and (b) then it is called injective and surjective.

Moreover, we have

$$c_n(S) = a_n(J_\infty S) \text{ and } d_n(S) = a_n(SQ_1),$$

where $J_\infty: Y \rightarrow l_\infty(B_{Y'})$ is the metric surjection defined by $J_\infty y = ((y, a))_{a \in B_{Y'}}$ and with values in the space $l_\infty(B_{Y'})$ of bounded sequences and where $Q_1: l_1(B_X) \rightarrow X$ is the metric surjection from $l_1(B_X)$ onto X , defined by $Q_1((\xi_x)) := \sum_{x \in B_X} \xi_x x$.

On the other hand, a s -numbers sequence (s_n) is called multiplicative if

$$s_{n+m-1}(TS) \leq s_n(T) s_m(S)$$

for $S \in L(X, Y), T \in L(Y, Z)$ and $m, n \in 1, 2, \dots$.

Now, we recall useful mixing multiplicativity property for an arbitrary s -number sequence $s = (s_n)$ from [4]. For $S \in L(X, Y)$ and $T \in L(Y, Z)$,

- a. $s_{n+m-1}(TS) \leq s_n(T)a_m(S)$ and $s_{n+m-1}(TS) \leq a_n(T)s_m(S)$.
- b. If $s = (s_n)$ is injective, then $s_{n+m-1}(TS) \leq c_n(T)s_m(S)$.
- c. If $s = (s_n)$ is surjective, then $s_{n+m-1}(TS) \leq s_n(T)d_m(S)$.

The following result can be easily deduced from the above inequalities. If $s = (s_n)$ is an injective and surjective s -number sequence, then

$$s_{n+m+l-1}(TSR) \leq c_n(T)s_m(S)d_l(R)$$

for $R \in L(X_0, X)$, $S \in L(X, Y)$ and $T \in L(Y, Y_0)$.

Let us now state a lemma that we frequently refer to in our proofs [15].

Lemma 2. Let $I \in L(X, Y)$ identity map. Then,

$$x_k(I: l_\infty^n \rightarrow l_2^n) = \left(\frac{n}{k}\right)^{\frac{1}{2}},$$

for $1 \leq k \leq n$.

A. Pietsch's principle of related operators in the context of operators on X factorizing through Y . And we give the following lemma which is quite useful as a result of the principle of related operators [5-7].

Definition 3. Let $S \in L(X)$ and $T \in L(Y)$. If there are maps $P \in L(X, Y)$ and $R \in L(Y, X)$ such that $S = RP$ and $T = PR$, then S and T are called related.

Lemma 3. Let $S \in L(X)$ and $T \in L(Y)$ be related operators and S power compact. Then T is power compact and

$$\sigma(S) \setminus \{0\} = \sigma(T) \setminus \{0\}, \quad m(S, \lambda) = m(T, \lambda) \text{ for all } 0 \neq \lambda \in \sigma(S).$$

Hence we have $\lambda_n(S) = \lambda_n(T)$ for all $n \in \mathbb{N}$.

We need another fact about the 2-summing norms due to Garling-Gordon [15].

Lemma 4. Let X_n be any n -dimensional Banach space. Then

$$\pi_2(I_{X_n}) = \sqrt{n}.$$

The following basic fact is quite important to prove the main result [5].

Lemma 5. Let $S \in C_\infty(X)$ be a compact operator and $\lambda_n(S) \neq 0$. Then there is a n -dimensional subspace X_n of X , invariant under S , such that the operator $S_n \in L(X_n)$ induced by S has exactly the eigenvalues $\lambda_1(S), \dots, \lambda_n(S)$.

The following theorems give the relationship between operators and their duals for some s -numbers, see [1] for similar relations.

Theorem 1. Let $S \in L(X, Y)$; then

$$c_n(S) = d_n(S'),$$

where S' is dual operator of S .

Theorem 2. Let $S \in C_\infty(X, Y)$; then

$$d_n(S) = c_n(S'),$$

where S' is dual operator of S .

3. Main results

In the first section, we have recalled that Weyl-type inequalities are optimal for estimating eigenvalues of operators in Banach spaces. We can see several Weyl-type inequalities in [5, 6, 16].

Let us give the Weyl-type inequalities expressing the relation between the eigenvalues and Weyl numbers established by Pietsch in [3]:

$$\left(\prod_{k=1}^{2n-1} |\lambda_k(S)| \right)^{\frac{1}{2n-1}} \leq \sqrt{2}e \left(\prod_{k=1}^n x_k(S) \right)^{\frac{1}{n}}$$

and

$$\left(\sum_{k=1}^n |\lambda_k(S)|^p \right)^{\frac{1}{p}} \leq c_p \left(\sum_{k=1}^n x_k^p(S) \right)^{\frac{1}{p}}$$

for $S \in C_\infty(X, Y)$.

3.1. Weyl-Type inequality by dual s -numbers of power compact operators

Power compact operators are a classical subject in the context of integral operators to relate the properties (e.i. kernel properties) of an operator to the decay of its eigenvalues [6]. So, we firstly obtained Weyl-type inequalities of power compact operators in Banach spaces through multiplicative injective and surjective s -numbers. Here $[x]$ denotes the integer part of x for $1 \leq x < \infty$ and if $0 < x \leq 1$ we put $[x] := 1$.

Theorem 3. Let $S \in L(X)$ is a power compact operator such that all complex Banach space X and $s = (s_n)$ be a multiplicative injective s -number sequence for $n \in \mathbb{N}$. Then,

$$\left(\prod_{k=1}^n |\lambda_k(S)| \right)^{\frac{1}{n}} \leq C(\delta) \sqrt{n} \sqrt{e} \left(\prod_{k=1}^m s_k(S) \right)^{\frac{1}{m}},$$

where $m := \left[\frac{n}{1+\delta} \right]$ and $0 < \delta \leq 1$, $C(\delta) = 2 \left(\frac{1+\delta}{\delta} \right)^{\frac{1}{2}}$ for $n, m \in \mathbb{N}$.

Proof. Since $S \in L(X)$ is a power compact we can find a n –dimensional subspace X_n of X invariant under S such that the restriction of S to X_n , $S_n = S|_{X_n}$ has precisely $\lambda_1(S), \dots, \lambda_n(S)$ as its eigenvalues. By Lemma 4, $\pi_2(I_{|X_n}) = \sqrt{n}$. Hence by the Grothendieck-Pietsch factorization $B \in L(H, X_n)$ with $BA = I_{|X_n}$ and $\|A\| = \pi_2(A) = \sqrt{n}$, $\|B\| = 1$. We may assume that the Hilbert space H is n –dimensional (by restriction), $H = l_2^n$ so that $B = A^{-1}$. Define $T_n = AS_nA^{-1} \in L(l_2^n)$; T_n has the same eigenvalues $(\lambda_j(S))_{j=1}^n$ as S_n with the principle of related operators. Using Weyl's inequality in Hilbert space and the multiplicative of s -number sequence, we obtain

$$\begin{aligned} \left(\prod_{k=1}^n |\lambda_k(S)| \right)^{\frac{1}{n}} &= \left(\prod_{k=1}^n |\lambda_k(S_n)| \right)^{\frac{1}{n}} \\ &= \left(\prod_{k=1}^n |\lambda_k(T_n)| \right)^{\frac{1}{n}} \\ &\leq \left(\prod_{k=1}^n s_k(T_n) \right)^{\frac{1}{n}}. \end{aligned} \tag{1}$$

Moreover, $0 < \delta \leq 1$ and a non-increasing sequence of positive numbers $(s_k)_{k \in \mathbb{N}}$ we use the estimate

$$\left(\prod_{k=1}^n s_k\right)^{\frac{1}{n}} \leq \left(\prod_{k=1}^m s_{[\delta k]+k-1}\right)^{\frac{1}{m}},$$

where $m := \left\lceil \frac{n}{1+\delta} \right\rceil$ and $n, m \in \mathbb{N}$. Thus,

$$\begin{aligned} \left(\prod_{k=1}^n s_k(T_n)\right)^{\frac{1}{n}} &= \left(\prod_{k=1}^n s_k(AS_n A^{-1})\right)^{\frac{1}{n}} \\ &\leq \left(\prod_{k=1}^m s_{[\delta k]+k-1}(AS_n A^{-1})\right)^{\frac{1}{m}}. \end{aligned} \tag{2}$$

The mixing multiplicative (b) property of an injective s -number sequence yields the estimate for the single s -numbers

$$\left(\prod_{k=1}^m s_{[\delta k]+k-1}(AS_n A^{-1})\right)^{\frac{1}{m}} \leq \left(\prod_{k=1}^m s_k(AS_n) c_{[\delta k]}(A^{-1})\right)^{\frac{1}{m}}. \tag{3}$$

Also using property (iii) of Definition 2, $\|A\| = \pi_2(A) = \sqrt{n}$, $\|B\| = 1$ by the Grothendieck-Pietsch factorization and Lemma 2 we have

$$\begin{aligned} s_k(AS_n) c_{[\delta k]}(A^{-1}) &\leq \|A\| s_k(S) c_{[\delta k]}(I_n B) \\ &\leq \sqrt{n} s_k(S) \|B\| c_{[\delta k]}(I_n: l_2^n \rightarrow l_2^n) \\ &= \sqrt{n} s_k(S) \|B\| x_{[\delta k]}(I_n: l_2^n \rightarrow l_2^n) \\ &\leq \sqrt{n} s_k(S) \sqrt{\frac{n}{[\delta k]}}, \end{aligned} \tag{4}$$

where $I_n: l_2^n \rightarrow l_2^n$ identity maps for $n \in \mathbb{N}$. From $m := \left\lceil \frac{n}{1+\delta} \right\rceil \geq \frac{n}{2(1+\delta)}$ and $[\delta k] \geq \frac{\delta k}{2}$ and Stirling's formula $e^m \geq \frac{m^m}{m!}$ we can combine Eqns. (1)-(4)

$$\begin{aligned}
 \left(\prod_{k=1}^n |\lambda_k(S)|\right)^{\frac{1}{n}} &\leq \sqrt{n} \left(\prod_{k=1}^m s_k(S) \left(\frac{n}{[\delta k]}\right)^{\frac{1}{2}}\right)^{\frac{1}{m}} \\
 &\leq \sqrt{n} \left(\prod_{k=1}^m \left(\frac{n}{[\delta k]}\right)^{\frac{1}{2}}\right)^{\frac{1}{m}} \left(\prod_{k=1}^m s_k(S)\right)^{\frac{1}{m}} \\
 &\leq \sqrt{n} \left(\prod_{k=1}^m \left(\frac{2n}{\delta k}\right)^{\frac{1}{2}}\right)^{\frac{1}{m}} \left(\prod_{k=1}^m s_k(S)\right)^{\frac{1}{m}} \\
 &\leq \sqrt{n} \left(\frac{2}{\delta}\right)^{\frac{1}{2}} \left(\frac{n^m}{m!}\right)^{\frac{1}{2m}} \left(\prod_{k=1}^m s_k(S)\right)^{\frac{1}{m}} \\
 &\leq \sqrt{n} \left(\frac{2}{\delta}\right)^{\frac{1}{2}} (e^m)^{\frac{1}{2m}} (2(1+\delta))^{\frac{1}{2}} \left(\prod_{k=1}^m s_k(S)\right)^{\frac{1}{m}} \\
 &\leq 2 \left(\frac{1+\delta}{\delta}\right)^{\frac{1}{2}} \sqrt{n} \sqrt{e} \left(\prod_{k=1}^m s_k(S)\right)^{\frac{1}{m}}.
 \end{aligned}$$

Finally, we obtain following inequality

$$\left(\prod_{k=1}^n |\lambda_k(S)|\right)^{\frac{1}{n}} \leq C(\delta) \sqrt{n} \sqrt{e} \left(\prod_{k=1}^m s_k(S)\right)^{\frac{1}{m}},$$

where $0 < \delta \leq 1$, $C(\delta) = 2 \left(\frac{1+\delta}{\delta}\right)^{\frac{1}{2}}$ and $n, m \in \mathbb{N}$.

Remark 2. If we put $\delta = 1$, $m = \lfloor \frac{n}{2} \rfloor = n - 1$ replace (s_n) by (x_n) then we have Pietsch's Weyl inequality

$$\left(\prod_{k=1}^n |\lambda_k(S)|\right)^{\frac{1}{n}} \leq 2\sqrt{2en^2}^{\frac{1}{2}} \left(\prod_{k=1}^{n-1} x_k(S)\right)^{\frac{1}{n-1}},$$

where $m, n \in \mathbb{N}$.

Theorem 4. Let $S \in L(X)$ be a power compact operator such that all complex reflexive Banach space X and $s = (s_n)$ be a multiplicative surjective s -number sequence for $n \in \mathbb{N}$. Then,

$$\left(\prod_{k=1}^n |\lambda_k(S)|\right)^{\frac{1}{n}} \leq C(\delta)\sqrt{n}\sqrt{e} \left(\prod_{k=1}^m s_k(S)\right)^{\frac{1}{m}},$$

where $m := \left\lceil \frac{n}{1+\delta} \right\rceil$ and $0 < \delta \leq 1$, $C(\delta) = 2 \left(\frac{1+\delta}{\delta}\right)^{\frac{1}{2}}$ for $n, m \in \mathbb{N}$.

Proof. If S is a compact power operator, the dual operator S' is also a compact power operator. Furthermore, the eigenvalues sequences of S and S' can be arranged in such a way that $\lambda_n(S') = \lambda_n(S)$ for all $n \in \mathbb{N}$, see e.g. [5]. For $n \in \mathbb{N}$ and any operator S , define $\tilde{s}_n(S) = s_n(S')$. $\tilde{s} = (\tilde{s}_n)$ is known to be a sequence of s -numbers [5]. Also, since the dual of a metric injection is a metric surjection [14], \tilde{s} is an injective s -number sequence. Then we obtain from Theorem 3 applied to S' that

$$\begin{aligned} \left(\prod_{k=1}^n |\lambda_k(S)|\right)^{\frac{1}{n}} &= \left(\prod_{k=1}^n |\lambda_k(S')|\right)^{\frac{1}{n}} \\ &\leq C(\delta)\sqrt{n}\sqrt{e} \left(\prod_{k=1}^m \tilde{s}_k(S')\right)^{\frac{1}{m}} \\ &\leq C(\delta)\sqrt{n}\sqrt{e} \left(\prod_{k=1}^m s_k(S'')\right)^{\frac{1}{m}}. \end{aligned}$$

We have $S'' = S$ since X is reflexive. Thus, the alleged inequality is proved.

3.2. Weyl-Type inequality of dual operators by arbitrary multiplicative injective and surjective s -numbers

We mentioned that Weyl numbers with minimum s -numbers are considered the best s -numbers for working with Weyl-type inequalities. Nevertheless, whether there exists a minimal multiplicative s -number sequence another from Weyl numbers for was investigated by [4].

We will obtain an important inequality between arbitrary multiplicative injective and surjective s -numbers (s_n) and (r_n) with the property that $s_n(S) \leq r_n(S)$ for all $S \in C_\infty(X)$ compact operators. We will also investigate the relation that $s = (s_n)$ s -numbers which is an

arbitrary multiplicative injective and surjective s -number sequence of S is compact operator and it's S' is dual operator in complex reflexive Banach space.

Theorem 5. Let (s_n) and (r_n) be multiplicative injective and surjective s -numbers sequence with the property that $s_n(S) \leq r_n(S)$ for all $S \in C_\infty(X)$ compact operators such that complex Banach space X . Then,

$$r_{2n-1}(S) \leq \sqrt{e} \left(\prod_{k=1}^n s_k(S) \right)^{\frac{1}{n}},$$

for $n = 1, 2, \dots$

Proof. Since (r_n) is an injective and surjective s -number sequence, we have that operator $Q_1 \in L(l_1^n, X)$ and $J_\infty \in L(X, l_\infty^n)$.

$$r_{2n-1}(S) = r_{2n-1}(J_\infty S Q_1) \leq \left(\prod_{k=1}^n r_{2k-1}(J_\infty S Q_1) \right)^{\frac{1}{n}} \tag{5}$$

We easily see that for Q_1 , an operator acting in Hilbert space, and (s_n) , a multiplicative injective and surjective s -number sequence, the following inequality holds.

$$\begin{aligned} \left(\prod_{k=1}^n r_{2k-1}(J_\infty S Q_1) \right)^{\frac{1}{n}} &= \left(\prod_{k=1}^n s_{2k-1}(J_\infty S Q_1) \right)^{\frac{1}{n}} \\ &\leq \left(\prod_{k=1}^n c_{\frac{k}{2}}(J_\infty) s_k(S) d_{\frac{k}{2}}(Q_1) \right)^{\frac{1}{n}}. \end{aligned} \tag{6}$$

Thus using property (iii) of Definition 2, J_∞ is an operator acting in Hilbert space, $\|J_\infty\| \leq 1$ and $\|Q_1\| \leq 1$ we obtain

$$\begin{aligned} \left(\prod_{k=1}^n c_{\frac{k}{2}}(J_\infty) s_k(S) d_{\frac{k}{2}}(Q_1) \right)^{\frac{1}{n}} &\leq \left(\prod_{k=1}^n c_{\frac{k}{2}}(I_n: l_\infty^n \rightarrow l_\infty^n) \|J_\infty\| s_k(S) \|Q_1\| d_{\frac{k}{2}}(I_n: l_1^n \rightarrow l_1^n) \right)^{\frac{1}{n}} \\ &\leq \left(\prod_{k=1}^n c_{\frac{k}{2}}(I_n: l_\infty^n \rightarrow l_\infty^n) s_k(S) d_{\frac{k}{2}}(I_n: l_1^n \rightarrow l_1^n) \right)^{\frac{1}{n}}, \end{aligned} \tag{7}$$

where I_n is a identity map. Since I_n is an operator acting in Hilbert space and combining Eqns. (5)-(7) we arrive

$$r_{2n-1}(S) \leq \left(\prod_{k=1}^n x_k(I_n: l_\infty^n \rightarrow l_\infty^n) s_k(S) x_k(I_n: l_1^n \rightarrow l_1^n) \right)^{\frac{1}{n}}.$$

We easily get the following estimates by using the identity maps I_n for $n = 1, 2, \dots$ with Lemma 2, from the last equation and known inequality $\frac{n^n}{n!} \leq e^n$,

$$\begin{aligned} r_{2n-1}(S) &\leq \left(\prod_{k=1}^n \left(\frac{2n}{k} \right) \right)^{\frac{1}{n}} \left(\prod_{k=1}^n s_k(S) \right)^{\frac{1}{n}} \\ &\leq 2 \left(\frac{n^n}{n!} \right)^{\frac{1}{n}} \left(\prod_{k=1}^n s_k(S) \right)^{\frac{1}{n}} \\ &\leq 2e \left(\prod_{k=1}^n s_k(S) \right)^{\frac{1}{n}}. \end{aligned}$$

Finally, we get that

$$r_{2n-1}(S) \leq 2e \left(\prod_{k=1}^n s_k(S) \right)^{\frac{1}{n}},$$

for $n = 1, 2, \dots$

Let's express the relation for dual operators under the conditions of Theorem 5.

Theorem 6. Let (s_n) and (r_n) be be multiplicative injective and surjective s -numbers sequence with the property that $s_n(S) \leq r_n(S)$ for all $S \in C_\infty(X)$ compact operators such that complex reflexive Banach space X . Then,

$$r_{2n-1}(S') \leq 2e \left(\prod_{k=1}^n s_k(S') \right)^{\frac{1}{n}}, \quad n \in \mathbb{N}$$

where S' is dual operator of S .

Proof. Since (r_n) is an injective and surjective s -number sequence, for operator $Q'_1 \in L(X', l_\infty^n)$ and $J'_\infty \in L(l_1^n, X')$ we have

$$r_{2n-1}(S') = r_{2n-1}(Q'_1 S' J'_\infty) \leq \left(\prod_{k=1}^n r_{2k-1}(Q'_1 S' J'_\infty) \right)^{\frac{1}{n}}. \tag{8}$$

We easily see that for J'_∞ , an operator acting in Hilbert space, and (s_n) , a multiplicative injective and surjective s -number sequence, we can write

$$\begin{aligned} \left(\prod_{k=1}^n r_{2k-1}(Q'_1 S' J'_\infty) \right)^{\frac{1}{n}} &= \left(\prod_{k=1}^n s_{2k-1}(Q'_1 S' J'_\infty) \right)^{\frac{1}{n}} \\ &\leq \left(\prod_{k=1}^n c_k(Q'_1)^{\frac{1}{2}} s_k(S') d_k(J'_\infty)^{\frac{1}{2}} \right)^{\frac{1}{n}}. \end{aligned} \tag{9}$$

Moreover we have from Theorem 1 and Theorem 2,

$$\left(\prod_{k=1}^n c_k(Q'_1)^{\frac{1}{2}} s_k(S') d_k(J'_\infty)^{\frac{1}{2}} \right)^{\frac{1}{n}} = \left(\prod_{k=1}^n d_k(Q_1)^{\frac{1}{2}} s_k(S') c_k(J_\infty)^{\frac{1}{2}} \right)^{\frac{1}{n}}. \tag{10}$$

Thus using property (iii) of Definition 2, J_∞ is an operator acting in Hilbert space, $\|J_\infty\| \leq 1$ and $\|Q_1\| \leq 1$ we obtain

$$\begin{aligned} \left(\prod_{k=1}^n d_k(Q_1)^{\frac{1}{2}} s_k(S') c_k(J_\infty)^{\frac{1}{2}} \right)^{\frac{1}{n}} &\leq \left(\prod_{k=1}^n \|Q_1\| d_k(I_n: l_1^n \rightarrow l_1^n) s_k(S') c_k(I_n: l_\infty^n \rightarrow l_\infty^n) \|J_\infty\| \right)^{\frac{1}{n}} \\ &\leq \left(\prod_{k=1}^n d_k(I_n: l_1^n \rightarrow l_1^n) s_k(S') c_k(I_n: l_\infty^n \rightarrow l_\infty^n) \right)^{\frac{1}{n}}, \end{aligned} \tag{11}$$

where I_n is a identity map. Since I_n is an operator acting in Hilbert space and combining Eqns. (8)-(11) we arrive

$$r_{2n-1}(S) \leq \left(\prod_{k=1}^n x_k(I_n: l_1^n \rightarrow l_1^n) s_k(S') x_k(I_n: l_\infty^n \rightarrow l_\infty^n) \right)^{\frac{1}{n}}.$$

We get the following estimates by using the identity maps I_n for $n = 1, 2, \dots$ with Lemma 2, from the last equation and known inequality $\frac{n^n}{n!} \leq e^n$,

$$r_{2n-1}(S') \leq 2e \left(\prod_{k=1}^n s_k(S') \right)^{\frac{1}{n}}.$$

4. Conclusion

In this study, the role and importance of s -numbers in the literature were investigated. First of all, the development of s -numbers in Banach spaces in the literature was given. Moreover, Weyl-type inequalities, which have an important place in applied mathematics, were presented. Information about the optimality of these Weyl-type inequalities was given. New Weyl-type inequalities were obtained by using multiplicative injective and surjective s -numbers and dual s -numbers in complex reflexive Banach spaces. In addition, important relations for dual operators were expressed.

References

- [1] Pietsch, A., *s-number of operators in Banach spaces*, Studia Math., 51, 201-233, 1974.
- [2] Weyl, H., *Inequalities between two kinds of eigenvalues of a linear transformation*, Proceedings of National Academy of Sciences USA, 35, 408-411, 1949.
- [3] Pietsch, A., *Weyl numbers and eigenvalues of operators in Banach spaces*, Mathematische Annalen, 247, 149-168, 1980.
- [4] Carl, B., Hincichs, A., *Optimal Weyl-type inequalities for operators in Banach spaces*, Positivity, 11, 41-55, 2007.
- [5] Pietsch, A., *Eigenvalues and s-numbers*, Cambridge University Press, 1987.
- [6] König, H., *Eigenvalues of compact operators with applications to integral operators*, Linear Algebra and its Applications, 84, 111-122, 1986.
- [7] König, H., *Eigenvalues of operators and application*, Handbook of Geometry of Banach Spaces, North-Holland, Amsterdam, 1, 941-974, 2001.
- [8] Carl, B., *On a Weyl inequalities of operators in Banach spaces*, Proceedings of the American Mathematical Society, 137, 155-159, 2009.
- [9] Carl, B., Hincichs, A., *On s-numbers and Weyl inequalities of operators in Banach spaces*, The Bulletin of the London Mathematical Society, 41, 2, 332-340, 2009.
- [10] Kochubei, A.N., *Symmetric Operators and Nonclassical Spektral Problems*, Matematicheskie Zametki, 25, 425-434, 1979.
- [11] Barramov, E., Öztürk Mert, R., Ismailov, Z.I., *Selfadjoint Extensions of a Singular Differential Operators*, Journal of Mathematical Chemistry, 50, 1100-1110, 2012.
- [12] Ismailov, Z.I, Cona L., Cevik, E.O., Guler, B.O., *Weyl Numbers of Diagonal Matrices*, AIP Conference Proceedings, Vol. 1611, 296-299, 2014.

- [13] Ismailov, Z.I, Cona L., Cevik, E.O., *Gelfand Numbers of Diagonal Matrices*, Hacettepe Journal of Mathematics and Statistics, 44(1), 75-81, 2015.
- [14] Pietsch, A., *Operator ideals*, North Holland, Amsterdam, New York, Oxford, 1980.
- [15] Pietsch, A., *History of Banach spaces and linear operators*, Birkhäuser, 2007.
- [16] Timoshenkox, A., *Theory of elastic stability*, Mc Grow-Hill, New York, 1961.
- [17] Ipek Al, P., Ismailov, Z.I., *Lorentz-Schatten characteristic of compact inverses of first order normal differential operators*, The Mediterranean International Conference of Pure Applied Mathematics and Related Areas (MICOPAM 2018), 200-203, 2018.
- [18] Ipek Al, P., Ismailov, Z.I., *Singular numbers of lower triangular one-band block operator matrices*, International Conference on Mathematics “An Istanbul Meeting for World Mathematicians” Minisymposium on Approximation Theory Minisymposium on Math Education (ICOM 2018), 184-189, 2018.
- [19] Öztürk Mert, R., Ipek Al, P., Ismailov, Z.I., *Lorentz-Schatten property of the inverses of second order differential operators with Dirichlet conditions*, Current Academic Studies in Natural Science and Mathematics Sciences, Mehmet Ali Kandemir, Fatma Erdoğan, Editor, IVPE, ss.155-161, 2019.
- [20] Ipek Al, P., Ismailov, Z.I., *Schatten-von Neumann characteristic of infinite tridiagonal block operator matrices*, Communications Faculty of Science University of Ankara Series A1 Mathematics and Statistics, 68(2), 1852-1866, 2019.
- [21] Ipek Al, P., Ismailov, Z.I., *Compact inverses of first order normal differential operators with Lorentz-Schatten properties*, 3. International Conference on Mathematics: An Istanbul Meeting for World Mathematicians (ICOM 2019), 359-363, 2019.
- [22] Ipek Al, P., Ismailov, Z.I., *Schatten-von Neumann characteristic of tensor product operators*, Filomat, 34(10), 2020.
- [23] Ipek Al, P., *Lorentz-Schatten classes of direct sum of operators*, Hacettepe Journal of Mathematics and Statistics, 49(2), 835-842, 2020.
- [24] Ipek Al, P., *Lorentz-Marcinkiewicz property of direct sum of operators*, Filomat, 34(2), 391-398, 2020.



Direct Product of Bitonic Algebras

Şule AYAR ÖZBAL^{1,*}

¹Yaşar University, Faculty of Science and Letter, Department of Mathematics, 35100, İzmir, Türkiye
sule.ayar@yasar.edu.tr, ORCID: 0000-0001-5933-5858

Received: 03.01.2022

Accepted: 21.04.2022

Published: 30.06.2022

Abstract

The purpose of this study is to construct the concept of direct product of bitonic algebras, and investigate some respective features. Also, the concept of direct product of commutative bitonic algebras, bitonic homomorphism are studied. Then the notion of direct product of bitonic algebras is expanded to finite family of bitonic algebras and their qualifications are practised.

Keywords: Bitonic algebras; Direct product; Homomorphisms; Filters.

Bitonic Cebirlerin Direkt Çarpımları

Öz

Bu çalışmanın amacı bitonic cebirlerin direkt çarpımları olup bitonic cebirlerin direkt çarpımlarının ilgili özelliklerini çalışmaktır. Ayrıca, değişmeli bitonic cebirlerinin direkt çarpımları, bitonic homomorfizmalar incelenmiş ve değişmeli bitonic cebirlerin direkt çarpımlarının da değişmeli olduğu elde edilmiş ve direkt çarpımların homomorfizmaları da çalışılmıştır.

Anahtar Kelimeler: Bitonic cebirleri; Direk çarpım; Homomorfizmalar; Süzgeçler.



1. Introduction

In 1984, the form of BCC-algebras was presented by Komori [1] and Dudek [2] as a generalization of BCK algebra that was introduced by Iseki [3] in 1966 and studied by him and Tanaka [4] in 1978. A dual BCC-algebra is an algebraic system $(X, *, 1)$ satisfies the following axioms: (D1) $(x * y) * ((y * z) * (x * z)) = 1$, (D2) $1 * x = x$, (D3) $x * 1 = 1$, (D4) $x * x = 1$, (D5) $x * y = 1$ and $y * x = 1$ imply $x = y$. The notion of dual BCC-algebra is a generalization of DBCK-algebras [5-7], Hilbert algebras [8-11], Heyting algebras [12, 13], implications algebras [14] and lattice implication algebras [15, 16]. The property (P): $x \leq y$ implies $z * x \leq z * y$ and $y * z \leq x * z$ is satisfied by all such algebras. Indeed, it can be said that these are the algebras that have the axiom (P). The notion of bitonic algebra as a generalization of dual BCC-algebra was introduced by Yong Ho Yon and Şule Ayar Özbal in 2018 [17]. The notion of direct product was firstly studied in group and some of their generalizations were obtained, such as the direct product of the group is a group and the direct product of the abelian group is again an abelian group are the ones that can be given as properties that are obtained in these studies. In 2016, the notion of direct product of B-algebra, 0-commutative B-algebra and B-homomorphism were studied by Lingcong and Endham [18]. In 2020, the concept of direct product of BP-algebras was given by Setani, Gemawati and Deswita [19]. The purpose of this study is to construct the concept of direct product of bitonic algebras, and investigate commutative direct product of commutative bitonic algebras and also homomorphisms on direct product of bitonic algebras are studied.

2. Preliminaries

Definition 1. [17] A bitonic algebra is an algebraic systems $(A, *, 1)$ where A is a set, 1 is an element in A and $*$ is a binary operation on A , satisfying the following axioms for every $a, b, c \in A$,

$$(B1) \ a * 1 = 1,$$

$$(B2) \ 1 * a = a,$$

$$(B3) \ a * b = 1 \text{ and } b * a = 1 \text{ implies } a = b,$$

$$(B4) \ a * b = 1 \text{ implies } (c * a) * (c * b) = 1 \text{ and } (b * c) * (a * c) = 1.$$

Example 1. [17] Let $N = \{1, x, y, z, w\}$ be a set. If we define a binary operation $*$ on N by the following table:

Table 1: Cayley table of binary operation $*$ on N

$*$	l	x	y	z	w
l	l	x	y	z	w
x	l	l	y	z	w
y	l	x	l	z	w
z	l	l	l	l	x
w	l	l	l	z	l

Then $(N, *, 1)$ is a bitonic algebra with Hasse diagram given below.

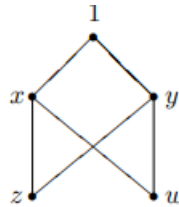


Diagram 1: Hasse diagram of the bitonic algebra N in Example 1

Definition 2. [17] Let A be a bitonic algebra a nonempty subset S of A is labeled a bitonic subalgebra of A if $x * y \in S$ for every $x, y \in S$ and F as a nonempty subset of A is labeled a filter of A if it performs:

(F1) $1 \in F$

(F2) $e \in F$ and $e * f \in F$ imply $f \in F$ for any $e, f \in F$.

Definition 3. [17] A bitonic algebra $(A, *, 1)$ is said to be commutative if $(a * b) * b = (b * a) * a$ for all $a, b \in A$.

3. Direct product of Bitonic algebras

Definition 4. Let $(A; *, 1_A)$ and $(B; *', 1_B)$ be bitonic algebras. The direct product of A and B is an algebraic nature $A \times B = (A \times B; \otimes, (1_A, 1_B))$ where $A \times B$ is the set $\{(a, b) | a \in A, b \in B\}$ and the binary operation \otimes is given by $(a_1, b_1) \otimes (a_2, b_2) = (a_1 * a_2, b_1 *', b_2)$.

Example 2. Let $A = \{1_A, a, b, c\}$ be a set. If a binary relation $*$ on A is illustrated by the following table:

Table 2: Cayley table of binary relation $*$ on A in Example 1

$*$	1_A	a	b	c
1_A	1_A	a	b	c
a	1_A	1_A	b	c
b	1_A	a	1_A	c
c	1_A	1_A	1_A	1_A

then $(A; *, 1_A)$ is a bitonic algebra.

Let $B = \{1_B, x, y, 0\}$ be a set. If we define a binary relation $*'$ on B by the following table:

Table 3: Cayley table of binary relation $*'$ on A in Example 1

$*'$	1_B	x	y	0
1_B	1_B	x	y	0
x	1_B	1_B	y	y
y	1_B	x	1_B	0
0	1_B	1_B	1_B	1_B

then $(B; *', 1_B)$ is a bitonic algebra. It is clear that the direct product of A and B is a bitonic algebra $A \times B = (A \times B; \otimes, (1_A, 1_B))$ whose Cayley table is given below

Table 4: Cayley table of binary relation \otimes on $A \times B$ given in Example 1

\otimes	$(1_A, 1_B)$	$(1_A, x)$	$(1_A, y)$	$(1_A, 0)$	$(a, 1_B)$	(a, x)	(a, y)	$(a, 0)$	$(b, 1_B)$	(b, x)	(b, y)	$(b, 0)$	$(c, 1_B)$	(c, x)	(c, y)	$(c, 0)$
$(1_A, 1_B)$	$(1_A, 1_B)$	$(1_A, x)$	$(1_A, y)$	$(1_A, 0)$	$(a, 1_B)$	(a, x)	(a, y)	$(a, 0)$	$(b, 1_B)$	(b, x)	(b, y)	$(b, 0)$	$(c, 1_B)$	(c, x)	(c, y)	$(c, 0)$
$(1_A, x)$	$(1_A, 1_B)$	$(1_A, 1_B)$	$(1_A, y)$	$(1_A, y)$	$(a, 1_B)$	$(a, 1_B)$	(a, y)	(a, y)	$(b, 1_B)$	$(b, 1_B)$	(b, y)	(b, y)	$(c, 1_B)$	$(c, 1_B)$	(c, y)	(c, y)
$(1_A, y)$	$(1_A, 1_B)$	$(1_A, x)$	$(1_A, 1_B)$	$(1_A, 0)$	$(a, 1_B)$	$(a, 1_B)$	(a, x)	$(a, 0)$	$(b, 1_B)$	(b, x)	$(b, 1_B)$	$(b, 0)$	$(c, 1_B)$	(c, x)	$(c, 1_B)$	$(c, 0)$
$(1_A, 0)$	$(1_A, 1_B)$	$(1_A, 1_B)$	$(1_A, 1_B)$	$(1_A, 1_B)$	$(a, 1_B)$	$(a, 1_B)$	$(a, 1_B)$	$(a, 1_B)$	$(b, 1_B)$	$(b, 1_B)$	$(b, 1_B)$	$(b, 1_B)$	$(c, 1_B)$	$(c, 1_B)$	$(c, 1_B)$	$(c, 1_B)$
$(a, 1_B)$	$(1_A, 1_B)$	$(1_A, x)$	$(1_A, y)$	$(1_A, 0)$	$(1_A, 1_B)$	$(1_A, x)$	$(1_A, y)$	$(1_A, 0)$	$(b, 1_B)$	(b, x)	(b, y)	$(b, 0)$	$(c, 1_B)$	(c, x)	(c, y)	$(c, 0)$
(a, x)	$(1_A, 1_B)$	$(1_A, 1_B)$	$(1_A, y)$	$(1_A, y)$	$(1_A, 1_B)$	$(1_A, 1_B)$	$(1_A, y)$	$(1_A, y)$	$(b, 1_B)$	$(b, 1_B)$	(b, y)	(b, y)	$(c, 1_B)$	$(c, 1_B)$	(c, y)	(c, y)
(a, y)	$(1_A, 1_B)$	$(1_A, x)$	$(1_A, 1_B)$	$(1_A, 0)$	$(1_A, 1_B)$	$(1_A, x)$	$(1_A, 1_B)$	$(1_A, 0)$	$(b, 1_B)$	(b, x)	$(b, 1_B)$	$(b, 0)$	$(c, 1_B)$	(c, x)	$(c, 1_B)$	(c, y)
$(a, 0)$	$(1_A, 1_B)$	$(1_A, 1_B)$	$(1_A, 1_B)$	$(1_A, 1_B)$	$(1_A, 1_B)$	$(1_A, 1_B)$	$(1_A, 1_B)$	$(1_A, 1_B)$	$(b, 1_B)$	$(b, 1_B)$	$(b, 1_B)$	$(b, 1_B)$	$(c, 1_B)$	$(c, 1_B)$	$(c, 1_B)$	$(c, 1_B)$
$(b, 1_B)$	$(1_A, 1_B)$	$(1_A, x)$	$(1_A, y)$	$(1_A, 0)$	$(a, 1_B)$	(a, x)	(a, y)	$(a, 0)$	$(1_A, 1_B)$	$(1_A, x)$	$(1_A, y)$	$(1_A, 0)$	$(c, 1_B)$	(c, x)	(c, y)	$(c, 0)$
(b, x)	$(1_A, 1_B)$	$(1_A, 1_B)$	$(1_A, y)$	$(1_A, y)$	$(a, 1_B)$	$(a, 1_B)$	(a, y)	(a, y)	$(1_A, 1_B)$	$(1_A, 1_B)$	$(1_A, y)$	$(1_A, y)$	$(c, 1_B)$	$(c, 1_B)$	(c, y)	(c, y)
(b, y)	$(1_A, 1_B)$	$(1_A, x)$	$(1_A, 1_B)$	$(1_A, 0)$	$(a, 1_B)$	(a, x)	$(a, 1_B)$	$(a, 0)$	$(1_A, 1_B)$	$(1_A, 1_B)$	$(1_A, x)$	$(1_A, 0)$	$(c, 1_B)$	(c, x)	$(c, 1_B)$	$(c, 0)$
$(b, 0)$	$(1_A, 1_B)$	$(1_A, 1_B)$	$(1_A, 1_B)$	$(1_A, 1_B)$	$(a, 1_B)$	$(a, 1_B)$	$(a, 1_B)$	$(a, 1_B)$	$(1_A, 1_B)$	$(1_A, 1_B)$	$(1_A, 1_B)$	$(1_A, 1_B)$	$(c, 1_B)$	$(c, 1_B)$	$(c, 1_B)$	$(c, 1_B)$
$(c, 1_B)$	$(1_A, 1_B)$	$(1_A, x)$	$(1_A, y)$	$(1_A, 0)$	$(1_A, 1_B)$	$(1_A, x)$	$(1_A, y)$	$(1_A, 0)$	$(1_A, 1_B)$	$(1_A, x)$	$(1_A, y)$	$(1_A, 0)$	$(1_A, 1_B)$	$(1_A, x)$	$(1_A, y)$	$(1_A, 0)$
(c, x)	$(1_A, 1_B)$	$(1_A, 1_B)$	$(1_A, 1_B)$	$(1_A, 1_B)$	$(1_A, 1_B)$	$(1_A, 1_B)$	$(1_A, 1_B)$	$(1_A, 1_B)$	$(1_A, y)$	$(1_A, y)$	$(1_A, y)$	$(1_A, y)$	$(1_A, y)$	$(1_A, y)$	$(1_A, y)$	$(1_A, y)$
(c, y)	$(1_A, 1_B)$	$(1_A, 1_B)$	$(1_A, 1_B)$	$(1_A, 1_B)$	$(1_A, x)$	$(1_A, x)$	$(1_A, x)$	$(1_A, x)$	$(1_A, 1_B)$	$(1_A, 1_B)$	$(1_A, y)$	$(1_A, 1_B)$	$(1_A, 0)$	$(1_A, 0)$	$(1_A, 0)$	$(1_A, 0)$
$(c, 0)$	$(1_A, 1_B)$	$(1_A, 1_B)$	$(1_A, 1_B)$	$(1_A, 1_B)$	$(1_A, 1_B)$	$(1_A, 1_B)$	$(1_A, 1_B)$	$(1_A, 1_B)$	$(1_A, 1_B)$	$(1_A, 1_B)$	$(1_A, 1_B)$	$(1_A, 1_B)$	$(1_A, 1_B)$	$(1_A, 1_B)$	$(1_A, 1_B)$	$(1_A, 1_B)$

The next theorem is one of the main theorems of this study.

Theorem 1. $(A; *, 1_A)$ and $(B; *', 1_B)$ are bitonic algebras if and only if $(A \times B; \otimes, (1_A, 1_B))$ is a bitonic algebra.

Proof. Let $(A; *, 1_A)$ and $(B; *', 1_B)$ be bitonic algebras, then we have $z * 1_A = 1_A$ and $f *' 1_B = 1_B$, $1_A * z = z$ and $1_B *' f = f$ for ant elements $z \in A$ and $f \in B$. The direct product of A and B is an algebraic nature $(A \times B; \otimes, (1_A, 1_B))$.

Thus, for all $(z, f) \in A \times B$ we have

$$(z, f) \otimes (1_A, 1_B) = (z * 1_A, f *' 1_B) = (1_A, 1_B). \quad (1)$$

Then axiom (B1) is satisfied.

We have

$$(1_A, 1_B) \otimes (z, f) = (1_A * z, 1_B *' f) = (z, f). \quad (2)$$

Then the axiom (B2) is satisfied.

Let $(z, f), (x, x) \in A \times B$. Then $(z, f) \otimes (x, x) = (1_A, 1_B)$ and $(x, x) \otimes (z, f) = (1_A, 1_B)$, that is $(z * x, f *' x) = (1_A, 1_B)$ and $(x * z, x *' f) = (1_A, 1_B)$. Since $z, x \in A$, $f, x \in B$ we have $z * x = 1_A$ and $x * z = 1_A$ imply $z = x$ and $f *' x = 1_B$ and $x *' f = 1_B$ imply $f = x$ we get $(z, f) = (x, x)$. So, axiom (B3) is satisfied.

Let $(z, f), (x, x), (q, q) \in A \times B$ and $(z, f) \otimes (x, x) = (1_A, 1_B)$. Hence, we get $z * x = 1_A$, $f *' x = 1_B$ for all $z, x \in A$, $f, x \in B$. Since A and B are bitonic algebras, we have $(z * z) * (z * x) = 1_A$ and $(q *' f) *' (q *' x) = 1_B$ and $(x * z) * (z * z) = 1_A$ and $(x *' q) *' (f *' q) = 1_B$. Then we have

$$\begin{aligned} ((z, q) \otimes (z, f)) \otimes ((z, q) \otimes (x, x)) &= (z * z, q *' f) \otimes (z * x, q *' x) \\ &= ((z * z) * (z * x), (q *' f) *' (q *' x)) \\ &= (1_A, 1_B) \end{aligned} \quad (3)$$

and

$$\begin{aligned} ((x, y) \otimes (p, q)) \otimes ((a, b) \otimes (p, q)) &= (x * p, y *' q) \otimes (a * p, b *' q) \\ &= ((x * p) * (a * p), (y *' q) *' (b *' q)) \end{aligned}$$

$$= (1_A, 1_B). \tag{4}$$

So, the axiom (B4) is satisfied. Finally, it is obvious that (B1), (B2), (B3), (B4) are satisfied for bitonic algebras. Hence, $A \times B$ is a bitonic algebra.

Conversely, let $A \times B$ be bitonic algebras and let $(a, b), (x, y), (p, q)$ be in $A \times B$. Then we have $(a, b) \otimes (1_A, 1_B) = (1_A, 1_B)$ that is $a * 1_A = 1_A$ and $b *' 1_B = 1_B$. So, axiom (B1) is satisfied for A and B .

Also, $(1_A, 1_B) \otimes (a, b) = (a, b)$, that is $1_A * a = a$ and $1_B *' b = b$. This means that axiom (B2) is satisfied for A and B .

We also have $(\mathfrak{z}, \mathfrak{f}) \otimes (\mathfrak{K}, \mathfrak{X}) = (1_A, 1_B)$ and $(\mathfrak{K}, \mathfrak{X}) \otimes (\mathfrak{z}, \mathfrak{f}) = (1_A, 1_B)$ implying that $(\mathfrak{K}, \mathfrak{X}) = (\mathfrak{z}, \mathfrak{f})$. That is $\mathfrak{z} * \mathfrak{K} = 1_A$ and $\mathfrak{K} * \mathfrak{z} = 1_A$ implying $\mathfrak{z} = \mathfrak{K}$, and $\mathfrak{f} *' \mathfrak{X} = 1_B$ and $\mathfrak{X} *' \mathfrak{f} = 1_B$ implying $\mathfrak{f} = \mathfrak{X}$. Hence, axiom (B3) is satisfied for A and B .

Additionally, $(a, b) \otimes (x, y) = (1_A, 1_B)$ implies that $((p, q) \otimes (a, b)) \otimes ((p, q) \otimes (x, y)) = (1_A, 1_B)$ and $((x, y) \otimes (p, q)) \otimes ((a, b) \otimes (p, q)) = (1_A, 1_B)$. So, $a * x = 1_A$ implies that $(p * a) * (p * x) = 1_A$ and $(x * p) * (a * p) = 1_A$ and $b *' y = 1_B$ implies that $(q *' b) *' (q *' y) = 1_B$ and $(y *' q) *' (y *' b) = 1_B$. Thus, axiom (B4) is satisfied for A and B . Therefore, A and B are bitonic algebras.

Also, we can generalize this product to any finite family of bitonic algebras.

Definition 5. Let $(A_i, *^i, 1_i)$ be a finite family of bitonic algebras for each $i \in \{1, \dots, s\}$. Then we can define direct product of A_i to be the structure $(\prod_{i=1}^s A_i; \otimes, (1_{A_1}, \dots, 1_{A_s}))$ whose operation is $(a_1, \dots, a_s) \otimes (x_1, \dots, x_s) = (a_1 *^1 x_1, \dots, a_s *^s x_s)$ for all $a_i, x_i \in A_i, i \in \{1, \dots, s\}$.

Then we have the following corollary.

Corollary 1. $(A_1, *^1, 1_1), (A_2, *^2, 1_2), \dots, (A_s, *^s, 1_s)$ are bitonic algebras if and only if $(\prod_{i=1}^s A_i; \otimes, (1_{A_1}, \dots, 1_{A_s}))$ is a bitonic algebra for $i \in \{1, \dots, s\}$.

Proof. Clear.

Corollary 2. Let $(A_i, *^i, 1_i)$ be a finite family of bitonic algebras for each $i \in \{1, \dots, s\}$. Then each A_i is commutative bitonic algebras if and only if $(\prod_{i=1}^s A_i; \otimes, (1_{A_1}, \dots, 1_{A_s}))$ is commutative.

Proof. Let each of $(A_i, *^i, 1_i)$ be commutative for all $i \in \{1, \dots, s\}$. If $(a_1, \dots, a_s), (b_1, \dots, b_s) \in \prod_{i=1}^s A_i$, then $(a_i *^i b_i) *^i b_i = (b_i *^i a_i) *^i a_i$ for all $a_i, b_i \in A_i$ and $i \in \{1, \dots, s\}$. Then we have

$$\begin{aligned}
 ((a_1, \dots, a_s) \otimes (b_1, \dots, b_s)) \otimes ((b_1, \dots, b_s)) &= ((a_1 *^1 b_1), \dots, (a_s *^s b_s)) \otimes (b_1, \dots, b_s) \\
 &= ((a_1 *^1 b_1) *^1 b_1, \dots, (a_s *^s b_s) *^s b_s) \\
 &= ((b_1 *^1 a_1) *^1 a_1, \dots, (b_s *^s a_s) *^s a_s) \\
 &= ((b_1 *^1 a_1), \dots, (b_s *^s a_s)) \otimes (a_1, \dots, a_s) \\
 &= ((b_1, \dots, b_s) \otimes (a_1, \dots, a_s)) \otimes ((a_1, \dots, a_s)). \tag{5}
 \end{aligned}$$

This implies $\prod_{i=1}^s A_i$ is commutative.

Conversely, let $\prod_{i=1}^s A_i$ be commutative. This is to say, if $a_i, b_i \in A_i$ for all $i \in \{1, \dots, s\}$ then $(a_1, \dots, a_s), (b_1, \dots, b_s) \in \prod_{i=1}^s A_i$. We have

$$\begin{aligned}
 ((a_1, \dots, a_s) \otimes (b_1, \dots, b_s)) \otimes ((b_1, \dots, b_s)) \\
 = ((b_1, \dots, b_s) \otimes (a_1, \dots, a_s)) \otimes ((a_1, \dots, a_s)). \tag{6}
 \end{aligned}$$

That is

$$\begin{aligned}
 ((a_1 *^1 b_1) *^1 b_1, \dots, (a_s *^s b_s) *^s b_s) &= ((b_1 *^1 a_1), \dots, (b_s *^s a_s)) \otimes ((a_1, \dots, a_s)) \\
 &= ((b_1 *^1 a_1) *^1 a_1, \dots, (b_s *^s a_s) *^s a_s). \tag{7}
 \end{aligned}$$

Hence, we get $(a_i *^i b_i) *^i b_i = (b_i *^i a_i) *^i a_i$ for all $a_i, b_i \in A_i$ and $i \in \{1, \dots, s\}$. Therefore, each A_i is commutative.

2. Homomorphisms of direct product of Bitonic algebras

Definition 6. Let $(X; *, 1_X)$ and $(Y; *', 1_Y)$ be bitonic algebras. An assignment $\beta: X \rightarrow Y$ is labeled a bitonic homomorphism if $\beta(x * y) = \beta(x) *' \beta(y)$ for any $x, y \in X$.

Theorem 2. Let $(A_i, *^i, 1_i)$ and $(B_i, *^i, 1_i)$ be a finite family of bitonic algebras and $\beta_i: A_i \rightarrow B_i$ be bitonic homomorphisms for each $i \in \{1, \dots, s\}$. If the mapping $\beta: \prod_{i=1}^s A_i \rightarrow \prod_{i=1}^s B_i$ given by $\beta(a_1, \dots, a_s) = (\beta(a_1), \dots, \beta(a_s))$, then β is a bitonic homomorphism with $\ker \beta = \prod_{i=1}^s \ker \beta_i$, $\beta(\prod_{i=1}^s A_i) = \prod_{i=1}^s \beta_i(A_i)$.

Proof. Let $(A_i, *^i, 1_i)$ and $(B_i, *^i, 1_i)$ be a finite family of bitonic algebras and $\beta_i: A_i \rightarrow B_i$ be bitonic homomorphisms for each $i \in \{1, \dots, s\}$ and let β be the mapping $\prod_{i=1}^s A_i \rightarrow \prod_{i=1}^s B_i$ given by $(a_1, \dots, a_s) \mapsto (\beta(a_1), \dots, \beta(a_s))$.

Let $(a_1, \dots, a_s), (b_1, \dots, b_s) \in \prod_{i=1}^s A_i$, then

$$\begin{aligned}
 \beta((a_1, \dots, a_s) \otimes (b_1, \dots, b_s)) &= \beta(a_1 *^1 b_1, \dots, a_s *^s b_s) \\
 &= (\beta_1(a_1 *^1 b_1), \dots, \beta_s(a_s *^s b_s)) \\
 &= (\beta_1(a_1) *^1 \beta_1(b_1), \dots, \beta_s(a_s) *^s \beta_s(b_s)) \\
 &= (\beta_1(a_1), \dots, \beta_s(a_s)) \otimes (\beta_1(b_1), \dots, \beta_s(b_s)) \\
 &= \beta((a_1, \dots, a_s)) \otimes \beta((b_1, \dots, b_s)). \tag{8}
 \end{aligned}$$

Thus, we have that β is a bitonic homomorphism. Also, if β is a bitonic homomorphism, then each β_i is a bitonic homomorphism.

Let $(a_1, \dots, a_s) \in \ker \beta$. Then

$$\begin{aligned}
 (a_1, \dots, a_s) \in \ker \beta &\Leftrightarrow \beta((a_1, \dots, a_s)) = (1_1, \dots, 1_s) \\
 &\Leftrightarrow (\beta_1(a_1), \dots, \beta_s(a_s)) = (1_1, \dots, 1_s) \\
 &\Leftrightarrow \beta_i(a_i) = 1_i \text{ for each } i \in \{1, \dots, s\} \\
 &\Leftrightarrow a_i \in \ker \beta_i \text{ for each } i \in \{1, \dots, s\} \\
 &\Leftrightarrow (a_1, \dots, a_s) \in \prod_{i=1}^s \ker \beta_i. \tag{9}
 \end{aligned}$$

That is to say $\ker \beta = \prod_{i=1}^s \ker \beta_i$.

Finally, let β be one-to-one. If $\beta_i(a_i) = \beta_i(b_i)$ for each $i \in \{1, \dots, s\}$, then

$$\begin{aligned}
 \beta((a_1, \dots, a_s)) &= (\beta_1(a_1), \dots, \beta_s(a_s)) \\
 &= (\beta_1(b_1), \dots, \beta_s(b_s)) \\
 &= \beta((b_1, \dots, b_s)). \tag{10}
 \end{aligned}$$

We have that β is one-to-one, therefore $(a_1, \dots, a_s) = (b_1, \dots, b_s)$. Hence, $a_i = b_i$ for each $i \in \{1, \dots, s\}$. That is β_i is one-to-one for each $i \in \{1, \dots, s\}$.

Conversely, let β_i be one-to-one for each $i \in \{1, \dots, s\}$. If $\beta((a_1, \dots, a_s)) = \beta((b_1, \dots, b_s))$, then

$$\begin{aligned} (\beta_1(a_1), \dots, \beta_s(a_s)) &= \beta((a_1, \dots, a_s)) \\ &= \beta((b_1, \dots, b_s)) \\ &= (\beta_1(b_1), \dots, \beta_s(b_s)). \end{aligned} \tag{11}$$

Since $\beta_i(a_i) = \beta_i(b_i)$ for each $i \in \{1, \dots, s\}$ and all β_i is one-to-one, we get $a_i = b_i$ for each $i \in \{1, \dots, s\}$ and hence $(a_1, \dots, a_s) = (b_1, \dots, b_s)$. So, β is one-to-one.

Finally, let β be onto. If $(b_1, \dots, b_s) \in \prod_{i=1}^s B_i$ then $(b_1, \dots, b_s) = \beta((a_1, \dots, a_s)) = (\beta_1(a_1), \dots, \beta_s(a_s))$. Hence $b_i = \beta_i(a_i)$ for some $i \in \{1, \dots, s\}$. Therefore, β_i is onto for all $i \in \{1, \dots, s\}$.

Conversely, let β_i be onto for all $i \in \{1, \dots, s\}$. If $(b_1, \dots, b_s) \in \prod_{i=1}^s B_i$ then $b_i \in B_i$ for all $i \in \{1, \dots, s\}$. So, there exists $a_i \in A_i$ such that $b_i = \beta_i(a_i)$ for some $i \in \{1, \dots, s\}$ since β_i is onto. Therefore, $(b_1, \dots, b_s) = (\beta_1(a_1), \dots, \beta_s(a_s)) = \beta((a_1, \dots, a_s))$. Hence, β is onto.

Theorem 3. Let $(A_i, *^i, 1_i)$ and $(B_i, *^i, 1_i)$ be a finite family of bitonic algebras and $\beta_i: A_i \rightarrow B_i$ be bitonic homomorphisms for $i \in \{1, \dots, s\}$ and let β be given by $\prod_{i=1}^s A_i \rightarrow \prod_{i=1}^s B_i$ given by $(a_1, \dots, a_s) \mapsto (\beta(a_1), \dots, \beta(a_s))$, then $\ker_\beta = \prod_{i=1}^s \ker_{\beta_i}$ is a filter.

Proof. Let $(A_i, *^i, 1_i)$ and $(B_i, *^i, 1_i)$ be a finite family of bitonic algebras and $\beta_i: X_i \rightarrow B_i$ be bitonic homomorphisms for $i \in \{1, \dots, s\}$. Then

$$\begin{aligned} \beta((1_1, \dots, 1_s)) &= \beta(a_1 *^1 1_1, \dots, a_s *^s 1_s) = (\beta_1(a_1 *^1 1_1), \dots, \beta_s(a_s *^s 1_s)) \\ &= ((\beta_1(a_1), \dots, \beta_s(a_s)) \otimes (\beta_1(1_1), \dots, \beta_s(1_s))) \\ &= (1_1, \dots, 1_s). \end{aligned} \tag{12}$$

So, $(1_1, \dots, 1_s) \in \ker_\beta, \ker_\beta \neq \emptyset$.

Let $(a_1, \dots, a_s) \in \ker_\beta$ and $(a_1, \dots, a_s) \otimes (b_1, \dots, b_s) \in \ker_\beta$. Consider

$$\begin{aligned} (1_1, \dots, 1_s) &= \beta((a_1, \dots, a_s) \otimes (b_1, \dots, b_s)) \\ &= \beta(a_1 *^1 b_1, \dots, a_s *^s b_s) \end{aligned}$$

$$\begin{aligned}
 &= (\beta_1(a_1) *^1 \beta_1(b_1), \dots, \beta_s(a_s) *^s \beta_s(b_s)) \\
 &= \beta((a_1, \dots, a_s)) \otimes \beta((b_1, \dots, b_s)) \\
 &= (1_1, \dots, 1_s) \otimes \beta((b_1, \dots, b_s)) \\
 &= \beta((b_1, \dots, b_s)). \tag{13}
 \end{aligned}$$

This implies $(b_1, \dots, b_s) \in \ker \beta$. Therefore, $\ker \beta$ is a filter.

Theorem 4. Let $(A_i, *^i, 1_i)$ and $(B_i, *^i, 1_i)$ be a finite family of bitonic algebras and $\beta_i: A_i \rightarrow B_i$ be bitonic homomorphisms for $i \in \{1, \dots, s\}$ and let $\beta: \prod_{i=1}^s A_i \rightarrow \prod_{i=1}^s B_i$ given by $\beta(a_1, \dots, a_s) = (\beta(a_1), \dots, \beta(a_s))$ then

- i) β is a bitonic monomorphism if and only if β_i is a bitonic monomorphism.
- ii) β is a bitonic onto homomorphism if and only if β_i is a onto homomorphism.

Proof. Let $(A_i, *^i, 1_i)$ and $(B_i, *^i, 1_i)$ be a finite family of bitonic algebras and $\beta_i: A_i \rightarrow B_i$ be bitonic homomorphisms for $i \in \{1, \dots, s\}$ and let $\beta: \prod_{i=1}^s A_i \rightarrow \prod_{i=1}^s B_i$ given by $\beta(a_1, \dots, a_s) = (\beta(a_1), \dots, \beta(a_s))$. Then

- i) Let β be a bitonic monomorphism and $\beta_i(a_i) = \beta_i(b_i)$ for $i \in \{1, \dots, s\}$. Then,

$$(\beta_1(a_1), \dots, \beta_s(a_s)) = (\beta_1(b_1), \dots, \beta_s(b_s)) \Rightarrow \beta((a_1, \dots, a_s)) = \beta((b_1, \dots, b_s)). \tag{14}$$

Since β is a bitonic monomorphism we have $(a_1, \dots, a_s) = (b_1, \dots, b_s)$, that is $a_i = b_i$ for $i \in \{1, \dots, s\}$. Hence, we get β_i is a bitonic monomorphism.

Conversely, let β_i be bitonic monomorphisms. And consider, $\beta((a_1, \dots, a_s)) = \beta((b_1, \dots, b_s))$ for $a_i, b_i \in \prod_{i=1}^s A_i$. Then $(\beta_1(a_1), \dots, \beta_s(a_s)) = (\beta_1(b_1), \dots, \beta_s(b_s)) \Rightarrow \beta_i(a_i) = \beta_i(b_i)$. Since β_i is bitonic monomorphism we have $a_i = b_i$ for $i \in \{1, \dots, s\}$. Therefore, $(a_1, \dots, a_s) = (b_1, \dots, b_s)$ and β is a bitonic monomorphism.

- ii) Let β be a bitonic onto homomorphism and let $b_i \in B_i$ for $i \in \{1, \dots, s\}$ then we have $(b_1, \dots, b_s) \in \prod_{i=1}^s B_i$. Since β is a onto homomorphism, then $(a_1, \dots, a_s) \in \prod_{i=1}^s A_i$ for all a_i for $i \in \{1, \dots, s\}$, so $(b_1, \dots, b_s) = \beta(a_1, \dots, a_s) = (\beta_1(a_1), \dots, \beta_s(a_s))$ implying that $b_i = \beta_i(a_i)$ for $i \in \{1, \dots, s\}$. Therefore, it is proved that β_i is an onto homomorphism.

Conversely, let β_i be a bitonic epimorphism for all $i \in \{1, \dots, s\}$ and $(b_1, \dots, b_s) \in \prod_{i=1}^s B_i$, then $b_i \in B_i$. Since β_i is an onto function, then there exists $a_i \in \prod_{i=1}^s A_i$ for all $i \in$

$\{1, \dots, s\}$ such that $b_i = \beta_i(a_i)$ implying that $(b_1, \dots, b_s) = (\beta_1(a_1), \dots, \beta_s(a_s)) = \beta(a_1, \dots, a_s)$. Hence, it is proved that β is a bitonic epimorphism.

Theorem 5. Let $\{A_i = (A_i, *^i, 1_i) | i \in \{1, \dots, s\}\}$ be a family of bitonic algebras and let J_i be a filter of A_i . Then $\prod_{i=1}^s J_i$ is a filter of $\prod_{i=1}^s A_i$ and $\prod_{i=1}^s A_i / \prod_{i=1}^s J_i \cong \prod_{i=1}^s (A_i / J_i)$.

Proof. Let $\{A_i = (A_i, *^i, 1_i) | i \in \{1, \dots, s\}\}$ be a family of bitonic algebras and let J_i be a filter of A_i . Then $(1_1, \dots, 1_s) \in \prod_{i=1}^s J_i$ since $1_i \in J_i$ for all $i \in \{1, \dots, s\}$ and so $\prod_{i=1}^s J_i$ is not empty. Let $(a_1, \dots, a_s) \in \prod_{i=1}^s J_i$ and $(a_1, \dots, a_s) \otimes (b_1, \dots, b_s) \in \prod_{i=1}^s J_i$. Then $(a_1 *^1 b_1, \dots, a_s *^s b_s) \in \prod_{i=1}^s J_i$. This is to say that $(a_i *^i b_i) \in J_i$ for $i \in \{1, \dots, s\}$. Since J_i is a filter of A_i we have $b_i \in J_i$. Hence, $(b_1, \dots, b_s) \in \prod_{i=1}^s J_i$. Therefore, $\prod_{i=1}^s J_i$ is a filter.

Let $J = \prod_{i=1}^s J_i$ and $A = \prod_{i=1}^s A_i$. Define $\varpi: A/J \rightarrow \prod_{i=1}^s (A_i / J_i)$ given by $\varpi((a_1, \dots, a_s)J) = (a_1 J_1, \dots, a_s J_s) \in A/J$ for all $(a_1, \dots, a_s)J \in A/J$.

Let $(a_1, \dots, a_s)J, (b_1, \dots, b_s)J \in A/J$. If $(a_1, \dots, a_s)J = (b_1, \dots, b_s)J$, then $(a_1, \dots, a_s) \sim_J (b_1, \dots, b_s)$, that is $(a_1 *^1 b_1, \dots, a_s *^s b_s) = (a_1, \dots, a_s) \otimes (b_1, \dots, b_s) \in J$. Thus, $a_i *^i b_i \in J_i$ for all $i \in \{1, \dots, s\}$, that is $a_i \sim_{J_i} b_i$ so that $a_i J_i = b_i J_i$. Therefore, $\varpi((a_1, \dots, a_s)J) = (a_1 J_1, \dots, a_s J_s) = (b_1 J_1, \dots, b_s J_s) = \varpi((b_1, \dots, b_s)J)$. Hence, ϖ is well - defined.

If $(a_1, \dots, a_s)J, (b_1, \dots, b_s) \in A/J$, then

$$\begin{aligned} \varpi((a_1, \dots, a_s)J *^i (b_1, \dots, b_s)J) &= \varpi(((a_1, \dots, a_s) \otimes (b_1, \dots, b_s))J) \\ &= \varpi((a_1 *^1 b_1, \dots, a_s *^s b_s)J) \\ &= ((a_1 *^1 b_1)J_1, \dots, (a_s *^s b_s)J_s) \\ &= (a_1 J_1 *^1 b_1 J_1, \dots, a_s J_s *^s b_s J_s) \\ &= (a_1 J_1, \dots, a_s J_s) \otimes (b_1 J_1, \dots, b_s J_s) \\ &= \varpi((a_1, \dots, a_s)J) \otimes \varpi((b_1, \dots, b_s)J). \end{aligned} \tag{15}$$

This gives us that ϖ is a homomorphism.

If $\varpi((a_1, \dots, a_s)J) = \varpi((b_1, \dots, b_s)J)$, then

$$\begin{aligned} (a_1J_1, \dots, a_sJ_s) &= \varpi((a_1, \dots, a_s)J) \\ &= \varpi((b_1, \dots, b_s)J) = (b_1J_1, \dots, b_sJ_s). \end{aligned} \tag{16}$$

Therefore, $a_iJ_i = b_i/J_i$ for all $i \in \{1, \dots, s\}$. Hence, $a_i \sim_{J_i} b_i$ that is $a_i *^i b_i \in J_i$ for all $i \in \{1, \dots, s\}$ so that $(a_1, \dots, a_s) \otimes (b_1, \dots, b_s) = (a_1 *^1 b_1, \dots, a_s *^s b_s) \in J$. Therefore, $(a_1, \dots, a_s) \sim_J (b_1, \dots, b_s)$ and so $(a_1, \dots, a_s)J = (b_1, \dots, b_s)J$. This implies ϖ is one-to-one.

If $(a_1J_1, \dots, a_sJ_s) \in \prod_{i=1}^s (A_i/J_i)$, then $a_i \in A_i$ for all $i \in \{1, \dots, s\}$, that is $(a_1, \dots, a_s) \in A$. It gives us that $(a_1J_1, \dots, a_sJ_s) = \varpi((a_1, \dots, a_s)J)$, where $(a_1, \dots, a_s)J \in A/J$. This follows that ϖ is onto. Therefore, ϖ is a bitonic isomorphism that is $\prod_{i=1}^s A_i / \prod_{i=1}^s J_i \cong \prod_{i=1}^s (A_i / J_i)$.

References

- [1] Komori, Y., *The class of BCC-algebras is not variety*, *Mathematica Japonica*, 29 (3), 391-394, 1984.
- [2] Dudek, W.A., *The number of subalgebras of finite BCC-algebras*, *Bulletin of the Institute of Mathematics*, 20 (2), 129-135, 1992.
- [3] Iseki, K., *An algebra related with a propositional calculus*, *Proceedings of the Japan Academy*, 42 (1), 26-29, 1966.
- [4] Iseki, K., Tanaka, S., *An Introduction to the theory of BCK-algebras*, *Mathematica Japonica*, 23, 1-26, 1978.
- [5] Borzooei, R.A., Khosravi Shoar, S., *Implication algebras are equivalent to the dual implicative BCK-algebras*, *Scientiae Mathematicae Japonicae*, 63 (3), 429-431, 2006.
- [6] Kim, K.H., Yon, Y.H., *Dual BCK-algebra and MV-algebra*, *Scientiae Mathematicae Japonicae*, 66 (2), 247-253, 2007.
- [7] Yon, Y.H., Kim, K.H., *On Heyting algebras and dual BCK-algebras*, *Bulletin of the Iranian Mathematical Society*, 38 (1), 159-168, 2012.
- [8] Diego, A., *Sur les algèbres de Hilbert*, *Collection de Logique Mathématique, Sér. A.*, 21, 1966.
- [9] Halas, R., *Remarks on commutative Hilbert algebras*, *Mathematica Bohemica*, 127 (4), 525-529, 2002.
- [10] Henkin, L., *An algebraic characterization of quantifiers*, *Fundamenta Mathematicae*, 37, 63-74, 1950.
- [11] Marsden, E.L., *Compatible elements in implicative models*, *Journal of Philosophical Logic*, 1, 156-161, 1972.
- [12] Curry, H.B., *Foundations of Mathematical Logic*, McGraw-Hill, New York, 1963.

[13] Birkhoff, G., *Lattice Theory*, American Mathematical Society Colloquium Publications, Providence, RI., 1967.

[14] Abbot, J.C., *Algebras of implication and semi-lattices*, Sèminaire Dubreil (Algèbre et théorie des nombres), 20e (2), exp., n° 20, 1-8, 1966-1967.

[15] Xu, Y., *Lattice implication algebras*, Journal of Southwest Jiaotong University., 1, 20-27, 1993.

[16] Xu, Y., *Lattice H implication algebras and lattice implication algebra classes*, Journal of Hebei Mining and Civil Engineering Institute, 3, 139-143, 1992.

[17] Yon, Y.H., Ayar Özbal, Ş., *On derivations and generalized derivations of bitonic algebras*, Applicable Analysis and Discrete Mathematics, 12, 110-125, 2018.

[18] Lingcong, J.A.V, Endam, J.C., *Direct product of B-algebras*, International Journal of Algebra, 10, 33-40, (2016).

[19] Setani, A., Gemawati, S., Deswita, L., *Direct product of BP-algebras*, International Journal of Mathematics Trends and Technology, 66 (10), 63-69, 2020.



On Two Efficient Numerical Schemes for Nonlinear Burgers' Type Equations

Bilge İNAN^{1,*}

¹*İskenderun Technical University, Faculty of Engineering and Natural Sciences, Department of Engineering Basic Sciences, 31200, Hatay, Türkiye
bilge.inan@iste.edu.tr, ORCID: 0000-0002-6339-5172*

Received: 24.12.2021

Accepted: 13.05.2022

Published: 30.06.2022

Abstract

In this work, we investigate two finite difference schemes to solve nonlinear Burgers' type equations. In the first stage, we define the numerical methods to solve the equations. Secondly, numerical solutions are obtained and compared with the exact solutions. In comparison with other defined results in the literature, it is deduced in a conclusive way that the methods are reliable and convenient alternative methods for solving nonlinear Burgers' type equations.

Keywords: The Burgers' type equations; The generalized Burgers-Huxley equation; Finite difference method; Logarithmic finite difference method.

Lineer Olmayan Burgers Tip Denklemler İçin Etkili İki Nümerik Yöntem Üzerine

Öz

Bu çalışmada, iki sonlu fark yöntemi kullanarak lineer olmayan Burgers tipi denklemlerin çözümleri incelenmiştir. İlk aşamada, denklemleri çözmek için nümerik yöntemler tanımlanmıştır. Daha sonra, nümerik çözümler elde edilmiş ve tam çözümlerle karşılaştırılmıştır. Literatürde tanımlanmış diğer sonuçlarla karşılaştırıldığında, yöntemlerin lineer olmayan Burgers tipi denklemlerin çözümü için güvenilir ve uygun alternatif yöntemler olduğu sonucu kesin bir şekilde elde edilmiştir.

* Corresponding Author

DOI: 10.37094/adyujsci.1041652



Anahtar Kelimeler: Burgers tip denklem; Genelleştirilmiş Burgers-Huxley denklemi; Sonlu fark yöntemi; Logaritmik sonlu fark yöntemi.

1. Introduction

In this manuscript, we consider the following initial-boundary-value problem:

$$\frac{\partial u}{\partial t} + \alpha u^\delta \frac{\partial u}{\partial x} - \frac{\partial^2 u}{\partial x^2} = \beta u(1 - u^\delta)(u^\delta - \gamma), \quad 0 \leq x \leq 1, \quad t \geq 0 \quad (1)$$

with the following initial condition

$$u(x, 0) = f(x) \quad (2)$$

and the boundary conditions

$$u(0, t) = g_1(t) \text{ and } u(1, t) = g_2(t) \quad (3)$$

where α , β , γ and δ are parameters that $\beta \geq 0$, $\delta > 0$, $\gamma \in (0,1)$. The equation is called the generalized Burgers-Huxley equation.

Nonlinear partial differential equations are generally obtained while modeling the problems in various fields like physics, chemistry, biology, mathematics and engineering. The generalized Burgers-Huxley equation which is a study in this paper is one of the nonlinear partial differential equations.

In the literature, many numerical methods have been defined for numerical solutions to the generalized Burgers-Huxley equation. Hashim et al. [1] used the Adomian decomposition method for solving the equation. Javidi [2, 3] applied the collocation method to solve the generalized Burgers-Huxley equation. Spectral collocation method for solving the equation was applied by Darvishi et al. [4]. Batiha et al. [5] presented the variational iteration method for the generalized Burgers-Huxley equation. Numerical solution of the equation was obtained by Sari and Gürarslan [6] using a polynomial differential quadrature method. A numerical method called Kansa's approach based on the collocation method using Radial basis functions was presented by Khattak [7] for the solution of the equation. The spectral collocation method uses Chebyshev polynomials for spatial derivatives and fourth order Runge-Kutta method for time integration to solve the equation applied by Javidi and Golbabai [8]. The differential transform method was used for the solution of the generalized Burgers-Huxley equation by Biazar and Mohammadi [9]. Bratsos [10] defined a fourth order finite-difference method in a two-time level recurrence relation for the generalized Burgers-Huxley equation. Çelik [11] solved the equation. El-Kady et al. [12] applied

cardinal Legendre and Chebyshev basis functions with the Galerkin method for the solution of the equation. Al-Rozbayani [13] used the discrete Adomian decomposition method for the solution of the generalized Burgers-Huxley equation.

When $\alpha = 0$, Eqn. (1) is reduced to the generalized Huxley equation. The generalized Huxley equation describes nerve pulse propagation in nerve fibers and wall motion in liquid crystals.

In literature, various numerical methods have been proposed by researchers for the numerical solutions of the generalized Huxley equation. The Adomian decomposition method for the numerical solution of the equation proposed by Hashim et al. [14]. The equation was solved numerically using the variational iteration method by Batiha and coworkers [15]. Hashemi et al. [16] applied the homotopy perturbation method and the Adomian decomposition method to solve the generalized Huxley equation. Tenth-order finite difference methods to obtain approximation solution of the generalized Huxley equation proposed by Sari et al. [17]. Hemida and Mohamed [18, 19] used the homotopy analysis method for solving the generalized Huxley equation. İnan [20] used an implicit exponential finite difference method for the numerical solution of the equation. Also, numerical solutions of the generalized Huxley and generalized Burgers Huxley equations were obtained by using explicit exponential finite difference methods by İnan [21]. Also, there are various numerical methods for the solutions of the Burgers type equations in the literature [32, 33].

On the other hand, the logarithmic finite difference method has been used by some authors. This method was obtained by getting inspired by the exponential finite difference method and used by El Morsy and El-Azab for the first time [22] in 2012 and they used the logarithmic finite difference method for the solution of the KdVB equation. Srivastava and coworkers [23, 24] proposed an implicit logarithmic finite difference method for numerical solutions of the one and two-dimensional coupled viscous Burgers' equations. Also, Srivastava et al. [25] used the method for the numerical solution of the two-dimensional unsteady nonlinear coupled viscous generalized Burgers' equation. Çelikten et al. [26] solved Burgers' equation with explicit logarithmic finite difference method. İnan, defined an explicit logarithmic method to the solutions of generalized Huxley equation and generalized Burgers-Huxley equation and these works were presented orally at congresses and published in the congresses' abstract books [27, 28]. Macías-Díaz and İnan presented a structural and numerical analysis of an implicit logarithmic method for diffusion equation [29]. Macías-Díaz solved the classical Fisher's equation and the Hodgkin-Huxley model using the explicit logarithmic finite difference method. Also, Macías-Díaz showed the existence

and the uniqueness of the numerical solutions obtained by the explicit logarithmic method and proved that the numerical model preserves the positivity, the boundedness, and the monotonicity of the solutions under suitable conditions and presented that the logarithmic scheme is stable and convergent [30]. Macías-Díaz and Hendy investigated stability and convergence of implicit logarithmic finite difference method for diffusion equations [31].

In this paper, the generalized Huxley and generalized Burgers-Huxley equations are solved by two different logarithmic finite difference methods which are explicit and implicit logarithmic finite difference methods. These methods are abbreviated as E-LOGFDM and I-LOGFDM and used respectively in the next part of the paper. To examine the effectiveness of the methods while solving the equations, we consider some examples. Additionally, obtained numerical solutions compared with the exact solutions and other numerical results. So, it concluded that the methods ensure high accuracy for the solution of the nonlinear generalized Huxley and Burgers-Huxley equations. In this paper, MATLAB R2015a was used for obtaining graphs and Fortran was used for computing.

2. Implementation of Logarithmic Finite Difference Methods

2.1. Explicit Logarithmic Finite Difference Method

If we rearrange Eqn. (1);

$$\frac{\partial u}{\partial t} = \frac{\partial^2 u}{\partial x^2} - \alpha u^\delta \frac{\partial u}{\partial x} + \beta u(1 - u^\delta)(u^\delta - \gamma), \quad (4)$$

$F(u)$ denote any continuous and differentiable function, multiplying equation Eqn. (1) by a derivative of F , we have

$$\frac{\partial F}{\partial u} \frac{\partial u}{\partial t} = F'(u) \left(\frac{\partial^2 u}{\partial x^2} - \alpha u^\delta \frac{\partial u}{\partial x} + \beta u(1 - u^\delta)(u^\delta - \gamma) \right) \quad (5)$$

and

$$\frac{\partial F}{\partial t} = F'(u) \left(\frac{\partial^2 u}{\partial x^2} - \alpha u^\delta \frac{\partial u}{\partial x} + \beta u(1 - u^\delta)(u^\delta - \gamma) \right) \quad (6)$$

If we use forward difference approximation for $\frac{\partial F}{\partial t}$ then the following equation is obtained

$$\frac{F(U_i^{n+1}) - F(U_i^n)}{k} = F'(u) \left(\frac{\partial^2 u}{\partial x^2} - \alpha u^\delta \frac{\partial u}{\partial x} + \beta u(1 - u^\delta)(u^\delta - \gamma) \right). \quad (7)$$

Where if we let $F(u) = F'(u) = e^u$, then we get explicit logarithmic finite difference method

$$F(U_i^{n+1}) = F(U_i^n) \left[1 + k \left(\frac{\partial^2 u}{\partial x^2} - \alpha u^\delta \frac{\partial u}{\partial x} + \beta u(1 - u^\delta)(u^\delta - \gamma) \right) \right] \quad (8)$$

and

$$U_i^{n+1} = U_i^n + \log_e \left[1 + k \left(\frac{\partial^2 u}{\partial x^2} - \alpha u^\delta \frac{\partial u}{\partial x} + \beta u(1 - u^\delta)(u^\delta - \gamma) \right) \right]. \quad (9)$$

If Eqn. (9) is arranged and the finite difference approximations are written in the equation, the following equations have been obtained;

$$\begin{cases} U_i^{n+1} = U_i^n + \log_e [1 + k\Phi_i^n] \\ \Phi_i^n = \frac{U_{i+1}^n - 2U_i^n + U_{i-1}^n}{h^2} - \alpha(U_i^n)^\delta \frac{U_{i+1}^n - U_{i-1}^n}{2h} + \beta U_i^n (1 - (U_i^n)^\delta)((U_i^n)^\delta - \gamma). \end{cases} \quad (10)$$

Eqn. (10) is the explicit logarithmic finite difference method for the solution of the generalized Burgers-Huxley equation. When $\alpha = 0$, the method (10) is the turned into to explicit logarithmic finite difference method for solution of the generalized Huxley equation. The explicit logarithmic finite difference method for Eqn. (1) takes linear form defined by Eqn. (10) were lying in the interval $1 \leq N \leq N - 1$.

2. 2. Implicit Logarithmic Finite Difference Method

Eqn. (9) is rearranged and considered finite difference approximations for the equation, we obtain the following implicit logarithmic finite difference method to the solution of the generalized Burgers-Huxley equation;

$$\begin{cases} U_i^{n+1} = U_i^n + \log_e [1 + k\Phi_i^{n+1}] \\ \Phi_i^{n+1} = \frac{U_{i+1}^{n+1} - 2U_i^{n+1} + U_{i-1}^{n+1}}{h^2} - \alpha(U_i^{n+1})^\delta \frac{U_{i+1}^{n+1} - U_{i-1}^{n+1}}{2h} + \beta U_i^{n+1} (1 - (U_i^{n+1})^\delta)((U_i^{n+1})^\delta - \gamma). \end{cases} \quad (11)$$

Eqn. (11) is the implicit logarithmic finite difference method for the solution of the generalized Burgers-Huxley equation. When $\alpha = 0$, the method (11) is turned into to implicit logarithmic finite difference method for the solution of the generalized Huxley equation. Eqn. (11) is a nonlinear difference equations system. Let us regard the nonlinear system of equations in the form

$$F(V) = 0, \quad (12)$$

where $F = [f_1, f_2, \dots, f_{N-1}]^T$ and $V = [U_1^{n+1}, U_2^{n+1}, \dots, U_{N-1}^{n+1}]^T$. Newton's method is applied to Eqn. (10) results in the following iteration:

1. Set $V^{(0)}$, an initial guess.
2. Solved $V^{(m+1)} = V^{(m)} - J(V^{(m)})^{-1}F(V^{(m)})$ for $m = 0, 1, 2, \dots$

where $J(V^{(m)})$ is the Jacobian matrix and the matrix is evaluated analytically. According to the nature of iteration methods, the solution at the previous time-step is considered as the initial estimate. The stopped criteria for Newton's iteration at each time-step is taken as $\|F(V^{(m)})\|_{\infty} \leq 10^{-4}$. The convergence is generally confirmed in two or three iterations.

While solving the problems the solution domain is discretized into the nodes set (x_i, t_n) in which $x_i = a + ih, (i = 0, 1, 2, \dots, N)$ and $t_n = nk, (n = 0, 1, 2, \dots)$, $h = \Delta x = \frac{b-a}{N}$ is the spatial mesh size and $k = \Delta t$ is the time step. Also, where U_i^n denotes the logarithmic finite difference approximation and $u(x, t)$ denotes the exact solution.

3. Stability Analysis

In this section, to investigate the stability of the method, the Fourier method is used. For the sake of examining the stability, the nonlinear term is accepted constant. So, stability can be discussed in the linearized sense. The stability analysis is ground on the von Neumann theory in which the growth factor of typical Fourier mode is defined as:

$$U_i^n = \xi^n e^{I\theta ih}, \quad I^2 = -1 \tag{13}$$

where h is the spatial mesh size and k is the time step, is determined from a linearization of the numerical scheme, so all the U_i^n are equal to local constant d , so that $u^\delta = (\epsilon d)^\delta$. Substituting Eqn. (13) in Eqn. (11) and $\xi^{n+1} = g\xi^n$ gives

$$g = \frac{1 - \frac{2k}{h^2} + \beta k(1 - (\epsilon d)^\delta)((\epsilon d)^\delta - \gamma)}{1 + \frac{2k}{h^2} \cos \frac{\theta h}{2} + \alpha (\epsilon d)^\delta \frac{k}{h} i \sin \theta h} \leq 1 \tag{14}$$

where h and k are usually a small quantity, and d represents the single speed and will usually be around unity. Hence, $|g| \leq 1$ will always be ensured for any problem. As a result, because $|g| \leq 1$, implicit logarithmic finite difference method is unconditionally stable. Also, the explicit logarithmic finite difference method is stable for $\frac{k}{h^2} \leq 0.5$.

4. Numerical Results

In this section, numerical solutions are presented obtained by logarithmic finite difference methods of the generalized Huxley and generalized Burgers-Huxley equations. The absolute error which is defined by the following form to measure the accuracy of the present method is used:

$$|u(x_i, t_n) - U(x_i, t_n)|.$$

Example 1. The generalized Huxley equation of the form;

$$\frac{\partial u}{\partial t} - \frac{\partial^2 u}{\partial x^2} = \beta u(1 - u^\delta)(u^\delta - \gamma), \quad 0 \leq x \leq 1, \quad t \geq 0 \quad (15)$$

with the initial condition

$$u(x, 0) = \left(\frac{\gamma}{2} + \frac{\gamma}{2} \tanh[\sigma\gamma x]\right)^{\frac{1}{\delta}}. \quad (16)$$

The exact solution of Eqn. (15) was derived by Wang [1] following for

$$u(x, t) = \left(\frac{\gamma}{2} + \frac{\gamma}{2} \tanh\left[\sigma\gamma\left(x + \left\{\frac{(1+\delta-\gamma)\rho}{2(1+\delta)}\right\}t\right)\right]\right)^{\frac{1}{\delta}} \quad (17)$$

where $\sigma = \delta\rho/4(1 + \delta)$, $\rho = \sqrt{4\beta(1 + \delta)}$ and β, γ and δ are parameters that $\beta \geq 0$, $\gamma \in (0,1)$.

Case 1. Table 1 presents numerical and exact solutions for various values of x , t and with $\delta = 1$, $\beta = 1$, $\gamma = 10^{-3}$. Also, numerical solutions were obtained by explicit and implicit logarithmic finite difference methods compared with exact solutions and those were obtained by another method in Table 1.

Case 2. In Table 2, absolute errors for various values of x , t and δ with $\beta = 10^{-2}$, $\gamma = 10^{-3}$ displayed.

Case 3. Table 3 presents absolute errors for various values of x , t and β with $\delta = 1$, $\gamma = 10^{-4}$.

Case 4. Table 4 shows absolute errors for various values of x , t and γ with $\beta = 10$, $\delta = 2$.

Table 1: Comparison of the solutions for $\delta = 1$

x	t	[16]	E-LOGFDM	I- LOGFDM	Exact
0.1	0.05	5.00005184E-04	5.000199E-04	5.000192E-04	5.000302E-04
	0.1	4.99992690E-04	5.000276E-04	5.000222E-04	5.000427E-04
	1	4.99767803E-04	5.002451E-04	5.002274E-04	5.002676E-04
0.5	0.05	5.00075895E-04	5.000777E-04	5.000586E-04	5.001009E-04
	0.1	5.00063401E-04	5.000749E-04	5.000285E-04	5.001134E-04
	1	4.99838513E-04	5.002758E-04	5.001874E-04	5.003383E-04
0.9	0.05	5.00146605E-04	5.001613E-04	5.000284E-04	5.001716E-04
	0.1	5.00134111E-04	5.001690E-04	5.000235E-04	5.001841E-04
	1	4.99909224E-04	5.003864E-04	5.002273E-04	5.004090E-04

Figure 1 displays absolute errors for $\delta = 1, 5, 10$, $\beta=1$, $\gamma = 10^{-3}$ at $t = 5$. Figure 2 shows absolute errors for $\beta=1, 10, 100$, $\delta = 2$, $\gamma = 10^{-3}$ at $t = 5$. Figure 3 demonstrates absolute errors for $\gamma = 10^{-3}, 10^{-4}, 10^{-5}$ for $\beta=1$, $\delta = 2$ at $t = 5$.

Table 2: Absolute errors for various values of x, t and δ

x	t	E-LOGFDM			I-LOGFDM		
		$\delta = 1$	$\delta = 2$	$\delta = 3$	$\delta = 1$	$\delta = 2$	$\delta = 3$
0.1	0.5	2.234E-10	9.995E-09	1.729E-07	1.966E-09	7.363E-08	8.082E-07
	1	2.248E-10	1.006E-08	1.739E-07	1.992E-09	7.460E-08	8.183E-07
	10	2.249E-10	1.006E-08	1.739E-07	1.993E-09	7.460E-08	8.182E-07
0.5	0.5	6.198E-10	2.773E-08	4.797E-07	9.378E-09	3.475E-07	3.672E-06
	1	6.246E-10	2.794E-08	4.832E-07	9.463E-09	3.507E-07	3.705E-06
	10	6.247E-10	2.794E-08	4.831E-07	9.463E-09	3.507E-07	3.704E-06
0.9	0.5	2.234E-10	9.994E-09	1.729E-07	1.611E-08	5.900E-07	5.963E-06
	1	2.249E-10	1.006E-08	1.740E-07	1.613E-08	5.910E-07	5.973E-06
	10	2.249E-10	1.006E-08	1.739E-07	1.613E-08	5.910E-07	5.972E-06

Table 3: Absolute errors for various values of x, t and β

x	t	E-LOGFDM			I-LOGFDM		
		$\beta = 1$	$\beta = 10$	$\beta = 100$	$\beta = 1$	$\beta = 10$	$\beta = 100$
0.1	0.5	2.235E-10	2.235E-09	2.235E-08	3.978E-10	2.786E-09	2.410E-08
	1	2.249E-10	2.250E-09	2.250E-08	4.017E-10	2.809E-09	2.426E-08
	10	2.249E-10	2.249E-09	2.244E-08	4.017E-10	2.808E-09	2.421E-08
0.5	0.5	6.201E-10	6.203E-09	6.203E-08	1.496E-09	8.972E-09	7.079E-08
	1	6.248E-10	6.249E-09	6.249E-08	1.509E-09	9.044E-09	7.133E-08
	10	6.248E-10	6.249E-09	6.235E-08	1.507E-09	9.044E-09	7.116E-08
0.9	0.5	2.235E-10	2.235E-09	2.235E-08	1.812E-09	7.259E-09	3.824E-08
	1	2.249E-10	2.250E-09	2.250E-08	1.816E-09	7.281E-09	3.841E-08
	10	2.249E-10	2.250E-09	2.244E-08	1.816E-09	7.280E-09	3.831E-08

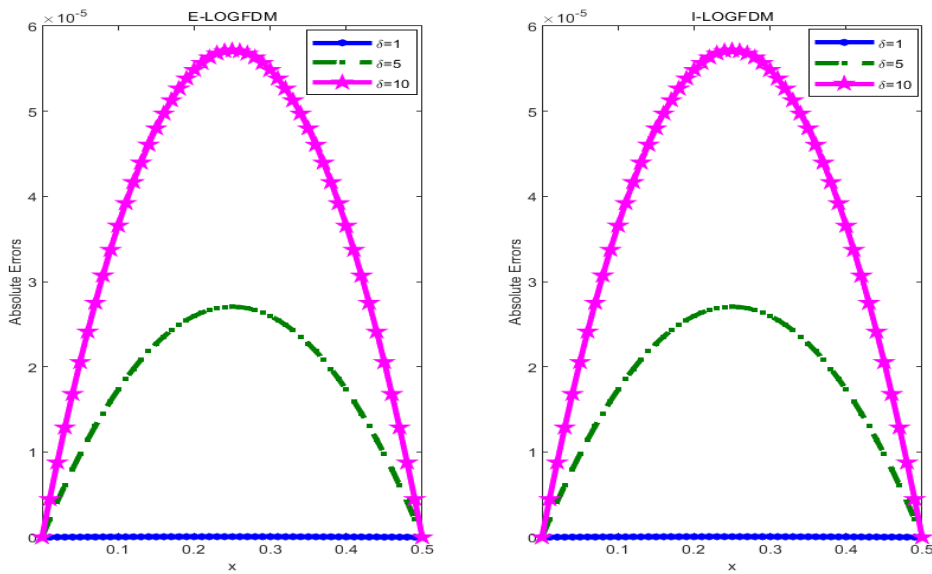


Figure 1: Absolute errors for different values of δ

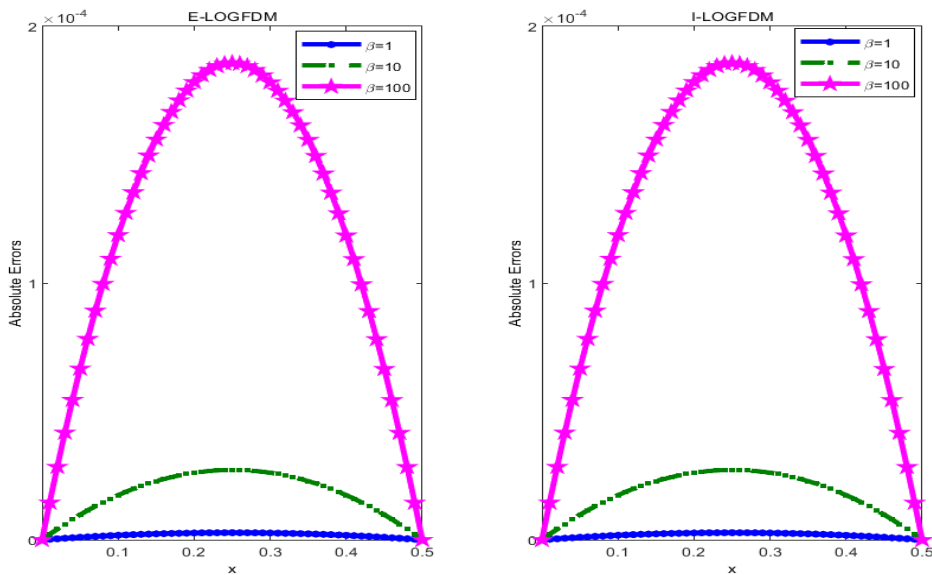


Figure 2: Absolute errors for different values of β

From Figs. 1, 2 and 3 and all of the computed results, it can be seen that the values of the errors are quite small. Also, it is observed that when δ, β and γ increase, the accuracy of the results decreases. From comparisons of the numerical solutions with the exact solutions and the others, it is concluded that the proposed method achieved highly accurate solutions. All of the computational works for Cases 1-4 and Figs. 1-3 are performed with $h = 10^{-2}$, $k = 10^{-5}$ and $h = 2 \times 10^{-2}$, $k = 10^{-4}$, respectively.

Table 4: Absolute errors for various values of x , t and γ

x	t	E-LOGFDM			I-LOGFDM		
		$\gamma = 10^{-3}$	$\gamma = 10^{-4}$	$\gamma = 10^{-5}$	$\gamma = 10^{-3}$	$\gamma = 10^{-4}$	$\gamma = 10^{-5}$
0.1	0.5	9.975E-06	3.160E-07	9.998E-09	1.198E-05	3.797E-07	1.201E-08
	1	1.001E-05	3.180E-07	1.006E-08	1.205E-05	3.826E-07	1.210E-08
	10	9.504E-06	3.166E-07	1.006E-08	1.143E-05	3.808E-07	1.210E-08
0.5	0.5	2.768E-05	8.771E-07	2.774E-08	3.777E-09	1.197E-06	3.785E-08
	1	2.781E-05	8.834E-07	2.795E-08	3.798E-09	1.206E-06	3.815E-08
	10	2.640E-05	8.794E-07	2.793E-08	3.605E-09	1.200E-06	3.814E-08
0.9	0.5	9.973E-06	3.161E-07	9.998E-09	2.827E-09	8.960E-07	2.834E-08
	1	1.001E-05	3.180E-07	1.006E-08	2.829E-09	8.987E-07	2.843E-08
	10	9.501E-06	3.166E-07	1.006E-08	2.684E-09	8.946E-07	2.842E-08

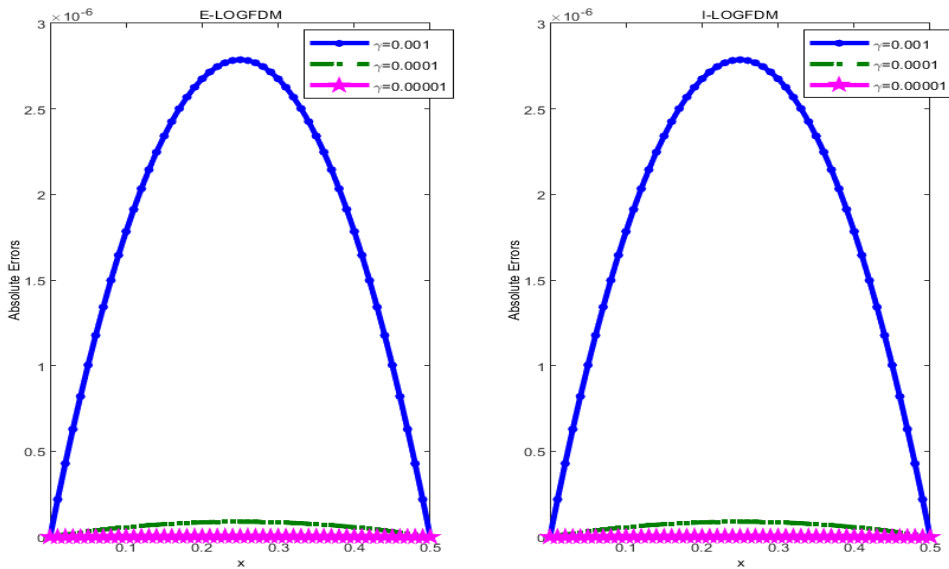


Figure 3: Absolute errors for different values of γ

Example 2. In this example, we consider the following generalized Burgers-Huxley equation,

$$\frac{\partial u}{\partial t} + \alpha u^\delta \frac{\partial u}{\partial x} - \frac{\partial^2 u}{\partial x^2} = \beta u(1 - u^\delta)(u^\delta - \gamma), \quad 0 \leq x \leq 1, \quad t \geq 0 \tag{18}$$

with the following initial condition taken from

$$u(x, 0) = \left(\frac{\gamma}{2} + \frac{\gamma}{2} \tanh[A_1 x] \right)^{\frac{1}{\delta}} \tag{19}$$

and the boundary conditions

$$u(0, t) = \left(\frac{\gamma}{2} + \frac{\gamma}{2} \tanh[-A_1 A_2 t]\right)^{\frac{1}{\delta}} \tag{20}$$

and

$$u(1, t) = \left(\frac{\gamma}{2} + \frac{\gamma}{2} \tanh[A_1(1 - A_2 t)]\right)^{\frac{1}{\delta}}. \tag{21}$$

The exact solution of Eqn. (18) is

$$u(x, t) = \left(\frac{\gamma}{2} + \frac{\gamma}{2} \tanh[A_1(x - A_2 t)]\right)^{\frac{1}{\delta}}, \tag{22}$$

where

$$A_1 = \frac{-\alpha\delta + \delta\sqrt{\alpha^2 + 4\beta(1+\delta)}}{4(1+\delta)}\gamma, A_2 = \frac{\gamma\alpha}{1+\delta} - \frac{(1+\delta-\gamma)(-\alpha + \sqrt{\alpha^2 + 4\beta(1+\delta)})}{2(1+\delta)}. \tag{23}$$

Case 5. Table 5 presents numerical and exact solutions for various values of x , t and with $\delta = 1$, $\alpha = 1$, $\beta = 1$, $\gamma = 10^{-3}$.

Case 6. Absolute errors for various values of x , t and δ with $\alpha = 0.1$, $\beta = 10^{-3}$, $\gamma = 10^{-4}$ shown in Table 6.

Case 7. Table 7 shows absolute errors for various values of x , t and β with $\alpha = \delta = 1$, $\gamma = 10^{-4}$.

Case 8. Absolute errors for various values of x , t and γ with $\alpha = 1$, $\beta = 10$, $\delta = 2$ presented in Table 8.

Case 9. Table 9 displays absolute errors for various values of x , t and α with $\beta = \delta = 1$, $\gamma = 10^{-4}$.

Case 10. Table 10 shows comparisons of the present method with Batiha et al. [5], Biazar&Mohammadi [7] and Al-Rozbayani [11] for $\alpha = \beta = \delta = 1$ and $\gamma = 10^{-3}$.

Table 5: Comparison of the solutions for $\delta = 1$

x	t	Exact Solution	E-LOGFDM		I-LOGFDM	
			Numerical Solution	Absolute Error	Numerical Solution	Absolute Error
0.1	0.05	0.000500037	0.000500022	1.545E-08	0.000500022	1.545E-08
	0.1	0.000500062	0.000500040	2.259E-08	0.000500040	2.259E-08
	1	0.000500512	0.000500478	3.373E-08	0.000500478	3.373E-08
0.5	0.05	0.000500087	0.000500053	3.470E-08	0.000500053	3.470E-08

	0.1	0.000500112	0.000500055	5.766E-08	0.000500055	5.766E-08
	1	0.000500562	0.000500468	9.370E-08	0.000500471	9.370E-08
0.9	0.05	0.000500137	0.000500122	1.545E-08	0.000500122	1.545E-08
	0.1	0.000500162	0.000500140	2.259E-08	0.000500140	2.259E-08
	1	0.000500612	0.000500578	3.373E-08	0.000500578	3.373E-08

Table 6: Absolute errors for various values of x, t and δ

x	t	E-LOGFDM			I-LOGFDM		
		$\delta = 1$	$\delta = 4$	$\delta = 8$	$\delta = 1$	$\delta = 4$	$\delta = 8$
0.1	1	5.551E-13	1.456E-09	1.989E-08	4.470E-13	1.456E-9	1.989E-8
	5	5.996E-13	1.457E-09	1.989E-08	4.431E-13	1.456E-9	1.989E-8
	10	5.996E-13	1.457E-09	1.989E-08	4.419E-13	1.456E-9	1.989E-8
0.5	1	1.459E-12	4.046E-09	5.525E-08	1.235E-12	4.045E-9	5.525E-8
	5	1.666E-12	4.046E-09	5.525E-08	1.232E-12	4.045E-9	5.524E-8
	10	1.666E-12	4.046E-09	5.524E-08	1.226E-12	4.045E-9	5.525E-8
0.9	1	5.551E-13	1.457E-09	1.989E-08	4.421E-13	1.456E-9	1.989E-8
	5	5.996E-13	1.457E-09	1.989E-08	4.421E-13	1.456E-9	1.989E-8
	10	5.996E-13	1.457E-09	1.989E-08	4.430E-13	1.456E-9	1.989E-8

Absolute errors displayed by Fig. 4 for $\delta = 1, 2, 3, \alpha = \beta = 1, \gamma = 10^{-3}, h = 0.02$ and $k = 10^{-4}$ at $t = 5$. Figure 5 displays absolute errors for $\beta = 1, 5, 10, \alpha = 1, \delta = 2, \gamma = 10^{-3}$. Figure 6 presents absolute errors for $\gamma = 10^{-3}, 10^{-4}, 10^{-5}, \alpha = \beta = 1, \delta = 2$. Figure 7 shows absolute errors for $\alpha = 0.1, 1, 10, \delta = 2, \beta = 1, \gamma = 10^{-3}$.

Table 7: Absolute errors for various values of x, t and β

x	t	E-LOGFDM			I-LOGFDM		
		$\beta = 1$	$\beta = 10$	$\beta = 100$	$\beta = 1$	$\beta = 10$	$\beta = 100$
0.1	0.05	1.546E-10	2.165E-09	2.436E-08	1.546E-10	2.165E-09	2.436E-08
	0.1	2.260E-10	3.165E-09	3.562E-08	2.261E-10	3.165E-09	3.562E-08
	1	3.375E-10	4.724E-09	5.316E-08	3.379E-10	4.725E-09	5.316E-08
0.5	0.05	3.471E-10	4.861E-09	5.471E-08	3.470E-10	4.861E-09	5.470E-08
	0.1	5.766E-10	8.076E-09	9.089E-08	5.770E-10	8.076E-09	9.089E-08
	1	9.370E-10	1.312E-08	1.477E-07	9.382E-10	1.312E-08	1.477E-07
0.9	0.05	1.546E-10	2.165E-09	2.436E-08	1.546E-10	2.165E-09	2.436E-08
	0.1	2.260E-10	3.165E-09	3.562E-08	2.261E-10	3.165E-09	3.562E-08
	1	3.375E-10	4.724E-09	5.316E-08	3.379E-10	4.725E-09	5.316E-08

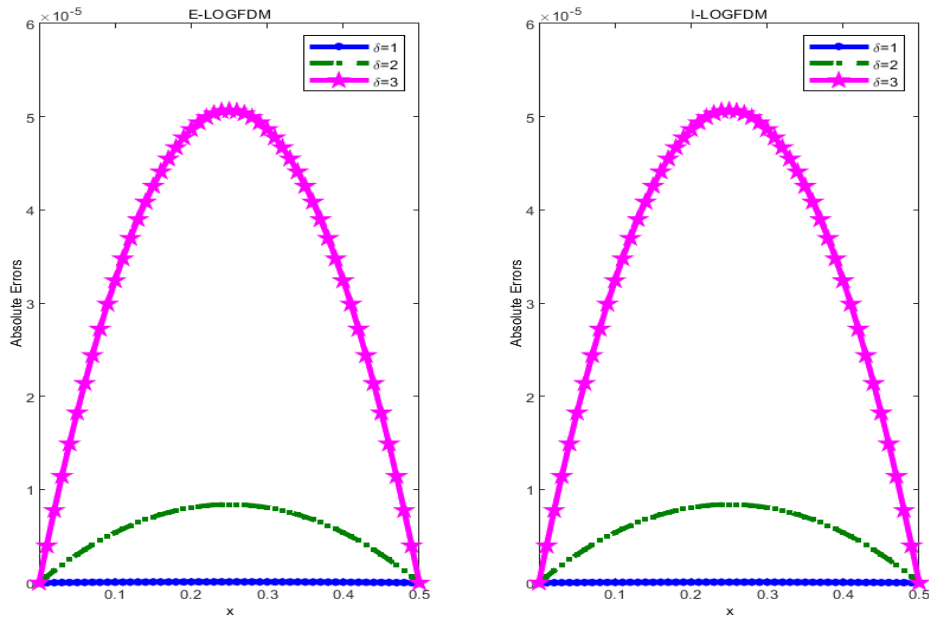


Figure 4: Absolute errors for different values of δ

As it can be observed from Tables 5-10 that the obtained results have excellent conform with the exact solutions. All numerical results for Cases 5-10 are obtained with the space step $h = 10^{-2}$ and the time step $k = 10^{-5}$. All numerical results shown in Figs. 5-7 are obtained for $h = 0.02$ and $k = 10^{-5}$ at $t = 5$. From all of the computed results and figures can be observed that the values of the errors are very small. Also, it is observed from all computations that the accuracy of the numerical results decreases when δ , β and γ increase. However, the accuracy of the results increases when α increased.

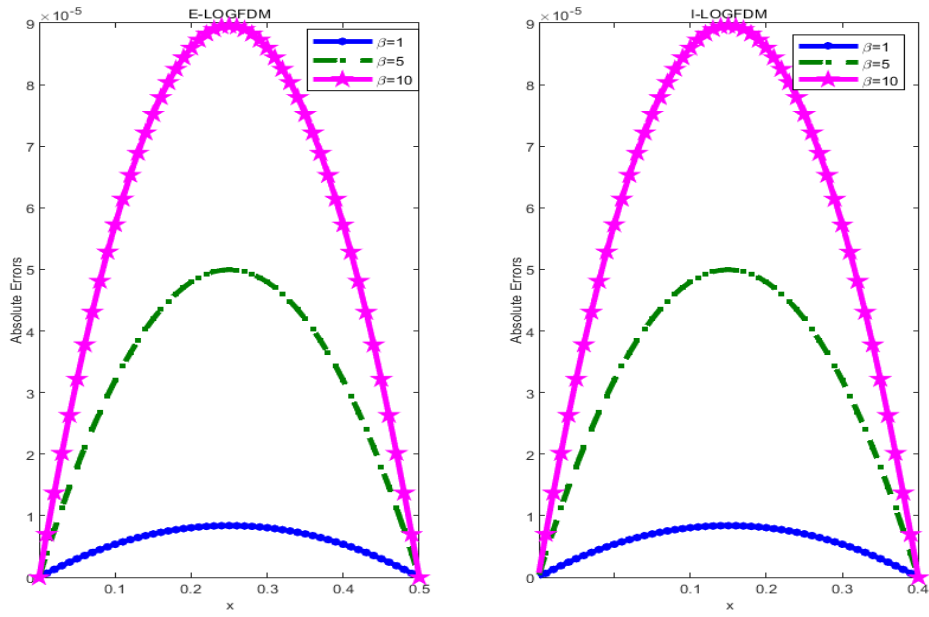


Figure 5: Absolute errors for different values of β

Table 8: Absolute errors for various values of x, t and γ

x	t	E-LOGFDM			I-LOGFDM		
		$\gamma = 10^{-3}$	$\gamma = 10^{-4}$	$\gamma = 10^{-5}$	$\gamma = 10^{-3}$	$\gamma = 10^{-4}$	$\gamma = 10^{-5}$
0.1	0.05	1.956E-05	6.195E-07	1.959E-08	1.956E-05	6.194E-07	1.959E-08
	0.1	2.856E-05	9.055E-07	2.864E-08	2.856E-05	9.055E-07	2.864E-08
	1	4.118E-05	1.348E-06	4.275E-08	4.118E-05	1.348E-06	4.275E-08
0.5	0.05	4.393E-05	1.391E-06	4.400E-08	4.392E-05	1.391E-06	4.399E-08
	0.1	7.290E-05	2.311E-06	7.309E-08	7.290E-05	2.311E-06	7.309E-08
	1	1.144E-04	3.743E-06	1.187E-07	1.144E-04	3.743E-06	1.187E-07
0.9	0.05	1.955E-05	6.194E-07	1.959E-08	1.955E-05	6.194E-07	1.959E-08
	0.1	2.856E-05	9.055E-07	2.864E-08	2.855E-05	9.055E-07	2.864E-08
	1	4.117E-05	1.347E-06	4.275E-08	4.117E-05	1.348E-06	4.275E-08

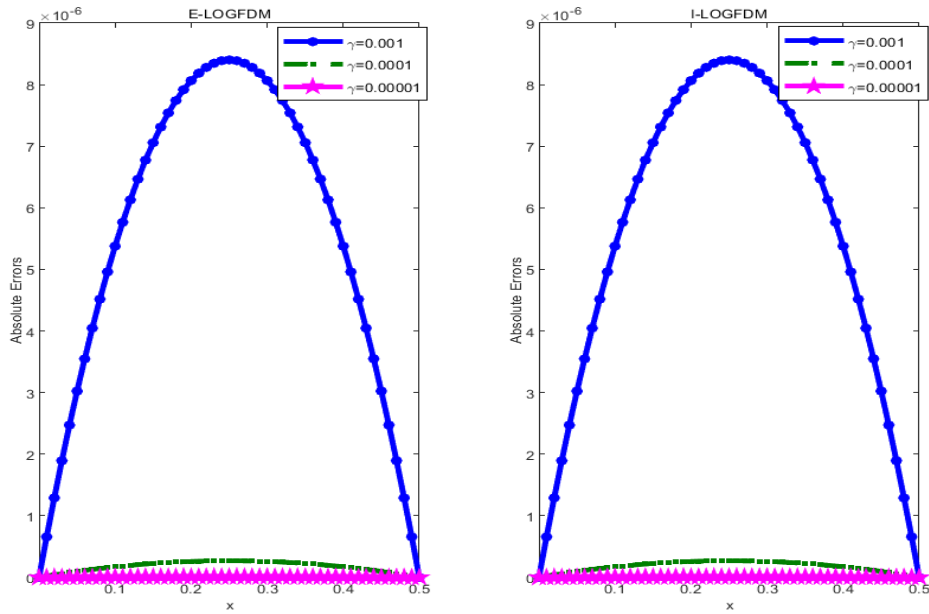


Figure 6: Absolute errors for different values of γ

Table 9: Absolute errors for various values of x, t and α

		E-LOGFDM			I-LOGFDM		
x	t	$\alpha = 0.1$	$\alpha = 1$	$\alpha = 5$	$\alpha = 0.1$	$\alpha = 1$	$\alpha = 5$
0.1	0.05	2.436E-10	1.546E-10	6.579E-11	2.437E-10	1.547E-10	6.576E-11
	0.1	3.561E-10	2.260E-10	9.618E-11	3.563E-10	2.261E-10	9.618E-11
	1	5.317E-10	3.375E-10	1.438E-10	5.321E-10	3.379E-10	1.442E-10
0.5	0.05	5.470E-10	3.471E-10	1.477E-10	5.470E-10	3.470E-10	1.476E-10
	0.1	9.087E-10	5.766E-10	2.454E-10	9.092E-10	5.770E-10	2.453E-10
	1	1.4769E-9	9.370E-10	3.993E-10	1.478E-09	9.382E-10	4.005E-10
0.9	0.05	2.436E-10	1.546E-10	6.579E-11	2.437E-10	1.546E-10	6.576E-11
	0.1	3.561E-10	2.260E-10	9.618E-11	3.563E-10	2.261E-10	9.618E-11
	1	5.317E-10	3.375E-10	1.438E-10	5.321E-10	3.379E-10	1.442E-10

Table 10: Comparisons of the absolute errors for $\delta = 1$

x	t	E-LOGFDM	I-LOGFDM	[5]	[9]	[13]
0.1	0.05	1.545E-08	1.545E-08	1.87405E-08	1.87406E-08	1.87406E-08
	0.1	2.259E-08	2.259E-08	3.74813E-08	3.74813E-08	3.74812E-08
	1	3.373E-08	3.373E-08	3.74812E-07	3.74813E-07	3.74812E-07
0.5	0.05	3.470E-08	3.470E-08	1.87405E-08	1.87406E-08	1.87406E-08
	0.1	5.766E-08	5.766E-08	1.37481E-08	3.74813E-08	3.74812E-08
	1	9.370E-08	9.370E-08	3.74813E-07	3.74813E-07	3.74812E-07
0.9	0.05	1.545E-08	1.545E-08	1.87405E-08	1.87406E-08	1.87406E-08
	0.1	2.259E-08	2.259E-08	3.74813E-08	3.74813E-08	3.74812E-08
	1	3.373E-08	3.373E-08	3.74813E-07	3.74813E-07	3.74812E-07

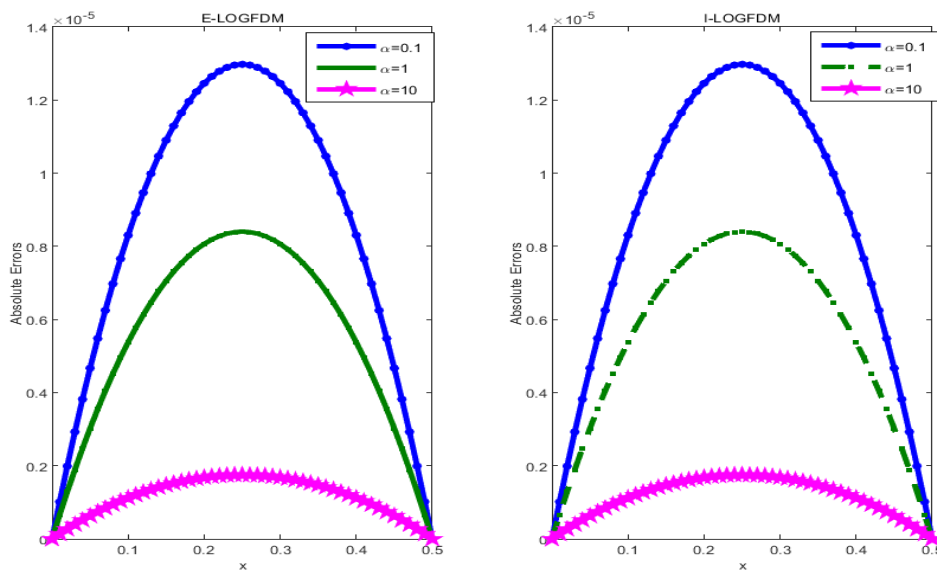


Figure 7: Absolute errors for different values of α

5. Conclusion

In this manuscript, we have designed explicit and implicit logarithmic finite difference methods has been proposed the generalized Huxley and Burgers-Huxley equations. The numerical solutions for different two test problems are presented through tables. The numerical results show that the solution using methods gives high accuracy and to obtain high accuracy results no restrictions for parameters are needed. As can be seen from comparisons and obtained results that the logarithmic finite difference methods are effective and reliable methods for solving a wide range of engineering problems.

References

- [1] Hashim, I., Noorani, M.S.M., Said Al-Hadidi, M.R., *Solving the generalized Burgers-Huxley Equation using the Adomian decomposition method*, *Mathematical and Computer Modelling*, 43, 1404-1411, 2006.
- [2] Javidi, M., *A numerical solution of the generalized Burger's-Huxley equation by pseudospectral method and Darvishi's preconditioning*, *Applied Mathematics and Computation*, 175, 1619-1628, 2006.
- [3] Javidi, M., *A numerical solution of the generalized Burger's-Huxley equation by spectral collocation method*, *Applied Mathematics and Computation*, 178, 338-344, 2006.
- [4] Darvishi, M.T., Kheybari, S., Khani, F., *Spectral collocation method and Darvishi's preconditionings to solve the generalized Burgers-Huxley equation* *Communications in Nonlinear Science and Numerical Simulation*, 13, 2091-2103, 2008.
- [5] Batiha, B., Noorani, M.S.M., Hashim, I., *Application of variational iteration method to*

the generalized Burgers-Huxley equation, *Chaos Soliton Fractals*, 36, 660-663, 2008.

[6] Sari, M., Gürarlan, G., *Numerical solutions of the generalized Burgers-Huxley equation by a differential quadrature method*, *Mathematical Problems in Engineering*, doi: 10.1155/2009/370765, 2009.

[7] Khattak, A. J., *A computational meshless method for the generalized Burger's-Huxley equation*, *Applied Mathematical Modelling*, 33, 3218-3729, 2009.

[8] Javidi, M., Golbabai, A., *A new domain decomposition algorithm for generalized Burger's-Huxley equation based on Chebyshev polynomials and preconditioning*, *Chaos Soliton Fractals*, 39, 849-857, 2009.

[9] Biazar, J., Mohammadi, F., *Application of differential transform method to the generalized Burgers-Huxley equation*, *Applications and Applied Mathematics: An International Journal (AAM)*, 5, 1726-1740, 2010.

[10] Bratsos, A.G., *A fourth order improved numerical scheme for the generalized Burgers-Huxley equation*, *American Journal of Computational Mathematics*, 1, 152-158, 2011.

[11] Çelik, İ., *Haar wavelet method for solving generalized Burgers-Huxley equation*, *Arab Journal of Mathematical Sciences* 18, 25-37, 2012.

[12] El-Kady, M., El-Sayed, S.M., Fathy, H.E., *Development of Galerkin method for solving the generalized Burger's Huxley equation*, *Mathematical Problems in Engineering*, doi: 10.1155/2013/165492, 2013.

[13] Al-Rozbayani, A.M., *Discrete Adomian decomposition method for solving Burger's-Huxley Equation*, *International Journal of Contemporary Mathematical Sciences*, 8, 623-631, 2013.

[14] Hashim, I., Noorani, M.S.M., Batiha, B., *A note on the Adomian decomposition method for the generalized Huxley Equation*, *Applied Mathematics and Computation*, 181, 1439-1445, 2006.

[15] Batiha, B., Noorani, M.S.M., Hashim, I., *Numerical simulation of the generalized Huxley equation by He's variational iteration method*, *Applied Mathematics and Computation*, 186, 1322-1325, 2007.

[16] Hashemi, S.H., Daniali, H.R.M., Ganji, D. D., *Numerical simulation of the generalized Huxley equation by He's homotopy perturbation method*, *Applied Mathematics and Computation*, 192, 157-161, 2007.

[17] Sari, M., Gürarlan, G., Zeytinoglu, A., *High-order finite difference schemes for numerical solutions of the generalized Burgers-Huxley equation*, *Numerical Methods for Partial Differential Equations*, 27, 1313-1326, 2010.

[18] Hemida, K., Mohamed, M.S., *Numerical simulation of the generalized Huxley equation by homotopy analysis method*, *Journal of Applied Functional Analysis*, 5, 344-350, 2010.

[19] Hemida, K., Mohamed, M.S., *Application of homotopy analysis method to fractional order generalized Huxley equation*, *Journal of Applied Analysis*, 7, 367-372, 2012.

[20] İnan, B., *A new numerical scheme for the generalized Huxley equation*, *Bulletin of Mathematical Sciences and Applications*, 16, 105-111, 2016.

[21] İnan, B., *Finite difference methods for the generalized Huxley and Burgers-Huxley equations*, *Kuwait Journal of Science*, 44, 20-27, 2017.

[22] El Morsy, S.A., El-Azab, M.S., *Logarithmic finite difference method applied to KdVB equation*, American Academic&Scholarly Research Journal, 4, 2, 2012.

[23] Srivastava, V.K., Awasthi, M.K., Singh, S., *An implicit logarithmic finite-difference technique for two dimensional coupled viscous Burgers' equation*, AIP Advances, 3, 122105, 2013.

[24] Srivastava, V.K., Tamsir, M., Awasthi, M.K., Singh, S., *One dimensional coupled viscous Burgers' equation and its numerical solution by an implicit logarithmic finite-difference method*, AIP Advances, 4, 037119, 2014.

[25] Srivastava, V.K., Tamsir, M., Rashidi, M.M., *Analytic and numeric computation of two dimensional unsteady nonlinear coupled viscous generalized Burgers' equation*, Asia Pacific Journal of Engineering Science and Technology, 2, 23-35, 2016.

[26] Çelikten, G., Göksu, A., Yagub, G., *Explicit logarithmic finite difference schemes for numerical solution of Burgers equation*, European International Journal of Science and Technology, 6, 57-67, 2017.

[27] İnan, B., *A logarithmic finite difference technique for numerical solution of the generalized Huxley equation*, Proceedings of 7th International Eurasian Conference on Mathematical Sciences and Applications, Kyiv, Ukraine, pp. 100-101, 2018.

[28] İnan, B., *High accuracy numerical solutions by logarithmic finite difference method for the generalized Burgers-Huxley equation*, Proceedings of 2nd International Conference on Mathematical and Related Sciences, Antalya, Turkey, pp.29, 2019.

[29] Macías-Díaz, J.E., İnan, B., *Structural and numerical analysis of an implicit logarithmic scheme for diffusion equations with nonlinear reaction*, International Journal of Modern Physics C, 30, 9, 1950065, 2019.

[30] Macías-Díaz, J.E., *On the numerical and structural properties of a logarithmic scheme for diffusion-reaction equations*, Applied Numerical Mathematics, 140, 104-114, 2019.

[31] Macías-Díaz, J.E., Hendy, A.S., *On the stability and convergence of an implicit logarithmic scheme for diffusion equations with nonlinear reaction*, Journal of Mathematical Chemistry, 58, 735-74, 2020.

[32] Uçar, Y., Yağmurlu, N.M., Çelikkaya, İ., *Numerical solution of Burger's type equation using finite element collocation method with strang splitting*, Mathematical Sciences and Applications E-Notes, 8(1), 29-45, 2020.

[33] Kutluay, S., Yağmurlu, N.M., *The modified Bi-quintic B-splines for solving the two-dimensional unsteady Burgers' equation*, European International Journal of Science and Technology, 1(2), 23-29, 2012.



Evaluation of Some Sulfonamide Derivatives as a Potential Inhibitors of The Carbonic Anhydrase IX/XII by ADME and Molecular Docking Method

Nuri YORULMAZ¹, Hilal ÖZTÜRK², Mustafa DURGUN^{3,*}

¹*Harran University, Faculty of Art and Science, Department of Physics, Şanlıurfa, Türkiye
nyorulmaz@harran.edu.tr, ORCID: 0000-0003-4959-2302*

²*Karadeniz Technical University, Faculty of Medicine, Department of Biophysics, Trabzon, Türkiye
hilal.ozturk@ktu.edu.tr, ORCID: 0000-0003-0079-5184*

³*Harran University, Faculty of Art and Science, Department of Chemistry, Şanlıurfa, Türkiye
mustafadurgun@harran.edu.tr, ORCID: 0000-0003-3012-7582*

Received: 22.03.2022

Accepted: 29.05.2022

Published: 30.06.2022

Abstract

Molecular docking is a simulation technique that calculates the binding score of the molecules of interest to protein structures and visualizes the bond structure. It is a widely used technique for foresight because it helps to determine bond relationships between molecular structures before laboratory applications in the development of new drugs. ADME studies also provide clues for the determination of the molecules analyzed by the molecular docking method to be drug candidates. In this study, inhibition of CA IX and CA XII enzymes by sulfonamide derivatives synthesized in our previous study was investigated using molecular docking method. The CA enzyme family has an important role in the survival and spread of cancer cells. Therefore, we aimed to find new drug candidates that inhibit these enzymes. We found that the sulfonamide derivative named **6** binds to the active sites of both CA IX and CA XII enzymes with -7.44 kcal/mol and -6.39 kcal/mol energy, respectively, closest to the binding of the reference molecule acetazolamide. In addition, the compatibility of all compounds used in the study with drug-like properties was investigated using the ADME method. In conclusion, it can be said that the



sulfonamide derivatives named 1-9 generally have the characteristic features of a drug (physicochemical and structural properties) and oral bioavailability.

Keywords: Molecular docking; ADME; CA IX; CA XII; Sulfonamide derivatives.

Karbonik Anhidraz IX/XII'nin Potansiyel İnhibitörleri Olarak Bazı Sülfonamit Türevlerinin ADME ve Moleküler Yerleştirme Metodu ile Değerlendirilmesi

Öz

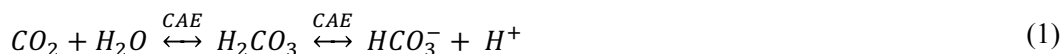
Moleküler yerleştirme, ilgili moleküllerin protein yapılarına bağlanma enerjilerini hesaplayan ve bağ yapısını görselleştiren bir simülasyon tekniğidir. Çeşitli hastalıklara ilişkin yeni ilaçların keşfi ve geliştirilmesinde, laboratuvar uygulamalarından önce moleküler yapılar arasındaki bağlanmaları belirlemeye yardımcı olması sebebiyle, yaygın olarak kullanılan bir tekniktir. ADME çalışmaları da moleküler yerleştirme yöntemiyle analiz edilen moleküllerin ilaç aday olma özelliklerinin belirlenmesinde ipuçları sağlamaktadır. Bu çalışmada, daha önceki çalışmamızda sentezlenen sülfonamit türevleri tarafından CA IX ve CA XII enzimlerinin inhibisyonu, moleküler yerleştirme yöntemi kullanılarak araştırılmıştır. Karbonik anhidraz (CA) enzim ailesi, kanser hücrelerinin hayatta kalmasında ve yayılmasında önemli bir role sahiptir. Bu nedenle bu enzimleri inhibe eden yeni ilaç adayları bulmayı amaçladık. 6 numaralı sülfonamit türevinin hem CA IX hem de CA XII enzimlerinin aktif bölgelerine sırasıyla -7,44 kcal/mol ve -6,39 kcal/mol enerji ile referans molekül asetazolamitin (AZM) bağlanmasına en yakın şekilde bağlandığını bulduk. Ayrıca çalışmada kullanılan tüm bileşiklerin ilaç benzeri özelliklerle uyumluluğu ADME yöntemi kullanılarak araştırılmıştır. Sonuç olarak, 1-9 olarak adlandırılmış sülfonamit türevlerinin genel olarak bir ilacın karakteristik özelliklerine (fizikokimyasal ve yapısal özellikler) ve oral biyoyararlanıma sahip olduğu söylenebilir.

Anahtar Kelimeler: Moleküler yerleştirme; ADME; CA IX; CA XII; Sülfonamit türevleri.

1. Introduction

The microenvironment is a key player in cancer cell survival and spread, in cancer research. Hypoxia and acidosis in the tumor microenvironment affect cancer biology. Therefore, the carbonic anhydrase family of enzymes, which maintains intracellular pH, has attracted the attention from cancer research [1].

Carbonic anhydrase (CA) enzymes are a family of metalloenzymes that are found in all living things and contain metal ions in their structure. CA enzymes catalyze the reversible conversion of carbon dioxide (CO₂) to bicarbonate (HCO₃⁻) and hydrogen ions (H⁺) (Eqn. (1)).



This protein chain consists of 260 amino acids and varies according to the metal ion they contain in their structure [2, 3]. The active site of the molecule is in the form of a centrally diffused cavity, with the zinc ion adjacent to the bottom of this cavity [4]. CA isoenzymes are encoded by seven distinct gene families, the α -carbonic anhydrase family is the species found in humans, and 16 different isoenzymes of this species have been found so far. Of these, five (CA I, II, III, VII, and XIII) are cytosolic, four (CA IV, IX, XII, and XIV) are membrane-bound, two (CA VA and VB) are mitochondrial, and one (CA VI) is in salivary and milk [5, 6].

The ability of sulfonamides to readily acquire an ionic form is essential for inhibiting an enzyme. The interaction of sulfonamides with the enzyme is as follows; First, the N atom in the R-SO₂-NH- compound must form an ionic bond with Zn²⁺ in the active site of the carbonic anhydrase enzyme. Second, it must form two hydrogen bonds with the THR-199 amino acid. This basic interaction mechanism is given in Fig. 1 [7, 8].

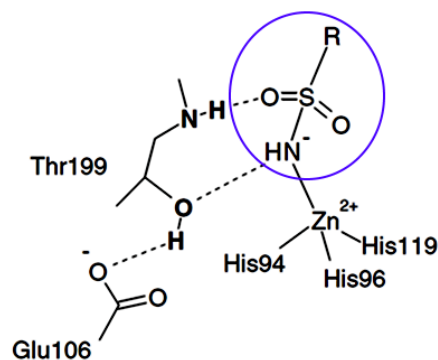


Figure 1: The mechanism of interaction between carbonic anhydrase enzyme and a sulfonamide derivative

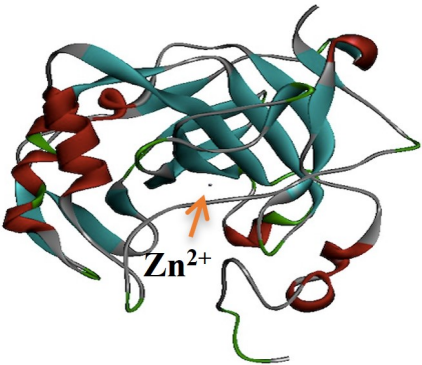
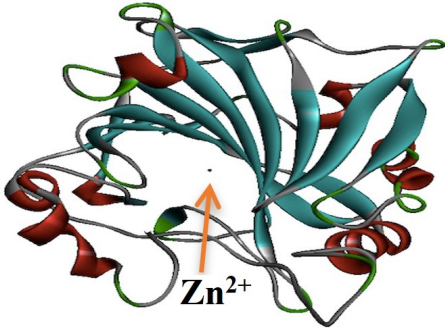
CA enzyme plays important roles in pH regulation, bone development/resorption, electrolyte secretion, calcification, lipogenesis, urea cycle, bicarbonate synthesis and many other physiological events apart from carboxylation reactions [9, 10]. In addition, CA IX and XII are overexpressed in some cancers due to their induction by the hypoxic environment in solid tumor cells. Overexpression of these enzymes in tumor cells supports survival in hypoxia and cell migration [11-13]. For this reason, besides cancer treatments such as chemotherapy and radiotherapy, drug studies that provide inhibition of related enzymes are important research areas for cancer treatment.

Sulfonamides are effective molecules in drug studies that have been used as anti-microbial for many years. Their broad biological activities such as anti-inflammatory, anti-tumor and antibacterial have made sulfonamides popular for drug studies [14-17]. Especially sulfonamide derivatives such as acetazolamide, which are used as CA enzyme inhibitors, are synthesized and their effectiveness in the treatment of various diseases is being investigated. In this study, we investigated the inhibition of CA IX and CA XII enzymes by some sulfonamide derivatives that we synthesized in our previous study [14, 18], using molecular docking method.

2. Materials and Methods

The crystal structures of both, first the extracellular domain of human CA XII and the other catalytic domain of tumor-associated human CA IX, were retrieved from the Protein Data Bank. The X-ray structures of both proteins are in complex with a classical, clinically used sulfonamide inhibitor, acetazolamide. PDB information of CA IX and CA XII are given in the Table 1. Before docking, the acetazolamide molecule and all heteroatoms were removed from the protein structures, polar hydrogens were added for a good imitation of the physiological environment.

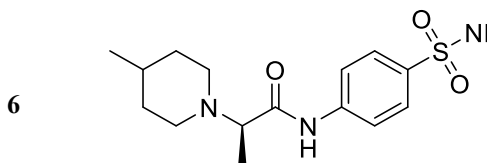
Table 1: The properties of CA IX and CA XII protein structures

PDB ID	Protein Structure	Resolution (Å)	Method
3IAI		2.2	XRD
1JD0		1.5	XRD

The molecular structures of the sulfonamide derivatives, which is binding to the active sites of CA IX and CA XII were examined, are shown in Table 2. Synthesized sulfonamides were evaluated experimentally for antimicrobial and cytotoxicity [14,18]. For the sulfonamide derivatives synthesized in our previous study, 1 and 2 were named for the starting materials, 3-10 for the derivatives. In addition, acetazolamide (AZM) was used as a reference molecule.

Table 2: Molecular structures of sulfonamide derivatives and reference molecule

Molecule Name	Molecule Structure	Molecule Name	Molecule Structure
1		7	
2		8	
3		9	
4		10	
5		AZM	



The docking studies of the molecules to CA IX and CA XII proteins was done using Autodock 4.2.6 software [19]. Ligand energy was optimized by Avogadro version 1.2 with Force Field type MMFF9, and saved in .mol2 format [20]. AutoDockTools was used to prepare molecules and receptors for docking. Docking studies were performed by Lamarckian genetic algorithm, with 50 as the total number of runs for each binding site. In each respective run, a population of 150 individuals with 27×10^3 generations and 25×10^6 energy evaluations were employed. In accordance with the mechanism described in Fig. 1, a different narrow region was chosen as the grid around Zn^{2+} , taking into account the size of each compound.

The binding of each sulfonamide derivative to the protein structures was determined by comparison with that of the reference molecule acetazolamide. The protein-ligand complexes were visualized and analyzed using AutoDockTools and Biovia Discovery Studio Visualizer 2020. It was also done using the SwissADME website to determine the physicochemical, pharmacokinetic and solubility (ADME) properties of the synthesized compounds [21].

3. Results and Discussion

3.1. Physicochemical properties and drug likeness screening

Chemical synthesis, biological screening (in vitro and in vivo) and investigation of pharmacokinetic properties are the basic steps in determining the drug potential of a chemical compound. First of all, it is necessary to determine the pharmacokinetic properties, metabolism, excretion (ADME) and toxicity data of newly synthesized compounds from in vivo test applications, which is a very costly task. Thus, weak drug candidate compounds that would lead to clinical failure can be eliminated [22]. SwissADME is a free web tool that offers applications for this purpose. It provides information on the size, solubility, lipophilicity, saturation, skin permeability, and intestinal absorption of compounds. The ADME results of synthesized compounds are given in Table 3.

All compounds synthesized are suitable based on the Lipinski, Veber and Ghose rules. The molecular weight of sulfonamide derivatives is small equal to 500 daltons, a hydrogen bond

acceptor number ≤ 10 , and a donor number ≤ 5 . Also, lipophilicity or logP value was calculated as ≤ 5 . The calculated hydrogen bond donor number for the compounds is less than 5 and the hydrogen bond acceptor number is less than 10. Based on all these rules, as given in Table 4, it can be said that the sulfonamide derivatives synthesized have the characteristic features of a good drug (physicochemical and structural properties) and have oral bioavailability (Fig. 2). Solubility is an important criterion in drug absorption, and when all compounds are evaluated on this scale, they are determined to have high solubility. All the pharmacokinetic properties of the compounds, including gastrointestinal absorption, blood-brain barrier crossing, skin permeability, and drug excretion, were investigated using the Boiled-Egg model and showed in Fig. 3. All sulfonamide derivatives in the study exhibited high GI and did not penetrate the blood-brain barrier. Skin permeability parameters, another pharmacokinetic property, were calculated in accordance with the criteria defined by Potts and Guy. These criteria are that skin permeability will decrease as the negativity of the LogK value increases, and Table 4 shows the values of the synthesized compounds. Finally, the synthesized compounds did not inhibit 5 important enzymes of the cytochrome P450 (CYP) system, which have an important role in the degradation of drug candidates for elimination from the body.

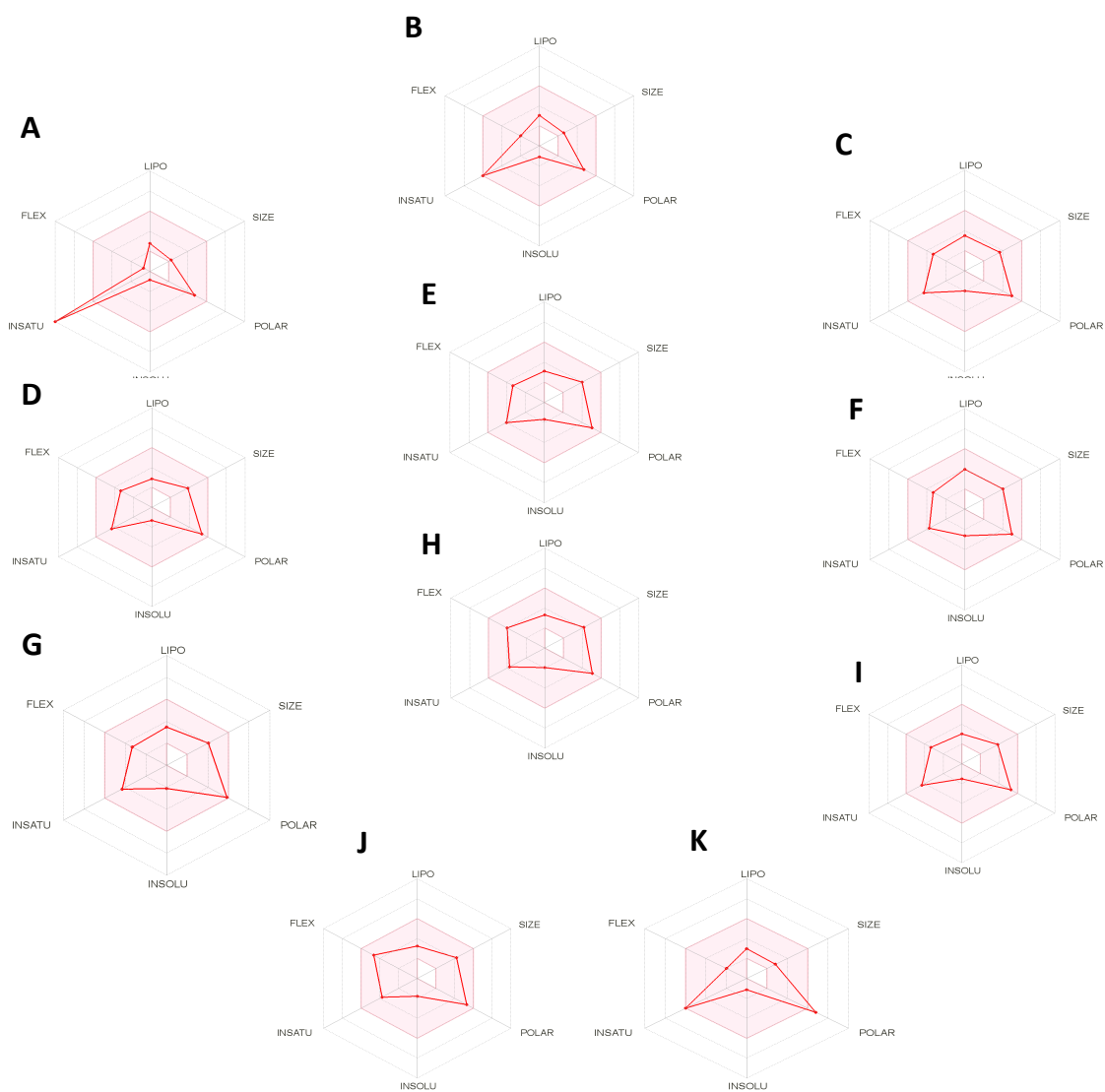


Figure 2: Bioavailability radar plot shows optimal physicochemical area for drug candidates as A)1 B)2 C)3 D)4 E)5 F)6 G)7 H)8 I)9 J)10 K)AZM (The pink area defines the optimal range for each properties)

Table 3: In-silico physic-chemical properties of sulfonamide derivatives.

ADME Properties	Molecule ID									
	1	2	3	4	5	6	7	8	9	10
	Acetazolamide									
	Physicochemical-properties									
Molecular weight (g/mol)	172.20	200.26	297.37	312.39	326.41	325.43	329.44	340.44	313.37	341.43
No. of heavy atoms	13	13	20	21	22	22	21	23	21	23
No. of rotatable bonds	3	3	5	5	5	5	5	6	5	7
No. of H-bond acceptors	6	4	5	6	6	5	5	6	6	6
No. of H-bond donors	2	2	2	3	2	2	2	2	2	2
Molar refractivity	45.22	49.92	80.48	87.20	92.10	90.10	88.07	96.91	81.57	89.64
TPSA (Å ²)	151.66	94.56	100.88	112.91	104.12	100.88	126.18	104.12	110.11	110.11
	Lipophilicity									
M LOGP	-2.34	0.12	0.14	-0.66	-0.40	0.66	0.14	-0.14	-0.66	-0.41
	Water solubility									
LogS (ESOL)	-1.14	-1.12	-1.97	-1.33	-1.70	-2.62	-2.12	-1.94	-1.51	-1.79
Solubility	Very soluble	Very soluble	Very soluble	Very soluble	Very soluble	Soluble	Soluble	Very soluble	Very soluble	Very soluble
	Pharmacokinetics									
Absorption	Low	High	High	High	High	High	High	High	High	High
BBB permeant	No	No	No	No	No	No	No	No	No	No
CYP1A2 inhibitor	No	No	No	No	No	No	No	No	No	No
CYP2C19 inhibitor	No	No	No	No	No	No	No	No	No	No
CYP2C9 inhibitor	No	No	No	No	No	No	No	No	No	No
CYP3A4 inhibitor	No	No	No	No	No	No	No	No	No	No
Log K _p (skin permeation-cm/s)	-7.84	-7.64	-7.67	-8.57	-8.33	-7.28	-7.91	-8.16	-8.38	-8.27
	Druglikeness									
Lipinski violation	Yes:0	Yes:0	Yes:0	Yes:0	Yes:0	Yes:0	Yes:0	Yes:0	Yes:0	Yes:0
Ghose violation	No:1 violation	Yes	Yes	Yes	Yes	Yes	Yes	Yes	Yes	Yes
Weber violation	No:1 violation	Yes	Yes	Yes	Yes	Yes	Yes	Yes	Yes	Yes
Bioavailability score	0.55	0.55	0.55	0.55	0.55	0.55	0.55	0.55	0.55	0.55

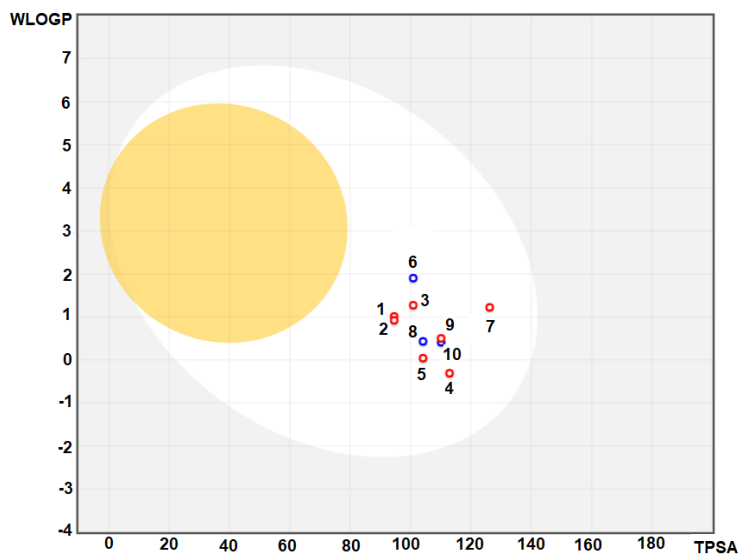


Figure 3: The Boiled-Egg model represents an intuitive evaluation of synthesized compound 1, 2, 3, 4, 5, 6, 7, 8, 9 and 10

3.2. Molecular Docking Study

Molecular docking results for both CA IX and CA XII were presented based on comparison of all molecules with the reference molecule. Acetazolamide, used as a reference, is a heterocyclic sulfonamide. It is a diuretic and carbonic anhydrase inhibitor medication that is used to treat several illnesses [23]. CA IX contains four domains [24, 25]: an N-terminal proteoglycan-like (PG) domain, a CA catalytic domain, a transmembrane segment (TM), and an intracytoplasmic (IC) portion. Similarly, CA XII includes these domains except the Pg domain. It is known that for the inhibition of these enzymes, they form a semi-covalent tetrahedral bond between the Zn ion in the active site and the inhibitor [26]. In particular, sulfonamide derivative inhibitors bond with Zn through nitrogen with consequent substitution of the zinc-bound water molecule, and by two H-bonds of the sulfonamide moiety with residue Thr199 [27-29]. An X-ray crystal structure of the catalytic domain of CA IX in complex with acetazolamide was determined [4]. In the structure with 3IAI ID from PDB, 2 hydrogen bonds are established between the native ligand acetazolamide and Thr199, and also formed a hydrogen bond with GLN92. The reference molecule was redocked to control the binding site and we observed the same bindings with the same amino acids (Fig. 4). Similarly, the binding properties of other compounds with the CA IX enzyme are given in Table 4.

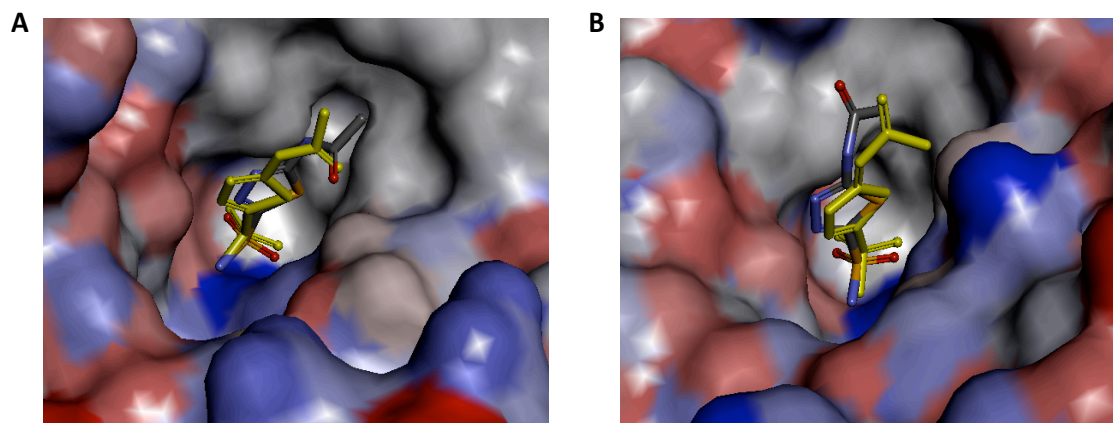


Figure 4: A) Redock image for the CA IX-Acetazolamide complex. The yellow colored molecule represents acetazolamide in complex with the enzyme in the original PDB file. RMSD: 1.0857 Å. B) Redock image for CA XII- Acetazolamide complex. The yellow colored molecule represents acetazolamide in complex with the enzyme in the original PDB file. RMSD: 1.1292 Å

Figure 5 shows that the hydrogen bonds of the reference molecule with CA IX are between THR199 and N, between THR199 and O, and between GLN92 and O. In addition, acetazolamide establishes several van der Waals interactions with residues HIS119, VAL143, VAL131, LEU91, LEU141 and THR200.

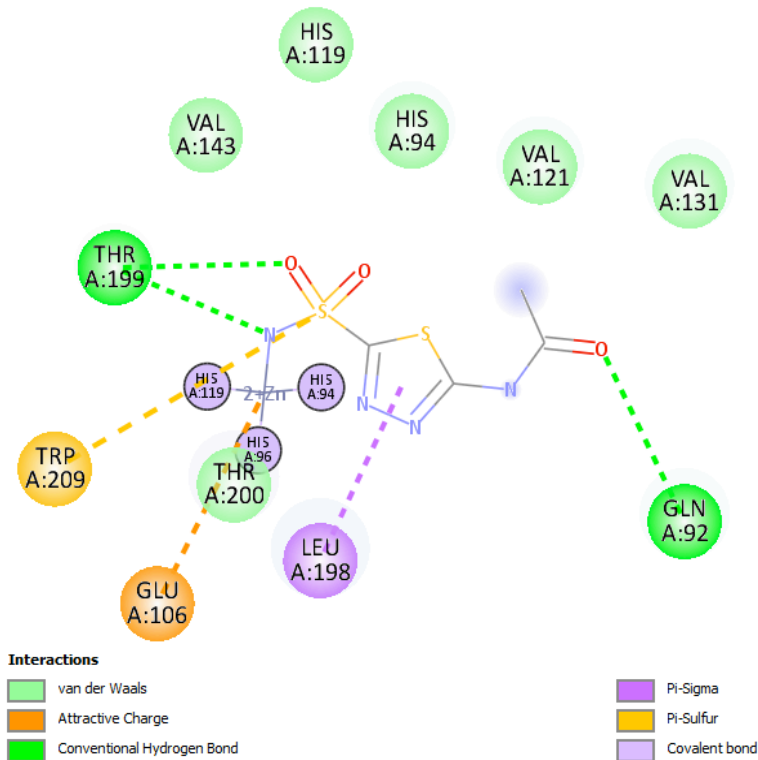


Figure 5: 2D plots of interactions of Acetazolamide with CA IX

Table 4: The docking scores for CA IX

Receptor	Molecule ID	Binding Energy (kcal/mol)	Inhibition Constant, Ki	Hydrogen Bonds (Donor - Acceptor)	The distance of hydrogen bonding (Å)
CA IX	1	-4.67	374.87 μ M	H18 – Glu106:OE2 H18 – THR199:OG1 O10 - THR199:N	3.05 1.62 2.94
	2	-5.65	71.95 μ M	H20 – Glu106:OE2 H20 – THR199:OG1 O9 – THR199:N H19 – Pro201:O H18 – Pro201:O	3.01 1.75 2.86 2.10 2.11
	3	-5.77	58.62 μ M	H30 – Glu106:OE2 H30 – THR199:OG1 O14 - THR199:N	2.91 1.70 2.90
	4	-6.19	28.85 μ M	H31 – Glu106:OE2 H31 – THR199:OG1 O12 - THR199:N	3.10 1.65 2.95
	5	-6.38	21.15 μ M	H31 – THR199:OG1 O12 - THR199:HN	1.65 1.97
	6	-7.44	3.52 μ M	H31 – Glu106:OE2 H31 – THR199:OG1 O12 - THR199:N	2.98 1.65 2.79
	7	-6.00	40.23 μ M	H31 – THR199:OG1 O12 - THR199:N	1.69 2.92
	8	-6.30	23.97 μ M	H31 – THR199:OG1 O12 - THR199:HN	1.79 1.87
	9	-6.29	24.51 μ M	H31 – THR199:OG1 O12 - THR199:N O16 – GLN92:NE2	1.69 3.04 2.81
	10	-5.99	40.68 μ M	H33 – Glu106:OE2 H33 – THR199:OG1 O12 – THR199:OG1 O12 - THR199:N O16 – GLN92:NE2	2.86 1.82 3.39 2.88 2.83
	Reference-Acetazolamide	-5.25	141.79 μ M	N1 – THR199:OG1 O1 – THR199:OG1 O1 - THR199:N O3 – GLN92:NE2	2.81 3.01 2.90 2.89
	Native Ligand Acetazolamide			N1 – THR199:OG1 O1 – THR199:OG1 O1 - THR199:N O3 – GLN92:NE2	2.75 3.28 2.85 3.25

In almost all adducts used in this study, the interaction of sulfonamide derivatives with enzyme active site is quite similar. All derivative molecules established hydrogen bonds with Thr199 of CA IX both through the oxygen and the hydrogen. Some of them also formed hydrogen bonds with GLU106. It is known that GLU106 is involved in the catalytic mechanism of the CA enzyme [30]. It has been observed that sulfonamide derivatives named 1, 2, 3, 4, 6 and 10 form H bond with this amino acid. The binding score of the sulfonamide named 6 is the highest, -7.44

kcal/mol. Moreover, when the binding diagrams were examined, it was determined that only one of them formed hydrogen bonds with GLN92, just like acetazolamide. This molecule, named **9**, also interacted with the enzyme structure with similar van der Waals interactions (Fig. 6).

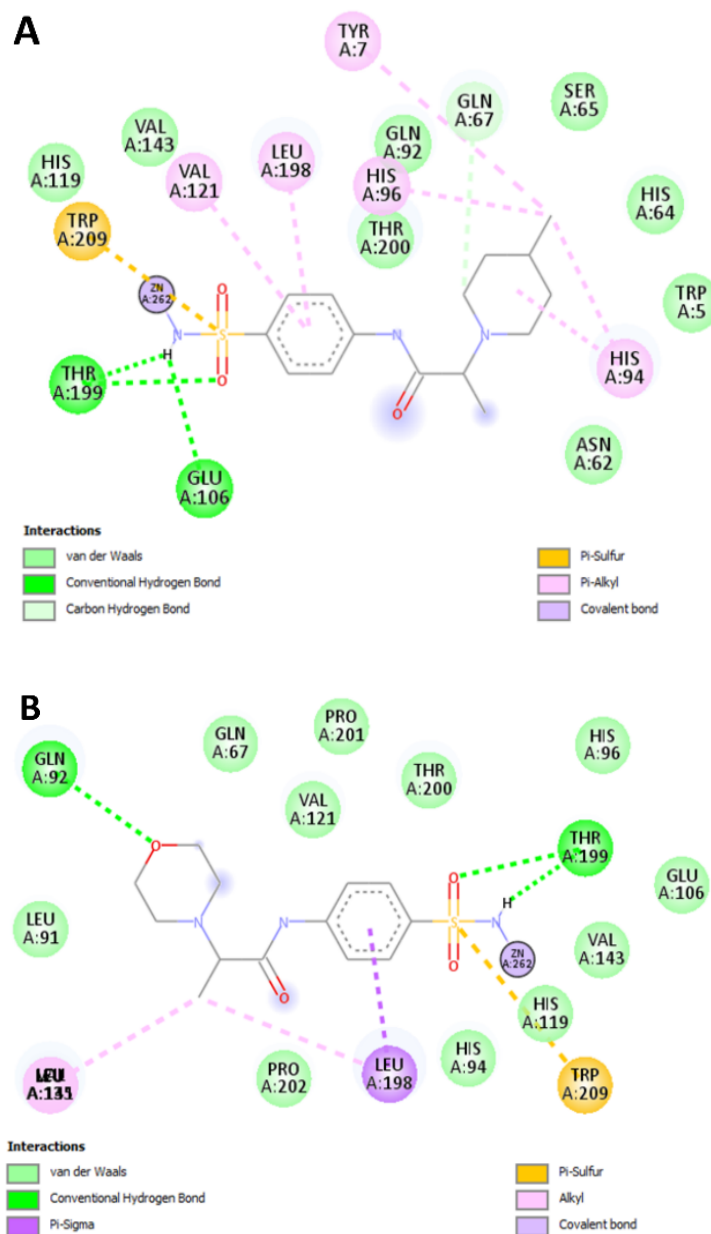


Figure 6: 2D plots of interaction of sulfonamide with enzyme. A) **6** with CA IX and B) **9** with CA IX

The docking results of all molecules with CA XII (PDB ID: 1JD0) are shared in Table 5. It was determined that 2 different hydrogen bonds were formed between acetazolamide and CA XII with the Thr199 residue. There were also van der Waals interactions with HIS199, VAL143, HIS94, THR200, VAL121 and LEU141.

Table 5: The docking scores for CA XII

Reseptör	Molecule ID	Binding Energy (kcal/mol)	Inhibition Constant, Ki	Hydrogen Bonds (Donor - Acceptor)	The distance of hydrogen bonding (Å)
CA XII	1	-3.92	1.33 mM	N11 – THR199:OG1 O10 – THR199:OG1 O10 - THR199:N	2.91 3.14 2.60
	2	-4.70	357.36 µM	H20 – Glu106:OE1 H20 – THR199:OG1 O9 - THR199:N H19 – THR200:OG1 H18 – PRO201:O	2.89 1.99 2.92 2.06 2.58
	3	-5.88	48.91 µM	H30 – THR199:OG1 O14 – THR199:OG1 O14 - THR199:N	2.24 3.39 2.94
	4	-5.29	132.08 µM	H31 – THR199:OG1 O12 - THR199:N	1.64 2.91
	5	-6.34	22.45 µM	H31 – THR199:OG1 O12 - THR199:N	1.91 2.94
	6	-6.39	20.75 µM	H31 – THR199:OG1 O12 - THR199:N	2.03 2.87
	7	-6.44	18.88 µM	H31 – THR199:OG1 O12 - THR199:N H30 – GLN92:OE1 S16 – TRP5:NE1	1.75 2.72 2.13 3.78
	8	-5.29	132.85 µM	H31 – THR199:OG1 O12 - THR199:N O4 – GLN92:NE2 N16 – SER135:OG	1.77 2.78 3.15 2.97
	9	-6.10	33.59 µM	H31 – THR199:OG1 O12 - THR199:N	1.82 2.85
	10	-5.10	183.52 µM	H33 – THR199:OG1 O12 – THR199:OG1 O12 - THR199:N O16 – SER135:OG	1.99 3.15 2.63 2.83
	Reference-Acetazolamide	-3.53	2.60 mM	N1 – THR199:OG1 O2 – THR199:OG1 O2 - THR199:N	2.76 3.00 2.80
	Native Ligand Acetazolamide			N1 – THR199:OG1 O2 - THR199:N	2.87 2.96

In silico studies revealed that all synthesized molecules showed average binding energies towards the target protein ranging from -6.44 to -3.32 kJ mol⁻¹. All sulfonamide derivatives formed hydrogen bonds with the key amino acid Thr199. Some are also linked by hydrogen bonds with different amino acids (**2**, **7**, **8**, and **10**). In addition, van der Waals interactions, which are important for enzyme inhibition, were examined. All derivatives have van der Waals interaction with HIS119 and VAL143 in common.

In this context, based on the binding between acetazolamide and CA XII, the molecules with the most similar and common bonds with CA XII are **6** and **9**, shown in Fig. 7.

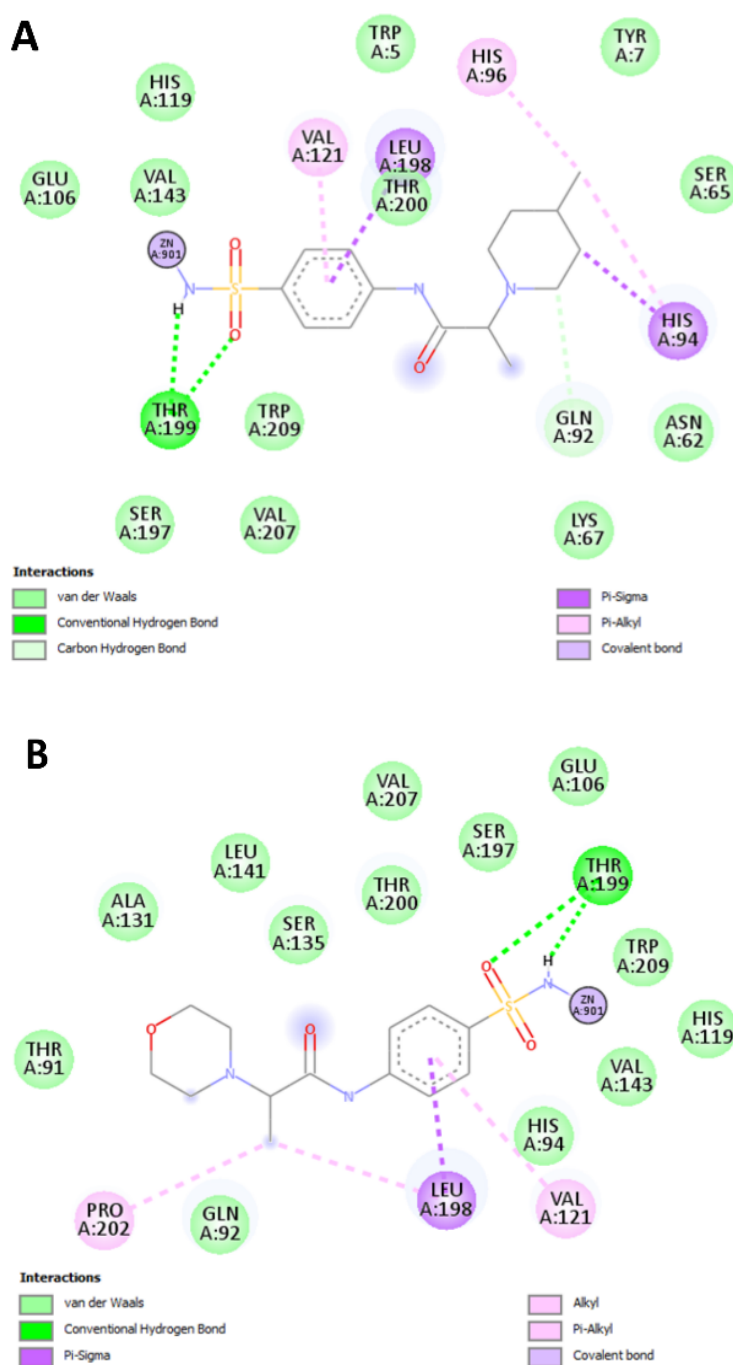


Figure 7: 2D plots interactions of sulfonamide with enzyme. A) **6** with CA XII and B) **9** with CA XII

4. Conclusion

In summary, overexpression of CA IX is associated with tumor hypoxia and is therefore being investigated as a diagnostic and therapeutic marker. Sulfonamides, which have efficacy in many different diseases, have the potential to be used as antitumor drugs. The availability of simulations to design selective CA enzyme inhibitors also contributes to this. In particular, CA

IX-targeted therapeutic agents have been developed and clinical trials have also yielded positive results [31]. In this study, we aimed to determine the anti-cancer properties of sulfonamide derivatives, which we synthesized and determined many properties in our previous study, and especially their contribution to CA IX and CA XII enzyme inhibition. In conclusion, we found good binding energies for both CA IX and CA XII of the sulfonamide derivative named **6** and **9**. In addition, compared to acetazolamide, we think that they may be candidates as an anti-tumor drug due to the similarity of the bond types and attachment to the active site of the enzyme (Fig. 8).

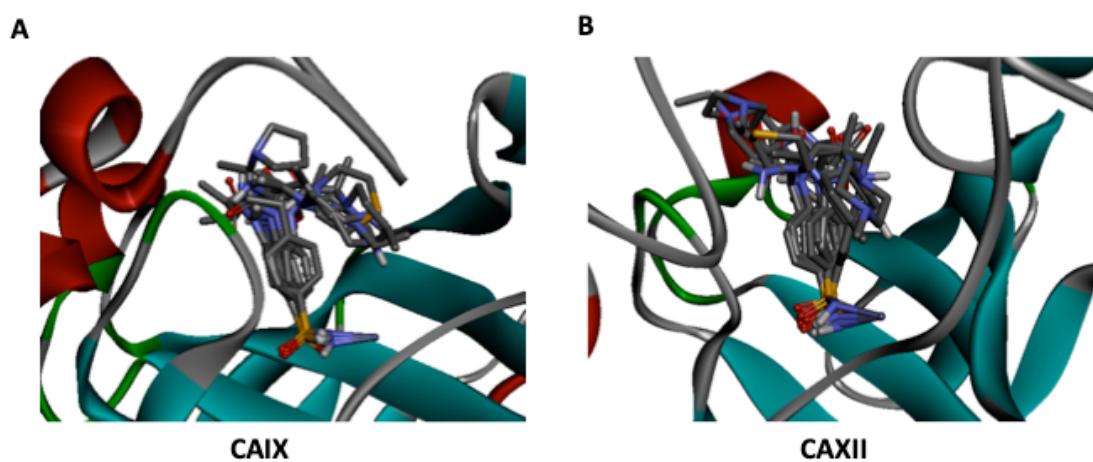


Figure 8: Superimposition of sulfonamide derivatives at the active site of the A) CA IX and B) CA XII

References

- [1] Andreucci, E., Ruzzolini, J., Peppicelli, S., Bianchini, F., Laurenzana, A., Carta, F., Supuran, C.T., Caalorini, L., *The carbonic anhydrase IX inhibitor SLC-0111 sensitises cancer cells to conventional chemotherapy*, *Journal of Enzyme Inhibition and Medicinal Chemistry*, 34(1), 117-123, 2019.
- [2] Supuran, C.T., Scozzafava, A., *Carbonic anhydrase inhibitors and their therapeutic potential*, *Expert Opinion on Therapeutic Patents*, 10(5), 575-600, 2000.
- [3] Supuran, C.T., *Structure and function of carbonic anhydrases*, *Biochemical Journal*, 473, 2023–2032, 2016.
- [4] Alterio, V., Hilvo, M., Di Fiore, A., Supuran, C.T., Pan, P., Parkkila, S., Scaloni, A., et al., *Crystal structure of the catalytic domain of the tumor-associated human carbonic anhydrase IX*, *PNAS*, 106(38), 16233-16238, 2009.
- [5] Chegwidde, W.R., Carter, N.D., Edwards Y.H., *The carbonic anhydrases*, Birkhauser, Boston, 2000.
- [6] Sly, W.S., Hu P.Y., *Human carbonic anhydrases and carbonic anhydrase deficiencies*, *Annual Review of Biochemistry*, 64, 375-401, 1995.

[7] Supuran, C.T., Scozzafava, A., *Carbonic Anhydrase Inhibitors*, Current Medicinal Chemistry, 363(1), 61-97, 2001.

[8] Supuran, C.T., Scozzafava, A., *Carbonic anhydrases as targets for medicinal chemistry*, Bioorganic & Medicinal Chemistry, 15, 4336–4350, 2007.

[9] Stadie, W.C., O'Brien, H., *The catalytic of the hydration of carbon dioxide and dehydration of carbonic acid by an enzyme isolated from red blood cells*, Journal of Biological Chemistry, 103, 521–529, 1933.

[10] Wassel, M.M.S., Ragab, A. et al., *Novel adamantine-pyrazole and hydrazine hybridized: design, synthesis, cytotoxic evaluation, SAR study and molecular docking simulation as carbonic anhydrase inhibitors*, Journal of Molecular Structure, 1223, 128966, 2021.

[11] Svastová, E., Hulíková, A., Rafajová, M., Zat'ovic'ová, M., Gibadulinová, A., Casini, A., Cecchi, A., Scozzafava, A., Supuran, C.T., Pastorek, J., et al., *Hypoxia activates the capacity of tumor-associated carbonic anhydrase IX to acidify extracellular pH*, FEBS Letters, 577, 439–445, 2004.

[12] Koyuncu, I., Temiz, E., Durgun, M., Kocyigit, A., Yuksekdag, O., Supuran, C.T., *Intracellular pH-mediated induction of apoptosis in HeLa cells by a sulfonamide carbonic anhydrase inhibitor*, International Journal of Biological Macromolecules, 2022.

[13] Temiz, E., Koyuncu, I., Durgun, M., Caglayan, M., Gonel, A., Güler, E. M., Kocyigit, A. and Supuran, C.T., *Inhibition of carbonic anhydrase IX promotes apoptosis through intracellular PH level alterations in cervical cancer cells*. International Journal of Molecular Sciences, 22(11), 6098, 2021.

[14] Durgun, M., Turkmen, H., Zengin, G., Zengin, H., Koyunsever, M., Koyuncu, I., *Synthesis, characterization, in vitro cytotoxicity and antimicrobial investigation and evaluation of physicochemical properties of novel 4-(2-methylacetamide) benzenesulfonamide derivatives*, Bioorganic Chemistry, 70, 163-172, 2017.

[15] Chohan, Z.H., Hassan, M., Khan, K.M., Supuran, C.T., *In-vitro antibacterial, antifungal and cytotoxic properties of sulfonamide derived Schiff's bases and their metal complexes*, Journal of Enzyme Inhibition and Medicinal Chemistry, 20(2), 183-188, 2004.

[16] Connor, E.E., *Sulfonamide antibiotics*, Primary Care Update for OB/GYNS, 5(1), 32-35, 1998.

[17] Turkmen, H., Zengin, G., Buyukkircali, B., *Synthesis of sulfonamide derivatives and investigation of in vitro inhibitory activities and antimicrobial and physical properties*, Bioorganic Chemistry, 39(3), 114-119, 2011.

[18] Durgun, M., Zengin, G., Zengin, H., Koyuncu, I., Turkoglu, S., Sonmez, H., Kuru, A., *Synthesis, characterization, cytotoxicity evaluation and physicochemical properties of some novel N⁴-substituted aminobenzenesulfonamides*, Indian Journal of Chemistry, 60B, 888-900, 2021.

[19] Morris, G.M. et al., *Auto dock 4 and auto dock tools 4: automated docking with selective receptor flexibility*, Journal of Computational Chemistry, 30, 2785–91, 2009.

[20] Hanwell, M.D., Curtis, D.E., Lonie, D.C., Vandermeersch, T., Zurek, E., Hutchison, G.R., *Avogadro: an advanced semantic chemical editor, visualization, and analysis platform*,

Journal of Cheminformatics, 4, 17, 2012.

[21] Daina, A., Michielin, O., Zoete, V., *SwissADME: a free web tool to evaluate pharmacokinetics, drug-likeness and medicinal chemistry friendliness of small molecules*, Scientific Reports, 7, 42717, 2017.

[22] Mishra, S., Dahima, R., *In-vitro ADME studies of TUG-891, a GPR-120 inhibitor using Swiss ADME predictor*, Journal of Drug Delivery and Therapeutics, 9(2-s), 266-369, 2019.

[23] Farzam, K., Abdullah, M., *Acetazolamide*. StatPearls Publishing, Treasure Island (FL), 2022.

[24] Opavsky, R., Pastorekova, S., Zelnik, V., Gibadulinova, A., Stanbridge, E.J., Zavada, J., Kettmann, R., Pastorek, J., *Human MN/CA9 gene, a novel member of the carbonic anhydrase family: structure and exon to protein domain relationships*, Genomics, 33, 480–487, 1996.

[25] Hilvo, M., Baranauskienė, L., Salzano, A.M., Scaloni, A., Matulis, D., Innocenti, A., Scozzafava, A., Monti, S.M., Di Fiore, A., De Simone, G., Lindfors, M., Janis, J., Valjakka, J., Pastorekova, S., Pastorek, J., Kulomaa, M.S., Nordlund, H.R., Supuran, C.T., Parkkila, S., *Biochemical characterization of CA IX, one of the most active carbonic anhydrase isozymes*. Journal of Biological Chemistry, 283, 27799–27809, 2008.

[26] Boyluğ, Z.E., *Yoğunluk Fonksiyonel Teori Temelli Kantitatif Yapı-Etki Analizleri (QSAR): Kumarin Moleküllerinin Karbonik Anhidraz Enzimine Karşı İnhibisyon Etkisinin Modellenmesi*. MSc Thesis, Aksaray University, Aksaray, Turkey, 2016.

[27] Supuran, C.T., Scozzafava, A., Casini, A., *Carbonic anhydrase inhibitors*, Medicinal Research Reviews, 23(2), 146–189, 2003.

[28] Stams, T., Christianson, D.W., *In the carbonic anhydrases. new horizons*; Chegwiddden, W.R., Carter, N.D., Edwards, Y.H., Eds. Birkhäuser Verlag: Basel, Switzerland, 159p., 2000.

[29] Lindahl, M., Vidgren, J., Eriksson, E., Habash, J., Harrop, S., Helliwell, J., Liljas, A., Lindeskog, M., Walker, N., *In Carbonic Anhydrase: From Biochemistry and Genetics to Physiology and Clinical Medicine*, Botre, F., Gros, G., Storey, B.T., Eds. VCH: Weinheim, Germany, 111p., 1991.

[30] Özensoy, Ö., *Kanser ile ilişkili Karbon Anhidraz IX ve XII izoenzimlerinin (CA-IX, CA-XII) ekspresyonu, saflaştırılması ve bazı bileşiklere karşı inhibisyon etkilerinin araştırılması*, PhD Thesis, Balıkesir University, Balıkesir, Turkey, 2006.

[31] Eckert, A.W., Lautner, M.H., Schutze, A., Bolte, K., Bache, M., Kappler, M., Schubert, J., Taubert, H., Bilkenroth, U., *Co-expression of Hif1alpha and CA IX is associated with poor prognosis in oral squamous cell carcinoma patients*, Journal of Oral Pathology and Medicine, 39, 313–317, 2010.



Microbiological Investigation of the Effects of Olanzapine with Thymoquinone on the Intestine

Ayşe Nilay GÜVENÇ^{1*}, Sebile AZIRAK², Deniz TAŞTEMİR KORKMAZ³, Sedat BİLGİÇ⁴, Nevin KOCAMAN⁵, Mehmet Kaya ÖZER⁶

¹University of Adiyaman, Vocational School of Health Services, Adiyaman, Türkiye
anguvenc@adiyaman.edu.tr, ORCID: 0000-0002-6464-0643

²University of Adiyaman, Vocational School of Health Services, Adiyaman, Türkiye
sazirak@adiyaman.edu.tr, ORCID: 0000-0001-9040-6773

³University of Adiyaman, Department of Medical Biology, Faculty of Medicine, Adiyaman, Türkiye
dtastemir@adiyaman.edu.tr, ORCID: 0000-0001-5844-8914

⁴University of Adiyaman, Vocational School of Health Services, Adiyaman, Türkiye
sbilgic@adiyaman.edu.tr, ORCID: 0000-0001-8410-2685

⁵University of Firat, Department of Histology, Faculty of Medicine, Elazig, Türkiye
drnkocaman@gmail.com, ORCID: 0000-0002-6682-6345

⁶University of Adiyaman, Department of Pharmacology, Faculty of Medicine, Adiyaman, Türkiye
mkayaozer@adiyaman.edu.tr, ORCID: 0000-0002-7961-4130

Received: 16.03.2022

Accepted: 02.06.2022

Published: 30.06.2022

Abstract

The aim of our study is to examine the effect of thymoquinone (TQ) in obese rats induced with the antipsychotic drug olanzapine (OL). Thirty-five female Spraque-Dawley rats were divided into five groups (n = 7): Control, OL (2 mg / kg OL daily), OL + TQ1 (2 mg / kg OL + 20 mg / kg TQ), OL + TQ2 (2 mg / kg OL + 40 mg / kg TQ) and the OL + TQ3 group (2 mg / kg OL + 80 mg / kg TQ). On the 15th day of treatment, intestinal tissue was removed for analysis. It has been found that TQ treatment affects the levels of Firmicutes and Bacteroides at varying rates in the intestinal flora in OL + TQ1, OL + TQ2, and OL + TQ3 groups, and also has a significant role in the apoptotic effect of TQ. In conclusion, with this study, it was determined that the



treatment of TQ has a protective property against the side effects of OL. TQ can be an effective treatment method to increase therapeutic effectiveness.

Keywords: Olanzapine; Thymoquinone; Obesity; *Firmicutes*; *Bacteroides*.

Olanzapin ile Timokinon'un Bağırsak Üzerindeki Etkilerinin Mikrobiyolojik Olarak Araştırılması

Öz

Çalışmamızın amacı, bir antipsikotik ilaç olanzapin (OL) ile indüklenen obez sıçanlarda timokinonun (TQ) etkisini incelemektir. Otuz beş dişi Spraque-Dawley sıçanı beş gruba ayrıldı (n = 7): Kontrol, OL (günlük 2 mg / kg OL), OL + TQ1 (2 mg / kg OL + 20 mg / kg TQ), OL + TQ2 (2 mg/kg OL + 40 mg/kg TQ) ve OL + TQ3 grubu (2 mg/kg OL + 80 mg/kg TQ). Tedavinin 15. gününde, analiz için bağırsak dokusu çıkarıldı. TQ tedavisinin, OL+TQ1, OL+TQ2 ve OL+TQ3 gruplarında bağırsak florasındaki *Firmicutes* ve *Bacteroides* düzeylerini değişen oranlarda etkilediği ve ayrıca TQ'nun apoptotik etkisinde önemli rolü olduğu tespit edilmiştir. Sonuç olarak, bu çalışma ile TQ tedavisinin OL'nin yan etkilerine karşı koruyucu özelliği olduğu belirlendi. TQ, terapötik etkinliği artırmak için etkili bir tedavi yöntemi olabilir.

Anahtar Kelimeler: Olanzapin; Timokinon; Obezite; *Firmicutes*; *Bacteroides*.

1. Introduction

Obesity is a disease that has increased in number in recent years and has become a serious problem in the world. In humans; cardiovascular, liver and gallbladder diseases, diabetes, osteoarthritis, hyperlipidemia, cancer, asthma, obstructive sleep apnea syndrome, and may result in death [1]. In 2015, 107.7 million children and 603.7 million adults were reported to be obese worldwide [2]. It is also estimated that obesity will affect 51%³ and about a quarter of the adult population by 2030 [4]. According to data from the World Health Organization, weight and obesity in Europe cause 80% of diabetes in adults, 35% of heart disease, 55% of hypertension, and deaths of more than one million people per year [5]. Since obesity develops due to changes in adipose tissue, we can say obesity = body mass index (BMI). BMI is calculated as the ratio of body weight to the square of the neck. 32 genes affecting BMI were identified, but the most effective factor was considered to be environmental factors caused by energy-intensive nutrition and reduced [6]. Recent research has shown that microbial changes in the intestine have an impact on obesity. Intestinal microbiota affects human metabolism. The presence of microbial flora and its metabolites are responsible for these effects. The microbiota has important effects on the

production of vitamins, destruction of non-breakable nutrients, metabolites, and immunity [3, 4, 7]. It benefits energy metabolism by producing short-chain fatty acids stimulating substances, affecting the metabolic pathway and insulin resistance in fat cells and peripheral organs. Alcohol, stress, smoking, socioeconomic status, and eating habits are effective on the microbiota. [3, 4, 8]. Dysbiosis with the change of the intestinal flora causes some metabolic disorders [9]. These metabolic disorders include impaired glucose, lipid levels, inflammation, altered intestinal permeability, insulin resistance, high calorie increase, obesity, and physiological balance changes [4, 10]. In the last decade, different results have been obtained on the effect of intestinal microbiota on obesity, leading studies to be in this direction [9]. Various methods of analysis, methods of taking samples, differences in body mass index classifications around the world and the increase in research findings have led to differences in the results of the study at the level of obesity relation of intestinal microbiota. Until the last five years, it has been known that the intestinal microbial flora of obese people is less than the weak ones, today it has been shown that this result is the opposite. As a result of the research findings, changes in the intestinal flora, namely intestinal dysbiosis, have gained importance [4, 7, 11]. In microbiome studies, it has been tried to understand the cause and effect relationships that cause obesity and intestinal microbiota connection, except for the types and rates of bacteria [12]. As is generally known, changes in the intestinal microbiota profile are important in obesity [9]. In healthy humans, the intestinal microbial consists of 6 classes: *Firmicutes*, *Bacteroidetes*, *Proteobacteria*, *Actinobacteria*, *Fusobacteria* and *Verrucomicrobia*. *Bacteroidetes* and *Firmicutes* make up 90% of the intestinal microbiota. *Bacteroides*, *Eubacterium*, *Clostridium*, *Ruminococcus*, *Peptococcus*, *Peptostreptococcus*, *Bifidobacterium*, *Fusobacterium* are the most obligatory anaerobes at the class level and the facultative anaerobes are *Escherichia*, *Enterobacter*, *Enterococcus*, *Klebsiella*, *Proteus* and *Lactobacillus*. *Bacteroidetes* / *Firmicutes* ratio is thought to be very effective on obesity [1]. It is known that some bacterial species belonging to *Bacteroidetes* and *Firmicutes* branches are dominant in the normal intestinal flora [13]. The main causes of obesity are not thought to be solely due to genetic changes and dietary differences. Genetic and environmental factors increase the tendency to obesity. Even antipsychotic drugs used are closely related to obesity, and antipsychotic drugs are known to cause weight gain in obesity. Olanzapine (OL), one of these antipsychotic drugs, has less side effects than other antipsychotic drugs [14]. However, significant weight gain leads to an increase in serum cholesterol and triglyceride levels. Again, OL has a stronger association with obesity and insulin resistance. Studies have shown that OL causes the most weight gain compared to other antipsychotic drugs. Therefore, patients taking antipsychotic drugs are thought to be at risk. The increase in the use of antipsychotic drugs worldwide and the numerous side effects of these drugs have necessitated the use of natural

products. One of these natural products is thymoquinone (TQ). TQ black seed (*Nigella Sativa*) is the most important bioactive component found in the essential oil of 18.4-24%. TQ has many beneficial effects such as antioxidant, antihyperlipidemic, antidiabetic, anti-inflammatory, gastroprotective and hepatoprotective. Studies have shown that TQ has hypoglycemic, hypolipidemic and hypocholesterolemic effects [15]. In our study, it is thought that atypical antipsychotic drugs can be removed with TQ which is a natural protective product against various metabolic changes such as weight gain induced by side effects.

The aim of our study is to determine to what extent the protective effect of TQ against OL, which is thought to cause obesity, on some *Bacteroides* and *Firmicutes* strains in the intestinal microflora. Recent studies show that more research is needed to determine the effect of intestinal microbiota on obesity. Our research will guide other studies in this field.

2. Materials and Methods

2.1. Chemicals

OL was obtained from Ali Arif Ilac Sanayi (ARIS), Istanbul, Türkiye. TQ (purity > 98 %) was purchased from Sigma. All other chemicals used were of the best analytical grade.

2.2. Animals

In this study, 35 female Sprague Dawley rats (230-280 g and 4 months old) were obtained from Firat University Laboratory Livestock and Research Center. The experiments were carried out according to the protocol (Protocol # 2015/36) approved by Firat University Faculty of Medicine Laboratory Animals Ethics Committee. The rats were provided with appropriate nutrition and shelter (rat food and tap water at 21 ± 1 °C for 12 hours without light and light). The drug and preservative application lasted 2 weeks.

2.3. Experimental design

In this study, 35 rats were randomly divided into 5 groups with 5 sherds. Doses of 25 mg, 50 mg, and 100 mg of TQ were administered. 1st group control, 2nd group OL, 3rd group OL + TQ1 (OL + 25 mg TQ), 4th group OL + TQ2 (OL + 50 mg TQ), and 5th group OL + TQ3 (OL + 100 mg TQ). Saline solution was given to the control group by gavage once a day. Apart from the first group, OL was given to all groups 4 mg/kg once a day in the first week and 8 mg/kg in the second week. The TQ was given 25 to the third group, 50 to the fourth group, and 100 mg/kg body weight/day to the third group. In female Sprague Dawley rats, OL and TQ doses and durations were determined according to certain methods, and TQ was administered daily between

08:00 and 09:00 a.m. by gastric tube [16,17]. All compounds were treated with saline and administered by gavage once a day. At the end of the application, which continued for 2 weeks, the rats were euthanized by cardiac puncture. Intestinal tissues and blood samples were stored at -80 °C.

2.4. Bacterial RNA isolation and quantitative real-time PCR (qRT-PCR)

In our study, 4 genus levels of *Lactobacillus* sp. (LAC), *Faecalibacterium* sp. (FAE) from Firmicutes branch, and 2 genera of *Bacteroides* sp. (BAC) and *Prevotella* sp. (PRE) from Bacteroidetes branch were determined in intestinal tissues. qRT-PCR was used to detect the mRNA expression of LAC, FAE, BAC and PRE receptors. RNA isolation of intestinal tissues was performed. 30 mg intestinal tissue homogenizer (Bioprep-24, Allsheng) was homogenized. Total RNAs were extracted using an ExiPrep™ Tissue Total RNA isolation kit (Bioneer, K-3325) and quantified by measuring the absorbance at 260/230 nm and 260/280 nm using a NanoDrop spectrophotometer (Denovix DS-11). RNA must first be reverse transcribed into cDNA in a reverse transcription (RT) reaction. We also used primer pairs (Bionner S-1001) for qRT-PCR in our study of AccuPower® RT PreMix (Bioneer K-2041) according to the instructions. The RT-PCR was conducted following the instructions of the AccuPower GreenStar qPCR PreMix (Bioneer, Cat No: K-6210). The level of the mRNA expression of the LAC, FAC, PRO and BAC genes, was detected using the ExiCycler™96 qRT-PCR system (Bioneer). The PCR conditions were 95 °C for 1 min, followed by 45 cycles at 95 °C for 5 sec, and 55 °C for 40 second. The $2^{-\Delta\Delta Ct}$ method was used to calculate the results 30-35 (Table 1).

Table 1: Primer sequences used to replicate the gene region

Primer Sets	F.	R.
<i>Lactobacillus</i> spp.	GAGGCAGCAGTAGGGAATCTTC	GGCCAGTTACTACCTCTATCCTTCTTC
<i>Faecalibacterium</i> spp.	GAAGGCGGCCTACTGGGCAC	GTGCAGGCGAGTTGCAGCCT
<i>Bacteroides</i> spp.	GAAGGTCCCCACATTG	CGCTACTTGGCTGGTTCAG
<i>Prevotella</i> spp.	AAGGTCCCCACATTGG	CCGCGGCKGCTGGCAC

2.5. Terminal deoxynucleotidyl transferase dUTP nick-end labeling (TUNEL) assay

TUNEL test was used to determine the rate of apoptosis in the intestinal samples of all study groups. Intestinal samples were waxed, sectioned, and placed on slides covered with polylysine. Apoptotic cells were identified with the ApopTag Plus Peroxidase In situ Apoptosis Detection Kit (Chemicon, Cat no: S7101, USA). Samples were examined, evaluated, and visualized using an imaging-assisted binocular light microscope (Eclipse Ni-U; Nikon, Tokyo,

Japan). Nuclei stained blue with hematoxylin were evaluated as normal, brown ones as apoptotic cells. 10 randomly selected areas in the sections were scanned and at least 400 cells were examined. Apoptotic index (AI) was calculated as apoptotic cells / total (normal + apoptotic) cells [18,19].

2.6. Statistical analysis

Statistical analyses were performed using a statistical software package (SPSS version 20.0, SPSS, Chicago, IL). For histopathological analysis, results were expressed as means \pm standard deviation. The statistically significant difference was determined by ANOVA followed by Tukey's multiple comparison test. Probability values (p) less than 0.05 were considered to be statistically significant.

2.7. qPCR relative assessment

In the study, it was assumed that the reactions work 100% efficiently. Increase or decrease in the number of bacteria compared to control. Control 1 was accepted. The number of bacteria in the groups is how many times it increases and how many times it decreases compared to the control. $2^{(\text{average Control ct} - \text{average sample ct})}$. Relative evaluation [20], 2^{nd} calculation [21].

3. Results

3.1. Evaluation of apoptosis in intestine tissue

Examination of TUNEL staining for the determination of apoptotic cells under light microscopy; TUNEL positivity was significantly increased in the OL group (Figure 1B), OL + TQ1 (Figure 1C), OL + TQ2 (Figure 1D) and OL + TQ3 (Figure 1E) compared to control group (Figure 1A) ($p < 0.05$). TUNEL positivity was significantly decreased in OL + TQ1, OL + TQ2 and OL + TQ3 groups compared to OL group ($p < 0.05$). However, no significant change was observed between OL + TQ1, OL + TQ2, and OL + TQ3 (Table 2, Fig. 1).

Table 2: Effects of olanzapine and thymoquinone on apoptotic index (%)

Groups	Apoptotic Index (%) (AI; mean \pm SD)
Control	4.66 \pm 1.75 ^{b,c,d}
OL	26.50 \pm 3.27 ^{a,c,d,e}
OL + TQ-1	11.51 \pm 1.51 ^{a,b}
OL + TQ-2	9.16 \pm 1.16 ^{a,b}
OL + TQ-3	10.16 \pm 2.85 ^{a,b}

The apoptotic index of all the groups. Values are mean \pm SD for seven rats in each group. a: Significant from control; b: Significant from OL; c: Significant from OL + TQ-1; d: Significant from OL + TQ-2; e: Significant from OL + TQ-3 ($p \leq 0.05$). Abbreviations: OL, olanzapine; TQ, thymoquinone; OL + TQ-1, OL + 25 mg/kg TQ; OL + TQ-2, OL + 50 mg/kg TQ; OL + TQ-3, OL + 100 mg/kg TQ. 4 mg/kg once a day for the first week, 8 mg/kg once a day for the second week of OL was given to all groups, except control group

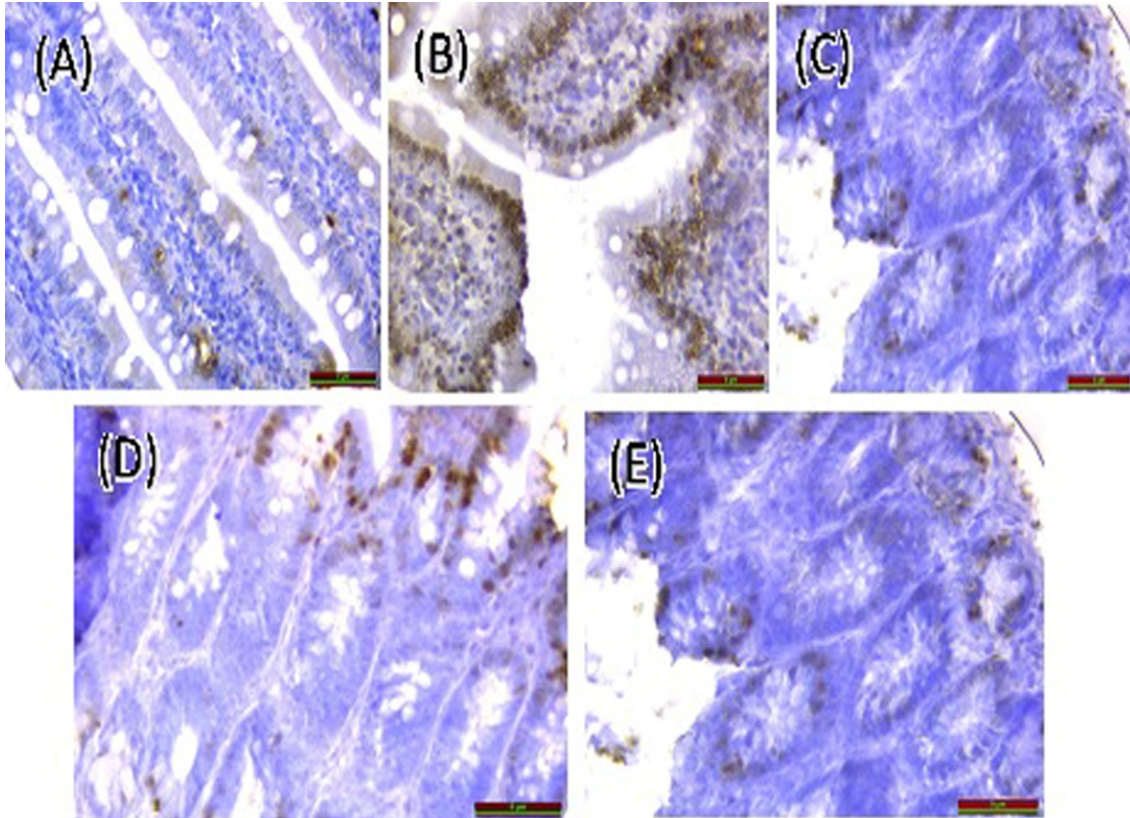


Figure 1: TUNEL staining for the determination of apoptotic cells

3.2. Evaluation of microbiological in intestine tissue

As a result of our study, the number of BAC was 5.8 times decreased in the OL group, OL + TQ1 decreased 3.36 times, OL + TQ2 group decreased 2.53 times, OL + TQ3 group decreased 6.06 times compared to the control (Table 3-4). According to the PRE control group OL group increased 149.08 times, OL + TQ1 12.64 times increased, OL + TQ2 group increased 9.98 times, and OL + TQ3 group decreased 81 times (Table 3-4). The number of LAC compared to the control group OL group 1.74 times, OL + TQ1 decreased 1.75 times, OL + TQ2 group decreased 2.11 times and OL + TQ3 group decreased 1.71 times (Table 3-4). The number of FAE compared to the control group OL group increased 5.89 times, OL + TQ1 decreased by 4.03 times, OL + TQ2 group increased 4.44 times, and OL + TQ3 group increased 3.56 times (Table 3-4).

Table 3: qPCR Relative Evaluation of bacterial levels

	Control Groups Avr Ct	OL Group			OL + TQ1			OL + TQ2			OL + TQ3		
		Avr Ct	ΔCt	Fold fark	AvrCt	ΔCt	Fold fark	AvrCt	ΔCt	Fold fark	AvrCt	ΔCt	Fold fark
Bac.	27.45 ± 2.29	30 ± 1.7	-2.55	5.8 d (0.17)	29.2 ± 3.2	-1.75	3.36 d (0.27)	28.8 ± 3.1	-1.34	2.53 d (0.395)	30.1 ± 3	-2.6	6.06 d (0.164)
Pre.	27.61 ± 5	20.39 ±1.16	7.22	149.08 i	23.94 ±2.01	3.66	12.64 i	24.29 ± 2.8	3.32	9.98 i	21.27 ±1.97	6.34	81 i
Lac.	19.79 ± 3.1	18.99 ±2.76	0.8	1.74 i	20.6 ±4.71	-0.81	1.75 d (0.57)	20.87 ±4.03	-1.08	2.11 d (0.473)	20.57 ± 6.2	-0.78	1,71 d (0.582)
Fae.	32.86 ± 2.12	30.30 ±5.64	2.56	5.89 i	34.87 ±1.87	-2.01	4.03 d (0.248)	30.71 ±3.08	2.15	4.44 i	31.03 ±1.39	1.83	3.56 i

(Increasing or decreasing the number of bacteria by control) = $2^{(average\ Control\ ct - average\ example\ ct)}$. (d: floor decreased compared to control, i: floor increased compared to control).

Table 4: qPCR Realistic Evaluation (Decrease in floor or multiplication according to control, if we accept control: 1)

Groups	BAC	PRE	LAC	FAE
Control	1	1	1	1
OL	1.17	149.08	1.74	5.89
OL + TQ1	0.279	12.64	0.57	0.248
OL + TQ2	0.395	9.98	0.473	4.44
OL + TQ3	0.164	81	0.582	3.56

4. Discussion

In our study, it was observed that the effect of TQ against the damage caused by OL in cells greatly reduced apoptotic cell damage and death. On the basis of this, TQ is thought to suppress apoptosis. Our results support other studies in terms of the antioxidant activity of TQ [22-27]. According to the microbiological results of our study, the decrease in the number of BAC in the OL group associated with obesity and the increase in the number of LAC and FAE belonging to the Firmicutes branch are similar to other studies [28-29]. The increase in the number of PRE from the Bacteroidetes phylum in the OL group was evaluated as a different result. The taxonomic categories within the phyla Firmicutes and Bacteroidetes cause changes in flora (dysbiosis) [4,11], as a result, the diversity on the basis of genus and species has become very important in different microbiota tables in obesity. *Bacteroides fragilis* and *Lactobacillus* sp. in a

study of microbiome levels in obese and overweight people. It has been reported that species are higher than lean ones and are directly proportional to body mass index [11]. In the OL + TQ1 group of our study, LAC and FAE decreased, the number of PRE increased, TQ was 25 mg. *Bacteroides* level in rat intestines with weight reduction was found to be higher than Firmicutes. It has been observed that the level of protection is in PRE and FAE, but not in BAC and LAC. In other studies, at the phylum level in obese; while an increase in the *Firmicutes* level was observed, a decrease in *Bacteroidetes* was reported, and the situation was reversed in people who were thin and dieted. [4, 7, 11, 30]. *Firmicutes* / *Bacteroidetes* ratio was higher in females with increased body mass index compared to males [11] and an increase in *Firmicutes* / *Bacteroidetes* ratio showed that the person was a candidate for obesity. *Firmicutes* bacteria break down non-degradable polysaccharides. Studies have shown that an increase in *Firmicutes* density and a decrease in *Bacteroidetes* take more energy and fat from foods than routine [4]. It has been found that there is an increase in the level of *Bacteroidetes* in people who lose weight with a poor calorie diet [31]. *Lactobacillus* sp. and *Bifidobacterium* sp. levels have been found to decrease in obese patients by reducing fatty food intake [32]. It has been determined that the intestinal microbiota in obese individuals varies according to the amount of calories taken with food, this variability is observed in thin individuals and not observed in obese individuals [33]. It has been reported that the composition of the gut microbiota is in mutual interaction with obesity, the level of *Bacteroidetes* in the microbiota in obese people is higher than *Firmicutes* in weight loss, and when these people have their previous eating habits and weight gain, the number turns in favor of *Firmicutes* [28-29]. In studies conducted with obese people, it was found that the number of Actinobacteria was high in the intestinal flora, the amount of *Firmicutes* was not affected and the number of *Bacteroidetes* decreased [34]. In another study, some *Lactobacillus* sp. numbers were thought to be associated with obesity [35]. In addition, it has been reported that the number of *Firmicutes* decreases with diet application in obese people [36]. It has been reported that the number of some *Firmicutes* species is increased in obese children compared to non-obese children [37]. *Bacteroidetes-Prevotella* sp. species have been found to increase after adolescent children lose weight [38]. In mice, intestinal microflora was observed in 12 obese subjects. The amount of *Bacteroidetes* in the non-obese control group was found to be less than the rate of excess *Firmicutes*. Then, it was observed that the number of *Bacteroidetes* increased and weight loss occurred in people who received food therapy [39]. Again, in a study on mice colon microbiota of obese mice was found to increase *Firmicutes* and decreased *Bacteroidetes* [40]. *Bacteroidetes* have fewer enzyme genes that concern less lipid and carbohydrate metabolism than *Firmicutes* [41]. *Bacteroidetes thetaiotaomicron* species have been found to have a good effect on food absorption in the body [42]. The variable *Firmicutes* / *Bacteroidetes* ratio was determined in the

intestinal flora of obese people. It was found that this ratio increased in some and was not related in others [43-48]. Studies have reported that high levels of *Lactobacillus* sp. species (from the *Firmicutes* family) are reported in obese patients compared to poor controls [43]. *Lactobacillus rhamnosus* probiotic species have been reported to lose weight at the end of a given period of time given to mice [49].

5. Conclusion

In conclusion, the results of our study revealed that there is an interaction between obesity and intestinal microflora. Our findings suggest that OL, an antipsychotic drug that causes obesity, affects the microflora in intestinal tissues at different levels, and the protective effect of TQ, which we use as a preservative, also creates differences in the groups. What type of microorganism is at what level and how on obesity is still unexplained. Our study will guide the comprehensive and well-equipped studies to be conducted regarding the interaction of metabolism and intestinal microbiota, which are still uncertain and need research.

Acknowledgments

This study was supported by Adıyaman University Scientific Research Fund with the grant number: SHMYOMAP/2015-0002. Also, we would like to thank Assoc. Prof. Dr. Hesna YİĞİT who helped us in microbiological calculations of this study.

Declaration of conflicting interests

No conflict of interest is reported by the authors.

References

- [1] Yıldırım, A.E., Altun, R., *Obezite ve Mikrobiyota*, *Güncel Gastroenteroloji*, 18(1) 106-111, 2014.
- [2] Collaborators, G.O., *Health effects of overweight and obesity in 195 countries over 25 years*, *The New England Journal of Medicine*, 377(1): 13-27, 2017.
- [3] Finkelstein, E.A., Khavjou, O.A., Thompson, H., et al., *Obesity and severe obesity forecasts through 2030*, *American Journal of Preventive Medicine*, 42(6):563-70, 2012.
- [4] Walters, W.A., Xu, Z., Knight, R., *Meta- analyses of human gut microbes associated with obesity and IBD*, *FEBS Letters*, 588(22): 4223-33, 2014.
- [5] Halk Sağlığı Genel Müdürlüğü. *Dünyada Obezitenin Görülme Sıklığı*. <https://hsgm.saglik.gov.tr/tr/obezite/dunyada-obezitenin-gorulme-sikligi.html> (Erişim tarihi: 2017).

- [6] Kaya, M., Sarıbaş, Z., *Obezite ve Mikroorganizmalar*, Hacettepe Tıp Dergisi, 38:173-176, 2007.
- [7] Bull, M.J., Plummer, N.T., *The human gut microbiome in health and disease*, Journal of Integrative Medicine, 13(6): 17-22, 2014.
- [8] Karabudak, S., Arı, O., Durmaz, B., Dal, T., Basyigit, T., Kalcioğlu, M.T., Durmaz, R., *Analysis of the effect of smoking on the buccal microbiome using next generation sequencing technology*, Journal of Medical Microbiology, 68 (8): 1148-1158, 2019.
- [9] Durmaz, B., *Bağırsak mikrobiyotası ve obezite ile ilişkisi*, Türk Hijyen ve Deneysel Biyoloji Dergisi, 76(3): 353-360, 2019.
- [10] Tseng, C.H., Wu, C.Y., *The gut microbiome in obesity*, Journal of the Formosan Medical Association, 118 (1): 3-9, 2018.
- [11] Castaner, O., Goday, A., Park, Y.M., Lee, S.H., Magkos, F., Shiow, S.A.T.E., Schröder, H., *The Gut Microbiome Profile in Obesity: A Systematic Review*, International Journal of Endocrinology, 2018: 9, 2018.
- [12] Qian, L.L., Li, H.T., Zhang, L., Fang, Q.C., Jia, W.P., *Effect of the Gut microbiota on obesity and its underlying mechanisms: an update*, Biomedical and Environmental Sciences, 28(11):839-47, 2015.
- [13] Shreiner, A.B., Kao, J.Y., Young, V.B., *The gut microbiome in health and in disease*, Current Opinion in Gastroenterology, 31(1): 69-5, 2015.
- [14] Bilgiç, S., Korkmaz, D.T., Azirak, S., Guvenc, A.N., Kocaman, N., Özer, M.K., *The protective effect of thymoquinone over olanzapineinduced side effects in liver, and metabolic side effects*, Bratislava Medical Journal, 118 (10) 618 – 625, 2017.
- [15] Abde Fattah, A.F.M., Matsumoto, K., Watanabe H., *Antinociceptive effects of Nigella sativa oil and its major component, thymoquinone in mice*, European Journal of Pharmacology, 400: 89-9, 2000.
- [16] Albaugh, V.L., Henry, C.R., Bello, N.T., Hajnal, A., Lynch, S.L., Halle, B., Lynch, C.J., *Hormonal and metabolic effects of olanzapine and clozapine related to body weight in rodents*, Obesity (Silver Spring), 14: 36–51, 2006.
- [17] Prabhakar, P., Reeta, K.H., Maulik, S.K., Dinda, A.K., Gupta, Y.K., *Protective effect of thymoquinone against high-fructose diet-induced metabolic syndrome in rats*, European Journal of Nutrition, 54 (7): 1117–27, 2015.
- [18] Tas, U., Ayan, M., Sogut, E., Kuloglu, T., Uysal, M., Tanriverdi, H., Senel, U., Ozyurt, B., Sarsilmaz, M., *Protective effects of thymoquinone and melatonin on intestinal ischemia–reperfusion injury*, Saudi Journal of Gastroenterology, 21: 284–289, 2015.
- [19] Can, N., Catak, O., Turgut, B., Demir, T., İlhan, N., Kuloglu, T., Ozercan, İ.H., *Neuroprotective and antioxidant effects of ghrelin in an experimental glaucoma model*, Drug Design, Development and Therapy, 2(9): 2819–2829, 2015.

[20] <https://www.youtube.com/watch?v=GQOnX1-SUrI>.

[21] http://www.rapidtables.com/calc/math/Exponent_Calculator.htm

[22] Yıldız, Ş., Turan, S., *Timokinon, Timol ve Karvakrolün Antioksidan Aktiviteleri ve Lipit Oksidasyonunu Önleme Kapasiteleri*, Atatürk Üniversitesi Ziraat Fakültesi Dergisi, 52 (1): 108-118, 2021.

[23] Nagi, M.N., Mansour, M.A., *Protective effect of thymoquinone against doxorubicin-induced cardiotoxicity in rats: a possible mechanism of protection*, Pharmacological Research, 41 (3): 283-289, 2000.

[24] Mansour, M.A., Nagi, M.N., El- Khatib, A.S., Al-Bekairi, A.M., *Effects of thymoquinone on antioxidant enzyme activities, lipid peroxidation and DT- diaphorase in different tissues of mice: A possible mechanism of action*. Cell Biochemistry and Function, 20 (2): 143-151, 2002.

[25] Badary, O.A., Taha, R.A., Gamal, E.D., Abdel-Wahab, M.H., *Thymoquinone is a potent superoxide anion scavenger*, Drug and Chemical Toxicology, 26 (2): 87-98, 2003.

[26] Bourgou, S., Pichette, A., Marzouk, B., Legault, J., *Bioactivities of black cumin essential oil and its main terpenes from Tunisia*, South African of Botany, 76: 210-216, 2010.

[27] Ahmad, S., Beg, Z.H., *Hypolipidemic and antioxidant activities of thymoquinone and limonene in atherogenic suspension fed rats*, Food Chemistry, 138 (2-3): 1116-1124, 2013.

[28] Jumpertz, R., Le, D.S., Turnbaugh, P.J., Trinidad, C., Bogardus, C., Gordon, J.I., Krakoff, J., *Energy-balance studies reveal associations between gut microbes, caloric load, and nutrient absorption in humans*, American Journal of Clinical Nutrition, 94(1): 58-65, 2011.

[29] Zhang, Y.J., Li, S., Gan, R.Y., Zhou, T., Xu, D.P., Li, H.B., *Impacts of gut bacteria on human health and diseases*, Int International Journal of Molecular Sciences, 16 (4): 7493-519, 2015.

[30] Khanna, S., Tosh, P.K., *A clinician's primer on the role of the microbiome in human health and disease*, Mayo Clinic Proceedings. Elsevier, 89(1):107-14, 2014.

[31] Stefanaki, C., Peppas, M., Mastorakos, G., Mastorakos, G., Chrousos, G.P., *Examining the gut bacteriome, virome, and mycobiome in glucose metabolism disorders: Are we on the right track?* Metabolism, 73: 52-6, 2017.

[32] Drapkina, O., Korneeva, O., *Gut microbiota and obesity: Pathogenetic relationships and ways to normalize the gut microflora*, Terapevticheskii Arkhiv, 88 (9): 135-42, 2016.

[33] Boulangé, C.L., Neves, A.L., Chilloux, J., Nicholson, J.K., Dumas, M.E., *Impact of the gut microbiota on inflammation, obesity, and metabolic disease*, Genome Medicine, 8 (1): 42, 2016.

[34] Turnbaugh, P.J., Hamady, M., Yatsunenkov, T., Cantarel, B.L., Duncan, A., Ley, R.E., Sogin, M.L., Jones, W.J., Roe, B.A., Affourtit, J.P., Egholm, M., Henrissat, B., Heath, A.C., Knight, R., Gordon, J.I., *A core gut microbiome in obese and lean twins*, Nature, 457:480-4, 2009.

[35] Million, M., Maraninchi, M., Henry, M., Armougom, F., Richet, H., Carrieri, P., Valero, R., Raccach, D., Vialettes, B., Raoult, D., *Obesity-associated gut microbiota is enriched in Lactobacillus reuteri and depleted in Bifidobacterium animalis and Methanobrevibacter smithii*, International Journal of Obesity, 36:817- 25, 2012.

[36] Duncan, S.H., Lopley, G.E., Holtrop, G., Ince, J., Johnstone, A.M., Louis, P., Flint, H.J., *Human colonic microbiota associated with diet, obesity and weight loss*, International Journal of Obesity, 32:1720-4, 2008.

[37] Balamurugan, R., George, G., Kabeerdoss, J., Hepsiba, K.J., Chandragunasekaran, A.M.S., Ramakrishna, B.S., *Quantitative differences in intestinal Faecalibacterium prausnitzii in obese Indian children*, British Journal of Nutrition, 103:335-8, 2010.

[38] Nadal, I., Santacruz, A., Marcos, A., Warnberg, J., Garagorri, J.M., Moreno, L.A., Matillas, M.M., Campoy, C., Martí, A., Moleres, A., Delgado, M., Veiga, O.L., Fuentes, M.G., Redondo, C.G., Sanz, Y., *Shifts in clostridia, bacteroides and immunoglobulin-coating fecal bacteria associated with weight loss in obese adolescents*, International Journal of Obesity, 33:758-67, 2009.

[39] Ley, R.E., Taunbaugh, P.J., Klein, S., Gordon, J.I., *Human gut microbes associated with obesity*, Nature, 444:1023, 2006.

[40] Turnbaugh, P.J., Backhed, F., Fulton, L., Gordon, J.I., *Diet-induced obesity is linked to marked but reversible alterations in the mouse distal gut microbiome*, Cell Host Microbe, 3:213-23, 2008.

[41] Kallus, S.J., Brandt L.J., *The intestinal microbiota and obesity*, Journal of Clinical Gastroenterology, 46:16-24, 2012.

[42] Hooper, L.V., Wong, M.H., Thelin, A., Hansson, L., Falk, P.G., Gordon, J.I., *Molecular analysis of commensal host-microbial relationships in the intestine*, Science, 291:881-4, 2001.

[43] Armougom, F., Henry, M., Vialettes, B., Raccach, D., Raoult, D., *Monitoring bacterial community of human gut microbiota reveals an increase in Lactobacillus in obese patients and methanogens in anorexic patients*, PLoS ONE, 4 (9):e 7125, 2009.

[44] Santacruz, A., Collado, M.C., Garcia, V.L., Segura, M.T., Lagos, J.A.M., Anjos, T., Romero, M.M., Lopez, R.M., Florida, J., Campoy, C., Sanz, Y., *Gut microbiota composition is associated with body weight, weight gain and biochemical parameters in pregnant women*, British Journal of Nutrition, 104:83-92. 2010.

[45] Mai, V., McCrary, Q.M., Sinha, R., Gleib, M., *Associations between dietary habits and body mass index with gut microbiota composition and fecal water genotoxicity: an observational study in African American and Caucasian American volunteers*, Nutrition Journal, 8:49, 2009.

[46] Arumugam, M., Rae, J., Pelletier, E., Paslier, D.L., Yamada, T., Mende, D.R., Fernandes, G.R., Tap, J., Bruls, T., Batto, J.M., Bertalan, M., Borrueal, N., Casellas, F., Fernandez, L., Gautier, L., Hansen, T., Hattori, M., Hayashi, T., Kleerebezem, M., Kurokawa, K., Leclerc, M., Levenez, F., Manichanh, C., Nielsen, H.B., Nielsen, T., Pons, N., Poulain, J., Qin, J., Ponten, T.S., Tims, S., Torrents, D., Ugarte, E., Zoetendal, E.G., Wang, J., Guarner, F., Pedersen, O., Vos,

W.M., Brunak, S., Doré, J., MetaHIT Consortium (additional members), Ehrlich, H.W.S.D., Bork, P., *Enterotypes of the human gut microbiome*, *Nature*, 473:174-80, 2011.

[47] Schwartz, A., Taras, D., Schafer, K., Beijer, S., Bos, N.A., Donus, C., Hardt, P.D., *Microbiota and SCFA in lean and overweight healthy subjects*, *Obesity*, 18:190-5, 2010.

[48] Collado, M.C., Isolauri, E., Laitinen, K., Salminen, S., *Distinct composition of gut microbiota during pregnancy in overweight and normal-weight women*, *The American Journal of Clinical Nutrition*, 88:894-9, 2008.

[49] Lee, H.Y., Park, J.H., Seok, S.H., Baek, M.W., Kim, D.J., Lee, K.E., Paek, K.S., Lee, Y., Park, J.H., *Human originated bacteria, Lactobacillus rhamnosus PL60, produce conjugated linoleic acid and show antiobesity effects in diet-induced obese mice*, *Biochimica et Biophysica Acta*, 1761:736-44, 2006.



Interstitial and Phytal Harpacticoid (Copepoda, Harpacticoida) Fauna of the Mediolittoral Zone of the Biga Peninsula (Çanakkale, Turkey)

Alper KABACA^{1*}, Serdar SAK², Alp ALPER²

¹Balikesir University, Necatibey Faculty of Education, Department of Biology Education, 10100, Balikesir, Turkey

alper.kabaca.10@gmail.com, ORCID: 0000-0001-8090-471X

²Balikesir University, Faculty of Science and Literature, Department of Biology, 10100, Balikesir, Turkey
serdarsak@gmail.com, ORCID: 0000-0002-4955-3162
alpalper80@gmail.com, ORCID: 0000-0001-5507-4072

Received: 09.05.2022

Accepted: 02.06.2022

Published: 30.06.2022

Abstract

In this study, interstitial and phytal harpacticoid copepods distributed along the mediolittoral zone of the Biga Peninsula were investigated. The samplings were made from 26 different stations seasonally between April - 2016, February - 2017. As a result, 73 species and subspecies belonging to 46 genera within 17 families were identified. In addition, 4 genera (*Troglophonte*, *Psammastacus*, *Stereoxiphos* and *Pteropsyllus*) and 20 species/subspecies (*Ameira divagans*, *Ameira reducta*, *Filexilia intermedia*, *Nitokra sewelli*, *Noodtiella enertha*, *Noodtiella intermedia*, *Noodtiella wellsi*, *Glabrotelson* sp., *Asellopsis intermedia*, *Echinolaophonte minuta*, *Heterolaophonte brevipes*, *Klieonychocamptus klei confluens*, *Troglophonte* sp., *Psammastacus confluens*, *Stereoxiphos operculatus*, *Schizopera minuta*, *Emertonia constricta orotavae*, *Thalestrella* sp., *Phyllopodopsyllus berrieri* and *Pteropsyllus plebeius furcatus*) are new records for the Turkish fauna. Besides, all identified taxa are new records for the Biga Peninsula.

Keywords: New record; Biodiversity; Meiofauna; Aegean Sea; Sea of Marmara.



Biga Yarımadası (Çanakkale, Türkiye) Mediollitoral Bölgesinin Kumiçi ve Fital Harpacticoid (Copepoda, Harpacticoida) Faunası

Öz

Bu çalışmada, Biga Yarımadası'nın mediollitoral bölgesinde yayılış gösteren kumiçi ve fital harpacticoid kopepodlar incelenmiştir. Örneklemeler Nisan – 2016, Şubat – 2017 tarihleri arasında 26 farklı istasyondan mevsimsel olarak yapılmıştır. Bu çalışma sonucunda 17 familya içerisinde 46 cinse ait 73 tür ve alttür tespit edilmiştir. Ek olarak 4 cins (*Troglophonte*, *Psammastacus*, *Stereoxiphos* ve *Pteropsyllus*) ve 20 tür/alttür (*Ameira divagans*, *Ameira reducta*, *Filexilia intermedia*, *Nitokra sewelli*, *Noodtiella enertha*, *Noodtiella intermedia*, *Noodtiella wellsi*, *Glabrotelson* sp., *Asellopsis intermedia*, *Echinolaophonte minuta*, *Heterolaophonte brevipes*, *Klieonychocamptus klei confluens*, *Troglophonte* sp., *Psammastacus confluens*, *Stereoxiphos operculatus*, *Schizopera minuta*, *Emertonia constricta orotavae*, *Thalestrella* sp., *Phyllopodopsyllus berrieri* ve *Pteropsyllus plebeius furcatus*) Türkiye faunası için yeni kayıttır. Ayrıca tespit edilen tüm taksonlar Biga Yarımadası için de yeni kayıt niteliğindedir.

Anahtar Kelimeler: Yeni Kayıt; Biyoçeşitlilik; Meiofauna; Ege Denizi; Marmara Denizi.

1. Introduction

The purpose of classification is to reveal biodiversity on the Earth [1]. The term biodiversity is used for many levels, e.g., genetic variations in populations, species variation in ecosystems. Taxonomic studies involve discovery, description, and analysis of the collected data [2]. The results of taxonomic studies are of great importance to understand of the biodiversity and the relationship between living things that are critical for conservation action [3].

Harpacticoida is one of the 10 orders of the subclass Copepoda [4, 5]. The biodiversity of the order is quite high; Wells [6] reported 58 families, 671 genera and approximately 4400 species except for the parasitic forms in his identification key. Later, Ahyong et al. [7] reported approximately 6000 harpacticoid species in 645 genera, which assigned to 59 families. Harpacticoid copepods are mainly marine, with merely one-tenth of species being freshwater. Most are benthic, a few are planktonic or are symbiotic with invertebrates and vertebrates [8 - 10]. Harpacticoids are also distributed on macroalgae and have great diversity [11].

The first record of harpacticoid copepods for Turkish fauna was given by Noodt [12], 52 species/subspecies belonging to 19 families were reported from the littoral zone of the Sea of

Marmara. Later, Bacesco [13] recorded *Leptastacus laticaudatus* Nicholls, 1935 and *Psammopsyllus operculatus* Nicholls, 1945 from the Bosphorus side of the Black Sea. Gündüz [14] reported *Mesochra aesturii* Gurney, 1921 from Bafra Lake (Samsun), which is a brackish lake. In the early 2000s, Toklu and Sarihan [15] recorded a pelagic form of *Euterpina acutifrons* Veal, 1852, from the Gulf of Iskenderun. *Taurocletodes tumenae* Karaytuğ and Huys, 2004; *Delamarella obscura* Huys, et al., 2005 and *Psammopsyllus ertunci* Karaytuğ and Sak, 2005 were described from the Black Sea coast of Turkey [16]. Karaytuğ and Sak [17] recorded 37 species and 1 subspecies belonging to 21 families from the Aegean and Sea of Marmara coasts of Balıkesir province. *Psammoleptastacus barani* Sak et al., 2008 was described from the Black Sea coast (Sahilköy/Istanbul) [18]. Sak et al. [19] reported the first record of *Pseudoleptomesochrella halophila* (Noodt, 1955) in Turkey from the coasts of Bartın and Kastamonu and presented the redescription of the genus *Pseudoleptomesochrella*. Sak et al. [20] established the genus *Ciplakastacus* within the family Leptastacidae to place *C. mersinensis*, a new species collected from the Mediterranean coast of Turkey. Pulat et al. [21] reported 6 phytal harpacticoid species belonging to 3 families from mediolittoral rocky biotopes on the coasts of Gümüldür (İzmir). Alper et al. [22] reported 49 species belonging to 18 families from Datça and Bozburun Peninsulas, 34 of these are new records for the Turkish coasts. Karaytuğ et al. [23] reported *Odaginiceps korykosensis* Karaytuğ et al., 2010 from Kızkalesi (Mersin). Kaymak et al. [24] recorded 8 species and subspecies belonging to the family Laophontidae from the Black Sea coasts of Turkey, 4 of these are new records for Turkey. Sönmez et al. [25] recorded 9 species belonging to the family Ectinosomatidae from the mediolittoral region of the Mediterranean coast of Turkey. On the other hand, Sönmez et al. [26] identified miraciid specimens, collected from the mediolittoral zone of the Aegean, Mediterranean and Black Sea coasts of Turkey and reported 18 species and subspecies. *Leptocaris emekdasi* Köroğlu et al. 2014; *Schizopera karanovici* Sönmez et al. 2014; *Diarthrodella ergeneae* Sönmez et al. 2015 were described in several studies which conducted on the Mediterranean and Aegean coasts [27 - 29]. Alper et al. [30] recorded 78 species and subspecies in 18 families from coast of Dilek Peninsula (Aydın), all the taxa reported herein are new records for the studied region, and more importantly 25 species and subspecies were also new records for the Turkish coasts. *Karaytugia aydini* (Kuru and Karaytuğ, 2015) described from Kızkalesi (Mersin) [31]. Karaytuğ and Koçak [32] recorded 24 species belonging to 20 genera from the Aegean and Mediterranean Sea of Turkey, and the northern coasts of Cyprus. Yıldız and Karaytuğ [33] reported 23 species belonging to 20 genera from the beaches of three islands in Bodrum. *Enhydrosoma serdarsaki* Sönmez et al., 2019 and *Pseudoameiropsis suphankaraytuği* Sönmez, 2019 were identified from the Mediterranean and Black Sea coasts of Turkey respectively [34, 35]. Two new louriniid species were described by Karaytuğ et al. [36]

from Mediterranean coast of Turkey. A total of 66 species/subspecies, 19 of which were new records for Turkey, were reported in a study conducted on the Sarımsaklı beach (Balıkesir) [37]. Another faunistic study conducted in Saros Bay, a total of 72 species/subspecies, 16 of these recorded for the first time from Turkish seas were identified [38]. According to the literature summarized above the total number of harpacticoid species reported from Turkish seas are reached to 232. All of these researches conducted on Harpacticoid fauna of the Turkish shores were carried out in the last two decade.

Despite all these studies there is not any research on harpacticoid copepods on the shores of Biga Peninsula (Çanakkale) which is located western part of Turkey and it has surrounded by Sea of Marmara and Aegean Sea. This study was aimed to reveal Harpacticoida fauna of the Biga Peninsula.

2. Materials and Methods

Biga Peninsula is located in the northwestern part of Turkey (Fig.) which is bounded by the Dardanelles Strait and the southwest coast of the Sea of Marmara to the north, Aegean Sea to the west and the Edremit gulf to the South. In general, it constitutes a transition between the Black Sea and Mediterranean climates. The Mediterranean climate is hot and dry during the summer season, and the Black Sea climate is cold and rainy in winters. It receives the most precipitation occurs in the autumn and winter seasons, and the summers are mostly dry [39].

Harpacticoid copepods were collected from 26 stations (Fig.; Table) from the shores of Biga Peninsula between April 2016 and February 2017. Of the sampling shore stations, 11 stations were located near the Aegean Sea, 8 stations were located on the shore of the Dardanelles, and 7 stations were located on the shores of the Sea of Marmara. Interstitial samples obtained from mediolittoral zone using Karaman – Chappius method [40]. Macroalgae were collected by bare hand from splash zone of shores where available. Collected samples were placed in polypropylene containers and then fixed with formalin solution (4% v/v) in situ. Harpacticoid copepods were extracted from detritus using PHYWE SMZ stereomicroscope in the laboratory and were next placed in concave slides by the stations. Specimens were mounted using lactophenol medium. Broken coverslip glass fibers were placed between slide and coverslip to prevent samples from being compressed or crushed. This method also allows to rotate specimen and facilitates to examine them from different angles [17]. The specimens were examined and identified using Olympus BX-50 equipped with DIC (differential interference contrast) attachment and CX-21 light microscopes. Descriptive terminology is adapted from Huys and Boxshall [4] and Huys et al. [41]. Lang [42, 43], Huys et al. [41], Wells [6] and other relevant literature were used for

identifications. Specimens were deposited in the collection of Balıkesir University, Faculty of Arts and Sciences, Department of Biology, in Turkey.

Table: Co-ordinates and sampling dates of stations

Station number	Locality	Sampling Habitats	Coordinates	Sampling Dates			
				I	II	III	IV
St.1	Küçükkuyu	Interstitial	39.53995° N 26.57687° E				
St.2	Assos Otel	Interstitial/Phytal	39.52196° N 26.46817° E				
St.3	Kadırga Bay	Interstitial	39.48644° N 26.36880° E				
St.4	Sokakağzı	Interstitial	39.46890° N 26.21017° E				
St.5	Akliman	Interstitial	39.51918° N 26.08333° E				
St.6	Gürpınar Beach	Interstitial	39.56645° N 26.10018° E				
St.7	Kavaklı Pier	Interstitial	39.65297° N 26.16035° E				
St.8	Ezine Beach	Interstitial	39.68654° N 26.16309° E				
St.9	Geyikli Beach	Interstitial	39.81913° N 26.16342° E				
St.10	Kumburun	Interstitial	39.87059° N 26.15126° E				
St.11	Yeniköy, Papaz Beach	Interstitial	39.91868° N 26.15511° E				
St.12	Güzelyalı Beach	Interstitial/Phytal	40.04484° N 26.34361° E	09.04.2016 – 11.04.2016	22.08.2016 – 23.08.2016	03.12.2016 – 05.12.2016	18.02.2017 – 20.02.2017
St.13	Dardanos Beach	Interstitial/Phytal	40.08096° N 26.36374° E				
St.14	Kepez Beach	Interstitial	40.10338° N 26.37427° E				
St.15	Yapıldak Altı Beach	Interstitial/Phytal	40.23373° N 26.54126° E				
St.16	Azmak Beach	Interstitial	40.27839° N 26.57071° E				
St.17	Suluca Village Beach	Interstitial/Phytal	40.29814° N 26.62553° E				
St.18	East of Lapseki	Interstitial/Phytal	40.36568° N 26.69161° E				
St.19	Çardaklı, Kumada Beach	Interstitial/Phytal	40.38310° N 26.71025° E				
St.20	Şevketiye	Interstitial/Phytal	40.39755° N 26.87440° E				
St.21	Kemer	Interstitial/Phytal	40.41533° N 27.06399° E				
St.22	Aksaz Beach	Interstitial/Phytal	40.44004° N 27.17658° E				
St.23	Biga, Kaleler Beach	Interstitial/Phytal	40.40735° N 27.31225° E				
St.24	Denizatı Beach	Interstitial	40.34784° N 27.37550° E				
St.25	Kumkent Beach	Interstitial	40.32112° N 27.44261° E				
St.26	Çanakkale-Balıkesir Province Border	Interstitial	40.30364° N 27.51508° E				

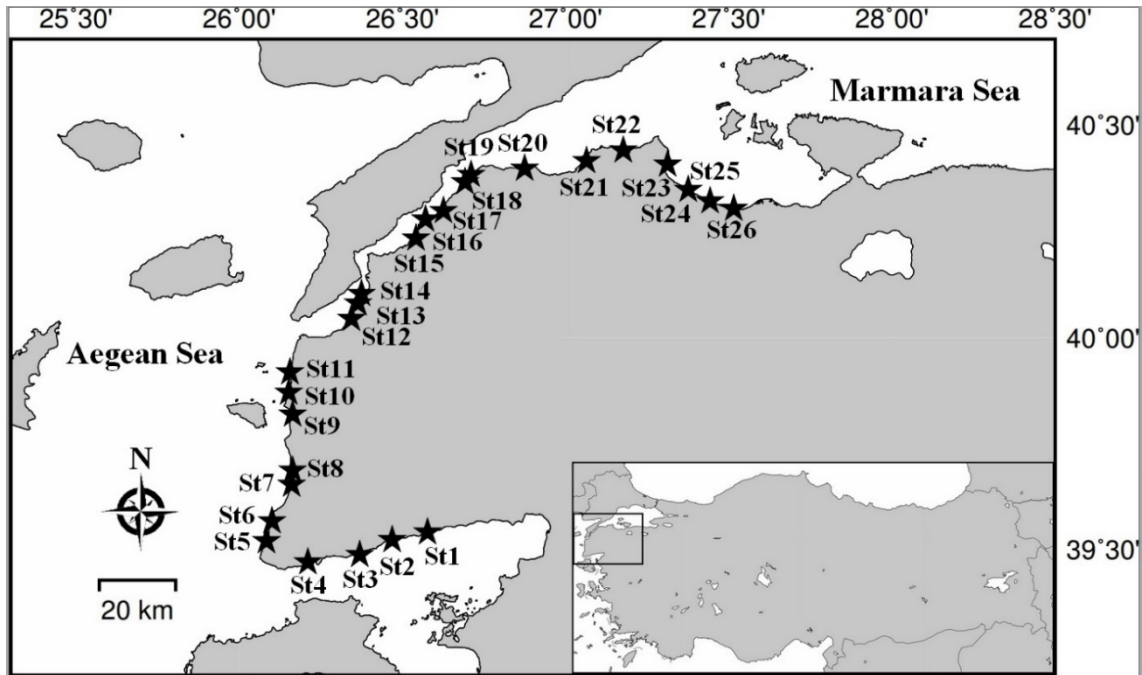


Figure: The sampling stations and study area

3. Results

A total of 73 species and subspecies belonging to 46 genera within 17 families were identified. Identified taxa are listed as follows:

Order: HARPACTICOIDA Sars, 1903

Family: AMEIRIDAE Boeck, 1865

Ameira atlantica mediterranea Kunz, 1975

Material examined: (II) St.4 (8♀♀, 1♂), St.21 (16♀♀, 2♂♂); (III) St.6 (5♀♀); (IV) St.1 (1♀), St.2 (3♀♀, 1♂)

Distribution in Turkey: Aegean Sea [38]

Ameira divagans Nicholls, 1939

Material examined: (III) St.21 (31♀♀, 5♂♂)

Distribution in Turkey: New Record.

Ameira parvula (Claus, 1866)

Material examined: (III) St.15 Phytal (3♀♀, 1♂♂), St.18 Phytal (7♀♀, 22♂♂); (IV) St.21 Pyhtal (3♀♀), St.23 Phytal (5♀♀), St.23 (5♀♀, 2♂♂)

Distribution in Turkey: Aegean Sea [17, 22, 30, 37, 38]

Ameira reducta Petkovski, 1954

Material examined: (I) St.2 (10♀♀, 6♂♂), St.3 (3♀♀), St.16 (16♀♀, 2♂♂), St.23 (7♀♀, 4♂♂), St. 24 (35♀♀, 5♂♂), St. 25 (8♀♀, 3♂♂), St.26 (20♀♀, 3♂♂); (II) St.2 (2♀♀, 3♂♂), St.16 (24♀♀, 8♂♂), St.17 (24♀♀, 8♂♂).

Distribution in Turkey: New Record.

Filexilia brevipes (Kunz, 1954)

Material examined: (II) St.21 (14♀♀, 1♂♂), St.22 (14♀♀, 2♂♂); (III) St.8 (19♀♀, 2♂♂); (IV) St.21 (10♀♀, 3♂♂), St.22 (6♀♀, 2♂♂).

Distribution in Turkey: Aegean Sea [37, 38]

Filexilia intermedia (Galhano, 1970)

Material examined: (I) St.22 (36♀♀, 2♂♂).

Distribution in Turkey: New Record.

Filexilia marinovi Conroy-Dalton and Huys, 1997

Material examined: (II) St.6 (8♀♀, 1♂♂); (III) St.12 (17♀♀, 10♂♂), St.13 (5♀♀, 2♂♂), St.14 (28♀♀, 5♂♂).

Distribution in Turkey: Aegean Sea [30, 37, 38].

Nitokra affinis Gurney, 1927

Material examined: (III) St.23 (10♀♀, 4♂♂).

Distribution in Turkey: Aegean Sea [22, 38].

Nitokra cari Petkovski, 1954

Material examined: (I) St.14 (7♀♀, 6♂♂).

Distribution in Turkey: Aegean Sea [37]

Nitokra sewelli Gurney, 1927

Material examined: (III) St.3 (2♀♀, 1♂♂).

Distribution in Turkey: New Record.

Nitokra typica Boeck, 1865

Material examined: (I) St.8 (10♀♀, 2♂♂), St.20 (7♀♀, 1♂); (II) St.15 (2♀♀), St.20 (4♀♀, 1♂); (IV) St.25 (1♀, 3♂♂).

Distribution in Turkey: Aegean Sea [30, 37, 38].

Pseudameira breviseta Klie, 1950

Material examined: (III) St.3 (13♀♀, 2♂♂).

Distribution in Turkey: Mediterranean Sea [33].

Pseudoleptomesochrella halophila (Noodt, 1952)

Material examined: (I) St.14 (6♀♀, 2♂♂); (II) St.14 (11♀♀, 2♂♂), St.24 (18♀♀, 3♂♂); (III) St.5 (6♀♀).

Distribution in Turkey: Aegean Sea [37, 38], Black Sea [20].

Psyllocamptus eridani Ceccherelli, 1988

Material examined: (II) St.15 (1♀, 1♂), St.23 (7♀♀, 1♂); (III) St.2 (22♀♀, 3♂♂), St.23 (10♀♀, 5♂♂).

Distribution in Turkey: Aegean Sea [30, 38], Mediterranean Sea [33].

Family: ARENOPONTIIDAE Martínez Arbizu Moura, 1994

Arenopontia nesaie Cottarelli, 1975

Material examined: (I) St.5 (21♀♀, 3♂♂), St.11 (5♀♀), St.17 (1♀, ♂), St.19 (16♀♀, 5♂♂); (II) St.5 (5♀♀, 5♂♂), St.6 (1♂), St.11 (2♀♀), St.17 (12♀♀); (III) St.2 (1♀), St.11 (9♀♀, 5♂♂), St.23 (1♀), St.25 (8♀♀, 2♂♂), St.26 (4♀♀, 1♂); (IV) St.10 (6♀♀, 3♂♂), St.11 (9♀♀, 1♂), St.22 (4♀♀).

Distribution in Turkey: Aegean Sea [30, 37, 38], The Black Sea [18].

Neoleptastacus acanthus Chappuis, 1954

Material examined: (II) St.4 (4♀♀, 1♂).

Distribution in Turkey: Aegean Sea [22, 30].

Psammoleptastacus barani Sak, Huys and Karaytuğ, 2008

Material examined: (I) St.7 (2♀♀, 1♂), St.21 (2♀♀), St.23 (2♀♀); (III) St.24 (5♀♀, 10♂♂).

Distribution in Turkey: The Black Sea [20], Aegean Sea [30, 38].

Family: CANTHOCAMPTIDAE Brady, 1880

Mesochra pygmaea (Claus, 1863)

Material examined: (III) St.24 (1♀).

Distribution in Turkey: Sea of Marmara [12], Aegean Sea [38].

Family: DARCYTHOMPSONIIDAE Lang, 1936

Leptocaris biscayensis (Noodt, 1955)

Material examined: (I) St.5 (1♂), St.21 (1♀), St.25 (2♀♀); (II) St.5 (8♀♀, 6♂♂), St.8 (1♀); (III) St.2 (1♀, 1♂), St.22 (10♀♀, 1♂); (IV) St.4 (8♀♀, 2♂♂).

Distribution in Turkey: Aegean Sea [27, 30, 37, 38].

Family: ECTINOSOMATIDAE Sars G.O., 1903

Arenosetella germanica Kunz, 1937

Material examined: (I) St.7 (25♀♀, 2♂♂), St.8 (19♀♀, 2♂♂), St.12 (8♀♀, 2♂♂), St.16 (1♀), St.17 (6♀♀), St.21 (8♀♀, 2♂♂); (II) St.9 (4♀♀), St.11 (1♀); (III) St.9 (4♀♀), St.12 (2♀♀), St.17 (30♀♀, 4♂♂), St.24 (10♀♀, 2♂♂), St.25 (8♀♀, 2♂♂); (IV) St.12 (12♀♀, 1♂), St.14 (1♀), St.16 (13♀♀), St.17 (5♀♀, 1♂).

Distribution in Turkey: Aegean Sea [17, 22, 37, 38], Mediterranean Sea [25].

Arenosetella lanceorostrata Sönmez, Sak and Karaytuğ, 2016

Material examined: (I) St.2 (1♀), St.7 (7♀♀, 1♂), St.22 (1♀, 1♂); (II) St.4 (4♀♀, 1♂), St.7 (4♀♀); (III) St.2 (3♀♀), St.4 (2♀♀), St.5 (2♀♀), St.8 (3♀♀); (IV) St.4 (11♀♀, 2♂♂), St.5 (1♀), St.7 (3♀♀), St.17 (5♀♀, 2♂♂).

Distribution in Turkey: Aegean Sea [37], Mediterranean Sea [44].

Ectinosoma melaniceps Boeck, 1865

Material examined: (II) St.25 (5♀♀), St.2 Phytal (7♀♀, 2♂♂), St.15 Phytal (18♀♀, 2♂♂); (III) St.8 (8♀♀, 2♂♂).

Distribution in Turkey: Sea of Marmara [12], Aegean Sea [17, 37, 38], Mediterranean Sea [25].

Ectinosoma reductum Bozic, 1955

Material examined: (II) St.20 Phytal (20♀♀, 2♂♂).

Distribution in Turkey: Aegean Sea [30, 38], Mediterranean Sea [25].

Ectinosoma soyeri Apostolov, 1975

Material examined: (I) St.1 (1♀, 1♂), St.23 (5♀♀, 1♂), St.25 (13♀♀, 2♂♂), St.26 (21♀♀, 3♂♂); (II) St.17 (2♀♀, 1♂), St.20 (12♀♀, 2♂♂); (IV) St.20 (16♀♀, 2♂♂), St.25 (9♀♀, 2♂♂), St.26 (25♀♀, 5♂♂).

Distribution in Turkey: Aegean Sea [22, 30, 37, 38], Mediterranean Sea [25].

Glabrotelson sp.

Material examined: (I) St.21 (2♀, 1♀ dissected in 6 slides, 3♂♂)

Distribution in Turkey: New Record.

Microsetella norvegica (Boeck, 1865)

Material examined: (I) St.3 (1♀), St.4 (7♀♀), St.5 (5♀♀); (II) St.2 (2♀♀, 3♂♂), St.6 (1♀), St.7 (10♀♀, 1♂), St.8 (7♀♀, 1♂), St.9 (6♀♀); (III) St.4 (2♀♀, 1♂), St.11 (3♀♀), St.12 (1♀); (IV) St.1 (1♀), St.3 (2♀♀), St.7 (3♀♀, 2♂♂).

Distribution in Turkey: Aegean Sea [22, 30, 32, 37], Mediterranean Sea [22].

Microsetella rosea (Dana, 1847)

Material examined: (III) St.13 (6♀♀, 4♂♂).

Distribution in Turkey: Aegean Sea [38], Mediterranean Sea [25].

Noodtiella enertha Lindgren, 1975

Material examined: (II) St.17 (2♀♀, 1♂); (III) St.11 (8♀♀, 1♂), St.25 (5♀♀, 1♂); (IV) St.9 (2♀♀).

Distribution in Turkey: New Record.

Noodtiella intermedia Wells, 1967

Material examined: (II) St.11 (2♂).

Distribution in Turkey: New Record.

Noodtiella wellsii Apostolov, 1974

Material examined: (I) St.21 (1♀).

Distribution in Turkey: New Record.

Family: HARPACTICIDAE Dana, 1846

Harpacticus compsonyx Monard, 1926

Material examined: (I) St. 15 Phytal (10♀♀, 2♂♂).

Distribution in Turkey: Aegean Sea [22].

Harpacticus littoralis Sars G.O., 1910

Material examined: (I) St.17 Phytal (10♀♀, 2♂♂); (II) St.20 Phytal (15♀♀, 3♂♂); (III) St.20 Phytal (9♀♀, 2♂♂); (IV) St.13 Phytal (20♀♀, 5♂♂), St.15 Phytal (11♀♀), St.17 Phytal (24♀♀, 1♂), St.18 Phytal (8♀♀, 1♂), St. 19 Phytal (9♀♀, 3♂♂), St.21 Phytal (5♀♀).

Distribution in Turkey: Aegean Sea [22, 30].

Family: LAOPHONTIDAE Scott T., 1904

Afrolaophonte pori Masry, 1970

Material examined: (I) St.4 (11♀♀, 2♂♂), St.8 (1♀); (II) St.4 (18♀♀, 1♂), St. 7 (1♀), St.8 (28♀♀, 6♂♂); (III) St.4 (12♀♀, 8♂♂); (IV) St.8 (15♀♀, 2♂♂).

Distribution in Turkey: Aegean Sea [22, 30, 37, 38].

Asellopsis intermedia (Scott T., 1895)

Material examined: (I) St.13 Phytal (15♀♀, 3♂♂).

Distribution in Turkey: New Record.

Echinolaophonte minuta Cottarelli and Forniz, 1991

Material examined: (II) St.2 Phytal (1♀, 1♂); (III) St.8 (4♀♀, 6♂♂).

Distribution in Turkey: New Record.

Heterolaophonte brevipes Roe, 1958

Material examined: (II) St.15 Phytal (5♀♀, 2♂♂).

Distribution in Turkey: New Record.

Heterolaophonte uncinata (Czerniavski, 1868)

Material examined: (II) St.2 Phytal (7♀♀, 6♂♂), St.15 Phytal (3♀♀), St.18 Phytal (14♀♀, 9♂♂); (III) St.12 Phytal (5♀♀); (IV) St.13 Phytal (6♀♀, 2♂♂), St.21 Phytal (7♀♀, 1♂), St.22 Phytal (8♀♀, 2♂♂).

Distribution in Turkey: Aegean Sea [22], The Black Sea [24].

Klieonychocamptus kliei adriaticus (Petkovski, 1954)

Material examined: (III) St.8 (2♀♀, 1♂); (IV) St.19 (3♀♀, 1♂), St.21 (1♂)

Distribution in Turkey: Aegean Sea [22], The Black Sea [24].

Klieonychocamptus kliei confluens Noodt, 1958

Material examined: (I) St.3 (6♀♀, 2♂♂).

Distribution in Turkey: New Record.

Klieonychocamptus ponticus (Serban and Plesa, 1957)

Material examined: (II) St.15 (10♀♀, 7♂♂), St.16 (3♀♀, 1♂), St.20 (14♀♀, 5♂♂), St.25 (8♀♀, 6♂♂), St.26 (27♀♀, 7♂♂); (III) St.5 (2♀♀, 4♂♂), St.16 (8♀♀, 2♂♂), St.17 (1♀, 1♂), St.20 (6♀♀, 5♂♂), St.21 (6♀♀).

Distribution in Turkey: Aegean Sea [30, 37, 38], The Black Sea [24].

Laophonte inornata Scott A., 1902

Material examined: (IV) St.18 Phytal (7♀♀, 2♂♂).

Distribution in Turkey: Sea of Marmara [12], The Black Sea [17].

Laophonte lignosa Hicks, 1988

Material examined: (I) St.15 Phytal (5♀♀, 2♂♂).

Distribution in Turkey: Aegean Sea [30].

Laophonte setosa Boeck, 1865

Material examined: (III) St.17 Phytal (2♀♀, 1♂); (IV) St.17 Phytal (2♀♀, 1♂), St.23 Phytal (25♀♀, 5♂♂).

Distribution in Turkey: Sea of Marmara [12], The Black Sea [24].

Lipomelum adriaticum (Petkovski, 1955)

Material examined: (I) St.3 (7♀♀, 2♂♂), St.5 (1♀); (II) St.3 (9♀♀, 5♂♂); (III) St.3 (15♀♀, 8♂♂), St.4 (3♀♀, 4♂♂); (IV) St.3 (2♀♀), St.4 (4♀♀, 2♂♂).

Distribution in Turkey: Aegean Sea [30, 33, 38].

Paralaophonte brevirostris (Claus, 1863)

Material examined: (III) St.17 Phytal (2♀♀, 1♂); (IV) St.17 Phytal (5♀♀, 2♂♂), St.23 Phytal (25♀♀, 5♂♂).

Distribution in Turkey: Sea of Marmara [12], Aegean Sea [21, 22, 30, 38].

Troglophonte sp.

Material examined: (IV) St.19 (4♀♀, 1♀ dissected in 6 slides; 2♂♂, 1♂ dissected in 6 slides).

Distribution in Turkey: New Record.

Family: LATIREMIDAE Bözić, 1969

Delamarella obscura Huys, Karaytuğ and Cottarelli, 2005

Material examined: (I) St.3 (1♀, 1♂), St.4 (1♀), St.7 (4♀♀), St.8 (5♀♀, 1♂), St.19 (2♀♀, 2♂♂), St.21 (1♀), St.22 (1♀), St.25 (6♀♀), St.26 (10♀♀, 2♂♂); (II) St.6 (4♀♀, 1♂), St.8 (1♀); (III) St.2 (2♀♀), St.3 (7♀♀, 1♂), St.4 (9♀♀, 2♂♂), St.21 (2♀♀), St.22 (3♀♀, 5♂♂), St.25 (22♀♀, 4♂♂), St.26 (24♀♀, 20♂♂); (IV) St.4 (2♀♀, 4♂♂), St.5 (1♀).

Distribution in Turkey: The Black Sea [45], Aegean Sea [17, 22, 37, 38].

Family: LEPTASTACIDAE Lang, 1948

Ciplakastacus mersinensis Sak, Karaytuğ and Huys, 2008

Material examined: (II) St.11 (8♀♀, 4♂♂).

Distribution in Turkey: Mediterranean Sea [19].

Minervella baccettii Cottarelli and Venanzetti, 1989

Material examined: (III) St.11 (1♂).

Distribution in Turkey: Aegean Sea [37].

Psammastacus confluens Nicholls, 1935

Material examined: (II) St.13 (2♀♀).

Distribution in Turkey: New Record.

Stereoxiphos operculatus (Masry, 1970)

Material examined: (I) St.11 (2♀♀, 1♂).

Distribution in Turkey: New Record.

Family: METIDAE Boeck, 1873

Metis ignea Philippi, 1843

Material examined: (I) St.15 (2♀♀, 1♂); (II) St.2 (1♀), St.18 Phytal (11♀♀), St.20 Phytal (10♀♀); (III) St.15 Phytal (5♀♀).

Distribution in Turkey: Aegean Sea [17].

Family: MIRACIIDAE Dana, 1846

Amphiascoides brevifurca (Czerniavsky, 1868)

Material examined: (IV) St.18 Phytal (5♀♀, 2♂♂).

Distribution in Turkey: Sea of Marmara [12], Aegean Sea [38]

Eoschizopera (Praeoschizopera) gligici (Petkovski, 1957)

Material examined: (I) St.5 (2♀♀), St.11 (1♀), St.14 (8♀♀, 5♂♂), St.22 (2♀♀), St.25 (3♀♀); (II) St.19 (1♀); (III) St.16 (17♀♀, 6♂♂), St.17 (5♀♀, 1♂).

Distribution in Turkey: Aegean Sea [17, 30, 37, 38], Mediterranean Sea [25].

Psammotopa vulgaris Pennak, 1942

Material examined: (I) St.14 (6♀♀, 4♂♂); (II) St.14 (6♀♀, 1♂); (III) St.11 (4♀♀, 1♂), St.14 (8♀♀, 2♂♂); (IV) St.11 (14♀♀, 5♂♂), St.14 (10♀♀, 13♂♂).

Distribution in Turkey: Aegean Sea [26, 30, 38].

Pseudamphiascopsis attenuatus (Sars G.O., 1906)

Material examined: (I) St.2 (2♀♀, 1♂); (III) St.15 (1♀).

Distribution in Turkey: Aegean Sea [22, 37].

Sarsamphiascus minutus (Claus, 1863)

Material examined: (II) St.22 (3♀♀, 1♂).

Distribution in Turkey: Sea of Marmara [12, 17], Aegean Sea [22, 30, 38].

Schizopera brusinae Petkovski, 1954

Material examined: (I) St.4 (5♀♀, 1♂), St.8 (2♀♀).

Distribution in Turkey: Aegean Sea [17, 22, 30, 38].

Schizopera karanovici Sönmez, Sak and Karaytuğ, 2015

Material examined: (I) St.11 (2♀♀, 1♂).

Distribution in Turkey: Mediterranean Sea [28].

Schizopera minuta Noodt, 1955

Material examined: (I) St.12 (4♀♀, 1♂), St.17 (3♀♀), St. 19 (1♀).

Distribution in Turkey: New Record.

Family: ORTHOPSYLLIDAE Huys, 1990

Orthopsyllus linearis (Claus, 1866)

Material examined: (III) St.18 Phytal (5♀♀, 3♂♂).

Distribution in Turkey: Aegean Sea [17].

Family: PARAMESOCHRIDAE Lang, 1944

Apodopsyllus arenicolus (Chappuis, 1954)

Material examined: (I) St.14 (1♀, 1♂), St.16 (5♀♀); (II) St.16 (3♀♀, 3♂♂), St.19 (4♀♀), St.21 (9♀♀, 1♂); (III) St.10 (2♀♀, 5♂♂), St.16 (1♀, 2♂♂); (IV) St.16 (7♀♀, 2♂♂), St.17 (3♀♀).

Distribution in Turkey: Aegean Sea [38]

Emertonia constricta orotavae (Noodt, 1958)

Material examined: (I) St.17 (3♀♀); (II) St.17 (14♀♀, 9♂♂); (III) St.2 (2♀♀, 1♂), St.5 (1♀, 1♂), St.12 (2♀♀); (IV) St.10 (7♀♀, 1♂), St.12 (14♀♀, 1♂), St.16 (6♀♀), St.17 (15♀♀, 2♂♂), St.21 (8♀♀), St.25 (9♀♀, 2♂♂).

Distribution in Turkey: New Record.

Leptopsyllus punctatus Mielke, 1984

Material examined: (I) St.21 (11♀♀, 1♂); (II) (11♀♀, 1♂); (III) St.21 (14♀♀, 7♂♂).

Distribution in Turkey: Aegean Sea [22, 30, 37].

Family: PARASTENHELIIDAE Lang, 1936

Parastenhelia spinosa (Fischer, 1860)

Material examined: (II) St.17 Phytal (7♀♀, 7♂♂); (III) St.15 Phytal (10♀♀, 3♂♂).

Distribution in Turkey: Aegean Sea [22, 30], Mediterranean Sea [33].

Thalestrella sp.

Material examined: (IV) St.22 (9♀♀, 1♀ dissected in 4 slides, 3♂♂).

Distribution in Turkey: New Record.

Family: PORCELLIDIIDAE Boeck, 1865

Porcellidium fimbriatum Claus, 1863

Material examined: (II) St.15 Phytal (5♀♀, 5♂♂); (III) St.12 Phytal (3♀♀, 2♂♂).

Distribution in Turkey: Aegean Sea [30].

Family: TETRAGONICIPITIDAE Lang, 1944

Phyllopodopsyllus berrieri Monard, 1936

Material examined: (III) St.16 (1♀, 1♂), St.22 (10♀♀, 12♂♂).

Distribution in Turkey: New Record.

Phyllopodopsyllus briani Petkovski, 1955

Material examined: (I) St.3 (14♀♀, 15♂♂); (II) St.3 (18♀♀, 19♂♂); (III) St.2 (4♀♀, 1♂).

Distribution in Turkey: Aegean Sea [17], Mediterranean Sea [33].

Phyllopodopsyllus thiebaudi Petkovski, 1955

Material examined: (II) St.22 (1♀, 1♂), St.23 (11♀♀, 11♂♂), St.24 (2♂♂).

Distribution in Turkey: Aegean Sea [17], Mediterranean Sea [33].

Pteropsyllus plebeius furcatus Kunz, 1938

Material examined: (II) St.8 (3♀♀, 2♂♂).

Distribution in Turkey: New Record.

Family: TISBIDAE Stebbing, 1910

Scutellidium ligusticum (Brian, 1920)

Material examined: (II) St.17 Phytal (5♀♀, 2♂♂), St.20 Phytal (2♀♀, 1♂); (III) St.12 Phytal (4♀♀).

Distribution in Turkey: Aegean Sea [30].

Scutellidium longicaudum (Philippi, 1840)

Material examined: (II) St.18 Phytal (7♀♀, 2♂♂); (IV) St.17 Phytal (7♀♀, 1♂), St. 18 Phytal (7♀♀, 1♂).

Distribution in Turkey: Aegean Sea [30, 37].

4. Discussion

As a result of the study, 73 species/subspecies belonging to 46 genera in 17 families were identified from 26 stations. In terms of species richness, the families Laophontidae and Ameiridae ranked first with 14 species each, belonging to 9 and 6 genera respectively; these two families followed by Ectinosomatidae with 11 species in 5 genera, Miraciidae with 8 species in 6 genera, Leptastacidae with 4 species in 4 genera, Tetragonicipitidae with 4 species in 4 genera, Arenopontiidae with 3 species in 3 genera, Paramesochridae with 3 species in 3 genera, Harpacticidae, Parastenheliidae and Tisbidae with 2 species in 1 genus each, and the remaining families represented by one species each. *Delamarella obscura* identified from 20 different samplings and in all samplings was the most common species followed by *Ectinosoma soyeri* (found in 18 samplings), *Arenosetella germanica* (found in 17 samplings) and *Arenopontia nesaie* (found in 16 samplings). In contrast, some harpacticoids were determined to be unique to one station and are not found in any other stations studied (see Results, Material examined). For example, *Neoleptastacus acanthus* was identified only at station St.4 and, *Pteropsyllus plebeius furcatus* was identified only from station St. 8.

Considering the distribution of harpacticoid species sampled from the stations mentioned in the present study, it can be suggested that some harpacticoids are specific for the sampled regions. Eleven species (*Pseudameira breviseta*, *Nitokra sewelli*, *Lipomelum adriaticum*, *Echinolaophonte minuta*, *Paralaophonte brevirostris*, *Stereoxiphos operculatus*, *Ciplakastacus mersinensis*, *Minervella bacetti*, *Schizopera brusinae*, *Schizopera karanovici* and *Pteropsyllus plebeius furcatus*) were determined from the stations located on the Aegean Sea coast. Seven species (*Filexilia intermedia*, *Ameira divagens*, *Nitokra affinis*, *Noodtiella wellsi*, *Glabrotelson* sp., *Sarsamphiascus minutus* and *Phyllopodopsyllus thiebaudi*) were determined from the stations

located from the shore of the Sea of Marmara. Six species (*Nitokra cari*, *Troglophonte* sp., *Psammastacus confluens*, *Schizopera minuta*, *Microsetella rosea* and *Phyllopodopsyllus berrieri*) were determined from the stations located along the Dardanelles Strait. On the contrary, fifteen species (*Ameira reducta*, *Nitokra typica*, *Psyllocamptus eridani*, *Pseudoleptomesochrella halophila*, *Arenopontia nesaei*, *Ectinosoma soyeri*, *Arenosetella lanceorostrata*, *Arenosetella germanica*, *Klieonychocamptus ponticus*, *Klieonychocamptus kliei*, *Klieonychocamptus adriaticus*, *Delameralla obscura*, *Eoschizopera (Praeoschizopera) gligici*, *Emertonia constricta orotavae* and *Apodopsyllus arenicolus*) were found widely distributed and determined from all three regions studied.

To date, 232 species of harpacticoid copepods have been reported from the Turkish coasts (See introduction). With the present study, additional 20 species/subspecies were recorded for the first time. Thus, the total number of harpacticoid copepod species determined from Turkish coasts has increased to 252.

Although faunistic studies on Turkish coasts have increased in the last two decades, they are still far from revealing the real harpacticoid diversity of Turkey. It is possible to speculate that one of the reasons for this situation is the faunistic results of almost all studies in Turkey were generally based on seasonal samplings that were carried out 3-4 times in a year. The most recent study were conducted by Alper [37] where, 9 stations on the mediolittoral zone of Sarımsaklı Beach (Balıkesir) were sampled 12 times in a year with monthly period. As a result of his examination, 66 species/subspecies were reported from a single beach. Apparently, the more sampling is conducted, the higher number of species can be identified. Another possible reason could be that only the mediolittoral regions were examined more intensively in the previous studies. Directing future studies to deeper regions, as well as examining symbiotic harpacticoids, will contribute to revealing the real biodiversity of Turkey's harpacticoid fauna.

Acknowledgements

This study was a part of a PhD thesis of Alper KABACA that is supported by Balıkesir University Scientific Research Projects Unit under Project number BAP 2017/017 and supervised by Dr. Serdar SAK. Thanks to Eray ERSOY (MSc) and İdris BAYRAM for their assistance in the fieldwork and the collection of the material.

References

- [1] Mayr E., *Principles of systematic zoology*, New York, McGraw-Hill, 428p. 1969.

[2] Colwell, R.K., III. *I Biodiversity: concepts, patterns, and measurement*, In: *The Princeton guide to ecology*, Princeton: Princeton University Press. 257-263p. 2009.

[3] McNeely, J.A., *The role of taxonomy in conserving biodiversity*, *Journal for Nature Conservation*, 10, 145-153, 2002.

[4] Huys, R., Boxshall, G.A., *Copepod evolution*, London: The Ray Society, 468p. 1991.

[5] Berera, R., Cottarelli, V., De Laurentiis, P., Galassi, D.M., Stoch, F., *Crustacea Copepoda Harpacticoida. Checklist e distribuzione della fauna Italiana*, *Memorie del Museo Civico di Storia Naturale di Verona*, 2, 97-99, 2005.

[6] Wells, J.B.J., *An annotated checklist and keys to the species of Copepoda Harpacticoida (Crustacea)*, *Zootaxa*, 1568, 1-872, 2007.

[7] Ahyong, S.T., Lowry J.K., Alonso M., Bamber R.N., Boxshall A.G., Castro P., Gerken S., Karaman G.S, Goy, J.W., Jones D.S., Meland K., Rogers D.C., Svavarsson J., *Subphylum Crustacea Brünnich, 1772. Animal biodiversity: an outline of higher-level classification and survey of taxonomic richness*, *Zootaxa* 3148, 165–191, 2011.

[8] Harris, R., *Copepods*. In: *Encyclopedia of ocean sciences*, Cambridge: Academic Press, 512-523, 2001.

[9] Chertoprud, E.S., Gheerardyn, H., Gómez, S., *Harpacticoida (Crustacea: Copepoda) of the South China Sea: faunistic and biogeographical analysis*, *Hydrobiologia*, 666, 45-57, 2011.

[10] Huys, R., *Harpacticoid copepods—their symbiotic associations and biogenic substrata: a review*. *Zootaxa*, 4174, 448–729, 2016.

[11] Hicks, G.R., *Structure of phytal harpacticoid copepod assemblages and the influence of habitat complexity and turbidity*, *Journal of experimental marine Biology and Ecology*, 44, 157-192, 1980.

[12] Noodt, W., *Marine Harpacticoiden (Crust. Cop.) aus dem Marmara Meer*, *Review of the Faculty of Science, University of Istanbul*, 20, 49-94, 1955.

[13] Băcescu, M., *Le role des îles dans la dispersion récente des espèces indo-pacifiques en Méditerranée occidentale et quelques observations sur la faune marine de L'île des serpents, en comparaison avec celle peuplants les parages prébosphoriques de la Mer Noire*. In: *V. Le peuplement des îles Méditerranéennes et la problème de l'insularité. Banyuls-sur-Mer*, Paris: Centre National de la Recherche Scientifique; 1961. 243–53

[14] Gündüz, E., *A new record of Mesochra aestuarii Gurney, 1921 (Copepoda, Harpacticoida) for Turkey*, *Doga Turkish Journal of Zoology*, 13, 228-232, 1989.

[15] Toklu, B., Sarihan, E., *The Copepoda and Cladocera (Crustacea) Fauna Along the Yumurtalık-Botaş Coastline in Iskenderun Bay*, *Su Ürünleri Dergisi*, 20, 63-68, 2003.

[16] Karaytuğ, S., Sak, S., *A new record of Psammopsyllus Nicholls, 1945 (Copepoda, Harpacticoida, Leptopontiidae), with a description of a new species from the Black Sea*, *Israel Journal of Ecology and Evolution*, 51, 135-146, 2005.

[17] Karaytuğ, S., Sak, S., *A contribution to the marine harpacticoid (Crustacea, Copepoda) fauna of Turkey*, Su Ürünleri Dergisi, 23, 2006.

[18] Sak, S., Huys, R., Karaytuğ, S., *Disentangling the subgeneric division of Arenopontia: resurrection of Psammoleptastacus Pennak, 1942, re-examination of Neoleptastacus spinicaudatus, and proposal of two new genera and a new generic classification (Copepoda, Harpacticoida, Arenopontiidae)*, Zoological Journal of the Linnean Society, 152, 409-458, 2008.

[19] Sak, S., Karaytuğ, S., Huys, R., *Ciplakastacus gen. nov., a primitive genus of Leptastacidae (Copepoda, Harpacticoida) from the Mediterranean coast of Turkey*, Journal of Natural History, 42, 2443-2459, 2008.

[20] Sak, S., Karaytuğ, S., Huys, R., *A review of Pseudoleptomesochrella Lang, 1965 (Copepoda, Harpacticoida, Ameiridae), including a redescription of P. halophila (Noodt, 1952) from the Black Sea and a key to species*, Zootaxa, 1758, 45-60, 2008.

[21] Pulat, İ., Özel, İ., Aker, H. V., *Gümüldür Sahili (Ege Denizi) Mediolittoral Kayalık Biyotoplarından Tespit Edilen Thalestridae ve Laophontidae (Copepoda, Harpacticoida) Türleri*, Su Ürünleri Dergisi, 26, 55-58, 2009.

[22] Alper, A., Karaytuğ, S., Sak, S., *Interstitial and phytal harpacticoida (Crustacea: Copepoda) inhabiting the mediolittoral zone of the Datça-Bozburun Peninsulas (Muğla, Turkey)*, Süleyman Demirel Üniversitesi Fen Edebiyat Fakültesi Fen Dergisi, 5, 16-28, 2010.

[23] Karaytuğ, S., Sak, S., Alper, A., *A new species of Odaginiceps Fiers, 1995 (Copepoda, Harpacticoida, Tetragnipitidae) from the Mediterranean coast of Turkey*, ZooKeys, 53, 2010.

[24] Kaymak, N.B., Karaytuğ, S., Sak, S., *Laophontidae fauna (Crustacea: Copepoda: Harpacticoida) of the Turkish Black Sea coast*, Journal of Anatolian Natural Sciences, 3, 23-36, 2012.

[25] Sönmez, S., Sak, S., Karaytuğ, S., *Meiobenthic ectinosomatids (Crustacea: Copepoda: Harpacticoida) of the Mediterranean sea coasts of Turkey*, Journal of Anatolian Natural Sciences, 3, 1-14, 2012.

[26] Sönmez, S., Sak, S., Karaytuğ, S., *Marine interstitial and phytal Miraciidae Dana, 1846 (Crustacea: Copepoda: Harpacticoida) inhabiting along the mediolittoral zone of Turkish coasts*, Journal of Anatolian Natural Sciences, 5, 52-87, 2014.

[27] Köroğlu, N.Ö., Kuru, S., Karaytuğ, S., *Marine darcythompsoniids of the Turkish coasts with a description of Leptocaris emekdasi sp. nov. (Copepoda: Harpacticoida: Darcythompsoniidae) from the Aegean coast of Turkey*, Marine Biodiversity, 45, 383-390, 2014.

[28] Sönmez, S., Sak, S., Karaytuğ, S., *A new species of the genus Schizopera Sars, 1905 (Copepoda: Harpacticoida: Miraciidae) from the Mediterranean coast of Turkey*, Marine Biodiversity, 45, 413-418, 2014.

[29] Sönmez, S., Karaytuğ, S., Sak, S., *First record of the genus Diarthrodella Klie, 1949 (Copepoda, Harpacticoida, Paramesochridae) from the Mediterranean Sea, with description of a new species from Turkey*, Turkish Journal of Zoology, 39, 174-181, 2015.

[30] Alper, A., Sönmez, S., Sak, S., Karaytuğ, S., *Marine harpacticoid (Copepoda, Harpacticoida) fauna of the Dilek Peninsula (Aydın, Turkey)*, Turkish Journal of Zoology, 39, 580-586, 2015.

[31] Kuru, S., Karaytuğ, S., *A new species of Parastenhelia Thompson & A. Scott, 1903 (Copepoda, Harpacticoida, Parastenheliidae) from Turkey*, Biharean Biologist, 9, 2015.

[32] Karaytuğ, S., Koçak, C., *Faunistic assessment of the marine Harpacticoida (Crustacea: Copepoda) fauna of Turkey with remarks on harpacticoid diversity in the eastern Mediterranean Sea*. *Marine Biodiversity*, 48, 273-280, 2018.

[33] Yıldız, N.Ö., Karaytuğ, S., *Harpacticoida (Crustacea: Copepoda) of the three islands on Aegean Sea (Turkey) with eight new records*, Mediterranean Fisheries and Aquaculture Research, 1, 57-65, 2018.

[34] Sönmez, S., Yıldız, I., Karaytuğ, S., *A new species of Enhydrosoma Boeck, 1872 (Copepoda: Harpacticoida: Cletodidae) from the Black Sea Coast of Turkey with some remarks on the taxonomic status of E. wellsi Bodin, 1968*, Turkish Journal of Fisheries and Aquatic Sciences, 19, 817-823, 2019.

[35] Sönmez, S., *Description of Pseudoameiropsis suphankaraytugi sp. nov. (Copepoda: Harpacticoida: Ameiridae) with the first report of the genus Pseudoameiropsis Pallares, 1982 outside of the South Atlantic Ocean*, Turkish Journal of Zoology, 43, 255-264, 2019.

[36] Karaytuğ, S., Sak, S., Alper, A., Sönmez, S., *Resolving the Lourinia armata (Claus, 1866) complex with remarks on the monophyletic status of Louriniidae, Monard 1927 (Copepoda: Harpacticoida)*, Zootaxa, 5051, 346-386, 2021.

[37] Alper, A., *Faunistic and ecological assessment of interstitial Harpacticoida (Crustacea, Copepoda) on a sandy beach in Balıkesir (Turkey)*, Nauplius, in press, 2022.

[38] Metin, O., Alper, A., Sak, S., *Interstitial harpacticoid (Copepoda, Harpacticoida) fauna inhabiting mediolittoral zone of the Gulf of Saros (Turkey)*, Balıkesir Üniversitesi Fen Bilimleri Enstitüsü Dergisi, in press, 2022.

[39] Günal, N., *Türkiye’de iklimin doğal bitki örtüsü üzerindeki etkileri*, Acta Turcica Çevrimiçi Tematik Türkoloji Dergisi, 5, 1-22, 2013.

[40] Deboutteville, C.D., *Eaux Souterraines Littorales de la Cote Catalane Française (Mise Au Point Faunistique)*, Vie et Milieu, 5, 408-451, 1954.

[41] Huys, R., Gee, J.M., Moore, C.G., Hamond, R., *Marine and brackish water Harpacticoid copepods. Part 1*. London: Field Studies Council, 353p. 1996.

[42] Lang, K., *Monographie der Harpacticiden, 2 vols*. Lund: Hakan Ohlsson, 1682p. 1948.

[43] Lang, K., *Copepoda Harpacticoida from the Californian pacific coast*, Kunliga Svenska Vetenskapsakademiens Handlingar, 4, 1-560, 1965.

[44] Sönmez, S., Sak, S., Karaytuğ, S., *A new species of Arenosetella Wilson, 1932 from Turkey with notes on the genus (Copepoda, Harpacticoida, Ectinosomatidae)*, *Zoosystematics and Evolution*, 92, 119-129, 2016.

[45] Huys, R., Karaytuğ, S., Cottarelli, V., *On the synonymy of Delamarella Chappuis and Latiremus Božić (Copepoda, Harpacticoida, Latiremidae), including the description of D. obscura sp. nov. from the Black Sea*, *Zoological Journal of the Linnean Society*, 145, 263-281, 2005.



Effects of Copper Substitution to Mn-site on Magnetic and Magnetocaloric Properties of $\text{La}_{0.7}\text{Sr}_{0.3}\text{Mn}_{1-x}\text{Cu}_x\text{O}_3$ Manganites

Selda KILIÇ ÇETİN¹, Gönül AKÇA^{1,*}, Mehmet Selim ASLAN¹, Ahmet EKİCİBİL¹

¹Çukurova University, Faculty of Science and Letters, Department of Physics, 01330, Adana, Türkiye
kilics@cu.edu.tr, ORCID: 0000-0003-4112-4475

¹Çukurova University, Faculty of Science and Letters, Department of Physics, 01330, Adana, Türkiye
gdayan@cu.edu.tr, ORCID: 0000-0001-7187-9516

¹Çukurova University, Faculty of Science and Letters, Department of Physics, 01330, Adana, Türkiye
mehmetselimaslan34@gmail.com, ORCID NO: 0000-0001-7086-9105

¹Çukurova University, Faculty of Science and Letters, Department of Physics, 01330, Adana, Türkiye
ahmetcan@cu.edu.tr, ORCID NO: 0000-0003-3071-0444

Received: 09.05.2022

Accepted: 10.06.2022

Published: 30.06.2022

Abstract

In present study, the effects of copper substitution on the magnetic and magnetocaloric properties of $\text{La}_{0.7}\text{Sr}_{0.3}\text{Mn}_{1-x}\text{Cu}_x\text{O}_3$ manganite samples were investigated. $\text{La}_{0.7}\text{Sr}_{0.3}\text{Mn}_{1-x}\text{Cu}_x\text{O}_3$ samples were obtained by using sol-gel method. X-ray diffraction analyses were performed to determine structural properties such as lattice parameters and crystal structure. The crystal structure of the samples is rhombohedral with space group $R\bar{3}c$. The Cu substitution to the Mn-site causes a decrease in the magnetic phase transition temperature (T_C) of the samples. By using Banerjee criterion and Landau theory, the type of magnetic phase transition is determined as second order. From isothermal magnetization measurements, magnetic entropy change ($-\Delta S_M$) values were calculated for different magnetic field changes of the samples. The maximum magnetic entropy change value ($-\Delta S_M^{max}$) determined from the temperature dependence of $-\Delta S_M$ curves for the samples is 3.39 and 2.78 $\text{JKg}^{-1}\text{K}^{-1}$ under 5 T, respectively. Relative cooling power (RCP) values of the samples were found as 249.52 and 111.98 Jkg^{-1} for 5 T, respectively.



Keywords: Magnetic refrigeration; Magnetic entropy change; Curie temperature; Manganite; Landau theory.

Mn Bölgesine Bakır Katkılmasının $\text{La}_{0.7}\text{Sr}_{0.3}\text{Mn}_{1-x}\text{Cu}_x\text{O}_3$ Manganitlerinin Manyetik ve Manyetokalorik Özellikleri Üzerindeki Etkileri

Öz

Bu çalışmada, Cu katkılmasının $\text{La}_{0.7}\text{Sr}_{0.3}\text{Mn}_{1-x}\text{Cu}_x\text{O}_3$ manganit numunelerinin manyetik ve manyetokalorik özelliklerine etkileri incelenmiştir. $\text{La}_{0.7}\text{Sr}_{0.3}\text{Mn}_{1-x}\text{Cu}_x\text{O}_3$ numuneleri sol-jel tekniği kullanılarak elde edilmiştir. Örgü parametreleri ve kristal yapı gibi yapısal parametreleri belirlemek için x-ışını kırınım analizleri yapılmıştır. Numunelerin kristal yapısı, $R\bar{3}c$ uzay grubu ile rombohedraldir. Mn bölgesindeki Cu katkılmasının manyetik faz geçiş sıcaklığını (T_C) düşürdüğü gözlenmiştir. Banerjee kriteri ve Landau teorisi kullanılarak manyetik faz geçişinin türü ikinci dereceden olarak belirlenmiştir. İzotermal manyetizasyon ölçümlerinden numunelerin farklı manyetik alan değişimleri için manyetik entropi değişimi ($-\Delta S_M$) değerleri hesaplanmıştır. Sıcaklığa bağlı $-\Delta S_M$ eğrilerinden belirlenen maksimum manyetik entropi değişim ($-\Delta S_M^{max}$) değeri 5 T altında örnekler için sırasıyla 3.39 ve 2.78 $\text{Jkg}^{-1}\text{K}^{-1}$ ' dir. Örneklerin bağlı soğutma gücü (RCP) değerleri 5 T için sırasıyla 249.52 ve 111.98 Jkg^{-1} olarak bulunmuştur.

Anahtar Kelimeler: Manyetik soğutma; Manyetik entropi değişimi; Curie sıcaklığı; Manganit; Landau teorisi.

1. Introduction

Developed and developing societies need various technologies in every field in order to raise their living standards and reach the level of comfort. One of the technologies widely used in almost every time of human life, including before and after, is cooling technologies [1]. Conventional cooling systems used today are technologies based on the principle of compression of gases with known negative effects on environment [2]. Many efforts have been carried out to reduce the negative effects of the gases used as refrigerants in these systems on the environment and to make improvements [3]. In addition to environmental factors, it is imperative to take the necessary steps to increase the energy efficiency of these systems, where energy consumption is high [4]. Efforts to reduce environmental impacts and energy consumption are not easy and inexpensive. Therefore, there is a need to develop and design new systems that can replace these systems [5]. Recently, intensive studies have been performed on magnetic refrigeration (MR) systems, which are accepted as an alternative technology to conventional systems [1, 2, 6]. Various MR systems have been developed; however, commercial use of these systems has not

yet been fully achieved. The most important reason for this is the problems encountered in the supply of materials to be used as cooling elements in these systems. The main purpose of studies performed for MR technologies is to find the best candidate material that can be used as a cooling element in applications of these systems operating according to the magnetocaloric effect (MCE) principle [7-10]. MCE can basically be explained as when a magnetic field is subjected to a magnetic material, the change in the entropy and temperature of the material [11]. For a magnetocaloric material to be considered as a candidate cooling material for applications, the material must meet certain criteria [12]. First, the magnetic entropy and adiabatic temperature change values, which define the magnetocaloric properties of the material, should be high enough to provide high performance under a low magnetic field and operating temperature range. Second, magnetic hysteresis related to the working efficiency of the material should be close to zero [13]. Thermal and magnetic hysteresis are associated with the magnetic phase transition type [13, 14]. The samples showing a first-order magnetic phase transition (FOMT) have large hysteresis, and the transition occurs in a narrow temperature range [15]. For the second-order magnetic phase transition (SOMT), the hysteresis is negligibly small and the transition is usually spread over a broad temperature range [16, 17]. This indicates that the RCP, defined as the amount of energy per unit mass of the magnetocaloric material, can be high [18]. In the operating temperature range, magnetocaloric materials with high RCP have a higher potential to be used as coolants in applications. In addition to the mentioned physical properties, the materials should meet certain economic and environmental merit such as low cost of raw material and synthesizing and not including poisonous or carcinogenic elements [13]. Although many material groups with high magnetic entropy and adiabatic temperature values have been discovered around room temperature, many of them exhibit properties that hinder their commercial use [13, 17, 19]. Manganites formulated with $R_{1-x}M_xMnO_3$ have critical advantages such as high chemical stability, low cost of preparation and raw materials and SOMT [13]. There are many studies describing the properties of manganites in detail and based on these studies [13, 20], it can be said that $La_{1-x}Sr_xMnO_3$ is one of the commonly studied compound systems in term of magnetic and magnetocaloric properties among manganite compounds [20, 21] for various applications such as MR and magnetic hyperthermia [22]. It is known that the magnetic and magnetocaloric properties of manganites are explained by double exchange interaction between Mn ions [20]. There are several factors that affect the physical properties of manganites; the Mn^{3+}/Mn^{4+} ratio, the average ionic radius of the A and/or B -site, oxygen deficiency, doping rate and the method chosen in material preparation are among the most important factors [23, 24]. Based on the information attained from the literature, in our present work, Cu substitution was made in Mn-site in order to bring the transition temperature to room temperature in the $LaSrMnO_3$ system. Sol-gel method

was chosen as the material preparation method because of its various advantages [25]. The effects of Cu substitution on the magnetic and magnetocaloric properties were investigated. To compare the results obtained by Maxwell relation, we calculated the $-\Delta S_M$ of the samples by using Landau theory. The type of magnetic phase transition was determined by Banerjee criteria and Landau parameters.

2. Materials and Methods

To obtain targeted $\text{La}_{0.7}\text{Sr}_{0.3}\text{Mn}_{1-x}\text{Cu}_x\text{O}_3$ ($x = 0.05$ and 0.1) manganite compounds, $\text{La}(\text{NO}_3)_3 \cdot 6\text{H}_2\text{O}$, SrO , CuO and $\text{Mn}(\text{NO}_3)_2 \cdot 4\text{H}_2\text{O}$ starting materials were used. Sol-gel method was chosen as material production method. The starting compounds were weighed according to stoichiometric ratios and brought into solution form using suitable solvents. The mixture obtained by mixing the solutions was heated in a magnetic stirrer and stirred continuously. Ethylene glycol and citric acid were added to the mixture to obtain a gel form. The processes of the sol-gel material fabrication technique used to prepare the $\text{La}_{0.7}\text{Sr}_{0.3}\text{Mn}_{1-x}\text{Cu}_x\text{O}_3$ ($x = 0.05$ and 0.1) compounds are given in Fig. 1. We have used a similar material fabrication process in our previous study [26]. The obtained samples were named as LSMC-0.05 and LSMC-0.10, respectively, depending on the Cu concentration. To determine the structural, magnetic and magnetocaloric properties of the samples, X-Ray Diffraction (XRD), scanning electron microscopy (SEM), and physical property measurement system (PPMS) were used. XRD measurements of the samples were performed by a Philips PANalytical Empyrean x-ray diffraction meter at room temperature in 0.0131 degree increments over the range of 20 and 80 . The crystal structures, lattice parameters and unit cell volume of the samples were analyzed with the Fullprof Programme. The grain size and elemental analysis of the samples were studied with a Scanning Electron Microscope (SEM) including Energy Dispersive X-Ray Spectrometry (EDS). In order to determine the transition temperature of the samples, temperature-dependent magnetization measurements were performed under 10 mT in zero field cooled (ZFC) and field cooled (FC) modes in the temperature range of 5 - 380 K. The isothermal magnetization measurements dependent magnetic field were carried out around the transition temperatures of the samples up to the field value of 5 T. By using the data obtained from isothermal magnetization measurements, the $-\Delta S_M$ values of the samples and the type of magnetic phase transition were determined. In addition, $-\Delta S_M$ value and magnetic phase transition type were determined according to Landau theory. Obtained experimental and theoretical results were compared with each other.

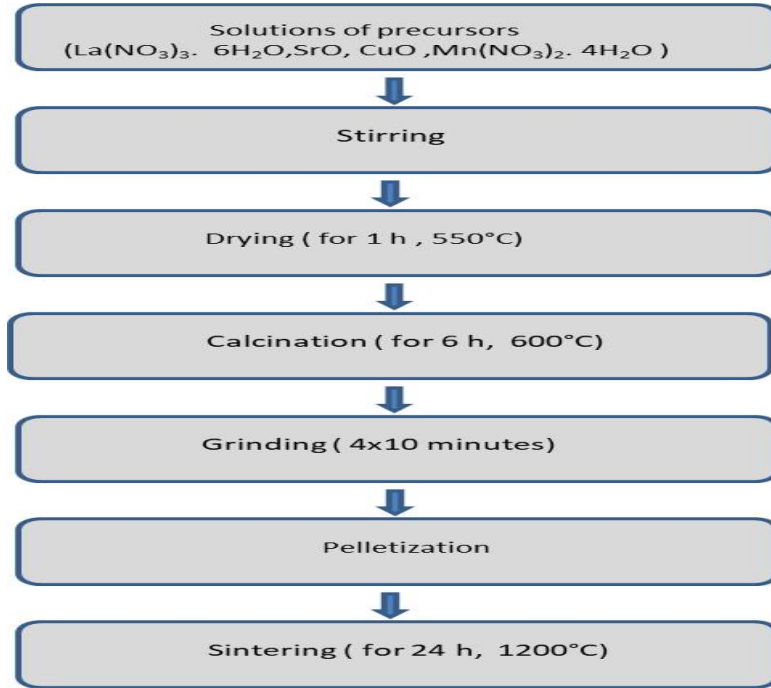


Figure 1: Processes of sol-gel material production technique used to prepare $\text{La}_{0.7}\text{Sr}_{0.3}\text{Mn}_{1-x}\text{Cu}_x\text{O}_3$ ($x = 0.05$ and 0.1) compounds

3. Results and Discussion

Figure 2 shows the XRD diffraction patterns of the compounds. It is seen from the XRD diffraction patterns of the samples the narrow-based and sharp diffraction peaks belonging to perovskite structure. The diffraction patterns of the samples have been analyzed in FullProof programs. In the figures, red circle and black line represent the observed and calculated data, respectively. The blue line is difference between them. Green vertical bars show Bragg position. The crystal structure and lattice parameters obtained from the end of analysis for the samples are indicated in Table 1. It is observed that a small change was observed in the lattice parameters and unit cell volume values with the increase of Cu concentration. However, no change has been observed in crystal structure. The perovskite structure is stable at certain values of the tolerance factor given by [27, 28]

$$t = \frac{r_A + r_O}{\sqrt{2}(r_{Mn} + r_O)} \quad (1)$$

equation where r_A and r_{Mn} are the effective radii of the A and Mn site, respectively. r_O represents the effective radii of the O ions. When t values are between 0.96 and 1, it can be said that the crystal structure is rhombohedral [27]. The t values of the samples were computed by taking into account Shannon's list of effective ion radii [29]. This value changes from 0.9798 to 0.9806 for

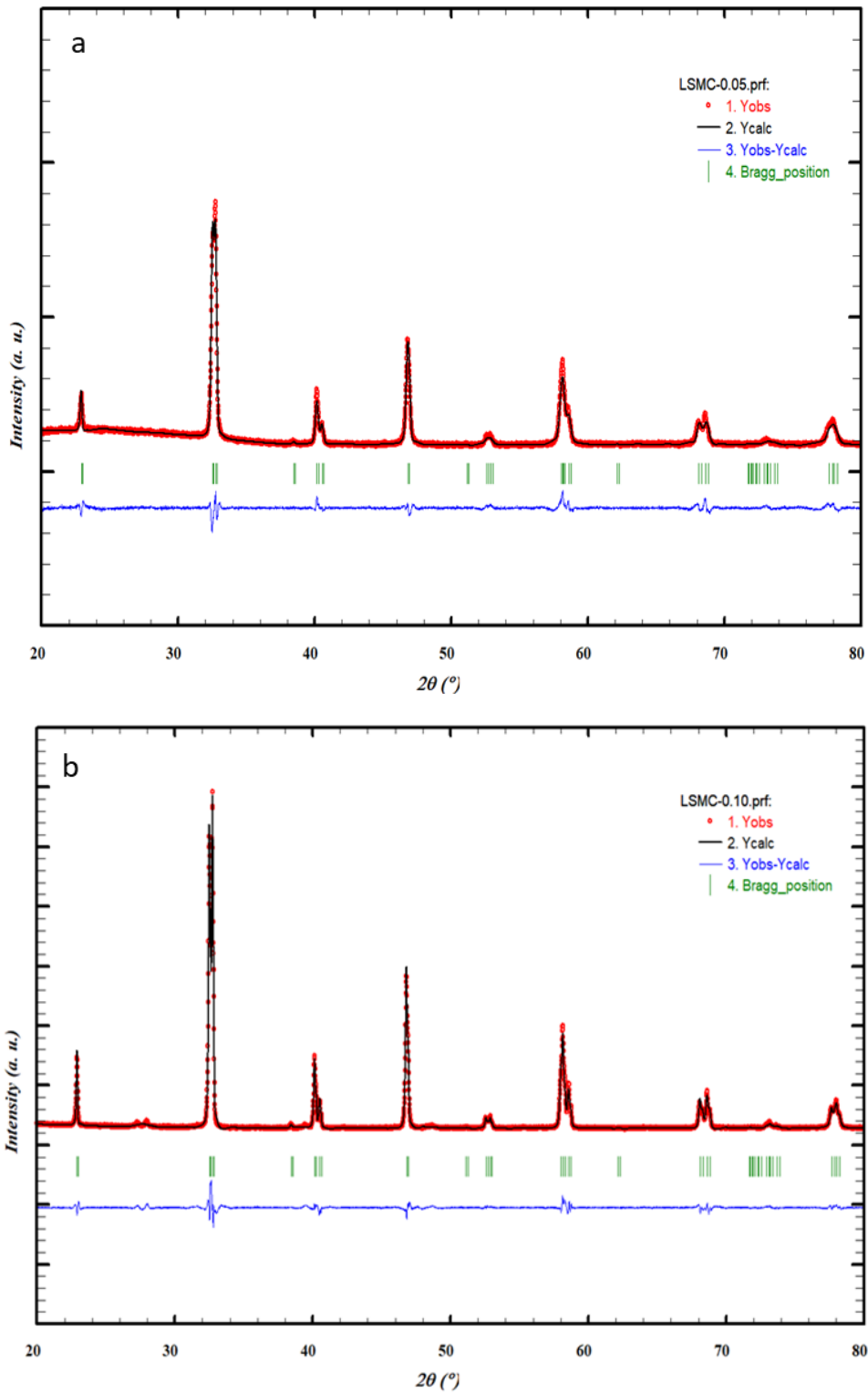


Figure 2: XRD patterns of the samples (a) LSMC-0.05 and (b) LSMC-0.10
 LSMC-0.05 and LSMC-0.10, respectively. These values confirm that they crystallize in rhombohedral crystal structures.

Table 1: Lattice parameter obtained from FULLPROF program and grain size of LSMC-0.05 and LSMC-0.10 samples

Sample Code	$a=b$ (Å)	c (Å)	V (Å ³)	d_{Mn-O} (Å)	$\theta_{Mn-O-Mn}$ (°)	Grain Size (μm)
LSMC-0.05	5.5073	13.3659	351.0815	1.9498	175.662	0.65
LSMC-0.10	5.5015	13.3449	349.7915	1.9505	175.654	0.47

In Figure 3, SEM images of the LSMC-0.05 and LSMC-0.10 samples are given. For Cu doped samples, different polygonal grain structures of different sizes, definite grain boundaries and mostly oval-like are seen. It is observed that the shape and size of the grains are not homogeneous and there is porosity between the grains. For the LSMC-0.05 sample, the size of the particles varies from 0.20 to 1.94 μm and the average particle size was calculated as 0.645 μm . From SEM images of LSMC-0.10 sample, it is seen that the clarity of the grain boundaries deteriorates. The size of the grains varied between 0.153 and 2.02 μm and the average particle size was calculated as 0.469 μm . It is observed that the grain size of the samples decreased with the increase of Cu concentration. The observed decrement in grain size may cause a variation in magnetic and magnetocaloric properties.

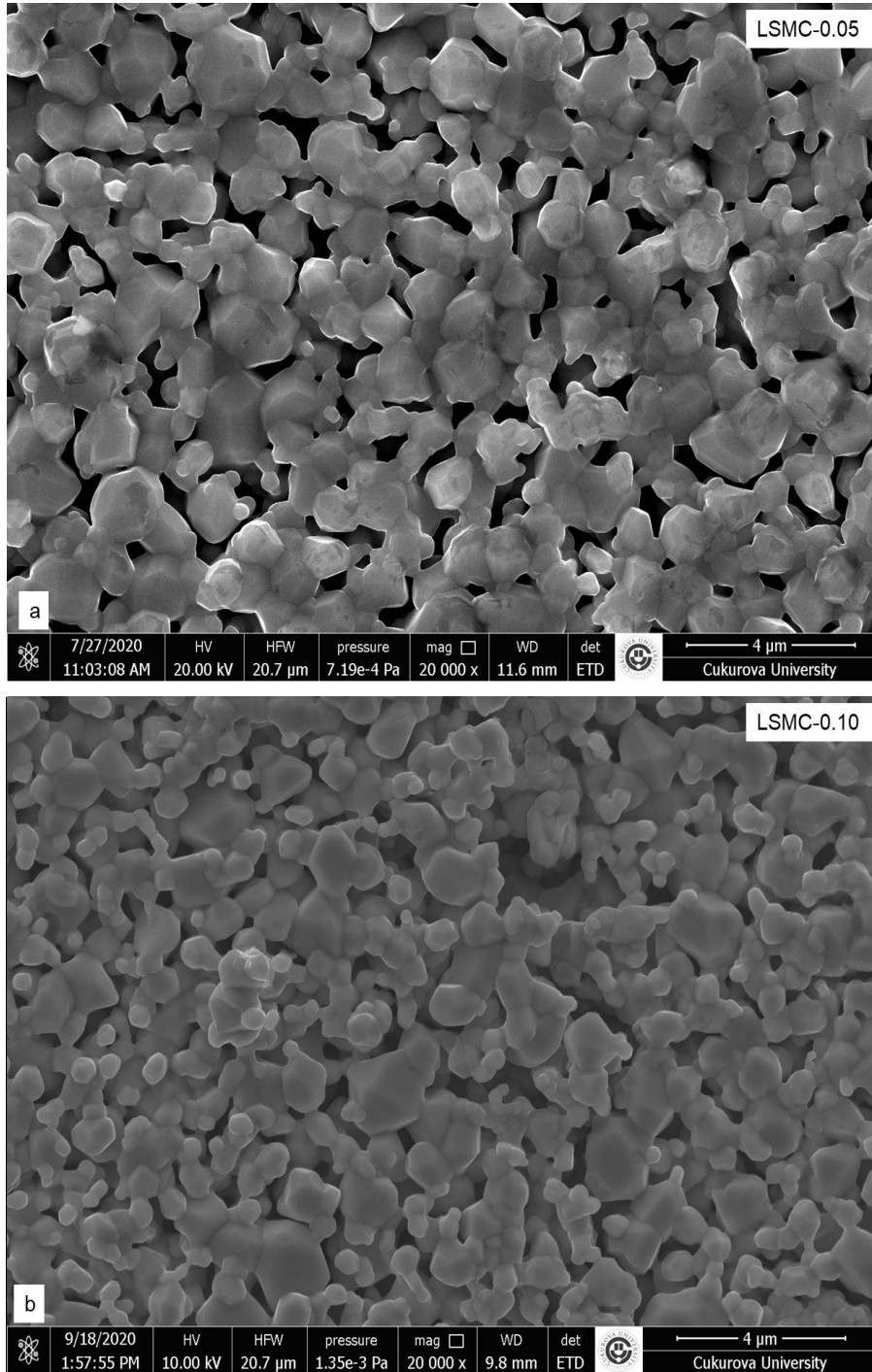


Figure 3: SEM images obtained at 20 kX magnifications of the samples (a) LSMC-0.05 and (b) LSMC-0.10

Figure 4 shows the EDS spectra of the samples. It is observed that the samples contain all expected elements and there are no traces of foreign elements that may interfere with the compound during the preparation and heat treatment process. The atomic percentages of the elements that compose the samples are summarized in Table 2. The obtained results are close to the expected atomic ratios for all samples.

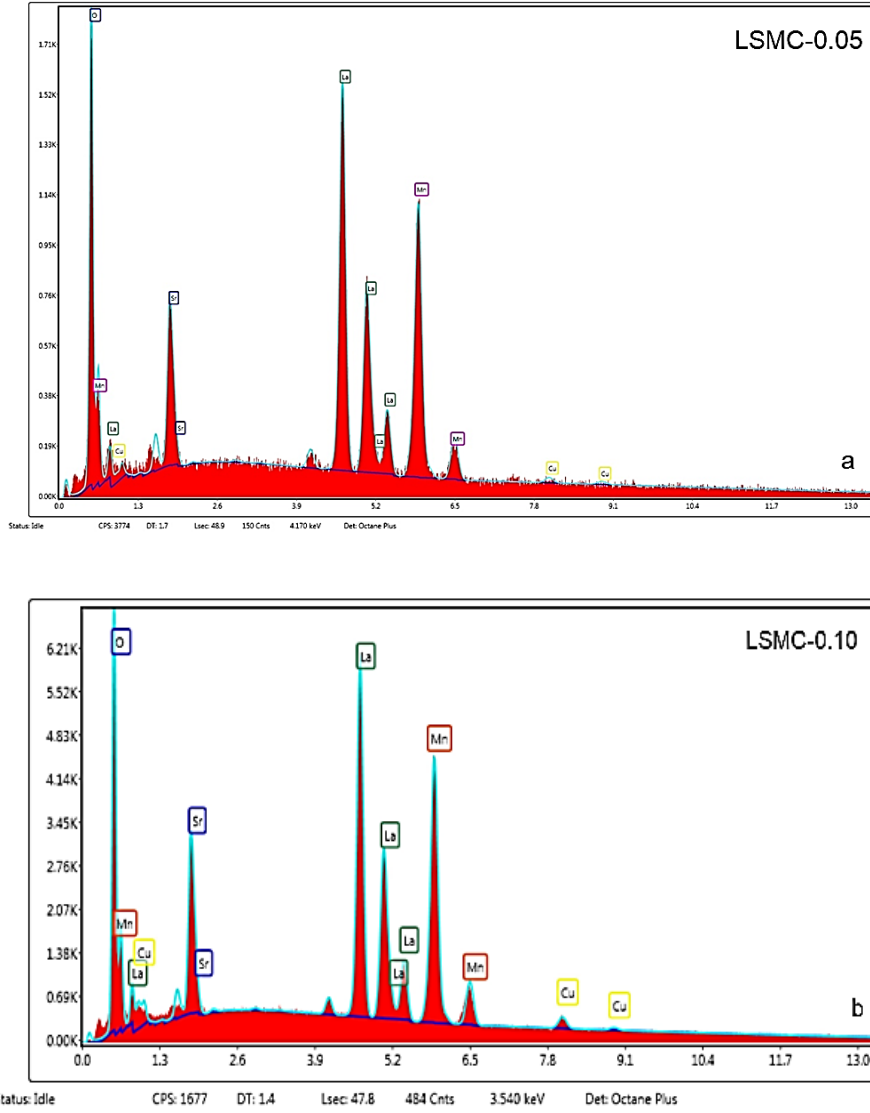


Figure 4: EDS spectra of LSMC-0.05 and LSMC-0.10 samples

Table 2: Atomic percentages of LSMC-0.05 and LSMC-0.10 samples

Sample Code	Atomic percentages %				
	La	Sr	Mn	Cu	O
LSMC-0.05	15.07	4.96	19.61	0.68	59.05
LSMC-0.10	15.29	5.51	19.73	1.47	58.01

To investigate the magnetic behavior dependent on temperature of the samples, magnetization measurements under low magnetic field (10 mT) were carried out in ZFC and FC modes. Thermomagnetic curves of the samples are given in Fig. 5. The $M(T)$ curves of the samples exhibit a transition from the ferromagnetic (FM) to the paramagnetic (PM) phase with the increase in temperature. It is seen that ZFC and FC curves are reversible in the paramagnetic region and

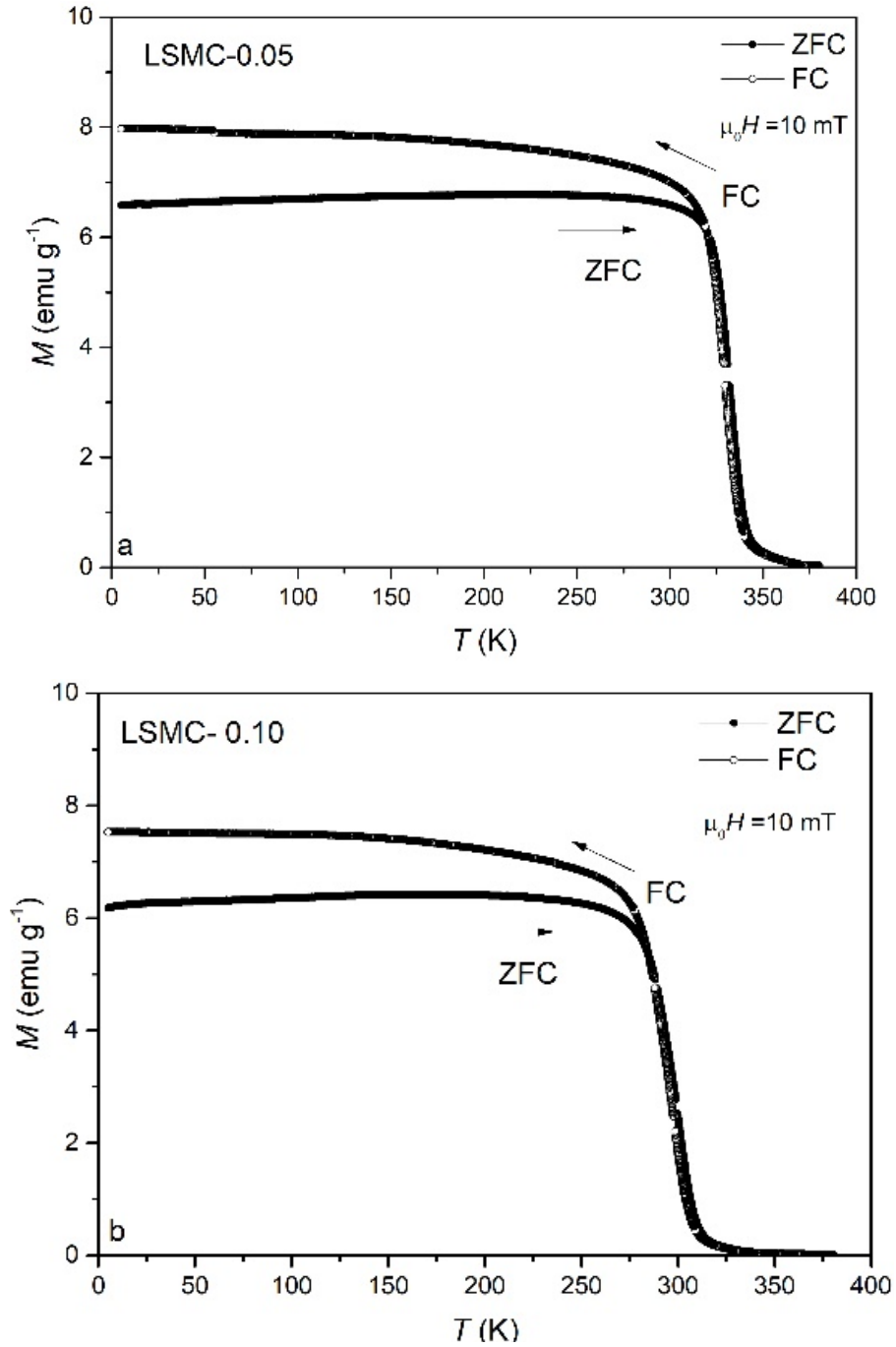


Figure 5: $M(T)$ curves of the samples (a) LSMC-0.05 and (b) LSMC-0.10 at ZFC and FC modes

follow an irreversible path by separating from each other in the ferromagnetic region. This separation between the ZFC and FC curves may arise from magnetic anisotropy effect and long-range magnetic interactions [30]. T_C is generally determined from the inflection point of the $dM(T)/d(T)$ curve. T_C values of LSMC-0.05 and LSMC-0.10 samples are 330 and 301 K, respectively. In our previous study, the T_C value of the LSM sample synthesized using the same material preparation method was reported as 363 K [26]. It was observed that the transition

temperature decreased when Cu was added to Mn-site. The ratio of $\text{Mn}^{4+}/\text{Mn}^{3+}$ ions was calculated as 0.58 and 0.80 for LSMC-0.05 and LSMC-0.10 materials, respectively. According to the results, it was observed that the number of Mn^{4+} increases with the increasing of Cu ratio. This results in decreasing the number of conduction electrons in the structure and T_C decreases. It is known that the change in Mn-O-Mn bond angle and Mn-O bond length causes a change in T_C value [31, 32]. For LSMC-0.05 and LSMC-0.10 samples, Mn-O-Mn bond angle and Mn-O bond length were determined from Rietveld refinement and given in Table 1. The Cu substitution to Mn-site induces a distortion in Mn-octahedra. This distortion limits the mobility of eg electrons [33]. As a result, double exchange interactions weaken and T_C reduces [32, 34]. The magnetic and magnetocaloric properties are also affected by the grain size of the samples as the smaller grain sizes may generate a strain that can disrupt the long-range FM order at the grain boundaries [35]. As mentioned above, the grain size of the samples decreased and the grain boundaries deteriorated with Cu substitution. This result supports the observed decrease in T_C .

In order to examine the magnetization behavior of the samples against the magnetic field, to calculate the magnetic entropy change values and to determine the type of magnetic phase transition, magnetization measurements were carried out depending on the magnetic field. Measurements have been performed below and above T_C of the samples in 4 K increments. The magnetic field has been applied to the samples up to field value of 5 T. The $M(H)$ curves are given in Fig. 6. It is seen that the $M(H)$ curves reach saturation rapidly when a low magnetic field is applied in the low temperature region. The $M(H)$ curves of the samples show a linear variation characteristic of the PM state at temperatures above the T_C .

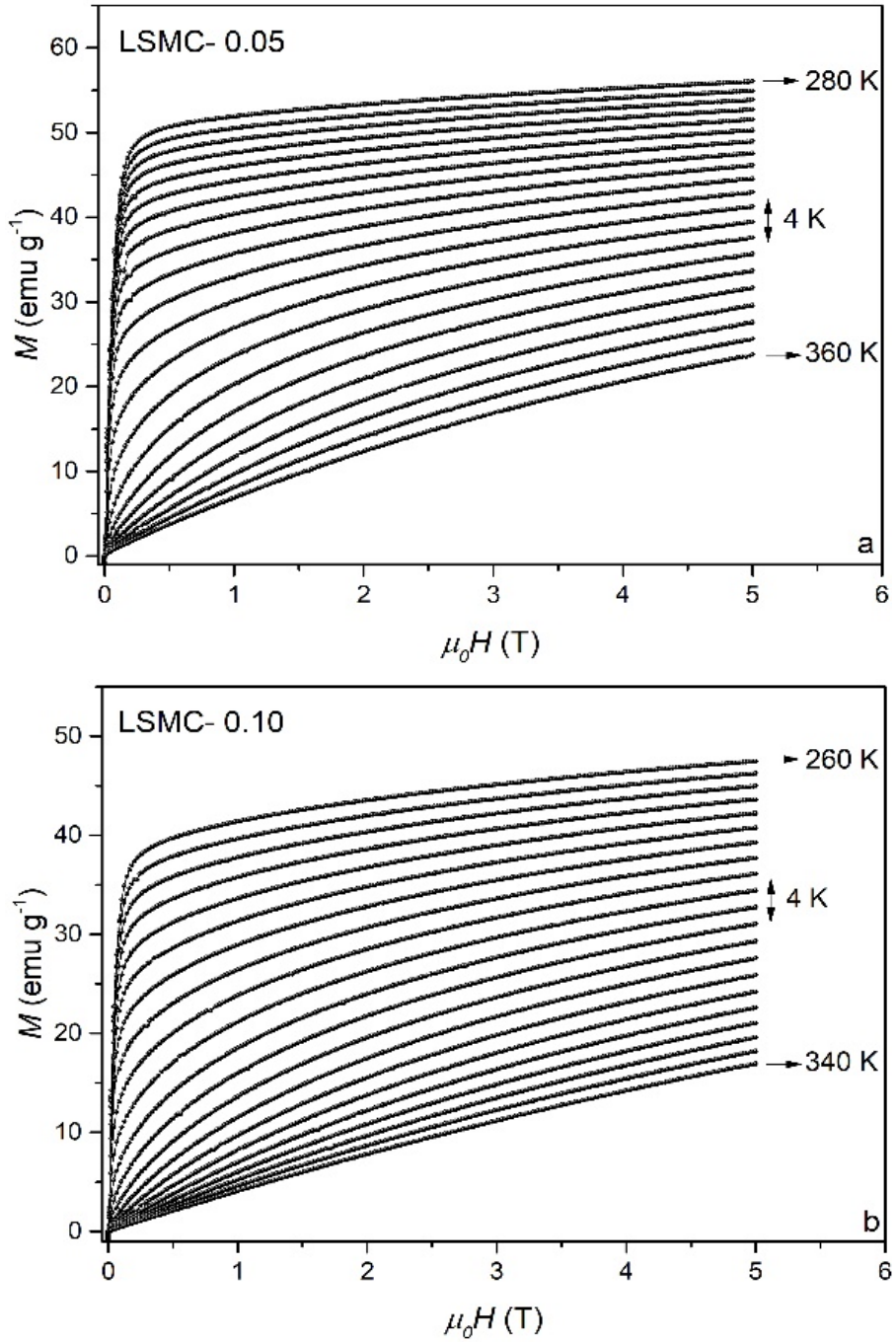


Figure 6: $M(H)$ curves of the samples (a) LSMC-0.05 and (b) LSMC-0.10

The kind of the magnetic phase transition is quite important for MR applications. The samples exhibiting FOMT show large $-\Delta S_M$ [13]. However, they have large hysteresis (magnetic and thermal), which affects the cooling efficiency and reversibility of a magnetic refrigerant [13]. Therefore, these group materials are not suitable for application. Compared to FOMT, materials showing SOMT have higher potential for use in applications since their thermal and magnetic hysteresis are negligible [16, 17]. The transition takes place over a wider temperature range than

another. For the reasons mentioned above, it is important to specify the type of magnetic phase transition. For identifying the type of magnetic phase transition, Banerjee criterion is generally used and Arrott plots are obtained from $M(H)$ measurements. [36]. Banerjee's criterion says that if the Arrott plots have a positive slope around T_C , the type of the magnetic phase transition is second order. Otherwise, it is first order. We have obtained the Arrott plots as given in Fig. 7. Around T_C , LSMC-0.05 and LSMC-0.10 samples have a positive slope. As a result, one can say that transition is second order.

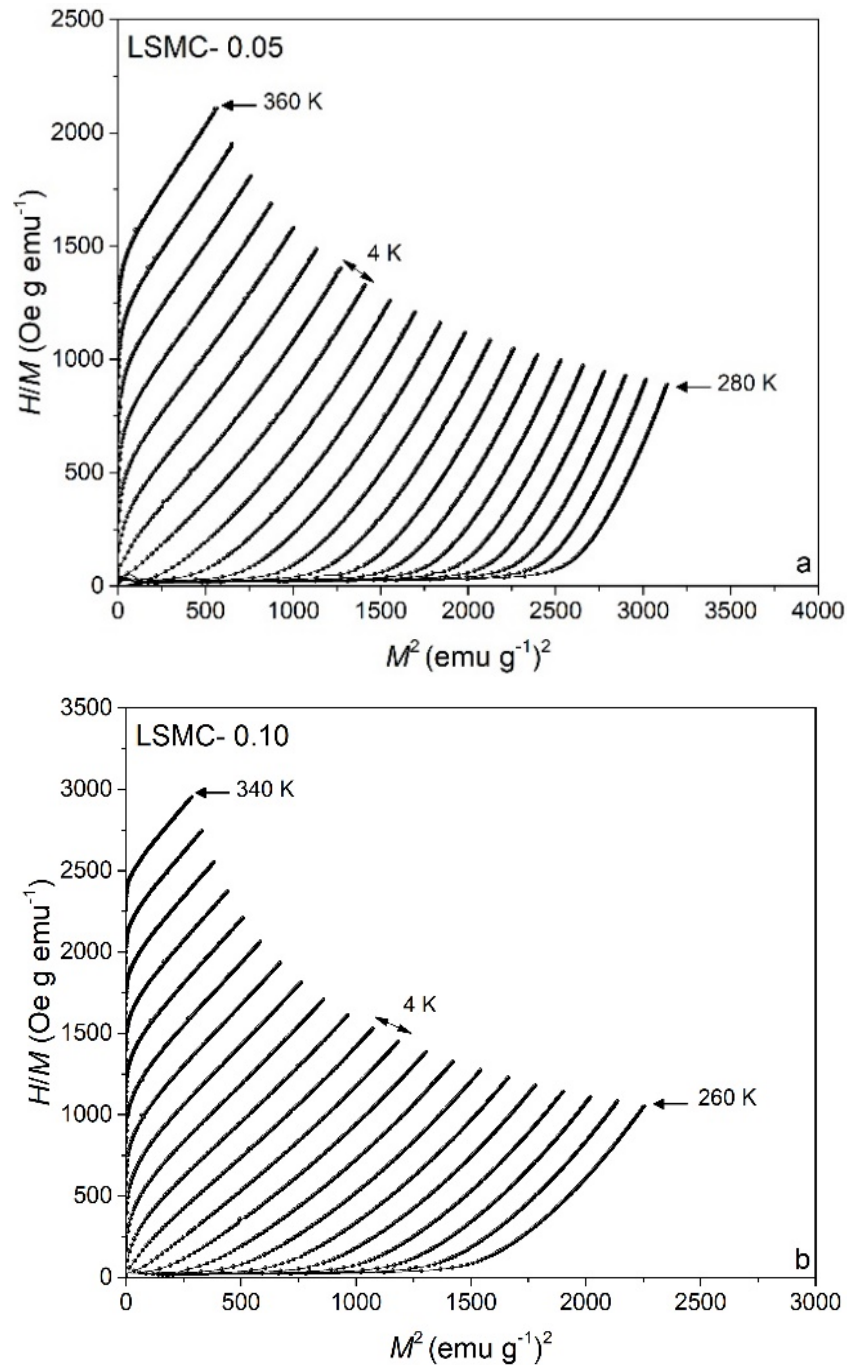


Figure 7: Arrott plot of the samples (a) LSMC-0.05 and (b) LSMC-0.10

$-\Delta S_M$ which is one of the components of MCE is calculated from $M(H)$ curves. Depending on Maxwell's relations and using numerical approximation, it can be practically written as follows [14];

$$-\Delta S_M(H, T) = \sum \frac{M_i - M_{i+1}}{T_{i+1} - T_i} \Delta H_i. \quad (2)$$

M_i and M_{i+1} parameters given in the equation are the magnetization values at T_i and T_{i+1} temperature, respectively. The $-\Delta S_M$ values corresponding to each temperature value of the samples were calculated. Figure 8 shows $-\Delta S_M(T)$ curves describing the temperature dependence of $-\Delta S_M$. The curves show a maximum peak defining maximum magnetic entropy change ($-\Delta S_M^{max}$) near T_C . The value of $-\Delta S_M^{max}$ for the samples has shown an increment with the increasing magnetic field. This is related to the increase in the number of magnetic moments oriented with the applied magnetic field [37]. It can be seen that the location of $-\Delta S_M^{max}$ peak is almost constant and does not show magnetic field dependency. This is observed when the Curie temperature is not dependent on the magnetic field. Otherwise, shifts are observed in the peak position [38]. The $-\Delta S_M^{max}$ values of LSMC-0.05 and LSMC-0.10 samples were calculated as 3.39 and 2.78 $\text{Jkg}^{-1}\text{K}^{-1}$ under 5 T magnetic fields, respectively. It has been observed that the substitution of Cu to Mn-site causes a decrease in $-\Delta S_M^{max}$ values, as in T_C . It is possible to say that this decrease is related to the decrease of conduction electrons in the structure. Relative cooling power (RCP), called as magnetic cooling efficiency, and is another important parameter for the technological applications of MR systems. Its value can be calculated by the following equation [2];

$$\text{RCP} = |-\Delta S_M^{max}| \times \delta T_{FWHM} \quad (3)$$

where δT_{FWHM} is the full width at half maximum of the magnetic entropy curves. For LSMC-0.05 and LSMC-010 samples RCP values were calculated as 249.52 and 111.98 Jkg^{-1} , respectively. RCP value has decreased with increasing of Cu concentration.

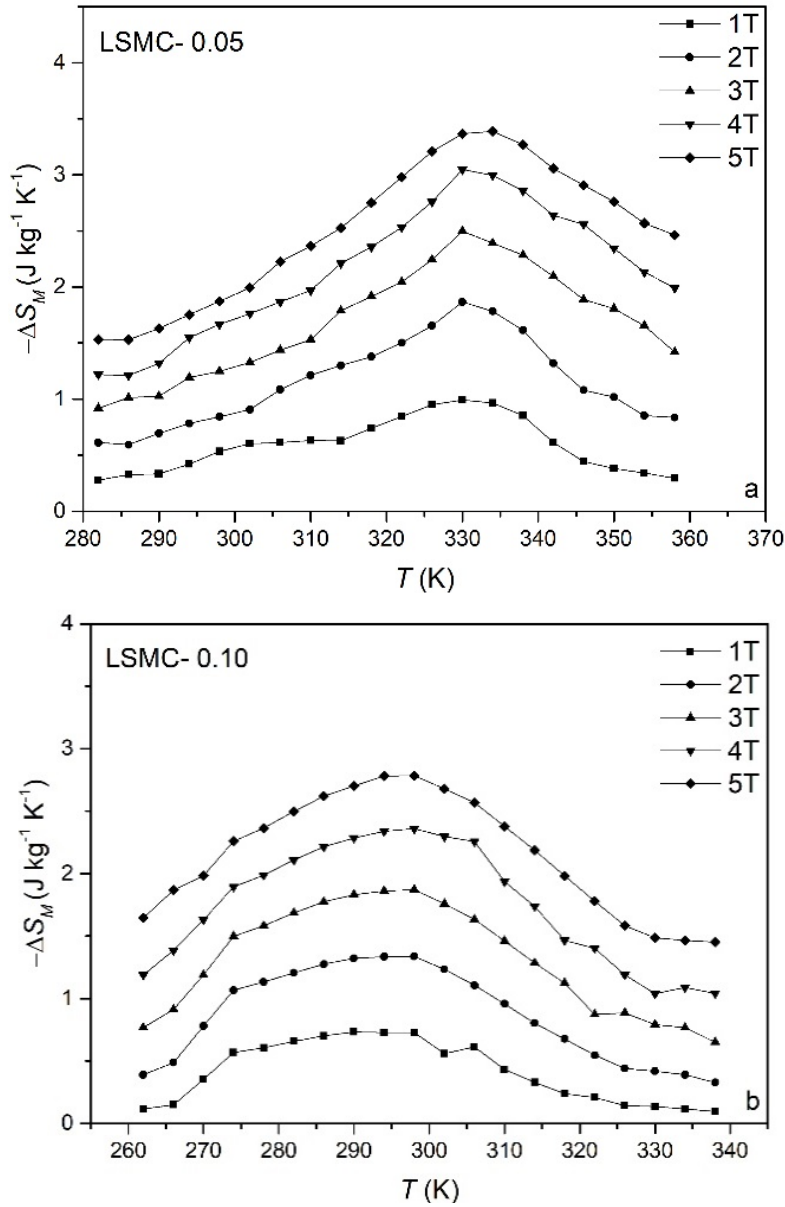


Figure 8: $-\Delta S_M(T)$ of the samples (a) LSMC-0.05 and (b) LSMC-0.10

The state equation of a magnetic system can be written based on the energy minimization as given following [39]:

$$\frac{H}{M} = a(T) + b(T)M^2 + c(T)M^4 \quad (4)$$

In the equation, there is a physical meaning of a , b , and c terms called Landau coefficients which change with temperature. First, the term a is related to magnetic susceptibility and is used to determine T_C [32]. The term b is related to the order of magnetic phase transition. At T_C , if term b has a positive slope, it is second order [40]. The term c is a constant. The temperature dependent

variation of a , b and c terms is given in Fig. 9 for LSMC-0.05 and LSMC-0.10 samples. As seen from figures, term b has positive value and it confirms that the order of transition is second order.

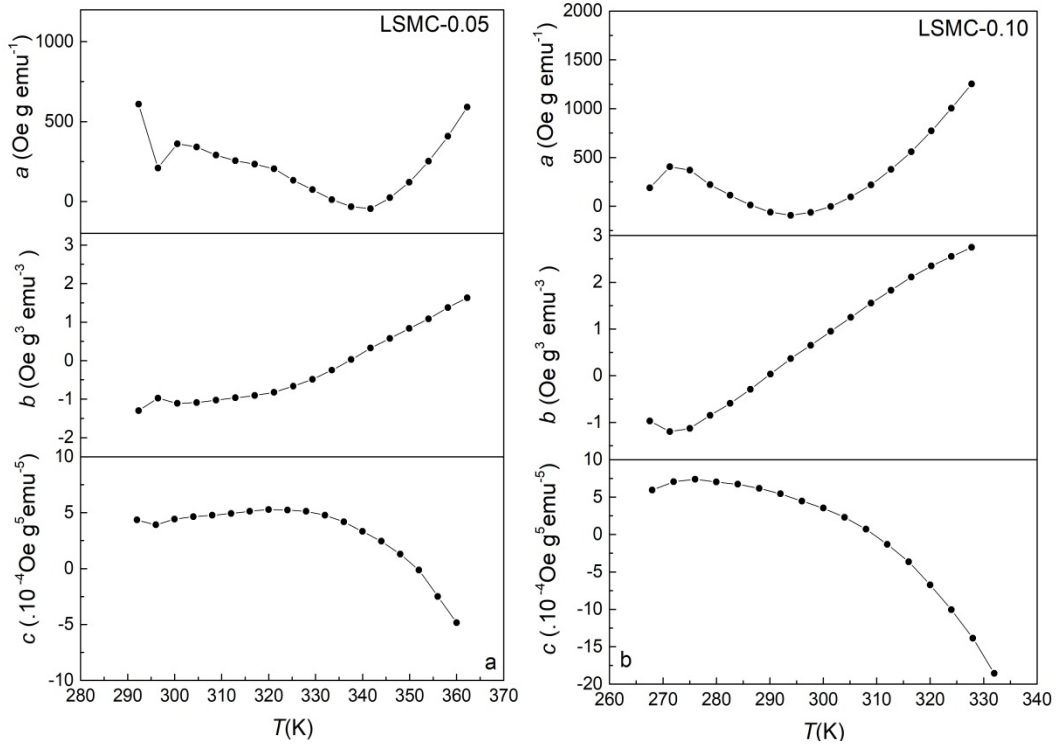


Figure 9: The temperature dependent variation of a , b and c terms for (a) LSMC-0.05 and (b) LSMC-0.10

The $-\Delta S_M$ can be theoretically calculated from following equation [39]

$$-\Delta S_M = \left(\frac{\partial G}{\partial T}\right)_H = \frac{1}{2} a'(T)M^2 + \frac{1}{4} b'(T)M^4 + \frac{1}{6} c'(T)M^6 \quad (5)$$

For both samples, the temperature dependence of the theoretical and experimental $-\Delta S_M$ curves under 5 T is given in Fig. 10. It is seen that there is a small difference between theoretical and experimental values for LSMC-0.05. It is considered that the Jahn–Teller effect, exchange interactions and micromagnetism may induce a difference between theoretical and experimental values of the $-\Delta S_M$ [41]. For LSMC-0.10 sample, the experimental and theoretical values are compatible with each other; this implies that $-\Delta S_M$ values and its temperature dependency are affected by magnetoelastic coupling and electron interactions [42, 43].

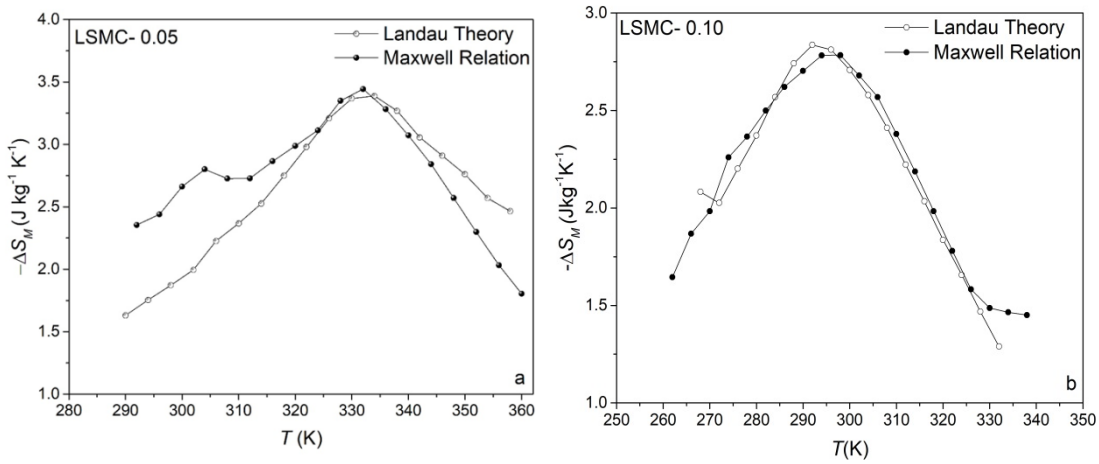


Figure 10: $-\Delta S_M(T)$ of the samples (a) LSMC-0.05 and (b) LSMC-0.10

4. Conclusion

In summary, magnetic and magnetocaloric properties as well as structural properties of LSM0.05 and LSMC-0.10 samples obtained by sol-gel method has been investigated. The structural properties of LSMC-0.05 and LSMC-0.10 samples were determined using XRD. Both samples were crystallized in rhombohedral structure. It is observed that a small change was observed in the lattice parameters and unit cell volume values with the increasing of Cu concentration. A decrement in the grain size and an increment in porosity between grains have been observed with Cu substitution to the Mn-site. The LSMC-0.05 and LSMC-0.10 samples show ferromagnetic- paramagnetic magnetic phase transition at 330 K and 301 K, respectively. It has been confirmed by the Landau and Banerjee criterion that the samples exhibit second-order phase transition. The $-\Delta S_M^{max}$ values of LSMC-0.05 and LSMC-0.10 samples have been calculated as 3.39 and 2.78 $\text{Jkg}^{-1}\text{K}^{-1}$ under 5 T magnetic fields, respectively. It has been observed that replacing Mn with Cu element in the structure causes a decrease in $-\Delta S_M^{max}$ values as well as in T_C . RCP values were calculated as 249.52 and 111.98 Jkg^{-1} for LSMC-0.05 and LSMC-010 samples, respectively. According to the results, we can say that the substitution of Cu to the Mn-site negatively affects the magnetic and magnetocaloric properties of the samples.

Acknowledgements

This work is supported by the TUBITAK (The Scientific and Technological Research Council of Turkey) under Grant Contract No. 119F069.

References

- [1] Sari, O., Balli, M., *From conventional to magnetic refrigerator technology*, International Journal of Refrigeration, 37, 8-15, 2014.
- [2] Brown, J.S., Domanski, P.A., *Review of alternative cooling technologies*, Applied Thermal Engineering, 64, 252-262, 2014.
- [3] Calm, J. M., *Emissions and environmental impacts from air-conditioning and refrigeration systems*, International Journal of Refrigeration, 25, 293-305, 2002.
- [4] Omer, A.M., *Energy use and environmental impacts: A general review*, Journal of Renewable and Sustainable Energy, 1, 053101, 2009.
- [5] Khosla, R., Miranda, N.D., Trotter, P.A., Mazzone, A., Renaldi, R., McElroy, C., Cohen, F., Jani, A., Perera-Salazar, R., McCulloch, M., *Cooling for sustainable development*, Nature Sustainability, 4, 201-208, 2021.
- [6] Crossley, S., Mathur, N., Moya, X., *New developments in caloric materials for cooling applications*, Aip Advances, 5, 067153, 2015.
- [7] Akça, G., Kılıç Çetin, S., Ekicibil, A., *Composite $x\text{La}_{0.7}\text{Ca}_{0.2}\text{Sr}_{0.1}\text{MnO}_3/(1-x)\text{La}_{0.7}\text{Te}_{0.3}\text{MnO}_3$ materials: magnetocaloric properties around room temperature*, Journal of Materials Science: Materials in Electronics, 31, 6796–6808, 2020.
- [8] Ayaş, A.O., Kılıç Çetin, S., Akyol, M., Akça, G., Ekicibil, A., *Effect of B site partial Ru substitution on structural magnetic and magnetocaloric properties in $\text{La}_{0.7}\text{Pb}_{0.3}\text{Mn}_{1-x}\text{Ru}_x\text{O}_3$ ($x=0.0, 0.1$ and 0.2) perovskite system*, Journal of Molecular Structure, 1200, 127120, 2020.
- [9] Dhahri, A., Dhahri, J., Dhahri, E., *Effect of potassium doping on physical properties of perovskites $\text{La}_{0.8}\text{Cd}_{0.2-x}\text{K}_x\text{MnO}_3$* , Journal of Alloys and Compounds, 489, 9-12, 2010.
- [10] Elghoul, A., Krichene, A., Boujelben, W., *Landau theory and critical behavior near the ferromagnetic-paramagnetic transition temperature in $\text{Pr}_{0.63}\text{A}_{0.07}\text{Sr}_{0.3}\text{MnO}_3$ ($A=\text{Pr}, \text{Sm}$ and Bi) manganites*, Journal of Physics and Chemistry of Solids, 108, 52-60, 2017.
- [11] Pecharsky, V.K., Gschneidner Jr, K.A., *Magnetocaloric effect and magnetic refrigeration*, Journal of Magnetism and Magnetic Materials, 200, 44-56, 1999.
- [12] Biswas, A., Chandra, S., Phan, M.H., Srikanth, H., *Magnetocaloric properties of nanocrystalline LaMnO_3 : Enhancement of refrigerant capacity and relative cooling power*, Journal of Alloys and Compounds, 545, 157-161, 2012.
- [13] Phan, M.H., Yu, S.C., *Review of the magnetocaloric effect in manganite materials*, Journal of Magnetism and Magnetic Materials, 308, 325-340, 2007.
- [14] Tishin, A.M., Spichkin, Y.I., *The Magnetocaloric Effect and its Applications*, IOP Publishing LTD, London, 2003.
- [15] Franco, V., Conde, A., Kuz'min, M. D., Romero-Enrique, J. M., *The magnetocaloric effect in materials with a second order phase transition: Are T_C and T_{peak} necessarily coincident?*, Journal of Applied Physics 105, 07A917, 2009.
- [16] Mleiki, A., Othmani, S., Cheikhrouhou-Koubaa, W., Cheikhrouhou, A., Hlil E. K., *Enhanced relative cooling power in Ga-doped $\text{La}_{0.7}(\text{Sr},\text{Ca})_{0.3}\text{MnO}_3$ with ferromagnetic-like canted state*, RSC Advances, 6, 54299–54309, 2016.
- [17] Lyubin, J., *Magnetocaloric materials for energy efficient cooling*, Journal of Physics D: Applied Physics, 50, 053002, 2017.

- [18] Paticopoulos, S.C., Caballero-Flores, R., Franco, V., Bla'zquez, J.S., Cond, A., Knipling, K.E., Willard, M.A., *Enhancement of the magnetocaloric effect in composites: Experimental validation*, Solid State Communications, 152, 1590–1594, 2012.
- [19] Monfared, B. Palm, B., *Material requirements for magnetic refrigeration applications*, International Journal of Refrigeration, 96, 25–37, 2018.
- [20] Coey, J. M. D., Viret, M., Von Molnár, S., *Mixed-valence manganites*, Advances in Physics, 48:2, Taylor & Francis, 167-293, 1999.
- [21] Rostamnejadi A., Salamati, H., Kameli, P., Ahmadvand, H., *Superparamagnetic behavior of $La_{0.67}Sr_{0.33}MnO_3$ nanoparticles prepared via sol-gel method*, Journal of Magnetism and Magnetic Materials, 321, 3126–3131, 2009.
- [22] Zverev, V.I., Pyatakov, A.P., Shtil, A.A., Tishin, A.M., *Novel applications of magnetic materials and technologies for medicine*, Journal of Magnetism and Magnetic Materials, 459, 182–186, 2018.
- [23] Thaljaou, R., Boujelben, W., Pekała, M., Pekała, K., Mucha, J., Cheikhrouhou, A., *Structural, magnetic and transport study of monovalent Na-doped manganite $Pr_{0.55}Na_{0.05}Sr_{0.4}MnO_3$* , Journal of Alloys and Compounds, 558, 236–243, 2013.
- [24] Levy, P., Parisi, F., Polla, G., Vega, D., Leyva, G., Lanza, H., *Controlled phase separation in $La_{0.5}Ca_{0.5}MnO_3$* , Physical Review B, 62, 6437-6441, 2000.
- [25] Walha, I., Smari, M., M'nasri, T., Dhahri, E., *Structural, magnetic, and magnetocaloric properties of Ag-doped in the $La_{0.6}Ca_{0.4}MnO_3$ compound*, Journal of Magnetism and Magnetic Materials, 454, 190–195, 2018.
- [26] Kılıç Çetin, S., Akça, G., Aslan, M. S., Ekicibil, A., *Role of nickel doping on magnetocaloric properties of $La_{0.7}Sr_{0.3}Mn_{1-x}Ni_xO_3$ manganites*, Journal of Material Science: Materials in Electronics, 32, 10458–10472, 2021.
- [27] Goldschmit, V.M., *Geochemische Verteilungsgesetz der Element 7*, Kristiania, Oslo, 1923-1938.
- [28] Bhalla, A. S., Guo, R., Roy, R., *The Perovskite Structure - a Review of its Role in Ceramic Science and Technology*,” Material Research Innovations 4, 3–26, 2000.
- [29] Shannon, R.D. , *Revised effective ionic radii and systematic studies of interatomic distances in halides and chalcogenides*, Acta Crystallographica A 32:5, 751–767, 1976.
- [30] Kılıç Çetin, S., Acet, M., Ekicibil, A., *Effect of Pr-substitution on the structural, magnetic and magnetocaloric properties of $(La_{1-x}Pr_x)_{0.67}Pb_{0.33}MnO_3$ ($0.0 \leq x \leq 0.3$) manganites*, Journal of Alloys and Compounds, 727, 1253-1262, 2017.
- [31] Sffir, I., Ezaami, A., Cheikhrouhou-Koubaa, W., Cheikhrouhou, A., *Structural, magnetic and magnetocaloric properties in $La_{0.7-x}Dy_xSr_{0.3}MnO_3$ manganites ($x = 0.00, 0.01$ and 0.03)*, Journal of Alloys and Compounds (696), 760–767, 2017.
- [32] Akça, G., Kılıç Çetin, S., Ekicibil, A., *Structural, magnetic and magnetocaloric properties of $(La_{1-x}Sm_x)_{0.85}K_{0.15}MnO_3$ ($x = 0.0, 0.1, 0.2$ and 0.3) perovskite manganites*, Ceramics International, 43, 15811–15820, 2017.
- [33] Bouzaïene, E., Dhahri, J., Hlil, E. K., Belmabrouk, H., Alrobei, H., *Three-dimensional Heisenberg critical phenomena in $La_{0.6}Bi_{0.1}Sr_{0.3-x}Ca_xMn_{0.9}Cu_{0.1}O_3$ manganites ($x = 0$ and 0.05)*, Journal of Material Science: Materials in Electronics, 31, 18186–18197, 2020.
- [34] Zhang, T., Wang, X. P., Fang, Q. F., Li, X. G., *Magnetic and charge ordering in nanosized manganites*, Applied Physics Reviews, 1, 031302, 2014

- [35] M'nassri, R., Boudjada, N. C., Cheikhrouhou, A., *Impact of sintering temperature on the magnetic and magnetocaloric properties in $Pr_{0.5}Eu_{0.1}Sr_{0.4}MnO_3$ manganites*, Journal of Alloys and Compounds, 626, 20–28, 2015.
- [36] Banerjee, B.K., *On a generalised approach to first and second order magnetic transitions*, Physics Letters, 12, 16–17, 1964.
- [37] Mansouri, M., Omrani, H., Cheikhrouhou-Koubaa, W., Koubaa, M., Madouri, A., Cheikhrouhou, A., *Effect of vanadium doping on structural, magnetic and magnetocaloric properties of $La_{0.5}Ca_{0.5}MnO_3$* , Journal of Magnetism and Magnetic Materials, 401, 593–599, 2016.
- [38] Zhang, L., Li, L., Li, R., Fan, J., Ling, L., Tong, W., Qu, Z., Tan, S., Zhang, Y., *Spin–lattice coupling studied by magnetic entropy and EPR in the $CdCr_2S_4$ system*, Solid State Communications, 150, 2109–2113, 2010.
- [39] Amaral, V.S., Amaral, J.S., *Magnetoelastic coupling influence on the magnetocaloric effect in ferromagnetic materials*, Journal of Magnetism and Magnetic Materials, 272–276, 2104–2105, 2004.
- [40] Amaral, V.S., Araújo, J.P., Pogorelov, Y. G., Tavares, P.B., Sousa, J.B, Vieira, J.M., *Discontinuous transition effects in manganites: magnetization study in the paramagnetic phase*, Journal of Magnetism and Magnetic Materials, 242–245, 655–658, 2002.
- [41] Yang, H., Zhang, P., Wu, Q., Ge, H., Pan, M., *Effect of monovalent metal substitution on the magnetocaloric effect of perovskite manganites $Pr_{0.5}Sr_{0.3}M_{0.2}MnO_3$ (M=Na, Li, K and Ag)*, Journal of Magnetism and Magnetic Materials, 324, 3727–3730, 2012.
- [42] Koubaa, M., Regaieg, Y., Koubaa, W.C., Cheikhrouhou, A., Ammar-Merah, S., Herbst, F., *Magnetic and magnetocaloric properties of lanthanum manganites with monovalent elements doping at A-site*, Journal of Magnetism and Magnetic Material, 323, 252–257, 2011.
- [43] Cherif, R., Hlil, E.K., Ellouze, M., Elhalouani, F., Obbade, S., *Study of magnetic and magnetocaloric properties of $La_{0.6}Pr_{0.1}Ba_{0.3}MnO_3$ and $La_{0.6}Pr_{0.1}Ba_{0.3}Mn_{0.9}Fe_{0.1}O_3$ perovskite-type manganese oxides*, Journal of Material Science, 49, 8244–8251, 2014.